



Summary
Report on
BAASS UAP
Analysis
Capabilities

November 23, 2010



Summary
Report on
BAASS UAP
Analysis
Capabilities

November 23, 2010

TABLE OF CONTENTS

	pg.
LIST OF FIGURES	4
LIST OF TABLES.....	9
1. EXECUTIVE SUMMARY	10
2. INTRODUCTION.....	13
2.1 HISTORICAL EVENTS AND STUDIES	13
2.2 BAASS' TWELVE TECHNOLOGY FOCUS AREAS	14
2.3 BAASS PERSONNEL, SOFTWARE, EQUIPMENT AND DATA WAREHOUSE	15
2.3.1 BAASS Personnel.....	15
2.3.2 ANSYS Multiphysics FEA.....	16
2.3.3 Equipment.....	16
2.3.4 Data Warehouse	19
3. TYPES OF UAPS OBSERVED	21
4. ANALYTICAL AND NUMERICAL SOLUTIONS FOR UAP INVESTIGATIONS.....	25
4.1 "TIC TAC" INCIDENT	25
4.1.1 Analytical Solutions of Velocities and Accelerations Associated with "Tic Tac" Performance	32
4.1.2 Summary of Analytical Velocity and Acceleration Solutions.....	32
4.1.3 Numerical Analysis of Compressible Flow	39
4.1.4 Summary and Conclusions of Compressible Numerical Analyses.....	46
4.1.5 Numerical Analysis of Incompressible Flow of a UAP Entering Water	47
4.1.6 Numerical Analysis of Incompressible Flow of a UAP Entering Water Results.....	48
4.1.7 Summary and Conclusions of Numerical Analysis of Incompressible Flow of a UAP Entering Water Results	58
4.2 ANALYSES OF SPHERICAL UAPS.....	58
4.2.1 Acoustical Analysis of a Spherical USO	58
4.2.2 ANSYS Multiphysics Electromagnetic Capabilities	82
4.2.3 Radar Cross Section Analysis of a Spherical UFO.....	83
5. SUMMARY AND CONCLUSION.....	98
6. REFERENCES.....	100
SYMBOLS AND ACRONYMS	102
ATTACHMENT I – ANSYS INPUT FILES.....	105

USO ANSYS Multiphysics Acoustics Input File Example	105
UAP ANSYS Multiphysics RCS Input File Example	112
ATTACHMENT II – "TIC TAC" CFD CONTOUR PLOTS FOR PRESSURE, TEMPERATURE AND MACH NUMBER.....	116
ATTACHMENT III – RIGHT CIRCULAR CYLINDER CFD CONTOUR PLOTS FOR PRESSURE, TEMPERATURE AND MACH NUMBER	128

LIST OF FIGURES

	pg.
Figure 1. The UFO Pattern: A Condensed Statement of Repeated Observations	21
Figure 2. Lockheed Martin Skunk Works SR-71 Black Bird	22
Figure 3. Lockheed F-117 Nighthawk Stealth Fighter	22
Figure 4. Northrop Grumman B-2 Spirit Stealth Bomber	23
Figure 5. Boeing Phantom Works B-2 Stealth X-45A UAV	23
Figure 6. Three Dimensional Rendering of a Cylindrical or "Tic Tac" UAP	24
Figure 7. Three Dimensional Rendering of a Metallic Spherical UAP	24
Figure 8. Location of the AAV during the F/A18 Intercept	26
Figure 9. FLIR in 'White Hot' Mode	30
Figure 10. FLIR in "Black Hot" mode	30
Figure 11. Tic Tac Parametric Velocities for Selected Times of Event Duration in ft/sec	35
Figure 12. Tic Tac Parametric Velocities for Selected Times of Event Duration in mph	36
Figure 13. Tic Tac Parametric Accelerations for Selected Times of Event Duration in ft/sec ²	37
Figure 14. Tic Tac Parametric Accelerations for Selected Times of Event Duration in g	38
Figure 15. Tic Tac Pressure at 1/6 Scale, Air Temperature 223K and 700 mph with Mixed Inlet and Supersonic Outlet	41
Figure 16. Tic Tac Temperature at 1/6 Scale, Air Temperature 223K and 700 mph with Mixed Inlet and Supersonic Outlet	41
Figure 17. Tic Tac Mach Number at 1/6 Scale, Air Temperature 223K and 700 mph with Mixed Inlet and Supersonic Outlet	42
Figure 18. Tic Tac Pressure at 1/6 Scale, Air Temperature 223K and 1500 mph with Supersonic Inlet and Supersonic Outlet	42
Figure 19. Tic Tac Temperature at 1/6 Scale, Air Temperature 223K and 1500 mph with Supersonic Inlet and Supersonic Outlet	43
Figure 20. Tic Tac Mach Number at 1/6 Scale, Air Temperature 223K and 1500 mph with Supersonic Inlet and Supersonic Outlet	43
Figure 21. Cylinder Temperature at 1/6 Scale, Air Temperature 223K and 700 mph with Mixed Inlet and Supersonic Outlet	44
Figure 22. Cylinder Mach Number at 1/6 Scale, Air Temperature 223K and 700 mph with Mixed Inlet and Supersonic Outlet	44
Figure 23. Cylinder Pressure at 1/6 Scale, Air Temperature 223K and 1500 mph with Supersonic Inlet and Supersonic Outlet	45
Figure 24. Cylinder Temperature at 1/6 Scale, Air Temperature 223K and 1500 mph with Supersonic Inlet and Supersonic Outlet	45
Figure 25. Cylinder Mach Number at 1/6 Scale, Air Temperature 223K and 1500 mph with Supersonic Inlet and Supersonic Outlet	46
Figure 26. Solid Three Dimensional Geometry of Disc and Water	50
Figure 27. Solid Three Dimensional Geometry Mesh of Disc and Water	51
Figure 28. Solid Three Dimensional Geometry Mesh of UAP Disc	52

Figure 29. User Generated Cut Analysis Plane	53
Figure 30. Animated Result, Fluid 2 Volume Fraction	54
Figure 31. Total Pressure Around UAP	55
Figure 32. Water Surface Effects From Solid Impact	56
Figure 33. Water Surface Effects From Solid Impact (Side View).....	57
Figure 34. Mesh Plot for 1,000 Hz with 25 Elements per Wavelength in Water.....	61
Figure 35. Mesh Plot for 1,000 Hz with 50 Elements per Wavelength in Water.....	62
Figure 36. Contour Plot of Real Component of Pressure (Pa) for 1,000 Hz with 50 Elements per Wavelength in Water	63
Figure 37. Contour Plot of Real Component of Pressure (Pa) for 1,000 Hz with 50 Elements per Wavelength in Water	64
Figure 38. Contour Plot of Imaginary Component of Pressure (Pa) for 1,000 Hz with 25 Elements per Wavelength in Water	65
Figure 39. Contour Plot of the Magnitude of Pressure (Pa) for 1,000 Hz with 25 Elements per Wavelength in Water	66
Figure 40. Steady State Real Component of Pressure (Pa) as a Function of Radial Distance (m) Plot for 1,000 Hz with 25 Elements per Wavelength in Water.....	67
Figure 41. Steady State Imaginary Component of Pressure (Pa) as a Function of Radial Distance (m) Plot for 1,000 Hz with 25 Elements per Wavelength in Water.....	68
Figure 42. Steady State Magnitude of Pressure (Pa) as a Function of Radial Distance (m) Plot for 1,000 Hz with 25 Elements per Wavelength in Water.....	69
Figure 43. Contour Plot of Real Component of Pressure (Pa) for 5,000 Hz with 25 Elements per Wavelength in Water	70
Figure 44. Contour Plot of Imaginary Component of Pressure (Pa) for 5,000 Hz with 25 Elements per Wavelength in Water	71
Figure 45. Contour Plot of the Magnitude of Pressure (Pa) for 5,000 Hz with 25 Elements per Wavelength in Water	72
Figure 46. Steady State Real Component of Pressure (Pa) as a Function of Radial Distance (m) Plot for 5,000 Hz with 25 Elements per Wavelength in Water.....	73
Figure 47. Steady State Imaginary Component of Pressure (Pa) as a Function of Radial Distance (m) Plot for 5,000 Hz with 25 Elements per Wavelength in Water.....	74
Figure 48. Steady State Magnitude of Pressure (Pa) as a Function of Radial Distance (m) Plot for 5,000 Hz with 25 Elements per Wavelength in Water.....	75
Figure 49. Contour Plot of Real Component of Pressure (Pa) for 10,000 Hz with 25 Elements per Wavelength in Water	76
Figure 50. Contour Plot of Imaginary Component of Pressure (Pa) for 10,000 Hz with 25 Elements per Wavelength in Water	77
Figure 51. Contour Plot of the Magnitude of Pressure (Pa) for 10,000 Hz with 25 Elements per Wavelength in Water	78
Figure 52. Steady State Real Component of Pressure (Pa) as a Function of Radial Distance (m) Plot for 10,000 Hz with 25 Elements per Wavelength in Water.....	79

Figure 53. Steady State Imaginary Component of Pressure (Pa) as a Function of Radial Distance (m) Plot for 10,000 Hz with 25 Elements per Wavelength in Water.....	80
Figure 54. Steady State Magnitude of Pressure (Pa) as a Function of Radial Distance (m) Plot for 10,000 Hz with 25 Elements per Wavelength in Water	81
Figure 55. Factors that Determine the Energy Returned by a Target.....	83
Figure 56. Effect of Distance from the radar to the Target on the Power Density.....	84
Figure 57. Reduction in the Strength of Target Echoes with Range.....	87
Figure 58. Geometry, Description and Maximum RCS.....	88
Figure 59. Radar Cross Section Comparison	89
Figure 60. Mesh of ½ Symmetry UFO Sphere with 25 Elements per Wavelength.....	90
Figure 61. Mesh of ½ Symmetry UFO Sphere with 50 Elements per Wavelength.....	91
Figure 62. Normalized radar Cross Section Plot for a ½ Symmetry 10 m Metallic Sphere with a 1 m Dielectric Coating in Decibels for 300 MHz and 25 Elements per Wavelength	93
Figure 63. Normalized radar Cross Section Plot for a ½ Symmetry 10 m Metallic Sphere with a 1 m Dielectric Coating in Decibels for 300 MHz and 50 Elements per Wavelength	95
Figure 64. Electric Filed Contour in V/m for a ½ Symmetry 10 m Metallic Sphere with a 1 m Dielectric Coating in Decibels for 300 MHz and 25 Elements per Wavelength	96
Figure 65. Tic Tac Pressure at 1/6 Scale, Air Temperature 223K and 100 mph with Subsonic Inlet and Subsonic Outlet.....	116
Figure 66. Tic Tac Temperature at 1/6 Scale, Air Temperature 223K and 100 mph with Subsonic Inlet and Subsonic Outlet.....	116
Figure 67. Tic Tac Mach Number at 1/6 Scale, Air Temperature 223K and 100 mph with Subsonic Inlet and Subsonic Outlet.....	117
Figure 68. Tic Tac Pressure at 1/6 Scale, Air Temperature 223K and 200 mph with Subsonic Inlet and Subsonic Outlet.....	117
Figure 69. Tic Tac Temperature at 1/6 Scale, Air Temperature 223K and 200 mph with Subsonic Inlet and Subsonic Outlet.....	118
Figure 70. Tic Tac Mach Number at 1/6 Scale, Air Temperature 223K and 200 mph with Subsonic Inlet and Subsonic Outlet.....	118
Figure 71. Tic Tac Pressure at 1/6 Scale, Air Temperature 223K and 300 mph with Subsonic Inlet and Subsonic Outlet.....	119
Figure 72. Tic Tac Temperature at 1/6 Scale, Air Temperature 223K and 300 mph with Subsonic Inlet and Subsonic Outlet.....	119
Figure 73. Tic Tac Mach Number at 1/6 Scale, Air Temperature 223K and 300 mph with Subsonic Inlet and Subsonic Outlet.....	120
Figure 74. Tic Tac Pressure at 1/6 Scale, Air Temperature 223K and 400 mph with Mixed Inlet and Subsonic Outlet	120
Figure 75. Tic Tac Temperature at 1/6 Scale, Air Temperature 223K and 400 mph with Mixed Inlet and Subsonic Outlet	121
Figure 76. Tic Tac Mach Number at 1/6 Scale, Air Temperature 223K and 400 mph with Mixed Inlet and Subsonic Outlet	121

Figure 77. Tic Tac Pressure at 1/6 Scale, Air Temperature 223K and 500 mph with Mixed Inlet and Subsonic Outlet	122
Figure 78. Tic Tac Temperature at 1/6 Scale, Air Temperature 223K and 500 mph with Mixed Inlet and Subsonic Outlet	122
Figure 79. Tic Tac Mach Number at 1/6 Scale, Air Temperature 223K and 500 mph with Mixed Inlet and Subsonic Outlet	123
Figure 80. Tic Tac Pressure at 1/6 Scale, Air Temperature 223K and 900 mph with Supersonic Inlet and Supersonic Outlet.....	123
Figure 81. Tic Tac Temperature at 1/6 Scale, Air Temperature 223K and 900 mph with Supersonic Inlet and Supersonic Outlet.....	124
Figure 82. Tic Tac Mach Number at 1/6 Scale, Air Temperature 223K and 900 mph with Supersonic Inlet and Supersonic Outlet.....	124
Figure 83. Tic Tac Pressure at 1/6 Scale, Air Temperature 223K and 1100 mph with Supersonic Inlet and Supersonic Outlet.....	125
Figure 84. Tic Tac Temperature at 1/6 Scale, Air Temperature 223K and 1100 mph with Supersonic Inlet and Supersonic Outlet.....	125
Figure 85. Tic Tac Mach Number at 1/6 Scale, Air Temperature 223K and 1100 mph with Supersonic Inlet and Supersonic Outlet.....	126
Figure 86. Tic Tac Pressure at 1/6 Scale, Air Temperature 223K and 1300 mph with Supersonic Inlet and Supersonic Outlet.....	126
Figure 87. Tic Tac Temperature at 1/6 Scale, Air Temperature 223K and 1300 mph with Supersonic Inlet and Supersonic Outlet.....	127
Figure 88. Tic Tac Mach Number at 1/6 Scale, Air Temperature 223K and 1300 mph with Supersonic Inlet and Supersonic Outlet.....	127
Figure 89. Cylinder Pressure at 1/6 Scale, Air Temperature 223K and 100 mph with Subsonic Inlet and Subsonic Outlet	128
Figure 90. Cylinder Temperature at 1/6 Scale, Air Temperature 223K and 100 mph with Subsonic Inlet and Subsonic Outlet	128
Figure 91. Cylinder Mach Number at 1/6 Scale, Air Temperature 223K and 100 mph with Subsonic Inlet and Subsonic Outlet	129
Figure 92. Cylinder Pressure at 1/6 Scale, Air Temperature 223K and 200 mph with Subsonic Inlet and Subsonic Outlet	129
Figure 93. Cylinder Temperature at 1/6 Scale, Air Temperature 223K and 200 mph with Subsonic Inlet and Subsonic Outlet	130
Figure 94. Cylinder Mach Number at 1/6 Scale, Air Temperature 223K and 200 mph with Subsonic Inlet and Subsonic Outlet	130
Figure 95. Cylinder Pressure at 1/6 Scale, Air Temperature 223K and 300 mph with Subsonic Inlet and Subsonic Outlet.....	131
Figure 96. Cylinder Temperature at 1/6 Scale, Air Temperature 223K and 300 mph with Subsonic Inlet and Subsonic Outlet.....	131
Figure 97. Cylinder Mach Number at 1/6 Scale, Air Temperature 223K and 300 mph with Subsonic Inlet and Subsonic Outlet.....	132
Figure 98. Cylinder Pressure at 1/6 Scale, Air Temperature 223K and 400 mph with Subsonic Inlet and Subsonic Outlet.....	132
Figure 99. Cylinder Temperature at 1/6 Scale, Air Temperature 223K and 400 mph with Subsonic Inlet and Subsonic Outlet.....	133

Figure 100. Cylinder Mach Number at 1/6 Scale, Air Temperature 223K and 400 mph with Subsonic Inlet and Subsonic Outlet.....	133
Figure 101. Cylinder Pressure at 1/6 Scale, Air Temperature 223K and 500 mph with Mixed Inlet and Subsonic Outlet.....	134
Figure 102. Cylinder Temperature at 1/6 Scale, Air Temperature 223K and 500 mph with Mixed Inlet and Subsonic Outlet.....	134
Figure 103. Cylinder Mach Number at 1/6 Scale, Air Temperature 223K and 500 mph with Mixed Inlet and Subsonic Outlet.....	135
Figure 104. Cylinder Pressure at 1/6 Scale, Air Temperature 223K and 700 mph with Mixed Inlet and Supersonic Outlet.....	135
Figure 105. Cylinder Pressure at 1/6 Scale, Air Temperature 223K and 900 mph with Supersonic Inlet and Supersonic Outlet.....	136
Figure 106. Cylinder Temperature at 1/6 Scale, Air Temperature 223K and 900 mph with Supersonic Inlet and Supersonic Outlet.....	136
Figure 107. Cylinder Mach Number at 1/6 Scale, Air Temperature 223K and 900 mph with Supersonic Inlet and Supersonic Outlet.....	137
Figure 108. Cylinder Pressure at 1/6 Scale, Air Temperature 223K and 1100 mph with Supersonic Inlet and Supersonic Outlet.....	137
Figure 109. Cylinder Temperature at 1/6 Scale, Air Temperature 223K and 1100 mph with Supersonic Inlet and Supersonic Outlet.....	138
Figure 110. Cylinder Mach Number at 1/6 Scale, Air Temperature 223K and 1100 mph with Supersonic Inlet and Supersonic Outlet.....	138
Figure 111. Cylinder Pressure at 1/6 Scale, Air Temperature 223K and 1300 mph with Supersonic Inlet and Supersonic Outlet.....	139
Figure 112. Cylinder Temperature at 1/6 Scale, Air Temperature 223K and 1300 mph with Supersonic Inlet and Supersonic Outlet.....	139
Figure 113. Cylinder Mach Number at 1/6 Scale, Air Temperature 223K and 1300 mph with Supersonic Inlet and Supersonic Outlet.....	140

LIST OF TABLES

	pg.
Table 1. Mach Regimes	32
Table 2. Velocities and Accelerations of Tic Tac for Parametric Time Durations of Event.....	34
Table 3. Properties of Water Used for ANSYS Harmonic Analyses	60
Table 4. Normalized radar Cross Section for a 10 m Metallic Sphere with a 1 m Dielectric Coating in Decibels for 300 MHz and 25 Elements per Wavelength	92
Table 5. Normalized radar Cross Section for a 10 m Metallic Sphere with a 1 m Dielectric Coating in Decibels for 300 MHz and 50 Elements per Wavelength	94

1. EXECUTIVE SUMMARY

The purpose of this report is to summarize the field data collection, in-house databases and computational capabilities that currently reside at Bigelow Aerospace Advanced Space Studies (BAASS) for the study of advanced aerospace technology. Between 2008 and 2010 BAASS was contracted by the Defense Warning Office of the Defense Intelligence Agency (DIA) to create, staff, and equip a new organization in order to examine and analyze the threat to national security associated with advanced aerospace technology. By selecting and modeling a few sentinel cases of encounters with advanced aerospace technology, this report demonstrates the in-house data collection, data storage and analysis resources built by BAASS under DIA contract HHM402-08-C-0072.

Throughout the millennia individuals have observed and reported unexplained phenomena in the sky. Some of these reports included bright and flashing lights, objects streaking across the sky or silently hovering, and multiple colored and flashing structures morphing into one. Cylindrical, cigar, spherical, lenticular, triangular and ellipsoid shaped structures have been reported hovering and/or accelerating at rapid rates from a stationary position. Some of these abrupt, high speed maneuvers have been harder to explain with conventional physics, considering the inherently poor aerodynamic properties of many of these objects. It should be stressed many, but not all, of these sightings may be explained by natural phenomena, or by unacknowledged aerospace technology.

Several official government studies were conducted from the late 1940s until around 1970, but many of these studies were superficial and lacking in rigor. Since 1970, because of an absence of research funding, the study of Unidentified Aerial Phenomena (UAP) has been characterized by cursory analysis and amateur, unscientific data collection.

Pilots, both civilian and military, have reported seeing unusual objects in the air, some of which have been independently confirmed by radar. During the 1960s and 1970s a series of incidents was reported along the so called Northern Tier of the United States where silent hovering objects were observed over military facilities housing nuclear weapons. One report in March 1967 involving the simultaneous disabling of multiple missiles for a period of time, while a UAP allegedly hovered nearby, stimulated considerable public interest when information of the event began to emerge. The 1967 incident, if true, as well as other Northern Tier incidents, arguably had national security implications.

Over the years, there have also been numerous reports of Unidentified Submerged Objects (USO), in all bodies of water. Some USO and UAP reportedly exhibited superior performance capabilities in velocity and acceleration underwater in the absence of detectable turbulence or cavitation signatures. While comparing our state of the art military equipment with these capabilities a reasonable individual may conclude there are national security implications.

Bigelow Aerospace Advanced Space Studies, LLC (BAASS) is a research organization focused on the identification, evaluation, and acquisition of novel and emerging future technologies worldwide as they specifically relate to air and space craft. Cutting edge research areas include propulsion systems, space applications of nanosensors, piezoelectric and nanowire fabrics, human performance, plasma stealth technologies, and directed high energy weapons. BAASS

was contracted to the Defense Intelligence Agency (DIA) in 2008 to investigate and analyze the possibility of a credible threat posed by UAPs. To accomplish this mission, BAASS over the past two years has focused on developing three separate resources, each unique to the study of UAP: 1) to obtain the most comprehensive suite of portable field sensors and personnel available, 2) to build the most all-inclusive database of UAP performance capabilities and behavior in the world and 3) to acquire world class computational methodology for analysis of UAP data. This report touches on all aspects of these resources, but concentrates on the in-house computational capabilities.

BAASS acquired the ANSYS Multiphysics Finite Element Analysis (FEA) program, for “a first of a kind” engineering and physics in-house resource devoted to providing a scientifically sound mathematical analysis and modeling of UAP behavior. Thus BAASS has acquired significant computational capability to convert field data into mathematical models and three dimensional simulations.

This report provides theory, analytical and numerical solutions for selected UAP and USO incidents through engineering and physics analyses. In particular, we examine a sentinel incident – the "Tic Tac" event – where F/A-18 aircraft from a United States Carrier Strike Group were vectored to a nearby unidentified contact in November 2004. The white object observed by four F/A-18F aircrew was described as 40 feet in length and shaped and colored like a "Tic Tac" candy.

Many analyses of UAP may use analytical or closed form solutions to solve the equations that describe the physics of an event. Where analytical solutions do not exist or the geometry is too complex, ANSYS multiphysics provides a powerful computational platform to solve large problems numerically, while combining and solving many different physical equations.

Compressible fluid flow analyses were performed to visualize the steady state pressure, temperature and Mach number contours around two craft shapes. An incompressible fluid flow problem around a solid disc shaped object descending through the air into a body of liquid was investigated to observe the disturbance produced on the surface of the water. A successful analysis of a USO was conducted using a full harmonic acoustics simulation; and computed values showed good agreement with the expected theoretical solutions. An analysis of a spherical UAP radar cross section (RCS) was conducted using a full harmonic electromagnetic simulation. Various other shapes of UAP and USOs may be evaluated by applying boundary conditions and transient physics equations to obtain a better understanding of the capabilities of these objects.

BAASS employees and contractors comprise scientists, engineers, analysts, intelligence and investigative professionals with a wide range of technical capabilities and backgrounds. Many of the professional staff members are considered national and international experts in their respective fields. BAASS' personnel have experience in performing work for government agencies such as the Department of Energy and Department of Defense. A broad mandate to research and develop future technology platforms pertaining to advanced propulsion, advanced non-aerodynamic lift capabilities, future material science breakthroughs including nanofabrication, novel power generation and signature reduction technologies, human interaction and effects of advanced technologies including field and radiation biological effects exists in

BAASS' work scope. BAASS' vision is to identify and acquire disruptive or discontinuous technologies that will form the basis of aerospace and defense applications through the year 2050, as well as those that pose potential threats to national security.

The company goal is to become a major entity in the research and development of future aerospace propulsion systems, controls, detection and tracking systems, stealth and directed energy uses by employing the best and brightest engineers and scientists available. The previous mentioned capabilities place BAASS in a strong position to provide technical results in both classified and unclassified endeavors.

2. INTRODUCTION

2.1 HISTORICAL EVENTS AND STUDIES

Disc, triangle, cigar and bell-shaped flying objects have been reported and documented on a global basis for millennia. The sighting by Kenneth Arnold on June 24, 1947 in the state of Washington garnered unprecedented global media attention and began the modern UFO era. While flying near Mt. Rainier, he observed a chain of nine unusual objects flying from north to south. Arnold reported that "two or three of them would dip or change course slightly, just enough for the sun to strike them at an angle that reflected brightly on my plane." The specific term "flying saucer" was never used by Arnold; however, he was quoted in a book stating: "As I described them at the time their flight was like speed boats on rough water or similar to the tail of a Chinese kite that I once saw blowing in the wind. As I put it to newsmen in Pendleton, Oregon, they flew like a saucer would if you skipped it across the water." (Arnold, 1953). Thus the moniker "flying saucer" was born. The terms "flying saucer" and "flying disc" were used commonly and interchangeably in the media to describe what are now known as UFOs (Unidentified Flying Object). Many sightings of UFOs were reported by commercial and military pilots during the late 1940s and a flying saucer allegedly crashed outside of Roswell, New Mexico, in early July 1947.

Shortly thereafter, a series of sightings of "green fireballs" began. These reports were almost exclusively over the state of New Mexico. Increasing significantly in number by December 1948, these sightings typically occurred over sensitive government installations, most notably the Los Alamos and Sandia National Laboratories. An investigation was initiated by meteor expert Dr. Lincoln La Paz. After personally witnessing a green fireball four to five degrees above the horizon on a horizontal trajectory on December 12, 1948, La Paz concluded the fireballs were structured, that is, not atmospheric phenomena. Initially they were thought to be of Russian origin. In April 1950, Project Twinkle was created to be a network of stations with the purpose of observing, studying, and collecting data on the fireball phenomena. This project did little to solve the mystery, and was disbanded later that year. Large numbers of UFO sightings continued in the late 1940s and as a result, some unease about the nature of the objects began to escalate in military circles, notably in the Air Force. For example, in September 1947, Air Force General Nathan Twining issued a memorandum stating "The reported operating characteristics such as extreme rates of climb, maneuverability (particularly in roll), and motion which must be considered evasive when sighted or contacted by friendly aircraft and radar, lend belief to the possibility some of the objects are controlled either manually, automatically or remotely." Twining recommended a detailed study of the UFO phenomenon. Based on increasing concern on the part of the military, the U.S. government initiated official studies of UFOs.

Project Sign was the first official U.S. government study of UFOs performed by the United States Air Force in early 1948 and concluded in early 1949. Project Sign officials argued UFOs were likely of extraterrestrial origin, and most of the project's personnel came to favor the extraterrestrial hypothesis. This hypothesis was rejected by the senior Air Force personnel. Project Sign eventually came to no official conclusion about UFOs with the final report stating the existence of flying saucers could neither be confirmed nor denied. Project Sign was concluded and restarted as Project Grudge in February 1949.

Project Grudge attempted to give each and every case a solution or an identifier tag. Grudge existed in various form and name until project completion in March 1952. The final Project Grudge report stated 22% of cases were categorized as unidentified, 69% identified, and 9% contained insufficient information to categorize.

In March 1952 Project Blue Book replaced Grudge and remained headquartered at the Air Technical Intelligence Center at Wright-Patterson Air Force Base in Ohio. Over the next seventeen years, Project Blue Book recorded approximately 15,000 UFO incidents, and Blue Book reported 701 of these incidents as "unidentified." The dramatic spike in UFO sightings in 1952 prompted the CIA to convene a scientific panel, headed by physicist Dr H. P. Robertson, in January 1953 to examine recent UFO data. It is widely stated among modern day UFO organizations that the Robertson Panel advocated a campaign to "debunk" UFOs.

Beginning on November 1, 1966, the Air Force Office of Scientific Research awarded \$313,000 to a research team at the University of Colorado, headed by physicist Dr. Edward Condon, to study the scientific implications of UFOs. The study was undertaken on the material furnished by Project Blue Book. The Condon Committee's final (and controversial) conclusion stated "we have recommended against the mounting of a major effort for continuing UFO study for scientific reasons." Secretary of the Air Force Robert C. Seamans, Jr. announced Blue Book would be closed due to the fact further funding "cannot be justified either on the grounds of national security or in the interest of science." The last publicly taken report for project Blue Book operations was December 17, 1969, but officially it closed on January 30, 1970.

Since the end of Blue Book numerous organizations have taken on the role of UFO/UAP investigations. Few of these groups have been professionally organized, trained, or equipped to properly investigate the phenomena. In contrast, one purpose of this report is to show BAASS is on the route to being the leading force in complete investigation and scientific analysis of the phenomena.

2.2 BAASS' TWELVE TECHNOLOGY FOCUS AREAS

BAASS is a research organization focused on the identification, evaluation, and acquisition of novel and emerging future technologies worldwide as they specifically relate to air and space craft. Cutting edge research areas include propulsion systems, space applications of nanosensors, piezoelectric and nanowire fabrics, human performance, plasma stealth technologies, and directed high energy technologies.

Research and development necessary for the procurement of the technology required for advanced space and weapons systems is conducted through use of computational Multiphysics FEA programs, development of computer code, experimentation, material science testing and manufacturing of prototypes in BAASS/Bigelow Aerospace in-house and in collaborating facilities and laboratories. Research areas of interest include Computational Fluid Dynamics, Heat Transfer, Nuclear Engineering, Electromagnetics and Radio Frequencies, Theoretical and Computational Physics, Biological Sciences and Chemistry.

Research performed through theoretical and computational applications, as well as modeling of components of non-conventional propulsion systems is under way to provide for future development of vehicles capable of operating in the atmosphere, under water and in space. BAASS research intends to provide innovative approaches and concepts for aircraft, propulsion, and flight technologies demonstrating significant advances in performance and capabilities beyond those in operation today.

BAASS' twelve key technology areas concentrate on how breakthrough technologies will provide for the development of advanced spacecraft concepts and weapon technologies through the year 2050 and beyond. The twelve areas are:

1. Lift
2. Propulsion
3. Control
4. Power Generation
5. Spatial Temporal Translation
6. Materials
7. Configuration, Structure
8. Signature Reduction
9. Human Interface
10. Human Effects
11. Armament
12. Other Peripheral Areas

2.3 BAASS PERSONNEL, SOFTWARE, EQUIPMENT AND DATA WAREHOUSE

Although the majority of this report is devoted to demonstrating BAASS' capabilities in mathematical modeling of various UAP performance parameters, the next section provides a short summary of some of the BAASS personnel, portable data collection sensors, as well as the current BAASS in-house database architecture.

2.3.1 BAASS Personnel

BAASS employees and contractors comprise scientists, engineers, analysts, intelligence and investigative professionals from diverse backgrounds. A majority of BAASS personnel have performed work for government agencies such as the Department of Energy and Department of Defense.

Research and development necessary for the procurement of the technology required for advanced space and weapons systems is conducted by numerical computational analysts through use of computational multiphysics FEA programs. Application and scientific programmers are involved in development of computer code that drives data mining and scientific applications used to evaluate historical and present UAP cases. Professionals in all areas conduct experimentation, material science testing and manufacturing of prototypes in both in-house facilities and collaborating facilities and laboratories. Areas of concentration include

Computational Fluid Dynamics (CFD), Heat Transfer, Nuclear Engineering, Electromagnetics and Radio Frequencies (RF), Theoretical and Computational Physics, Biological Sciences and Chemistry.

2.3.2 ANSYS Multiphysics FEA

The ANSYS Workbench platform is a powerful multi-domain simulation environment that harnesses the core physics from ANSYS, enables their interoperability, and provides common tools for interfacing with CAD, repairing geometry, creating meshes and post-processing results. To our knowledge, this powerful computational capability has not been previously utilized in the 64 year history of UFO study. It is hypothesized that through this more broad ranging analysis, additional theoretical constructs can be generated regarding UAP and USO behavior. These in turn can provide the scaffolding for advanced engineering concepts.

2.3.3 Equipment

2.3.3.1 Field Investigative Equipment

BAASS has amassed a considerable amount of field investigative equipment. The inventory includes a variety of imaging devices, along with Global Positioning Systems (GPS) and range finding items. Of note are the following:

2.3.3.1.1 Canon 5D MK II Digital SLR Cameras

Two Canon 5D MK II, 21.1 Megapixel, Digital SLR cameras were selected based on their capability for low light photography when combined with the Canon EF 300 mm ultrasonic, and the Canon EF 24-105 mm ultrasonic lenses. The 21.1 Megapixel size allows for RAW images suitable for scientific examination and analysis.

2.3.3.1.2 Sony A350 Digital SLR camera

The Sony A350 is a 14.2 Megapixel, digital SLR camera, with a Sony N 50-300 mm, a Sony N 50-70 mm lens, and a Sony Macro 2.8/50 mm lens. The a350 while a high quality camera, is compact and portable. It also allows for close-up and one-to-one photography.

2.3.3.1.3 Sony High Definition Video Cameras

Three Sony High Definition Video (HDV) 1080i, High Definition Video cameras, with low light capability were chosen for video capture in various field conditions.

2.3.3.1.4 Sony Handicam, Digital Video Cameras

Four Sony Handicam, digital video cameras with 80 GB hard drive storage capacity. These cameras are compact and portable, and using the HDD allow for up to 4 hours of continuous video recording with no tapes or other external media. They can also capture still images.

2.3.3.1.5 ATT PVS-7, Night Vision Devices

Seven ATT PVS-7, Night Vision Devices – military quality, state-of-the-art night vision devices.

2.3.3.1.6 Oasys Universal Thermal Monocular (UTM)

This device is a ruggedized thermal imaging and designation system. It includes a digital magnetic, both still and video capture capability as well as a digital PC interface allowing for real-time review of images in the field.

2.3.3.1.7 Garmin Global Positioning Systems

One Colorado 400t and two Oregon 400t, Global Positioning Systems, allowing for route mapping as well as waypoint storage in the field.

2.3.3.1.8 Leica Rangemaster 1200 Laser Range Finders

These two range finders are accurate out to 1500 meters, extremely compact and user friendly.

2.3.3.1.9 Sony CyberShot Cameras

Three Sony CyberShot 10.1 megapixel digital cameras – compact and portable for quick reaction to opportunities while actively investigating.

These equipment items give BAASS considerable capability when investigating events in the field. In addition to the items listed above a wide range of other support type items are in the BAASS inventory. These include Toshiba laptop computers, digital voice recorders, digital Game Cameras, IR spot lights, power invertors, several pieces of older night vision equipment, and packaging and storage items for solid, liquids, and hazardous materials.

In addition, BAASS obtained Technical Surveillance Countermeasures (TSCM) equipment in an effort to enhance the security of BAASS facilities. In addition to the below listed TSCM equipment BAASS personnel are trained by Research Electronics International in Cookeville, TN; also the manufacturer of the equipment.

- OSCOR 5000E, Omni-Spectral Correlator covering the radio frequency range from 50 kHz to 3 GHz
- ORION Non-Linear Junction Detector
- TALAN Telephone Analyzer
- CPM-700 Broadband Detector

2.3.3.2 Scientific Equipment

2.3.3.2.1 Veho VMS-001 200X 1.3 Megapixel Digital USB Microscope

This instrument is a very portable (4.4 x 1.3 inches) digital microscope which expands the capability of the field investigators. The microscope allows detailed images to be taken and connects directly to a laptop. Illumination is via 4 built in white LED lights.

2.3.3.2.2 Celestron 44340 3.5" LCD Digital Microscope

This instrument is a bench top digital microscope. The microscope has magnification capabilities of 40–400X extending up to 1600X with digital zoom. Images can be uploaded to a PC or laptop via a USB connection. It could also be taken into the field if required.

2.3.3.2.3 Niton XL3t 900S GOLDD Analyzer

This instrument is an X-ray fluorescence (XRF) analyzer. The device analyzes the emission of characteristic "secondary" (or fluorescent) X-rays from a material that has been excited by bombarding with high-energy X-rays. BAASS field teams deploy the Niton and conduct on-site elemental analysis.

2.3.3.2.4 Colibri TTC Handheld Dose Rate Meter

This instrument package allows for the detection and quantification of alpha, beta and gamma radiation in the field. The ability to accurately measure and quantify these three types of radiation adds another critical level of capability to the BAASS arsenal of analysis.

2.3.3.2.5 Hand held Spectrum Analyzer Pro Bundle 3 (NF-5030 and HF-60100)

These are instruments designed to detect and measure a broad spectrum of electromagnetic (EMF) radiation and high frequency radio waves. The NF-5030 measures three dimensional magnetic fields from as low as background up to 20 Gauss. Combining the two instruments electric fields are measured from 0.1 V/m to 20 kV/m and frequencies from 1 Hz to 9.4 GHz.

2.3.3.6 Hardware for ANSYS Workbench Platform

The research and work performed by BAASS ranges from technical design and prototyping, all the way up to advanced theoretical and computational studies of partial differential equations describing multiphysics problems. An expandable twelve core Hewlett Packard server with 48 GB of RAM and 1 TB of storage is used to perform parallel processing solutions for structural, fluid flow, heat transfer, high and low frequency electromagnetic problems along with coupled physics of two or more of those listed previously.

2.3.4 Data Warehouse

BAASS developed a Data Warehouse to support research on UAP and related anomalies and titled it "Project CAPELLA". The BAASS Data Warehouse is revolutionary because it: 1) incorporates a format based on the Valleé-Davis Six Layer Model for analyzing UAP, 2) includes several new databases developed by BAASS, and 3) includes databases developed by others which have never been collectively analyzed. The Data Warehouse currently consists of eleven separate databases and their associated supporting documentation in electronic format such as witness interviews, photographs, videos, recordings, sketches, analytical reports, etc. Each of the databases contains UAP sighting events relating to the purpose of that particular database, although some of the reported cases do overlap. Four of the databases will continue to catalogue current and future sighting reports. Seven of the databases have been completed and fully integrated and populated with all pertinent information captured by the CAPELLA format. BAASS will continue to input historical data in the CAPELLA format and will expand the Data Warehouse with additional databases and unusual aerial phenomena information.

The eleven databases currently included in the Data Warehouse are:

1. NIDS Database
2. Dominique Weinstein's Pilot Database
3. Sign/Grudge/Blue Book Database
4. UFOCAT Database
5. MUFON Case Management System Database
6. Project Colares Database
7. Canadian Release Database
8. United Kingdom Release Database
9. BAASS Database
10. Utah Ranch Database
11. Post-Utah Ranch Effects Database

The BAASS Data Warehouse is an electronic repository for historical, ongoing, and future UAP reporting and investigations. The Data Warehouse is designed to facilitate sophisticated analyses and data mining to improve our understanding of the extent, structure, and frequency of UAP, as well as their potential correlation to known physical, environmental, biological, or socio-political factors.

2.3.4.1 CAPELLA Format

The CAPELLA database format is based upon the "Six Layer Model for Anomalous Phenomena" developed by Dr. Jacques Valleé and Dr. Eric Davis (Valleé and Davis, 2003). This six layer model encapsulates all of the potential characteristics of UAP events that can be studied. The six layers are:

1. The Physical Layer – those physical characteristics associated with a UAP event
2. The Anti-Physical Layer – the patterns that conflict with those predicted in modern physics
3. The Psychological Layer – the psychological impacts to the witness(es) and the social conditions that surround them
4. The Physiological Layer – the effects perceived by humans
5. The Psychic Layer – the effects commonly found in parapsychology literature
6. The Cultural Layer – the primary and secondary effects upon society.

Additionally, the CAPELLA format captures administrative details associated with the UAP event, such as witness information, location, date, time, duration, etc.

2.3.4.2 Data Warehouse Upgrade

BAASS is undergoing a database upgrade project to further enhance data security and integrity, and increase processing power for greater analytical capability. The CAPELLA framework and methodologies will be preserved in the upgraded system. This upgrade will increase efficiency and effectiveness, and will allow databases to be analyzed individually or collectively.

2.3.4.3 Statistical Analysis

BAASS has completed a first-level, yet comprehensive statistical analyses for three of the databases: Dominique Weinstein's Pilot Database, Project Sign/Grudge/Blue Book Database, and the Utah Ranch Database. The analyses on the Weinstein and Blue Book databases are focused on identifying patterns of technical information from the case reports. The Utah Ranch analysis delves into patterns and aspects of when anomalous activity is reported in an attempt to identify potential times and improve the means of future detection methods.

3. TYPES OF UAPS OBSERVED

NASA aeronautical engineer Mr. Paul Hill made important inroads into attempts to delineate some quantitative characteristics of UFO performance by close examination of, and derivation of numerical parameters from, well investigated sentinel UFO cases (Hill, 1995). In addition, computer scientist Dr. Jacques Valleé has attempted to compute estimates of optical power output derived from UFO reports (Valleé, 1998). This report attempts to extend and broaden these preliminary studies using considerably enhanced computational power and mathematical modeling capabilities.

Figure 1, taken from (Hill, 1995) depicts illustrations of the various shapes associated with the UAP phenomena.

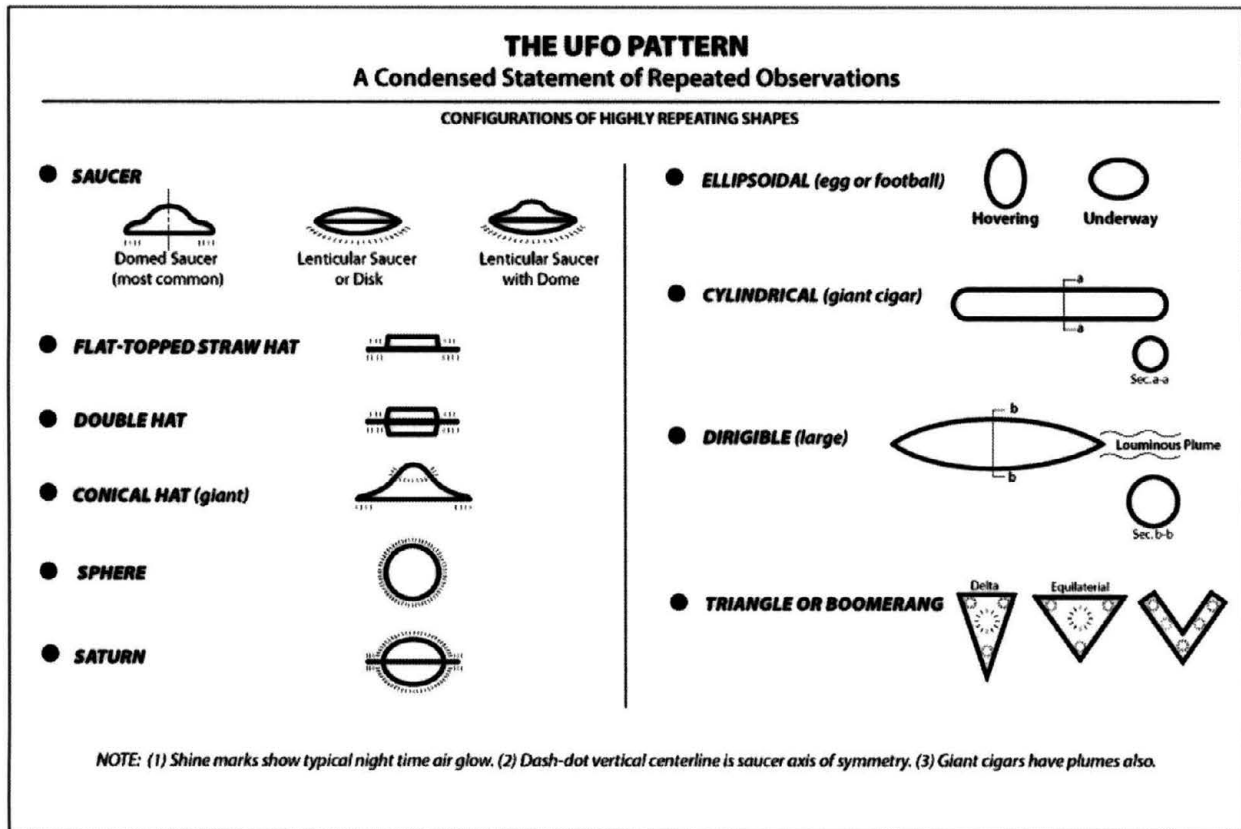


Figure 1. The UFO Pattern: A Condensed Statement of Repeated Observations

As an important component of these studies, BAASS understands a considerable number, possibly a majority, of UAP reports can be explained by simple misidentification of current advanced technology platforms. Some recent black triangle and even possibly some saucer and hat shaped UAP reports over the last several decades may have been explained by aircraft sightings of the Lockheed SR-71 Blackbird (Figure 2), Lockheed F-117 Nighthawk Stealth Fighter (Figure 3), Northrop Grumman B-2 Spirit Stealth Bomber (Figure 4) and Boeing Phantom Works Stealth X-45A Unmanned Aerial Vehicles (UAV) (Figure 5). Nevertheless, a significant number of cylindrical and cigar shapes along with spherical, lenticular and ellipsoid

shaped UAPs which appear to hover and/or accelerate at rapid rates from a stationary position have been harder to explain considering the inherently poor aerodynamic properties of these objects. It is this latter subset of UAP reports that BAASS has focused on.



Figure 2. Lockheed Martin Skunk Works SR-71 Black Bird



Figure 3. Lockheed F-117 Nighthawk Stealth Fighter

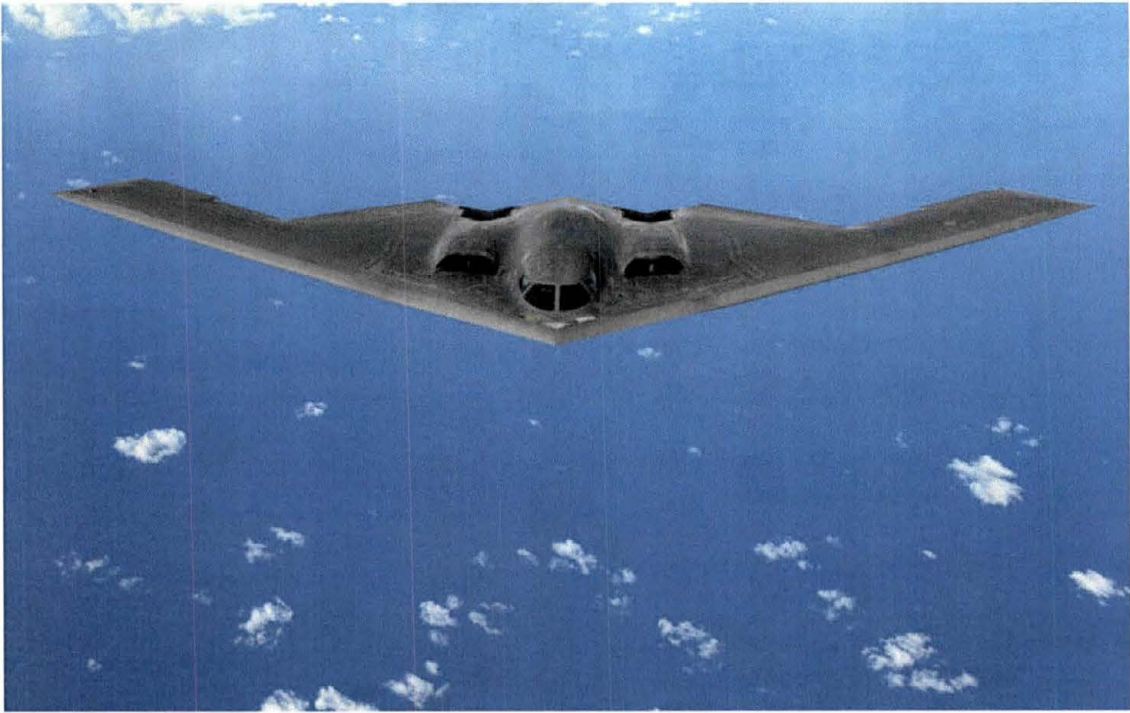


Figure 4. Northrop Grumman B-2 Spirit Stealth Bomber



Figure 5. Boeing Phantom Works B-2 Stealth X-45A UAV

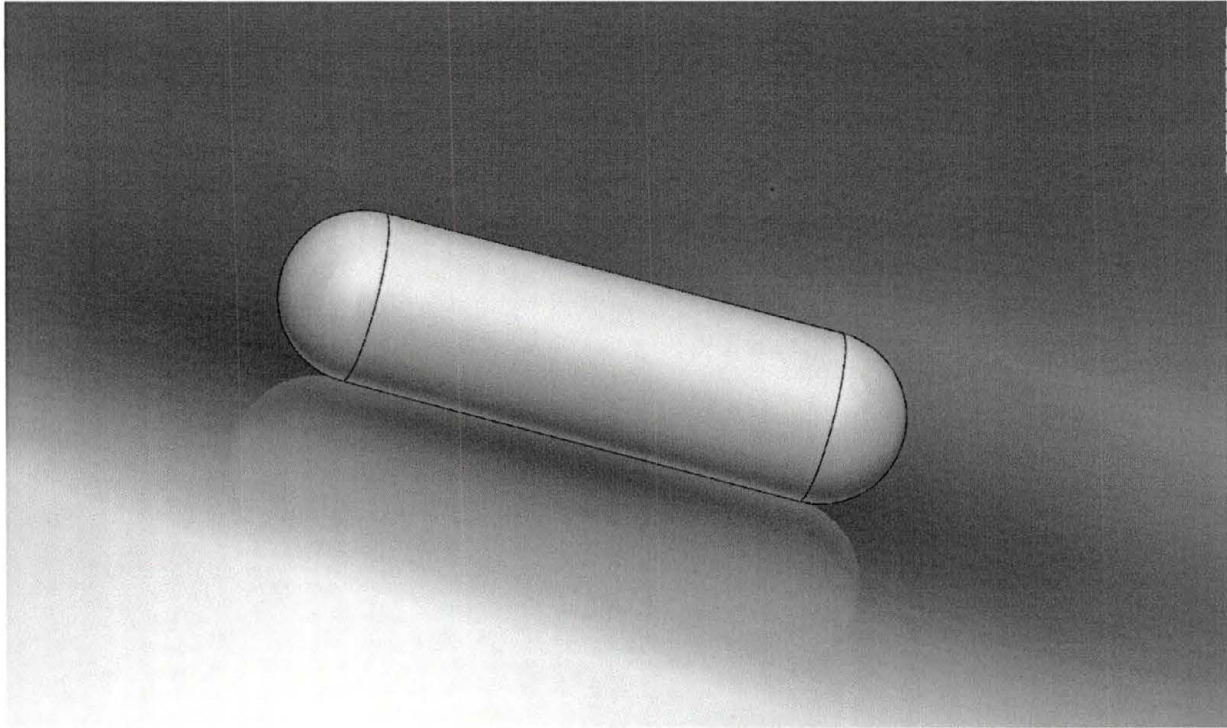


Figure 6. Three Dimensional Rendering of a Cylindrical or "Tic Tac" UAP

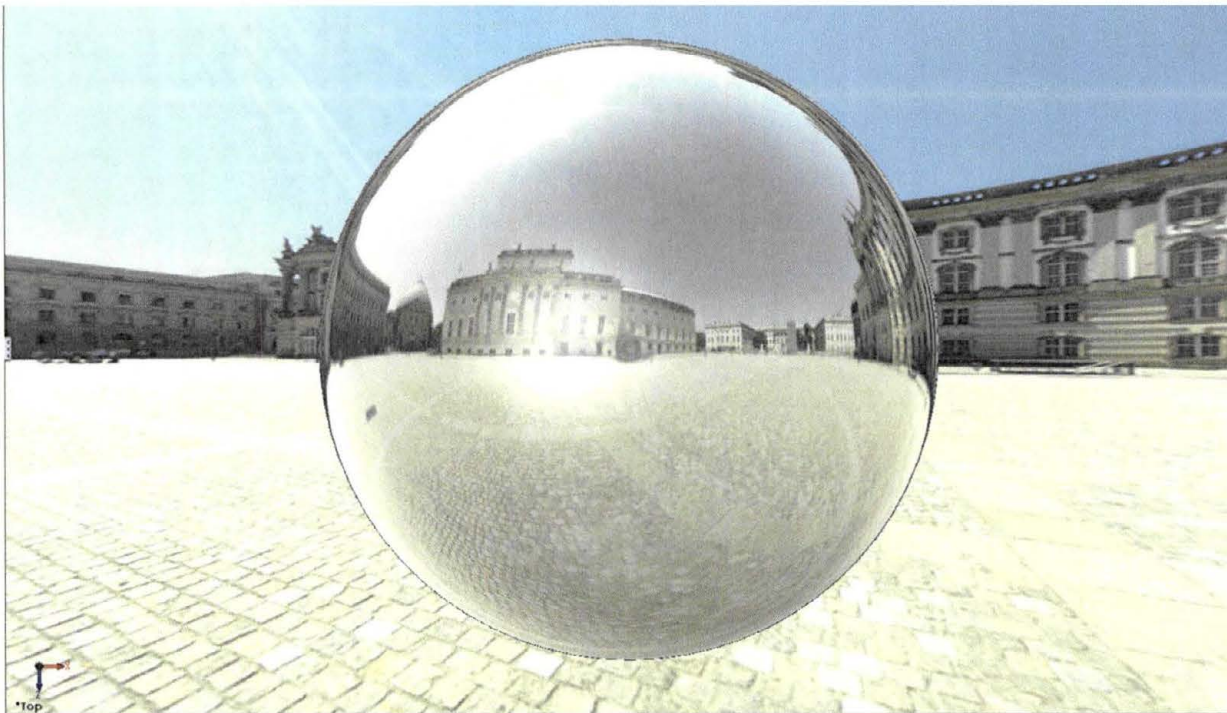


Figure 7. Three Dimensional Rendering of a Metallic Spherical UAP

4. ANALYTICAL AND NUMERICAL SOLUTIONS FOR UAP INVESTIGATIONS

4.1 "TIC TAC" INCIDENT

The following summary is excerpted from the report of an investigation conducted by personnel assigned to DIA of an observation by elements of the Nimitz Carrier Strike Group of UAP off the coast of Mexico in November 2004. Note: The DIA personnel who wrote the report utilized the term Anomalous Aerial Vehicle (AAV) rather than the more common Unidentified Aerial Phenomenon (UAP) or Unidentified Flying Object (UFO). All three terms, AAV, UAP, and UFO are used at different times in this section and should be considered interchangeable.

During the period of approximately 10-16 November 2004, the Nimitz Carrier Strike Group (CSG) was operating off the western coast of the United States in preparation for their deployment to the Arabian Sea. The USS Princeton on several occasions detected multiple Anomalous Aerial Vehicles (AAVs) operating in and around the vicinity of the CSG. The AAVs would descend "very rapidly" from approximately 60,000 feet down to approximately 50 feet in a matter of seconds. They would then hover or stay stationary on the radar for a short time and depart at high velocities and turn rates. On 14 November after again detecting the AAV, the USS Princeton took the opportunity of having a flight of two F/A-18Fs returning from a training mission to further investigate the AAV. The USS Princeton took over control of the F/A-18s from the E-2C Airborne Early Warning aircraft and vectored in the F/A-18s for intercept leading to visual contact approximately one mile away from the AAV, which was reported to be "an elongated egg or a 'Tic Tac' shape with a discernable midline horizontal axis." It was "solid white, smooth, with no edges. It was "uniformly colored with no nacelles, pylons, or wings." It was approximately 46 feet in length. The F/A-18Fs radar could not obtain a 'lock' on the AAV; however it could be tracked while stationary and at slower speeds with the Forward Looking Infrared (FLIR). The AAV did take evasive actions upon intercept by the F/A-18 demonstrating an advanced acceleration (g), aerodynamic, and propulsion capability. The AAV did not take any offensive action against the CSG; however, given its ability to operate unchallenged in close vicinity to the CSG it demonstrated the potential to conduct undetected reconnaissance leaving the CSG with a limited ability to detect, track, and/or engage the AAV.

According to Senior Chief Blila, the AAVs would descend from a very high altitude into the scan volume of the AN/SPY-1 at a high velocity. The top of the scan volume would put the AAVs at higher than 60,000 feet. The AAVs would descend "very rapidly" from approximately 60,000 feet down to approximately 50 feet in a matter of seconds. They would then hover for a short time and depart at high velocities and at turn rates demonstrating an advanced acceleration (g) capability. Senior Chief Blila added that based on his experience, which is 17 years as a Fire Control on Aegis cruisers, the AAV exhibited ballistic missile Characteristics in reference to its appearance, velocity, and indications on the radar. Since the radar was in the mode to handle Air Intercept of conventional aircraft it never obtained an accurate track of the AAVs and was quickly "dropped" by the radar meaning it was eliminated by the computer to reduce the amount of clutter on the radar, as any other false target is handled. If the radar were set up in a mode for Ballistic Missile tracking they likely would have had the capability to track the AAV. They were detected three separate times during the week operating off the western coast of the United States and Mexico. The Tactical Air Officer onboard the Princeton could not identify the radar contact

and given the high speed and altitude was perplexed. On 14 November 2004, after again detecting an AAV took the opportunity of two F/A-18s airborne in the vicinity to task them for airborne reconnaissance of the AAV.

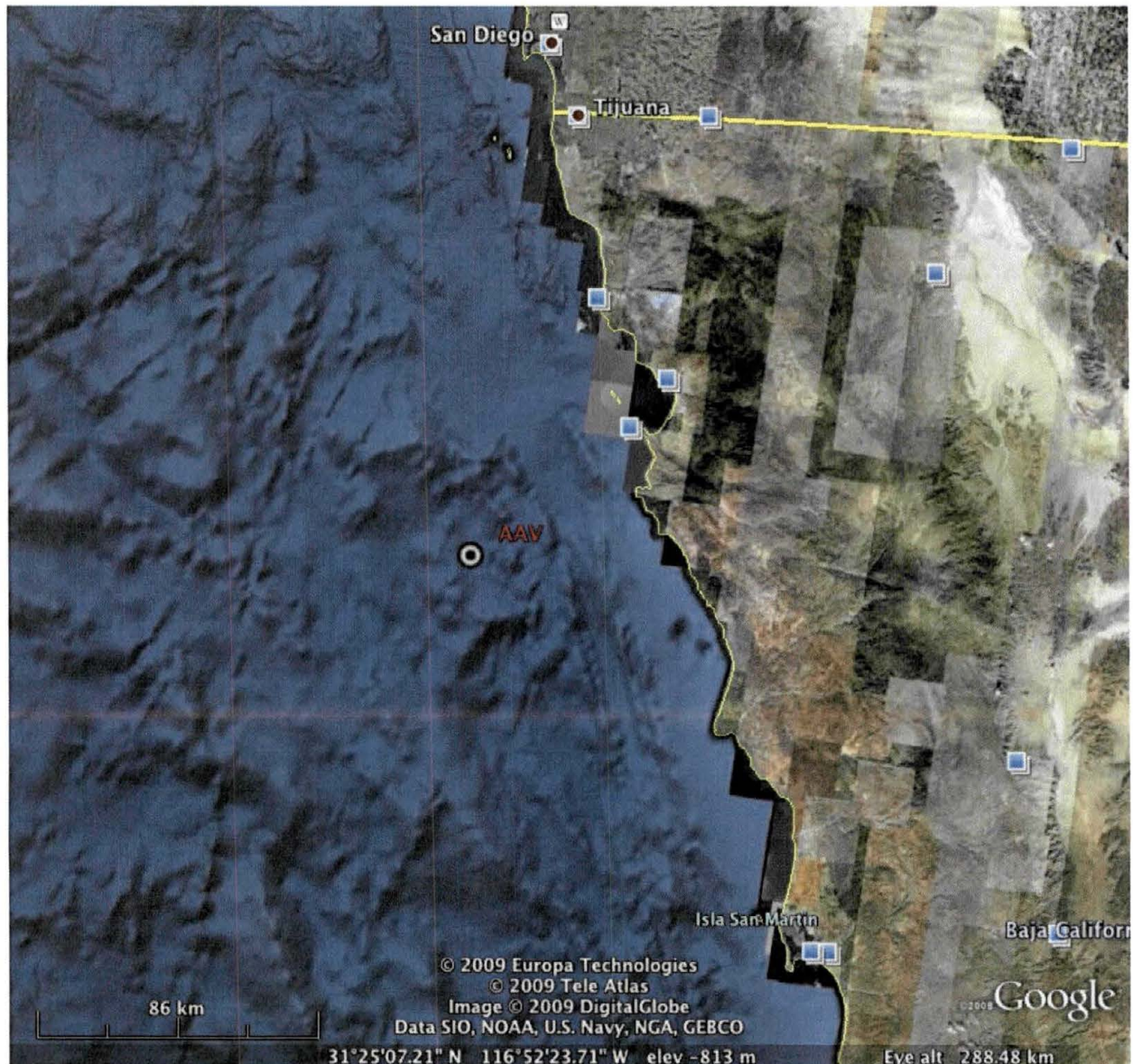


Figure 8. Location of the AAV during the F/A18 Intercept

Lt. Col Douglas “Cheeks” Kurth, Commanding Officer VMFA-232, was flying a single seat F/A-18C that launched from the USS Nimitz at approximately 1030L to conduct a Functional Check Flight of an aircraft that had recently completed significant maintenance. He noted the weather that day was blue skies, no clouds, and unlimited visibility. After 30 minutes into his flight he received a radio call from his air controller asking him to investigate an unidentified airborne contact. This was not a standard request. Additionally the controller asked if he had ordnance onboard, which was odd since no controller had ever asked that question during a

situation of identifying an unknown contact over U.S. or International territory. He responded that he had no ordnance onboard. The controller provided vectors to the vicinity of Figure 8. The object was reported to be at "slow speed and low altitude."

While en route at approximately 250 knots indicated/400 knots groundspeed at medium altitude (15-25,000 feet), he gained radar contact of what he believed to be two F/A-18Fs that were approaching the AAV from the west at low altitude (500- 5,000 feet). There was no other traffic on the radar. The controller informed him to remain above 10,000 feet, as there was other fighter traffic at low altitude investigating the AAV. As he approached approximately 15nm from the AAV descending through approximately 15,000 feet, he could see a water disturbance in the ocean surface. He recalled that the sea state was low (calm). At approximately 5-10 nm away from the AAV, the controller told him to "skip it" and return to his operating area. Since he was close he elected to fly over the water disturbance to try and see what was causing it.

The disturbance appeared to be 50 to 100 meters in diameter and close to round. It was the only area and type of whitewater activity that could be seen and reminded him of images of something rapidly submerging from the surface like a submarine or ship sinking. It also looked like a possible area of shoal water where the swell was breaking over a barely submerged reef or island. He overflew the disturbance and turned back to the northwest. As he was flying away he could see the disturbance clearing and could no longer identify the place where it occurred. He did not see any object or vessel associated with the disturbance either above the surface, on the surface, or below the surface. He also never made visual contact with the other fighter aircraft that were vectored to the location or the AAV. It is possible that the disturbance was being caused by an AAV but that the AAV was 'cloaked' or invisible to the human eye.

Lt Col Kurth recovered aboard the Nimitz at approximately 1200L. He reported to the Carrier Intelligence Center (CVIC) and was asked by his Intelligence Officer, 1stLt Cory Knox, if he saw the "supersonic Tic Tac"? We questioned now Capt. Knox to determine if he had any further information but based on his position in CVIC at the time he was not involved in any further discussions concerning the AAV.

CDR David "Sex" Fravor, Commanding Officer VFA-41, was the pilot of FastEagle 01. He and LT Joshua "Noodle" Appezzato were in the lead aircraft of the first F/A-18F section airborne that day from VFA-41, call sign FastEagle 01. The flight walked, started and launched with no issue. They completed their departure from the USS Nimitz and flew to the working area to conduct the training portion of the flight. After they completed their training the E-2C controller handed them off to the USS Princeton call sign 'Poison' where they received vectors via Bearing Range Altitude Aspect (BRAA) to an unknown contact flying into the working area from the south. Poison asked what ordnance they had on board. LT Appezzato told Poison control that they had two captive training AIM-9Ms (CATM-9) and no other ordnance. The flight descended to between 20-24,000 feet and proceeded to the contact. CDR Fravor did not recall any indications via on-board sensor of the object. Their aircraft was not carrying a Forward Looking Infrared (FLIR) pod onboard. As CDR Fravor remembers it, the radar Attack Display was clean (no targets).

CDR Fravor and LT Appezzato were attempting acquire the object visually as they heard “merge plot” from Poison. According to CDR Fravor the first indication he had of the unknown contact was a visual of a disturbance on the water below the AAV. As he scanned the area he gained a visual on the object. It is important to note that when asked to describe the disturbance on the water he stated that it was localized underneath the object, did not appear as a trail or wake, and looked like frothy waves and foam almost as if the water was boiling.

At this point CDR Fravor detached FASTEAGLE02, which held at approximately 20,000 feet, and FASTEAGLE01 descended to between 12-16,000 feet. CDR Fravor attempted a “helmet lock” that was unsuccessful. It is important to note that CDR Fravor was using the Joint Helmet Mounted Cueing System which will cue the aircraft sensors such as the radar to ‘lock on’ to what the pilot is looking at and it also has a recording capability. It may have been useful in this situation but typically because of the large amount of head movement it is not practical. CDR Fravor stated that the helmet’s recording capability was rarely used therefore he did not think to use it that day.

LT Appezzato communicated what they were seeing with Poison control and said that he had a running dialogue on the interflight radio with FastEagle 02. CDR Fravor stated that the object was “holding like a Harrier.” (Referring to the AV-8B jet aircraft, which is capable of hovering and Vertical/Short Takeoff and Landing (V/STOL) via thrust vectoring.) According to CDR Fravor, the object’s shape was like an elongated egg or a ‘Tic Tac’ and had a discernable midline horizontal axis. However, the object was uniformly white across the entire body. It was approximately 46 feet in length. LT Appezzato described it as “solid white, smooth, with no edges. It was uniformly colored with no nacelles, pylons, or wings.” When asked to describe the appearance, if it glowed or reflected sunlight he said, “neither, it looked like it had a white candy-coated shell, almost like a white board.” His report differs from CDR Fravor in that he reported the object traveling level at approximately 500-1000 feet at approximately 500 knots.

The object was pointed in a north/south orientation and was moving both north & south and east & west, while maintaining a consistent altitude. These displacements, according to CDR Fravor, were minor. CDR Fravor stated he then began a descent with the intention to take a close aboard pass with the object in an attempt to visually identify it. They began the decent as they rolled in from about 10,000 ft and approximately 350 knots to take the object close aboard. CDR Fravor pulled nose on and then pulled trail (aft) of the object. As they were maneuvering, the object appeared, according to CDR Fravor: “to recognize us.” He assessed this from the fact the object “pointed” (realigned its axis) in the direction of their aircraft. At this time, according to CDR Fravor, the disturbance on the water ceased.

As they completed this maneuver, the object ascended quickly and pulled lift vector on and aft of them at a supersonic speed. CDR Fravor commanded the radar through the Short Range radar set and asked for a picture from Poison. Poison initially reported that the “picture was clean” (no contact) but then stated “you’re not going to believe this, it’s at your CAP” meaning that the AAV had flown to their training CAP, which was located in the southern end of the training area and had climbed to approximately 24,000 feet. CDR Fravor stated that the flight attempted to locate both the object and the disturbance with no success. CDR Fravor stated that nothing was seen on the surface or subsurface and that there were no indications of the previous disturbance.

Following the engagement, the flight rejoined and returned to the USS Nimitz. When asked how the jets functioned and if there was any indications of a system malfunction, he stated that, “the jets were brand new, less than 100 hrs on them.

They were working perfectly.” LT Appezzato, when asked, said that all aircraft systems were functional. That there were no mission computer issues or avionics issues and that there was no radio or communication interference and that they had entry into the Link-16 network. When asked, LT Appezzato couldn’t confirm any physiological or psychological feelings that were out of the ordinary.

USN Lt ‘Nutz’ Underwood was a member of VFA-41 and was the Weapons and Sensors Officer (WSO) flying with LT Page Fellini. They were a part of the second F/A-18F section airborne that day from VFA-41. Their flight launched following the FASTEAGLE flight. The crews spoke with each other in the paraloft, discussed the object and that the flights were scheduled for the same working area. FASTEAGLE flight told LT Underwood’s flight what they saw and to try to see and record what they could.

There were no clouds and there was a discernable horizon. The time was approximately 1500L. All on board systems were functioning normally. The radar was in a standard search mode (RWS/ 80NM/ 4bar/ intr) and the FLIR was in L+S slave (the FLIR would point in direction of an L+S track). There was no radio or communication interference and they had entry into the Link-16 network. Initial awareness of an object came via the radar. According to the radar display, the initial tracks were at approximately 30-40 nm to the south of the aircraft. LT Underwood was controlling the radar and FLIR and attempted multiple times to transition the radar to Single Target Track (STT) mode on the object. The radar could not take a lock, the b-sweep would raster around the hit, build an initial aspect vector (which never stabilized) and then would drop and continue normal RWS b-sweep. When asked, LT Underwood stated that there were no jamming cues (strobe, champagne bubbles, “any normal EA indications”). It “just appeared as if the radar couldn’t hack it.” The radar couldn’t receive enough information to create a single target track file. The FLIR, in L+S slave, pointed in the direction of the initial track flies as the radar attempted lock. The FLIR showed an object at 0 ATA and approximately -5 deg elevation (Figure 9). According to LT Underwood, “the target was best guess co-altitude or a few thousand feet below,” estimating the object to be between 15-20 thousand feet. The object, according to the FLIR, appeared stationary (Figure 10). There was no discernable movement from the object with the only closure being a result of the aircraft’s movement. As LT Underwood watched the object it began to move out of FLIR field of view to the left. LT Underwood made no attempt to slew the FLIR and subsequently lost situational awareness to the object. The Flight continued with training mission with no further contact with object.

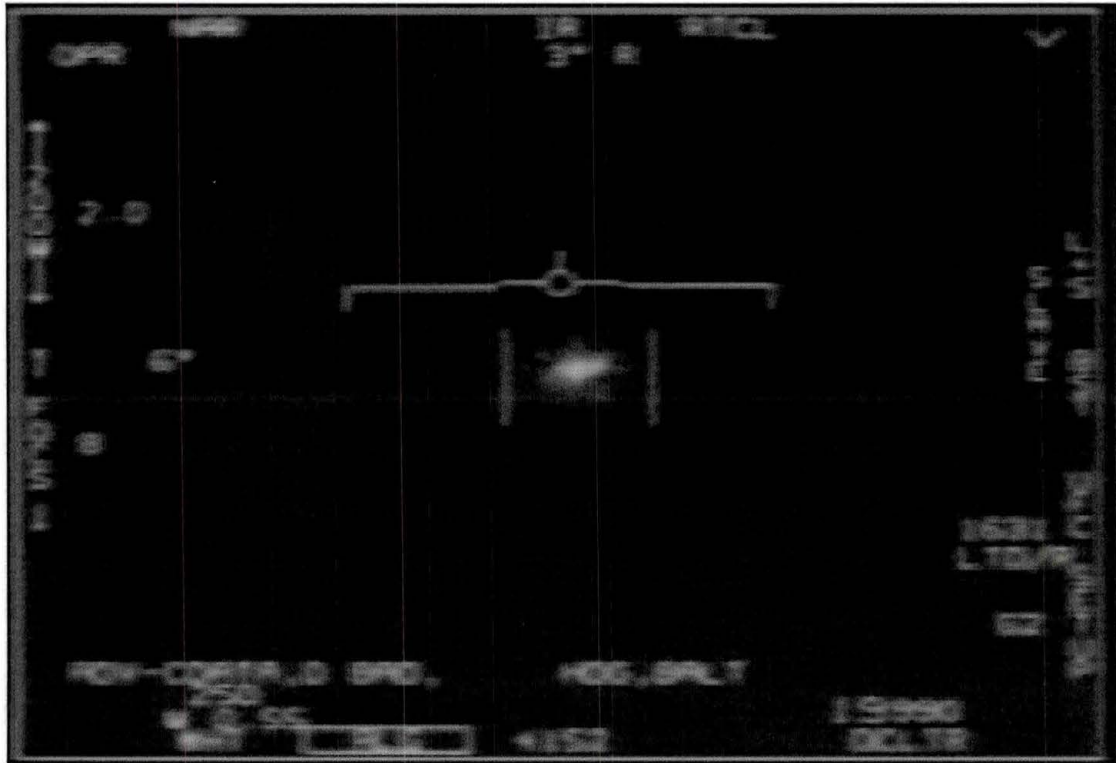


Figure 9. FLIR in 'White Hot' Mode



Figure 10. FLIR in "Black Hot" mode

LT Underwood was clear in that he couldn't confirm that it was the same object as described by FASTEAGLE flight. He never had visual, only seeing the object via the FLIR. He reaffirmed that all systems were functional. Following completion of the training portion, the section returned to the ship for a normal approach, landing and shutdown. The crew met in CVIC and debriefed. LT Underwood said that the CIVC section attempted to collect his tapes but he refused.

They proceeded to their ready room where they debriefed with CDR Fravor and his flight. Copies of the tapes were made with a set being turned into the intelligence section. LT Underwood was not asked to sign any non-disclosure agreement and he is uncertain how far up the chain the reporting went past his commanding officer. When asked, LT Underwood couldn't confirm any physiological or psychological feelings that were out of the ordinary. He only expressed a feeling of confusion during the event.

According to former LT Daniel Goodwin now a civilian working for the US Navy, who was a qualified Submarine Officer onboard the Louisville in November 2004 during the AAV activity there were no unidentified sonar contacts in the vicinity of the aerial sightings or anytime during the operations off the coast of California. The former commander of the USS Louisville, CAPT David Kirk, confirmed that there was no anomalous undersea activity during this period. There was a live fire exercise conducted by the USS Louisville during the period of and in the vicinity of the AAV sightings; however, the weapon in use did not match the flight profile or visible characteristics of the AAV. Additionally any live fire would have been coordinated throughout the CSG and all air traffic would have been well aware of the launch and operation of the weapon system. Aircraft would not have been vectored for the intercept of a US Weapon in flight. Based on the lack of detection of any unidentified sonar contacts it is highly unlikely that an AAV operated below the surface of the ocean; it is possible that the AAV demonstrated the ability to be cloaked or invisible to the human eye based on pilot reporting of the water disturbance with no visible craft. Based on the assessment of Mr. Goodwin, if the AAV did operate underwater undetected it would represent a highly advanced capability given the advanced capability of our sensors.

Key Assessments According to DIA Report

- The Anomalous Aerial Vehicle (AAV) was no known aircraft or air vehicle currently in the inventory of the United States or any foreign nation.
- The AAV exhibited advanced low observable characteristics at multiple radar bands rendering US radar based engagement capabilities ineffective.
- The AAV exhibited advanced aerodynamic performance with no visible control surfaces and no visible means to generate lift.
- The AAV exhibited advanced propulsion capability by demonstrating the ability to remain stationary with little to no variation in altitude transitioning to horizontal and/or vertical velocities far greater than any known aerial vehicle with little to no visible signature.
- The AAV possibly demonstrated the ability to 'cloak' or become invisible to the human eye or human observation.

The AAV possibly demonstrated a highly advanced capability to operate undersea completely undetectable by our most advanced sensors. The so called "Tic Tac" incident has many physics and engineering aspects that may be studied with regards to understanding the performance capabilities and propulsion mechanisms of the craft. Since there was little hard data, most analyses of the incident had to be made using either parametric studies or assumptions based on eye witness testimony.

4.1.1 Analytical Solutions of Velocities and Accelerations Associated with "Tic Tac" Performance

An initial starting point consisted of using basic physics formulas for the calculation of velocities and accelerations based on the distance s the object traveled and the duration time t of the incident. Since no exact duration was known, as the radar operator noted that it occurred in a matter of "seconds," a parametric range from 0.5 seconds to 10 seconds was studied (assuming instantaneous velocities and accelerations).

$$v = \frac{ds}{dt}$$

$$a = \frac{dv}{dt}$$

Flight is classified in six categories as shown in the table below.

Table 1. Mach Regimes

Regime	Subsonic	Transonic	Sonic	Supersonic	Hypersonic	High-hypersonic	Re-entry Speeds
Mach Number	< 1.0	0.8 – 1.2	1.0	1.0 – 5.0	5.0 – 10.0	10.0 – 25.0	> 25.0

Due to the lack of data, only the instantaneous velocity of the craft v and the instantaneous acceleration a , were computable. For the velocity and deceleration witnessed, a negative sign is implied to represent the direction component of the vector.

Assumptions:

1. *Elevation of 60,000 ft to Sea Level* – It was reported by radar observation the object descended from approximately 60,000 ft to sea level in a matter of seconds.
2. *Matter of Seconds* – A range of 0.5 seconds to 10 seconds was used for a parametric study.

4.1.2 Summary of Analytical Velocity and Acceleration Solutions

Table 2 provides the computed values of instantaneous velocities and decelerations in ft/s and mph and ft/sec^2 and g respectively for each chosen Δt . Figure 11 through Figure 14 show

non-continuous plots for velocity and acceleration in each unit for a specific Δt event duration. As one may observe from the table and graphs, extremely small and small duration times specifically between 0.5 and 5 seconds provide high velocities and accelerations. Most of the values in the table represent extraordinary velocities and all fall between hypersonic and re-entry speed Mach regimes. Acceleration values also show a very high number of g.

An examination of Table 2 at a Δt of 5.0 sec reveals the average velocity of the craft was 12,000 ft/sec (8,182 mph or Mach 10.7). A very high deceleration value is also witnessed at 2400 ft/sec² or 75 g. These are extraordinarily high values and would require some form of acceleration manipulation to limit what a human pilot would experience and be able to survive.

Table 2. Velocities and Accelerations of Tic Tac for Parametric Time Durations of Event

Δs 60000 feet
 Δs 11.36364 miles

Δt (sec)	V (ft/s)	v (mph)	Mach Number ¹	a (ft/s ²)	a (g)
0.0	0	0	0.0	32.2 ²	1 ²
0.5	120,000	81,818	107.5	240,000	7,453
1.0	60,000	40,909	53.7	60,000	1,863
1.5	40,000	27,273	35.8	26,667	828
2.0	30,000	20,455	26.9	15,000	466
2.5	24,000	16,364	21.5	9,600	298
3.0	20,000	13,636	17.9	6,667	207
3.5	17,143	11,688	15.4	4,898	152
4.0	15,000	10,227	13.4	3,750	116
4.5	13,333	9,091	11.9	2,963	92
5.0	12,000	8,182	10.7	2,400	75
5.5	10,909	7,438	9.8	1,983	62
6.0	10,000	6,818	9.0	1,667	52
6.5	9,231	6,294	8.3	1,420	44
7.0	8,571	5,844	7.7	1,224	38
7.5	8,000	5,455	7.2	1,067	33
8.0	7,500	5,114	6.7	938	29
8.5	7,059	4,813	6.3	830	26
9.0	6,667	4,545	6.0	741	23
9.5	6,316	4,306	5.7	665	21
10.0	6,000	4,091	5.4	600	19

¹ Computed using the speed of sound at sea level under standard conditions

² Standard acceleration due to gravity

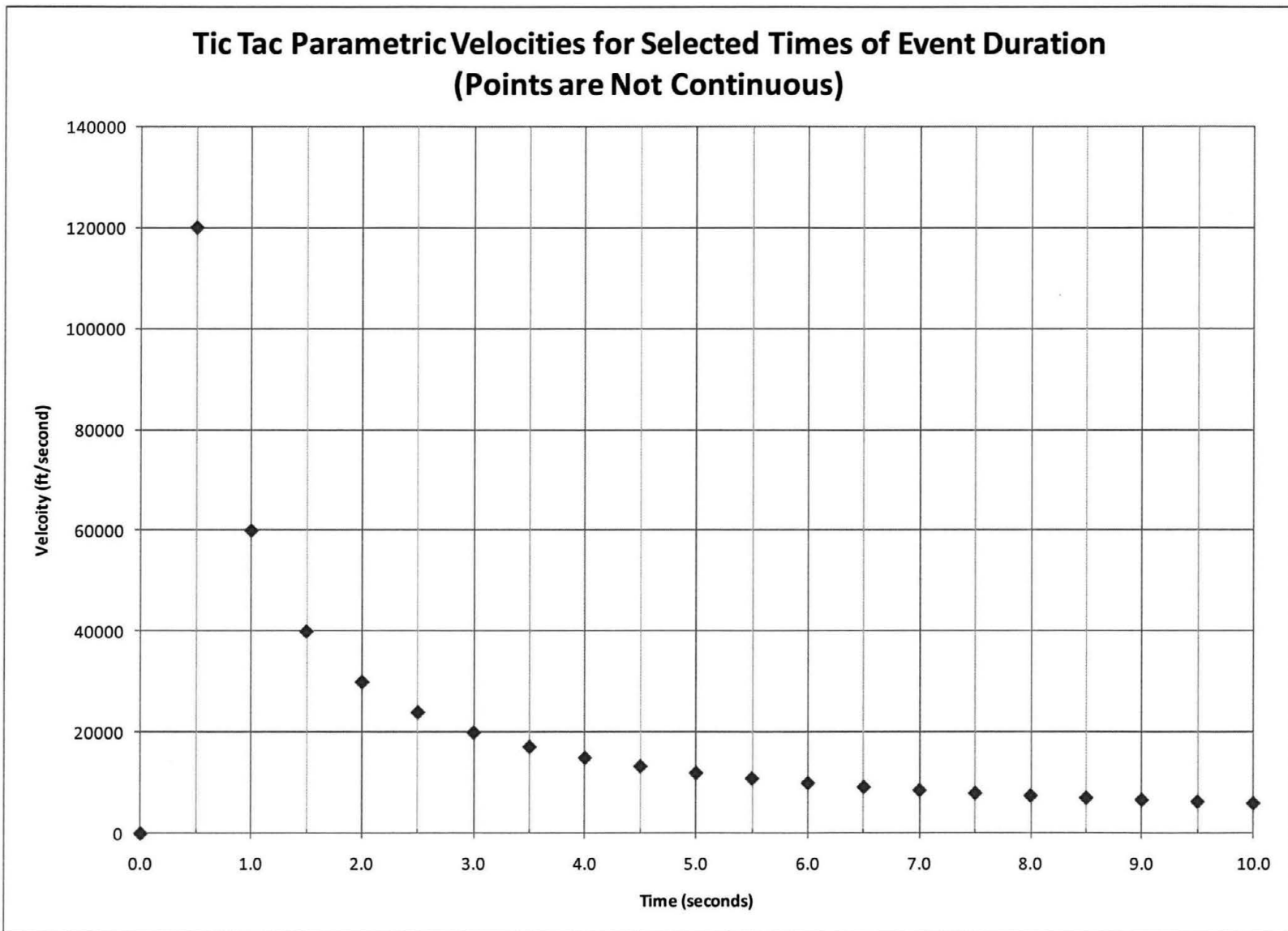


Figure 11. Tic Tac Parametric Velocities for Selected Times of Event Duration in ft/sec

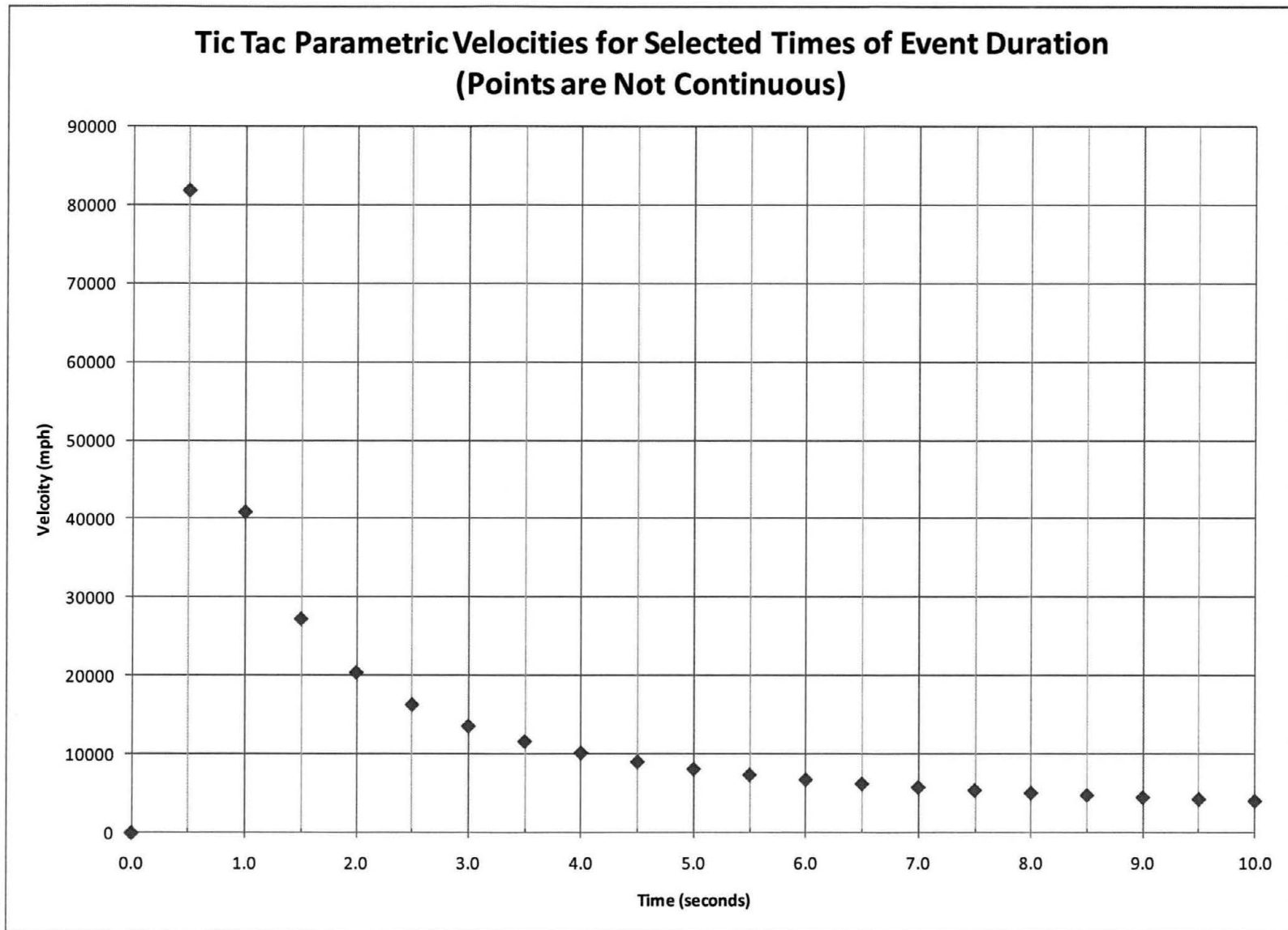


Figure 12. Tic Tac Parametric Velocities for Selected Times of Event Duration in mph

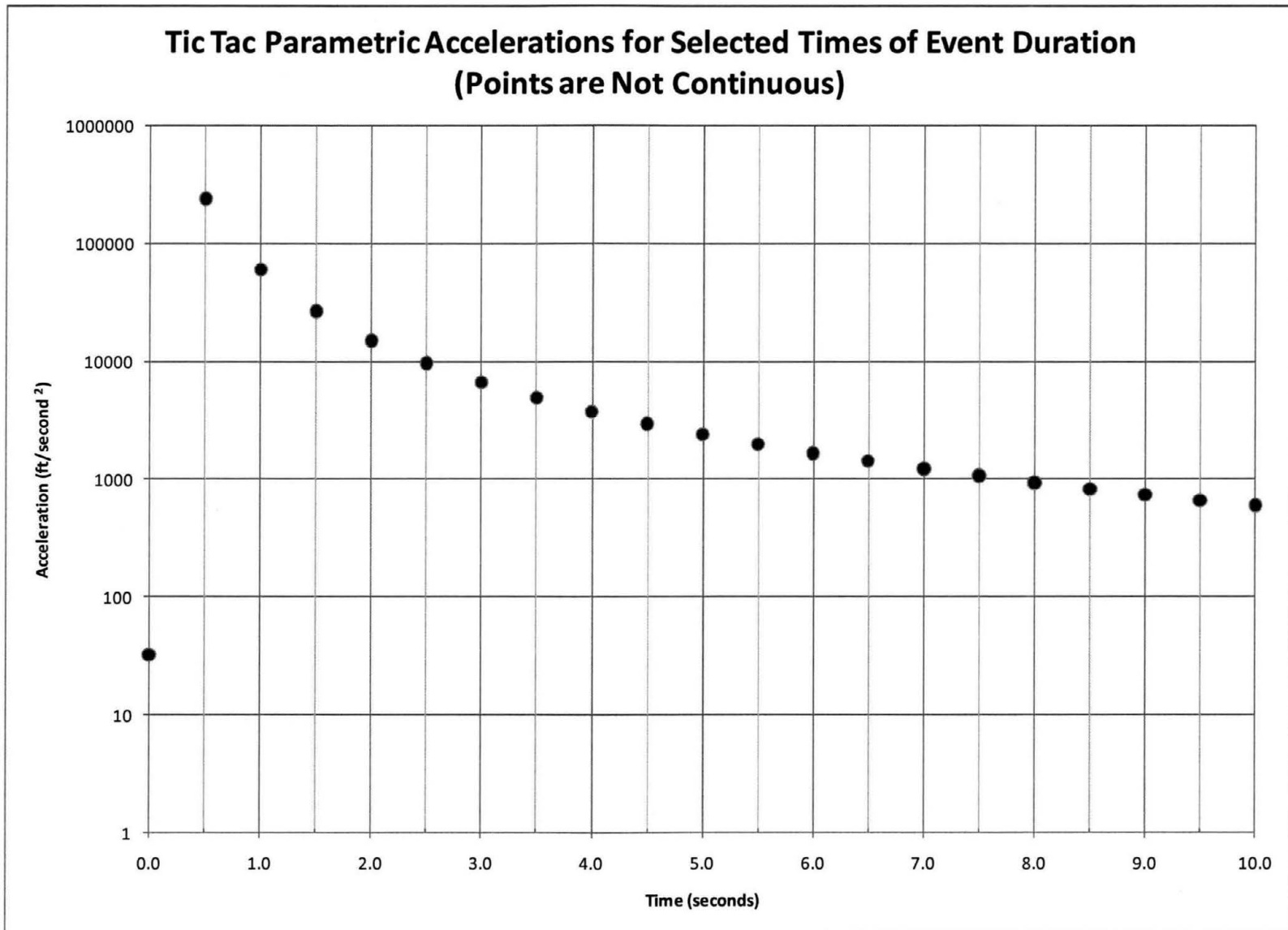


Figure 13. Tic Tac Parametric Accelerations for Selected Times of Event Duration in ft/sec²

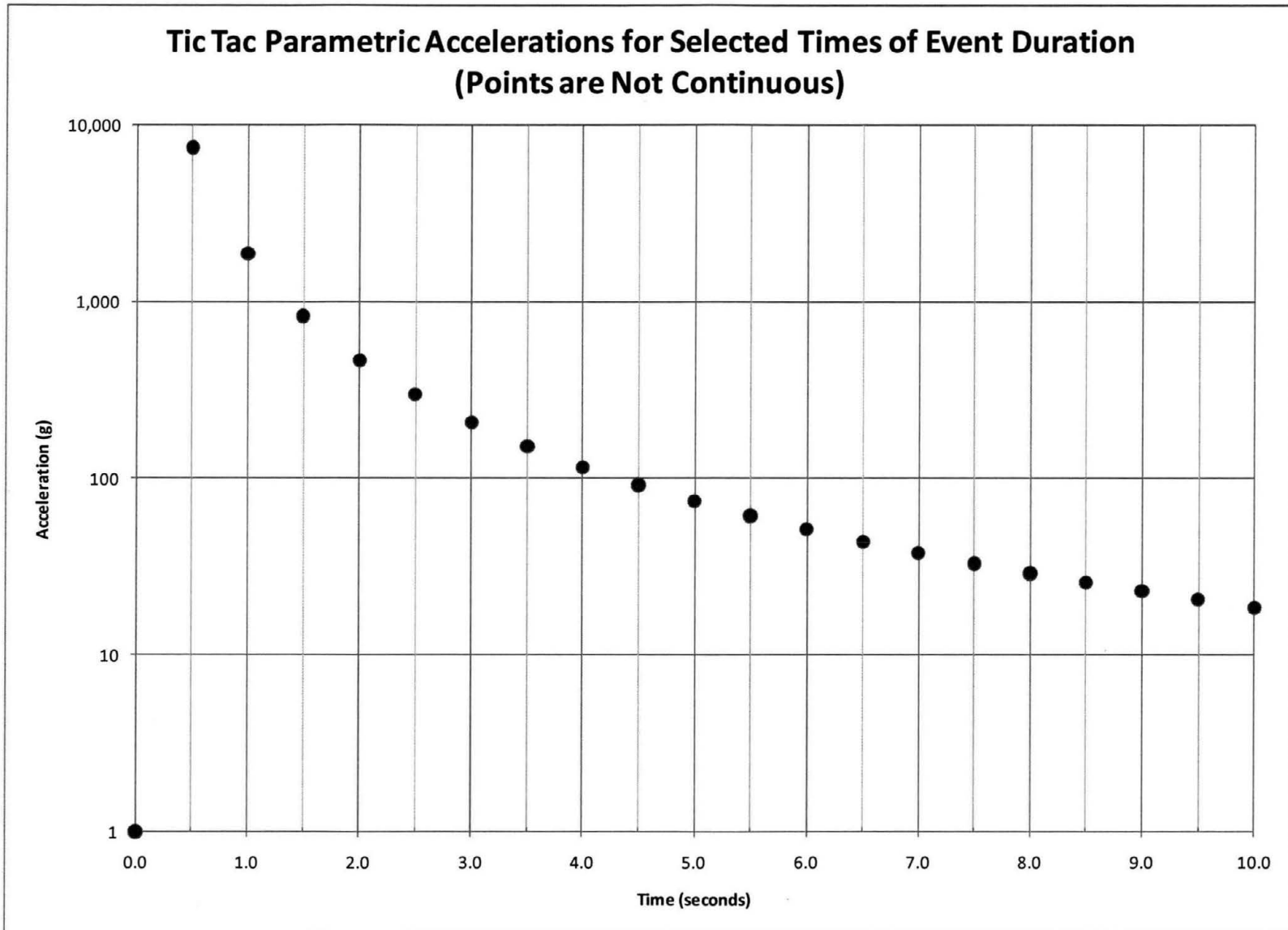


Figure 14. Tic Tac Parametric Accelerations for Selected Times of Event Duration in g

4.1.3 Numerical Analysis of Compressible Flow

Compressible fluid flow analyses were performed to visualize the steady state pressure, temperature and Mach number contours around two craft shapes ("Tic Tac" and right circular cylinder). The use of compressible fluid flow and modeling of air as an ideal gas assumed the aerodynamics over the craft were not being controlled or modified through other means.

Steady state solutions for pressure, temperature and Mach number contours around both a "Tic Tac" shape and a right circular cylinder were obtained under subsonic, supersonic and mixed conditions. The CFX module was capable of solving the three dimensional unsteady Navier–Stokes equations in their conservation form as shown below in Cartesian coordinates in the x, y and z directions numerically. For the steady state solutions, the transient terms were unchanging and fall out of the equations below.

Momentum:

$$\rho \left(\frac{\partial u}{\partial t} + u \frac{\partial u}{\partial x} + v \frac{\partial u}{\partial y} + w \frac{\partial u}{\partial z} \right) = -\frac{\partial p}{\partial x} + \mu \left(\frac{\partial^2 u}{\partial x^2} + \frac{\partial^2 u}{\partial y^2} + \frac{\partial^2 u}{\partial z^2} \right) + \rho g_x$$
$$\rho \left(\frac{\partial v}{\partial t} + u \frac{\partial v}{\partial x} + v \frac{\partial v}{\partial y} + w \frac{\partial v}{\partial z} \right) = -\frac{\partial p}{\partial y} + \mu \left(\frac{\partial^2 v}{\partial x^2} + \frac{\partial^2 v}{\partial y^2} + \frac{\partial^2 v}{\partial z^2} \right) + \rho g_y$$
$$\rho \left(\frac{\partial w}{\partial t} + u \frac{\partial w}{\partial x} + v \frac{\partial w}{\partial y} + w \frac{\partial w}{\partial z} \right) = -\frac{\partial p}{\partial z} + \mu \left(\frac{\partial^2 w}{\partial x^2} + \frac{\partial^2 w}{\partial y^2} + \frac{\partial^2 w}{\partial z^2} \right) + \rho g_z.$$

Continuity:

$$\frac{\partial \rho}{\partial t} + \frac{\partial(\rho u)}{\partial x} + \frac{\partial(\rho v)}{\partial y} + \frac{\partial(\rho w)}{\partial z} = 0.$$

Energy:

$$\left[\frac{1}{2} v_1^2 + g z_1 + \varepsilon_1 + \frac{p_1}{\rho_1} \right] \rho_1 A_1 v_1 \Delta t + \left[\frac{1}{2} v_2^2 + g z_2 + \varepsilon_2 + \frac{p_2}{\rho_2} \right] \rho_2 A_2 v_2 \Delta t = 0$$

where:

A – Area (m²)

g – gravitational acceleration (9.8 m/s²)

g_x – x directional component of gravitational acceleration

g_y – y directional component of gravitational acceleration

g_z – z directional component of gravitational acceleration

ε – specific internal energy (J/kg)

ρ – density of the fluid (kg/m³)

μ – dynamic viscosity of the fluid (Pa·s)

p – pressure (Pa)

t – time (sec)

u – x velocity (m/s)
 v – y velocity (m/s)
 w – z velocity (m/s)
 x – x coordinate
 y – y coordinate
 z – z coordinate

The following sections provide steady state pressure, temperature and Mach number contours over the "Tic Tac" and right circular cylinder for velocities of 700 mph and 1500 mph with an environmental air temperature of 223 K (-58°F). Attachment II and Attachment III show contours for subsonic speeds below 700 mph and supersonic increments between 700 mph and 1500 mph for the "Tic Tac" and a right circular cylinder respectively. A comparison of the profiles of the "Tic Tac" geometry and that of a right circular cylinder was performed due to other numerous reports of craft with similar capabilities but lacking curvature at the ends of the craft. A flat 90° surface moving through the air would be expected to cause greater resistance during flight.

Assumptions:

1. *Elevation of 30,000 ft* – It was reported by radar observation the object descended from approximately 60,000 ft to sea level in a matter of seconds. An average Δs is computed by:

$$\Delta s = \frac{s_2 - s_1}{2} = \frac{60,000ft - 0ft}{2} = 30,000ft$$

2. *Ambient Air Temperature of 223 K (-58F)* – An approximate ambient environmental temperature of 223 K was chosen in accordance with an average elevation in the range of 30,000 ft (which varies with weather conditions) as a starting point for computational investigations.
3. *Air Modeled as an Ideal Gas* – Air Temperature, pressure and density are all interdependent and are given by the relationship of the ideal gas law:

$$p = \frac{\rho R_u T}{M}$$

where:

R_u – Gas Constant (8.314472 m³·Pa·K⁻¹·mol⁻¹)
 M – Molar Mass (g/mol)
 T – Temperature (K)

Since the temperature and density of air decreases with altitude, so does the speed of sound, hence a given true velocity results in a higher Mach number at higher altitudes. The slice used for the contours was taken axially for each geometric configuration. Reports from aircrew on sight indicate the object flew in a horizontal position. A 0° angle of attack was used in all cases to try to replicate observed flight conditions.

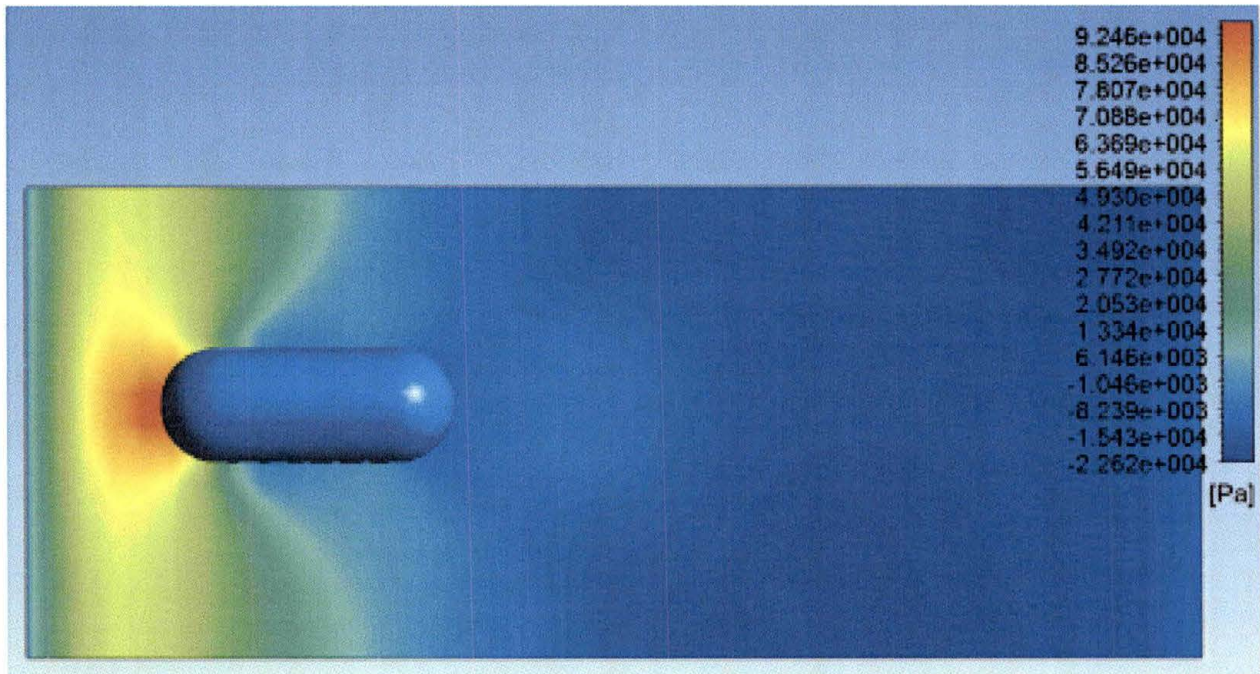


Figure 15. Tic Tac Pressure at 1/6 Scale, Air Temperature 223K and 700 mph with Mixed Inlet and Supersonic Outlet

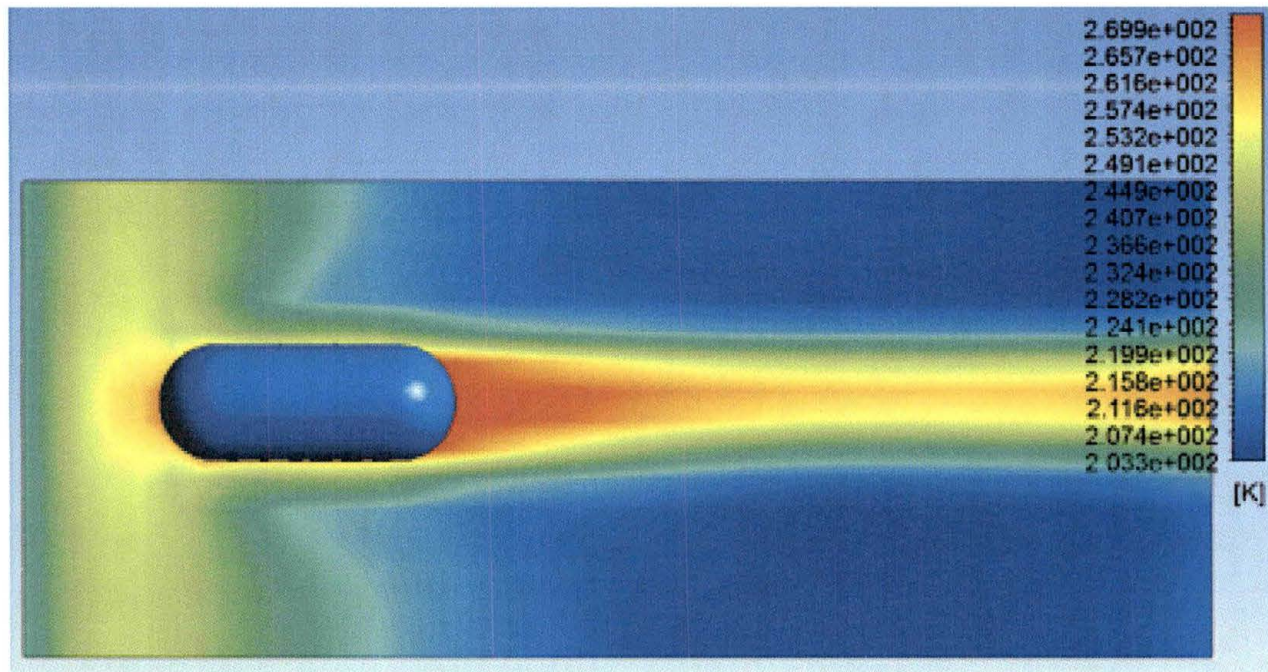


Figure 16. Tic Tac Temperature at 1/6 Scale, Air Temperature 223K and 700 mph with Mixed Inlet and Supersonic Outlet

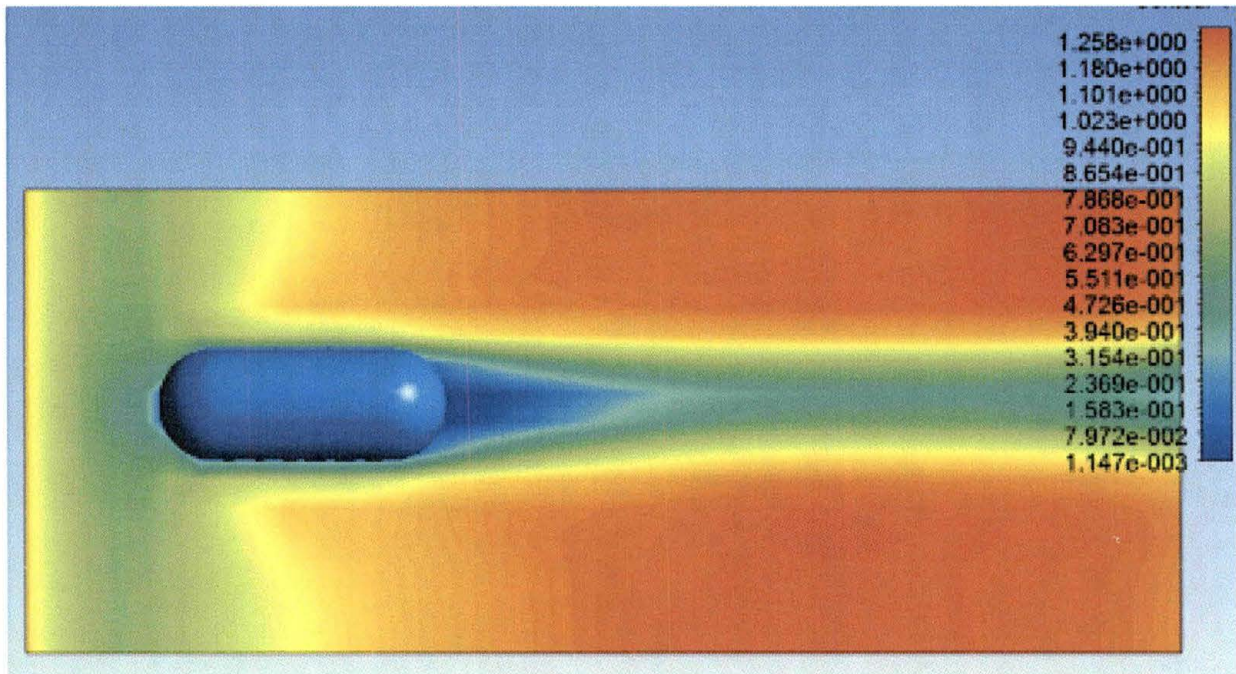


Figure 17. Tic Tac Mach Number at 1/6 Scale, Air Temperature 223K and 700 mph with Mixed Inlet and Supersonic Outlet

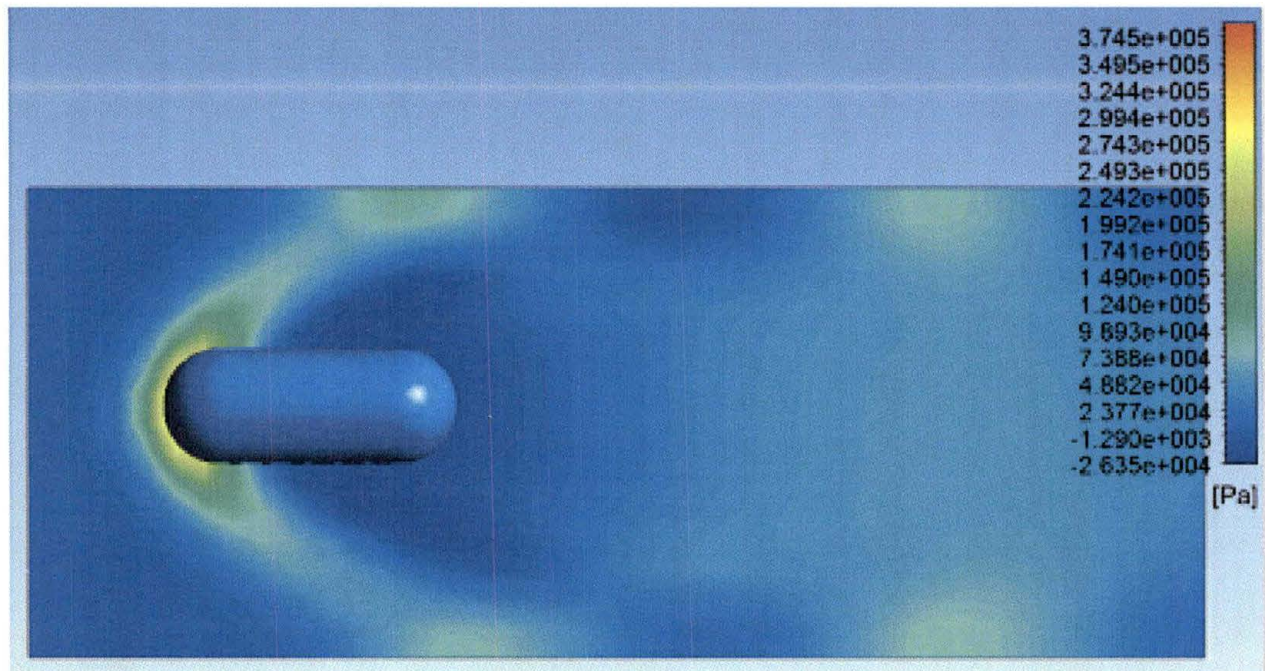


Figure 18. Tic Tac Pressure at 1/6 Scale, Air Temperature 223K and 1500 mph with Supersonic Inlet and Supersonic Outlet

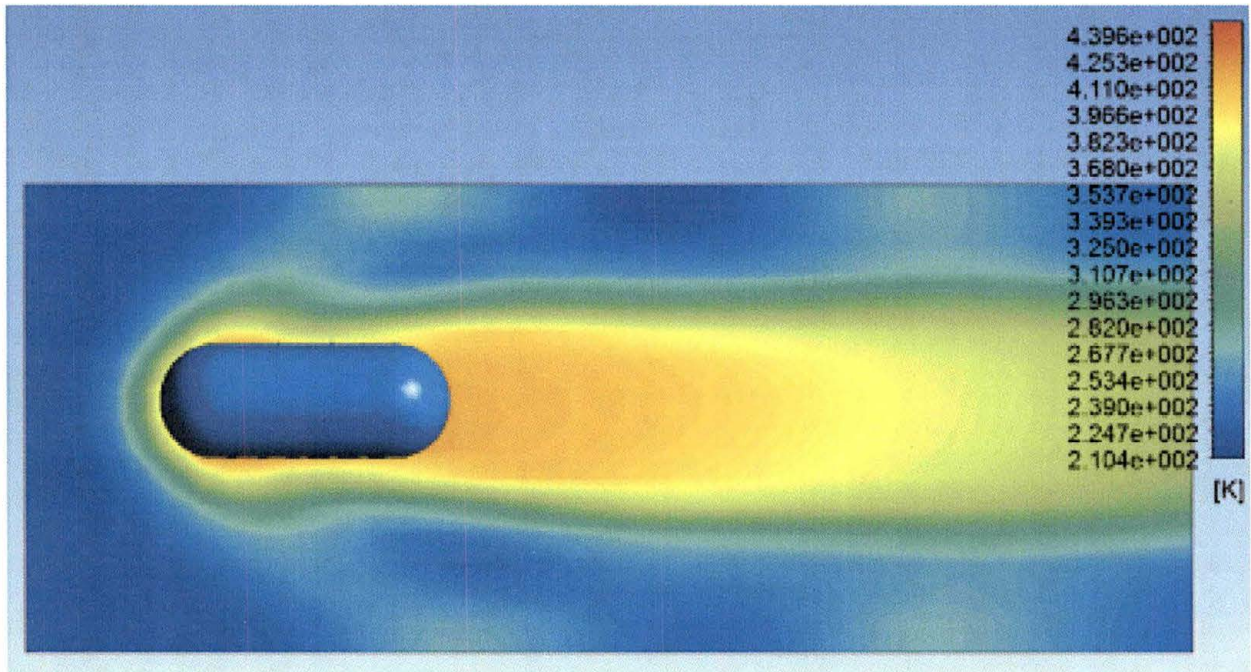


Figure 19. Tic Tac Temperature at 1/6 Scale, Air Temperature 223K and 1500 mph with Supersonic Inlet and Supersonic Outlet

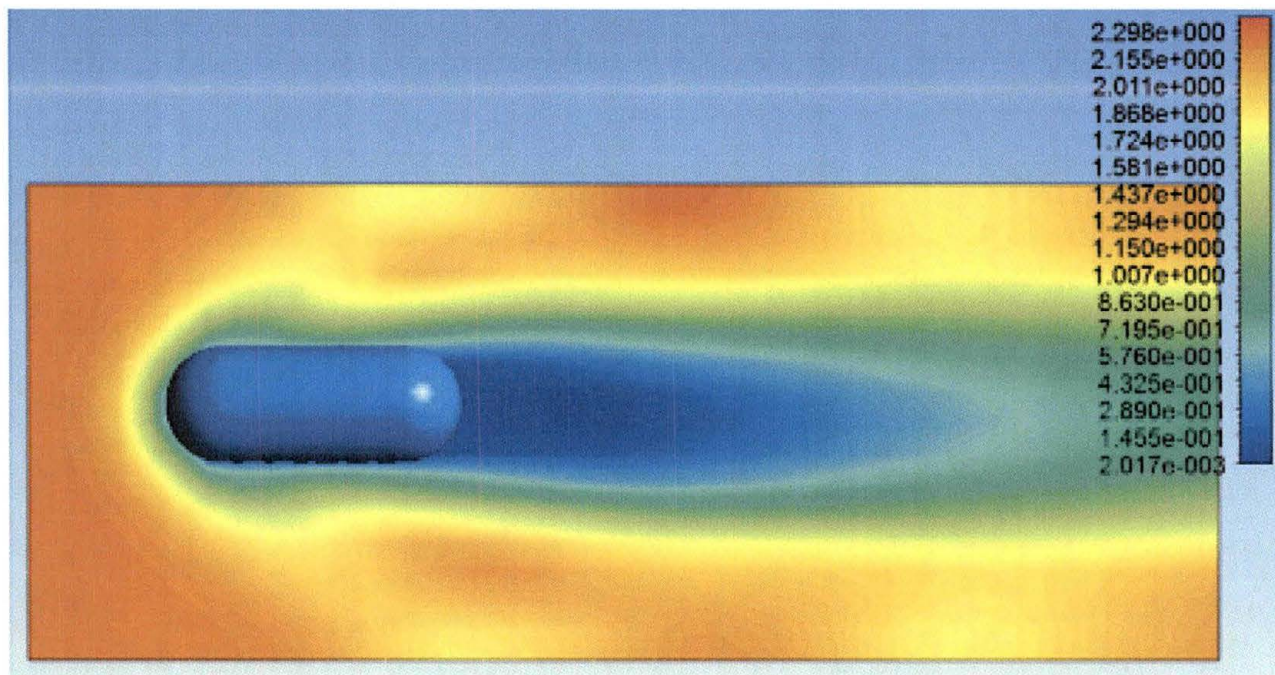


Figure 20. Tic Tac Mach Number at 1/6 Scale, Air Temperature 223K and 1500 mph with Supersonic Inlet and Supersonic Outlet

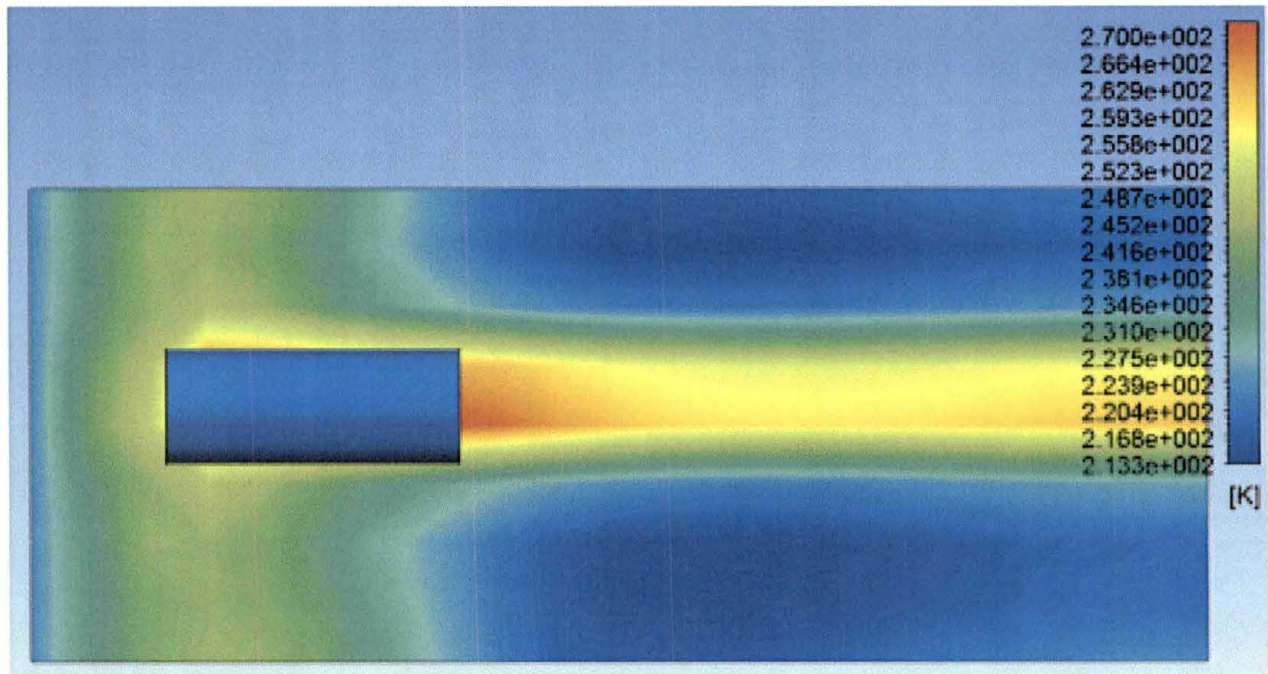


Figure 21. Cylinder Temperature at 1/6 Scale, Air Temperature 223K and 700 mph with Mixed Inlet and Supersonic Outlet

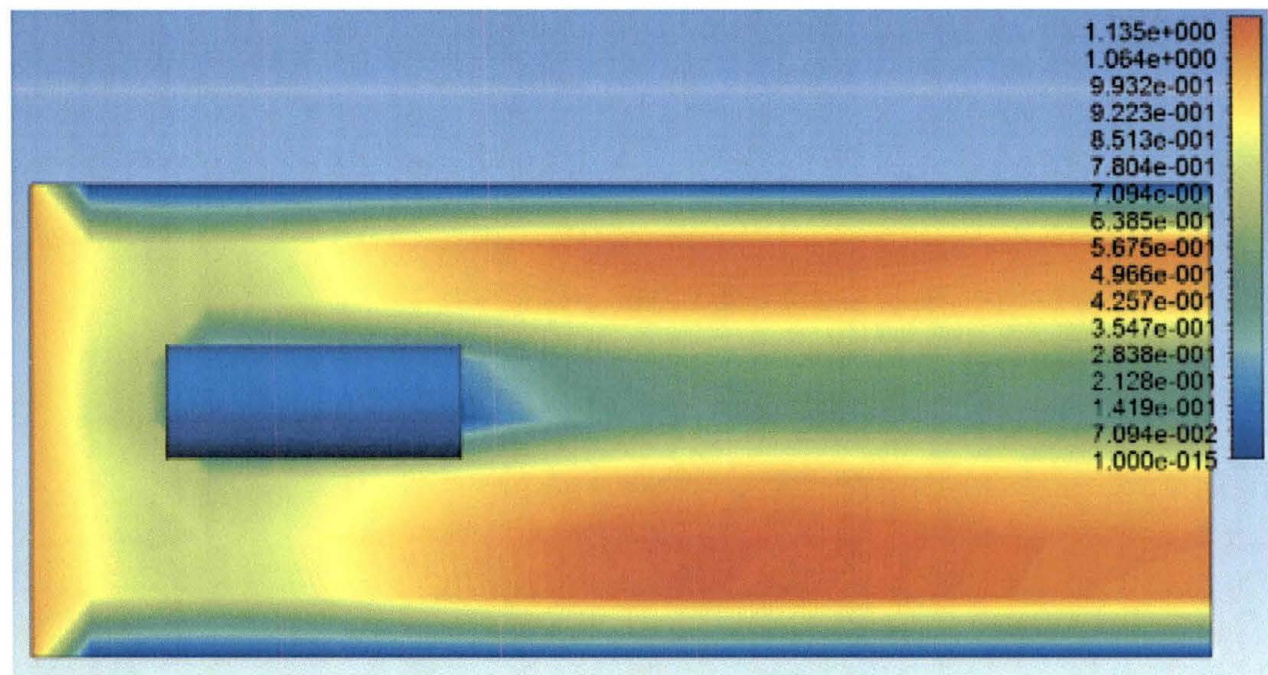


Figure 22. Cylinder Mach Number at 1/6 Scale, Air Temperature 223K and 700 mph with Mixed Inlet and Supersonic Outlet

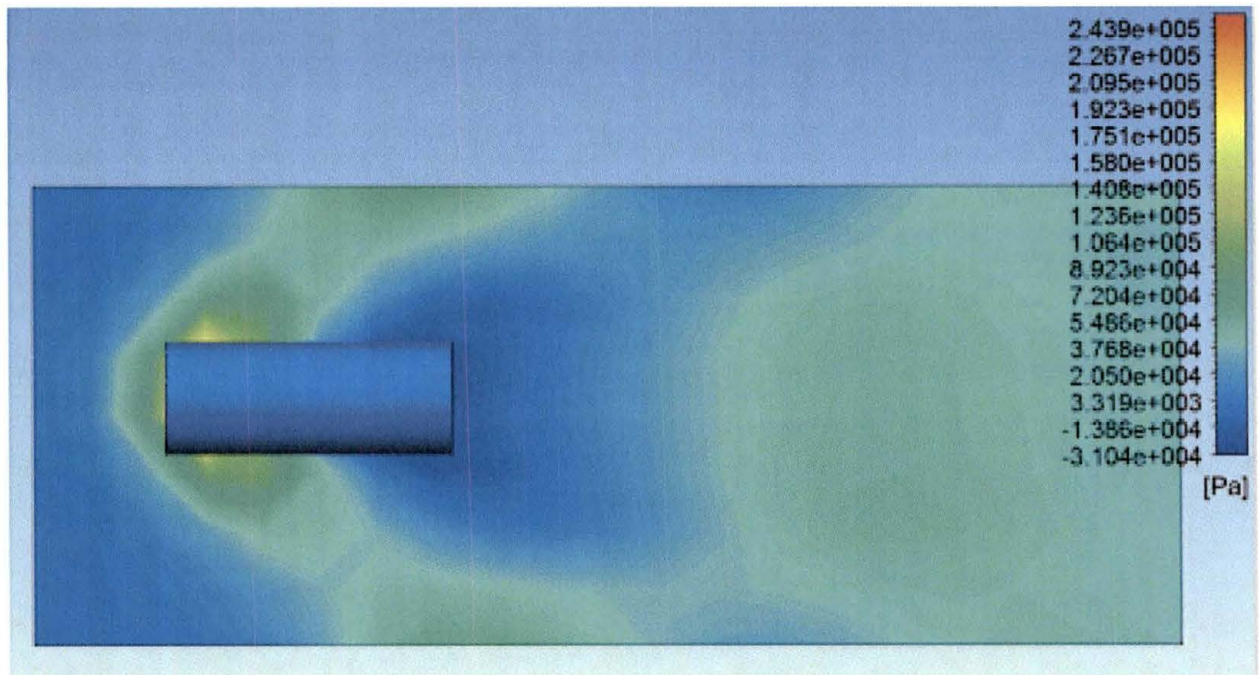


Figure 23. Cylinder Pressure at 1/6 Scale, Air Temperature 223K and 1500 mph with Supersonic Inlet and Supersonic Outlet

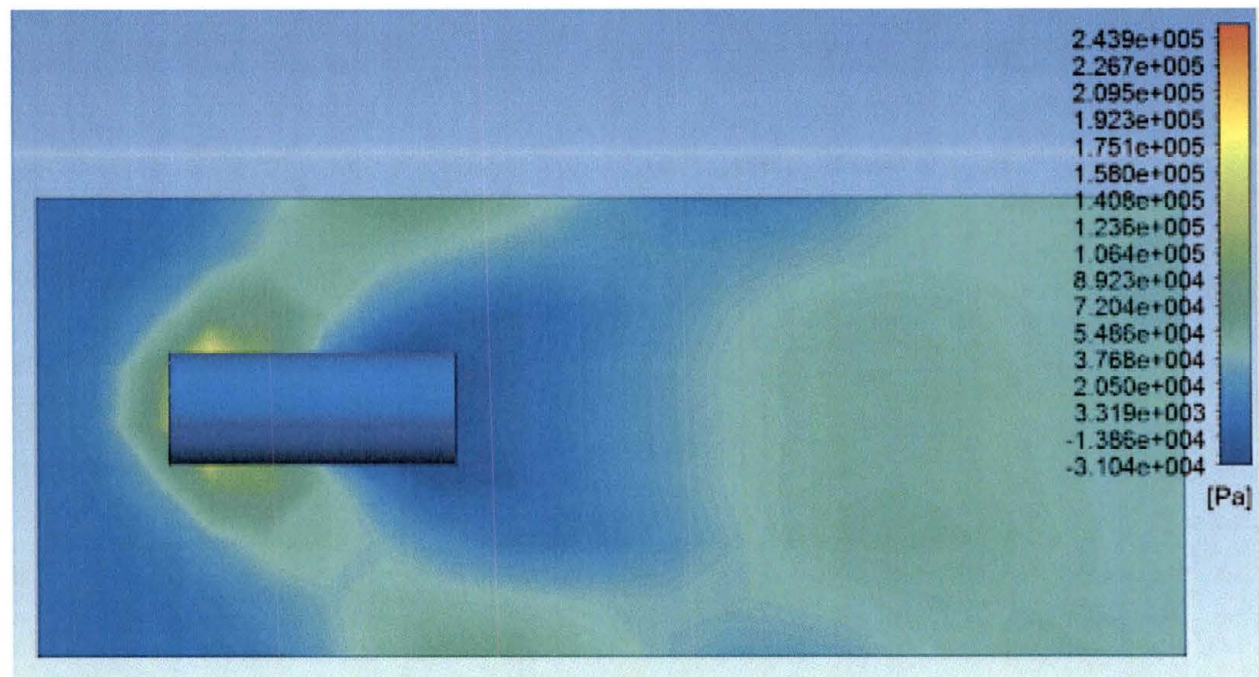


Figure 24. Cylinder Temperature at 1/6 Scale, Air Temperature 223K and 1500 mph with Supersonic Inlet and Supersonic Outlet

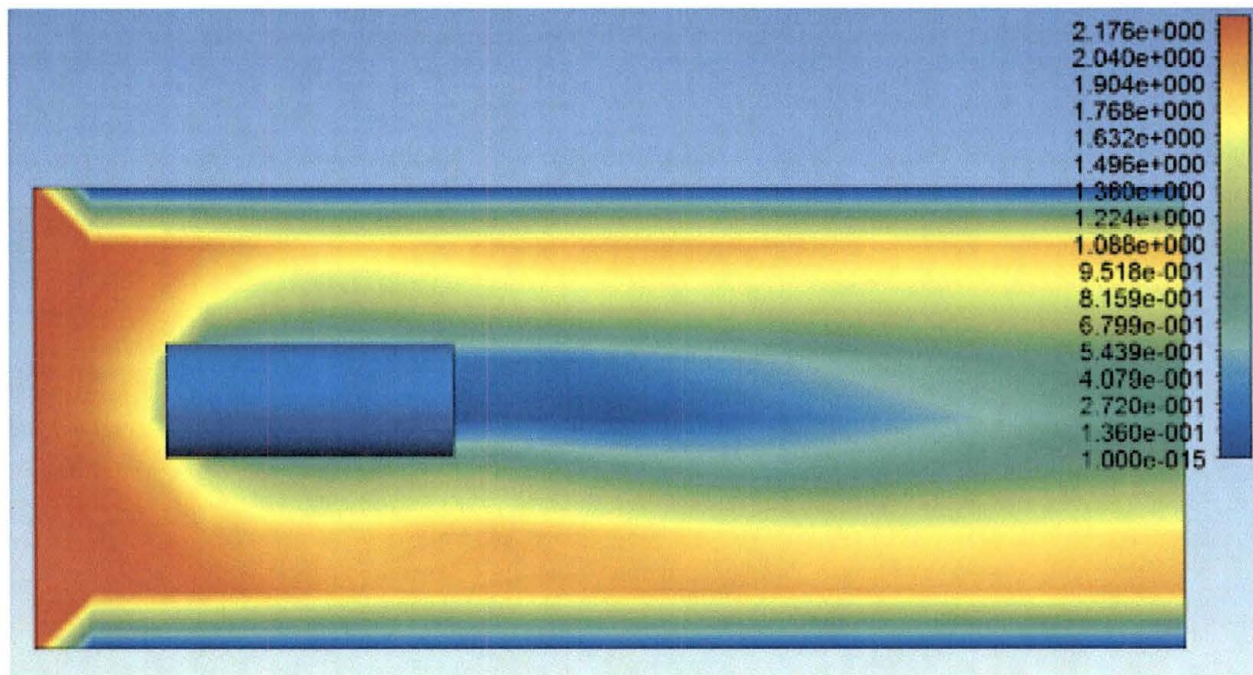


Figure 25. Cylinder Mach Number at 1/6 Scale, Air Temperature 223K and 1500 mph with Supersonic Inlet and Supersonic Outlet

4.1.4 Summary and Conclusions of Compressible Numerical Analyses

In the field of UAP studies, it is believed this preliminary analysis of the "Tic Tac" incident is the first of its kind to utilize a multi-industry standard FEA code to perform computational studies. The cases used are provided as a basic demonstration of the CFX fluid flow module and illustrate some of its capabilities, as well as a sample of some visualization tools.

4.1.4.1 "Tic Tac" Geometry

For the contour plots of pressure, temperature from 100 mph up to 500 mph, gradual increases in values are observed, with the most significant value change at the front of the object. The Mach number values increase at the front sides of the object. Disturbance of air flow is witnessed in the pressure and Mach contour profiles around the body.

Nearing the speed of sound at 700 mph, contours for pressure and Mach number started to show a more pronounced shock as would be expected. Temperature values also showed a higher increase at the front nose due to higher flow and air resistance over the body. Velocities higher than 700 mph showed a drastic difference in values compared to those at 100 mph with pressure differences in orders of magnitude. At 1,100 mph, the temperature rises not only at the attack nose, but started to even increase on the sides and in the wakes of air flow. Detached shock waves were witnessed in the pressure and Mach contours starting at 700 mph all the way up to 1,500 mph.

4.1.4.2 Circular Cylinder Geometry

It would seem counter intuitive to have a craft with a flat face pushing through the air due to a major increase in air resistance. However, there have been many reports of objects of just the sort seen maneuvering in the skies. A comparison of the detrimental aerodynamic effects was sought in relation to the smoother edged body.

At lower speeds, no large differences in values of pressures, temperatures or Mach numbers were observed. There were, however, slight differences in the location and profiles of the values of the "Tic Tac" geometry compared to the cylinder. None of these differences would indicate a drastic difference in conventional lift performance between the two geometries. The same appeared to hold true for higher speed scenarios, indicating no significantly different aerodynamic lift advantages between the two geometries.

4.1.4.3 Outcome

Success was achieved in implementing the ANSYS Multiphysics and SolidWorks Solid modeling program to create and run input cases for compressible fluid flow over both the "Tic Tac" geometry and that of a right circular cylinder to illustrate pressure, temperature and Mach contour profiles over both shapes. Separated shockwaves were witnessed in higher velocity cases indicating that the possibility of a sonic boom or vibration may have been perturbed into the environment. The actual propagation distance of these was not of interest in this study and may be looked at in the future. It is doubtful the aircrew would have felt a shock wave in the cockpit unless extremely close to the object while traveling at high rates of speed, which the fighter jets were not. These basic geometries and assumptions helped provide an excellent starting point to create more complex transient cases that possibly incorporate heat generation, electromagnetic effects, and acoustics. This is demonstrated in a basic model that FEA algorithms describing multiphysics can provide to be an invaluable tool in gaining insight into UAP flight characteristics and even possibly rule out improbable scenarios.

4.1.5 Numerical Analysis of Incompressible Flow of a UAP Entering Water

The problem studied was that of a solid disc shaped object descending through the air into a body of liquid. The model created, details the descent of a solid disc shaped UAP into water. It is assumed normal ambient conditions with a solid steel disc moving at a speed of 5 m/s in the negative y (downward) direction. The water surface is approximately 10 feet below the bottom of the UAP. Water and air temperatures are held at constant at 25°C and the gravitational acceleration constant at 9.81 m/s². Ambient pressure was a constant 1 atm, buoyancy effects within the water were accounted for and the UAP was taken to be isothermal (no heat transfer between the system and the surroundings). Three distinct phases were created; a gaseous phase (air), the solid phase (UAP) and the liquid phase (water). Figure 26 displays the three dimensional geometry depicting the distinct regions and boundaries.

The geometry was completed, and the necessary mesh was created in order to carry out the FEA analysis. Meshing is the discretization of a continuous domain into a set of discrete sub-domains called elements and is shown Figure 27. The governing equations were then solved for all

elements within the domain. The accuracy of the solution increases with increasing number of elements (refining of the mesh).

Typically, meshes are refined near domain borders or other places of interest; specifically where the solution is desired (for example the edge of solid object where it is desired to determine the amount of heat loss from the object). The solid UAP body was more refined than the air and water domains because it was of primary importance to study fluid flow around the UAP and not the flow of air/water further away from the solid domain. A close-up view of the refined mesh in the solid UAP domain is seen in Figure 28.

Once the mesh was generated, then boundary and initial conditions were assigned to replicate approximate physical conditions during the event. As the name implies, boundary conditions are exact solutions to differential equations that exist on the outskirts of the different geometries. These conditions must be met if the solution is to be correctly determined. Initial conditions are time dependent relationships that describe the initial state of the problem. Thermophysical data must be defined for each domain. The governing equations include the properties of the materials involved (c_p , μ , etc.) and an accurate analysis depends as much on the proper accounting of these properties as on the proper identification of boundary conditions.

Boundary conditions on the solid UAP edges were set as a no slip surface. A no slip boundary sets the fluid velocity at 0. That is to say that a fluid coming in contact with the surface will not move (not slip). This is a typical boundary condition used when a fluid comes in contact with a solid body. In addition, the outside walls of the boundary were set as no slip. It was assumed that the walls were located far enough away from the UAP–water impact zone to play no part in determination of fluid movement around the solid UAP body.

Thermophysical data was determined by material identification within the problem setup. The UAP was defined as being made of steel, the liquid body was set as water and the gaseous body was set to air. The initial velocity for the UAP was 0 m/s, that is to say the UAP initially starts at rest. Total simulation time was set to 10 seconds with 0.2 seconds per time step (for a total of 50 time steps).

4.1.6 Numerical Analysis of Incompressible Flow of a UAP Entering Water Results

Upon completion of the simulation; an output file was created and stored for use in the post processing portion of Workbench called CFX-Post. Once the output file has been imported to CFX-Post; a variety of results may be obtained. For this investigation, a fluid dynamic analysis was performed. To best view the results; a plane (parallel to the y axis) was created to bisect the geometry (see Figure 29).

The creation of a plane contained within the geometry allows for easy analysis of the solution. CFX-Post was used to determine the velocities of the air and water fluid domain, the pressure of the system and through examination of the volume fraction of water; a recreation of the appearance of a solid entering the water. An animated representation of the transient results was created in an effort to understand how the trends in the specified variable change over time. Figure 30 displays a still image of an animated result showing how the volume fraction of water changed as the UAP descended into the water domain.

Manipulation of the created plane view allowed for a two dimensional analysis for a variety of parameters. Figure 31 displays a still frame of the animation depicting how pressure varied throughout geometry.

Figure 31 displayed the expected trend of an increasing pressure with increasing depth. A re-creation of the physical appearance of the UAP impacting and descending into water may be achieved through analysis of the transient animated results of volume fraction of water. Figure 32 displays a still shot of this animation after the UAP has impacted and entered the water domain.

The radially expanding concentric circles display the resulting ripple effect after the solid has penetrated through the surface of the water. Figure 33 displays a side view of the same result. The original result animations from which the still screenshots (Figure 29 through Figure 33) were taken are provided in .mpeg form. In addition to the preceding results, several animations depicting transient trends of fluid density and fluid velocity have been provided.

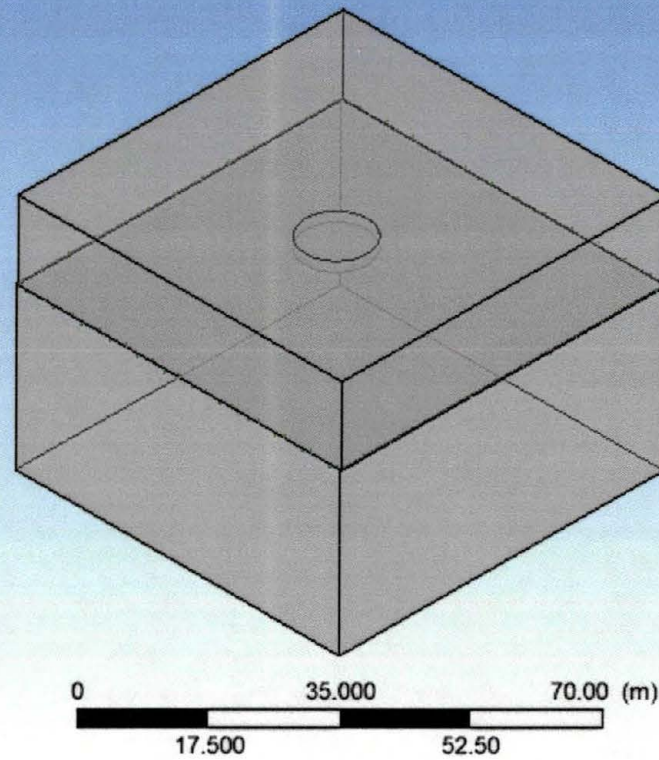


Figure 26. Solid Three Dimensional Geometry of Disc and Water

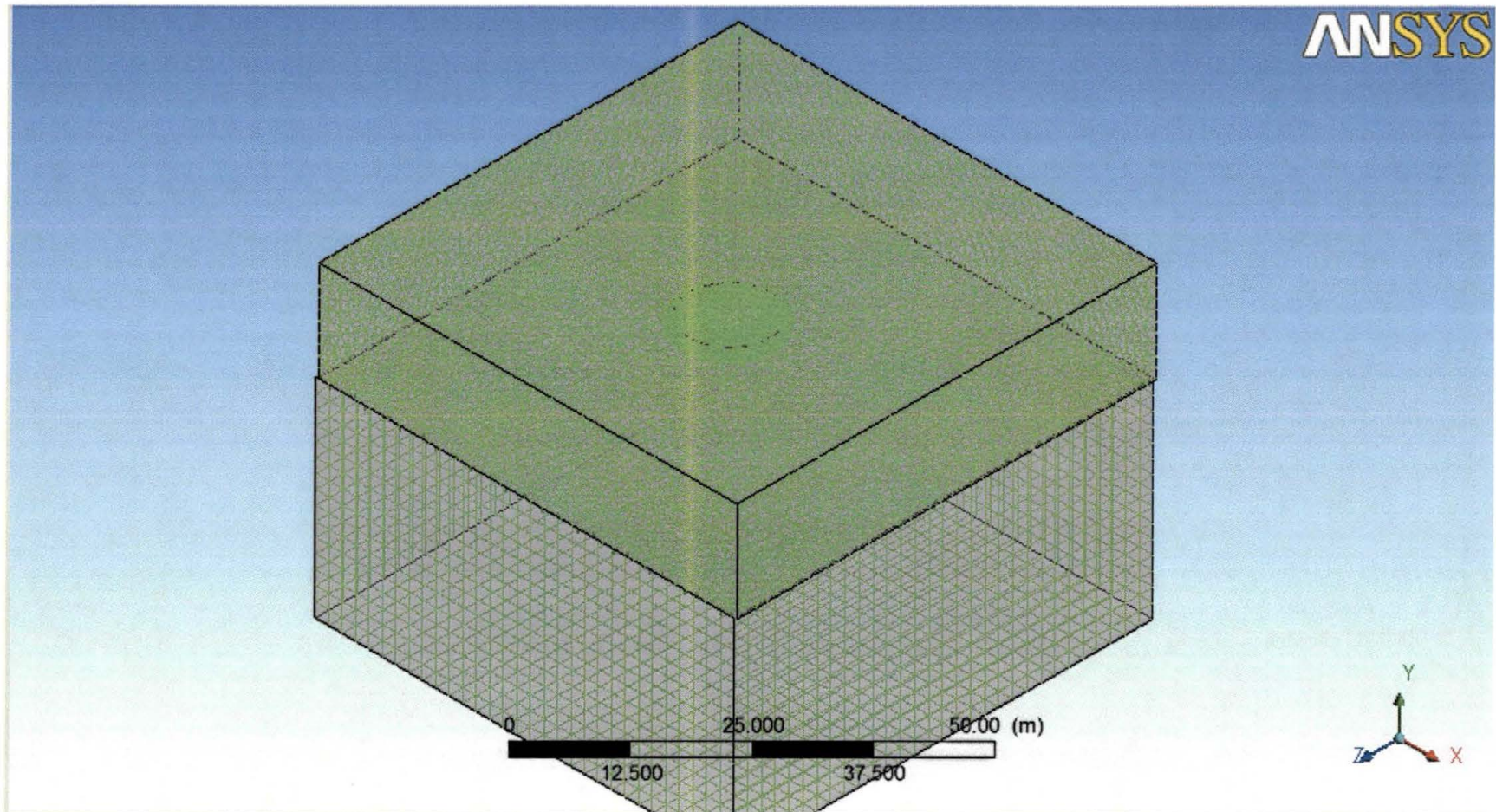


Figure 27. Solid Three Dimensional Geometry Mesh of Disc and Water

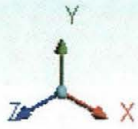
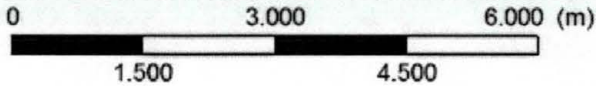
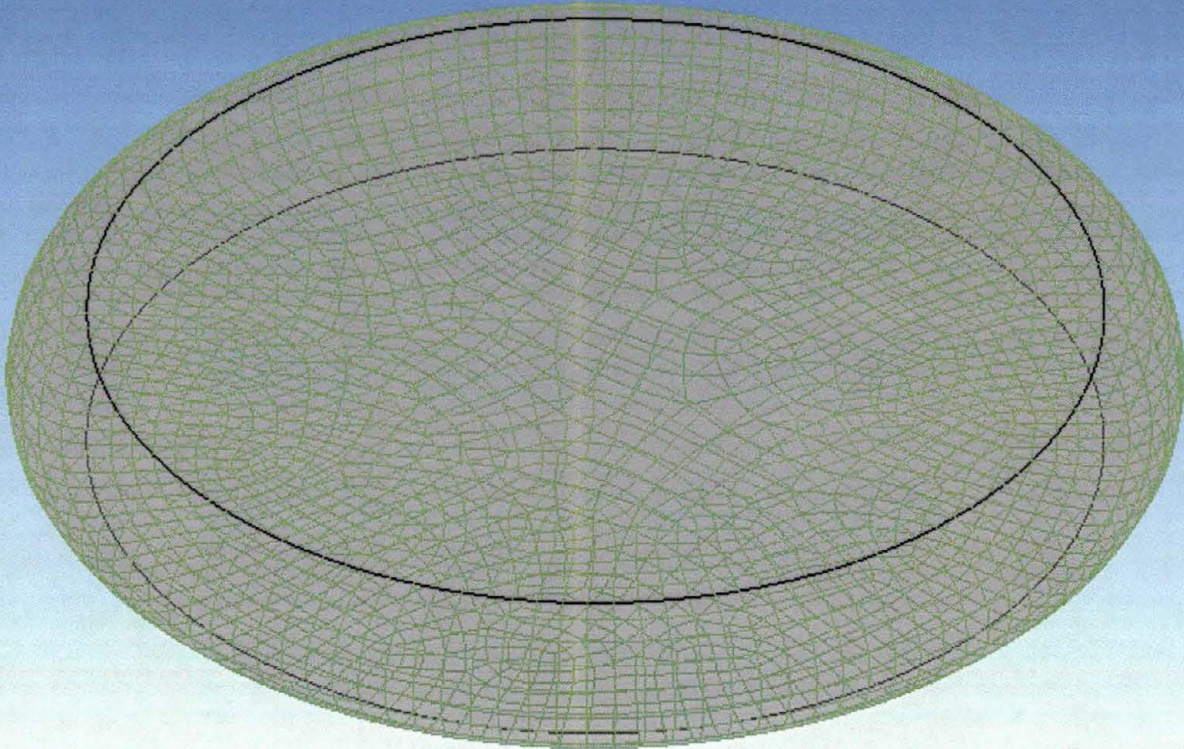


Figure 28. Solid Three Dimensional Geometry Mesh of UAP Disc

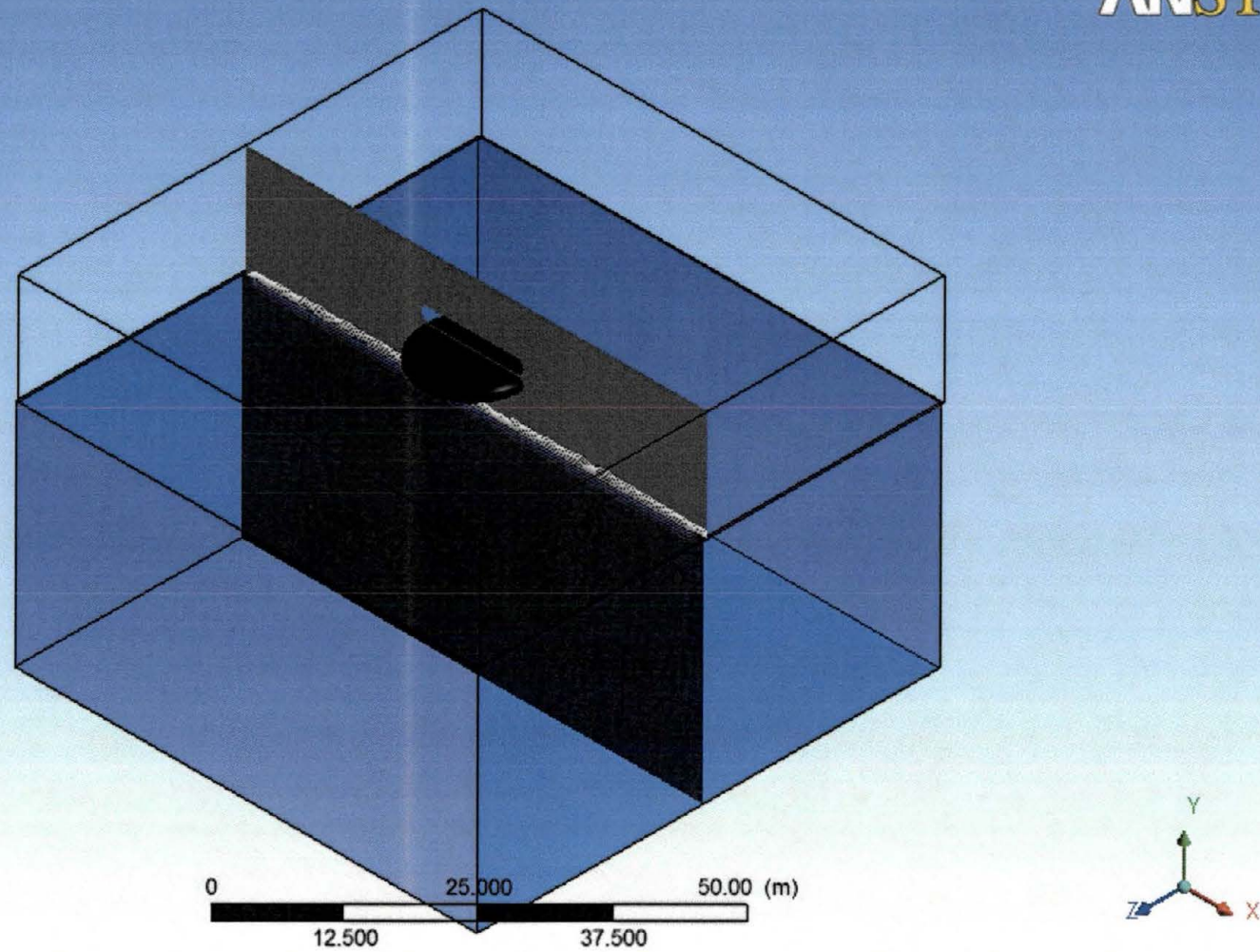


Figure 29. User Generated Cut Analysis Plane

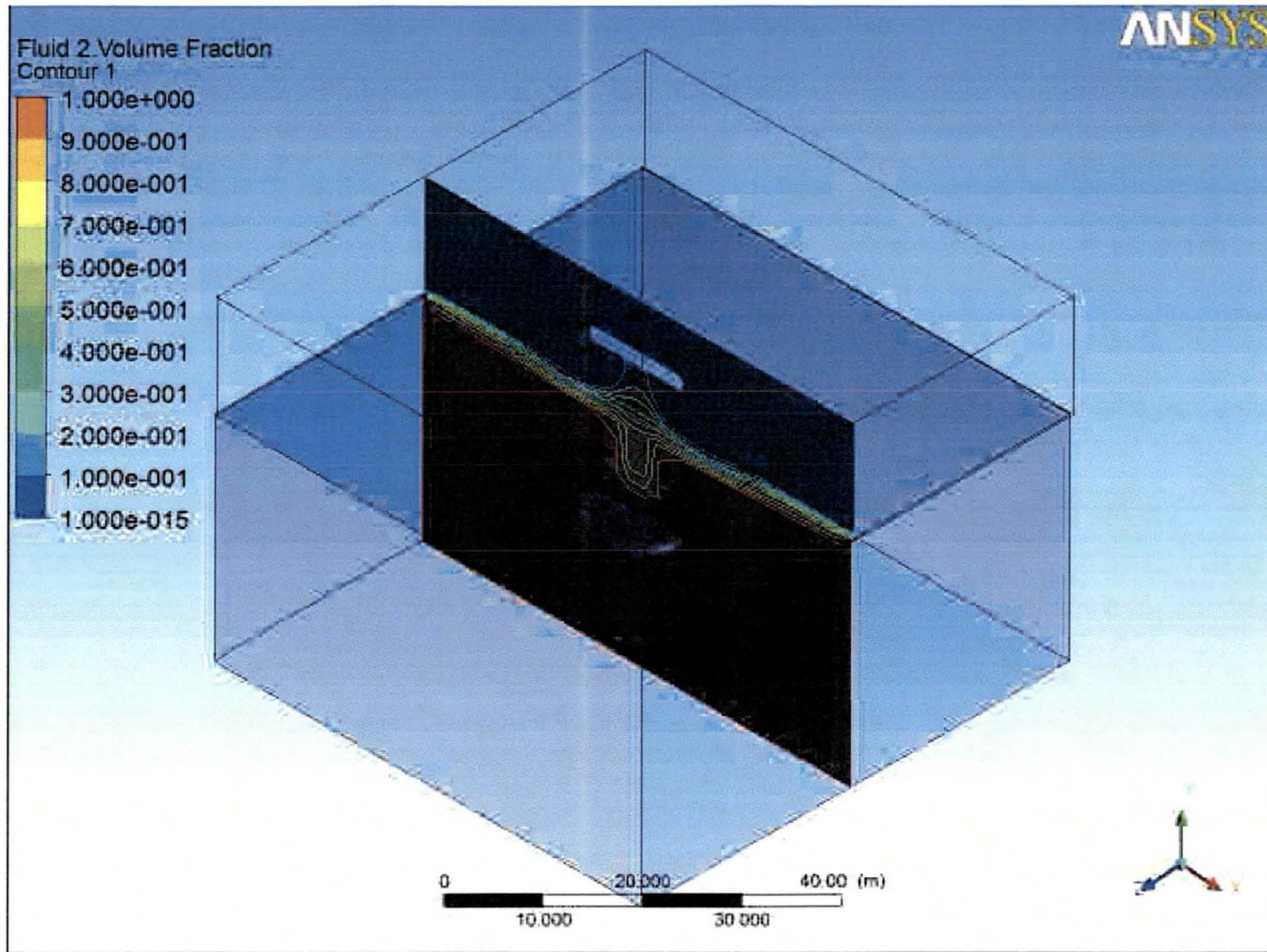


Figure 30. Animated Result, Fluid 2 Volume Fraction

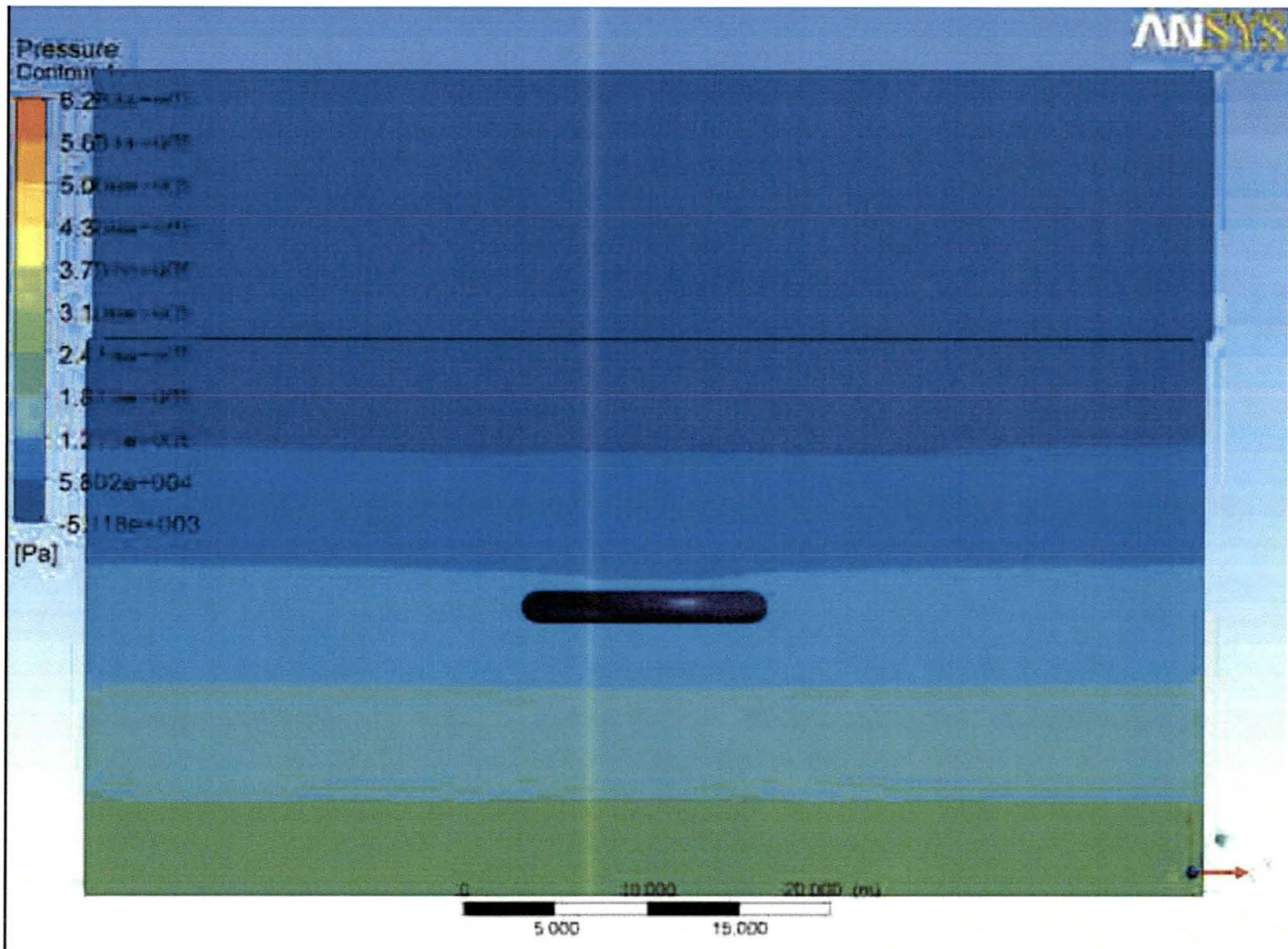


Figure 31. Total Pressure Around UAP

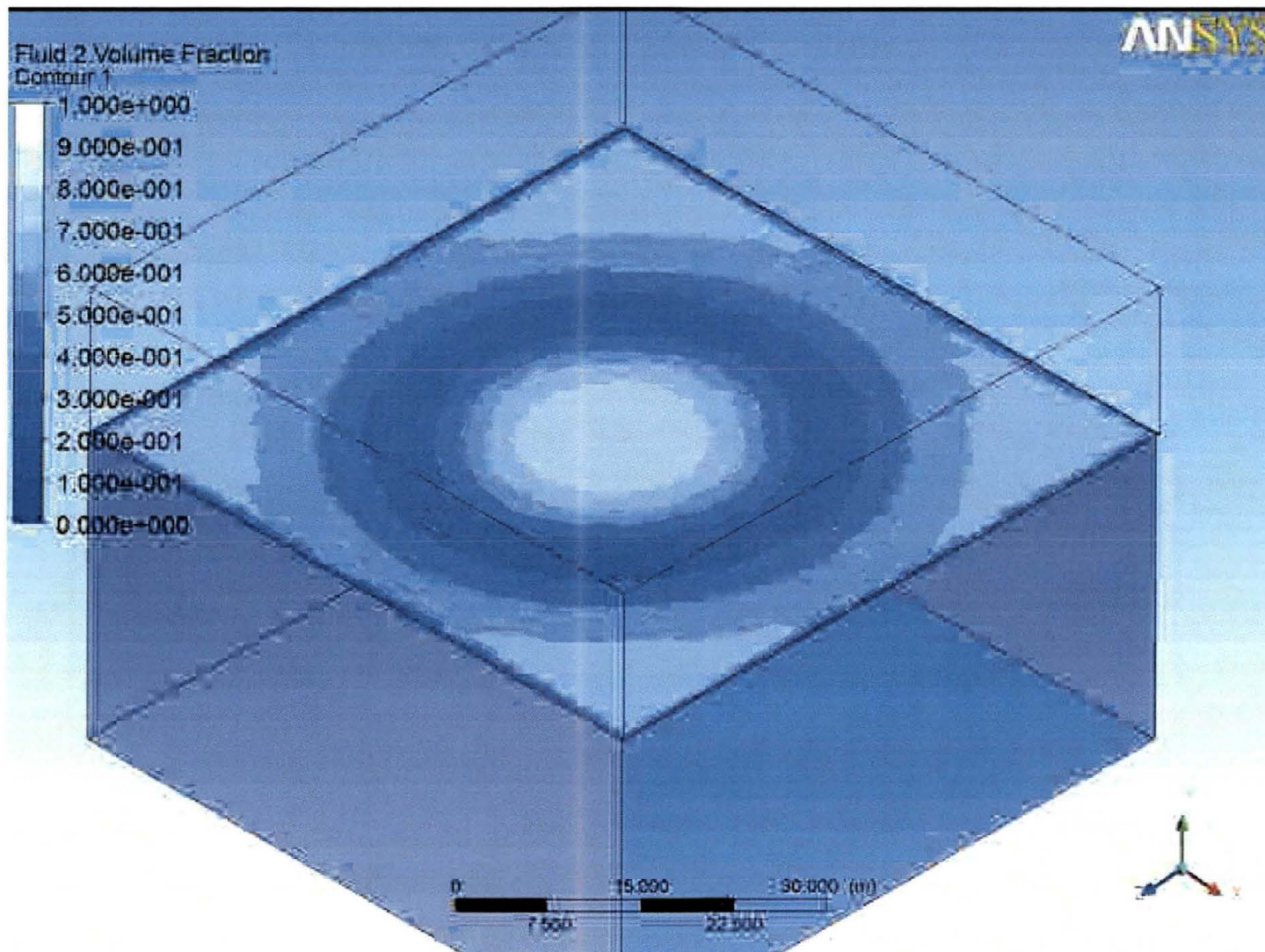


Figure 32. Water Surface Effects From Solid Impact

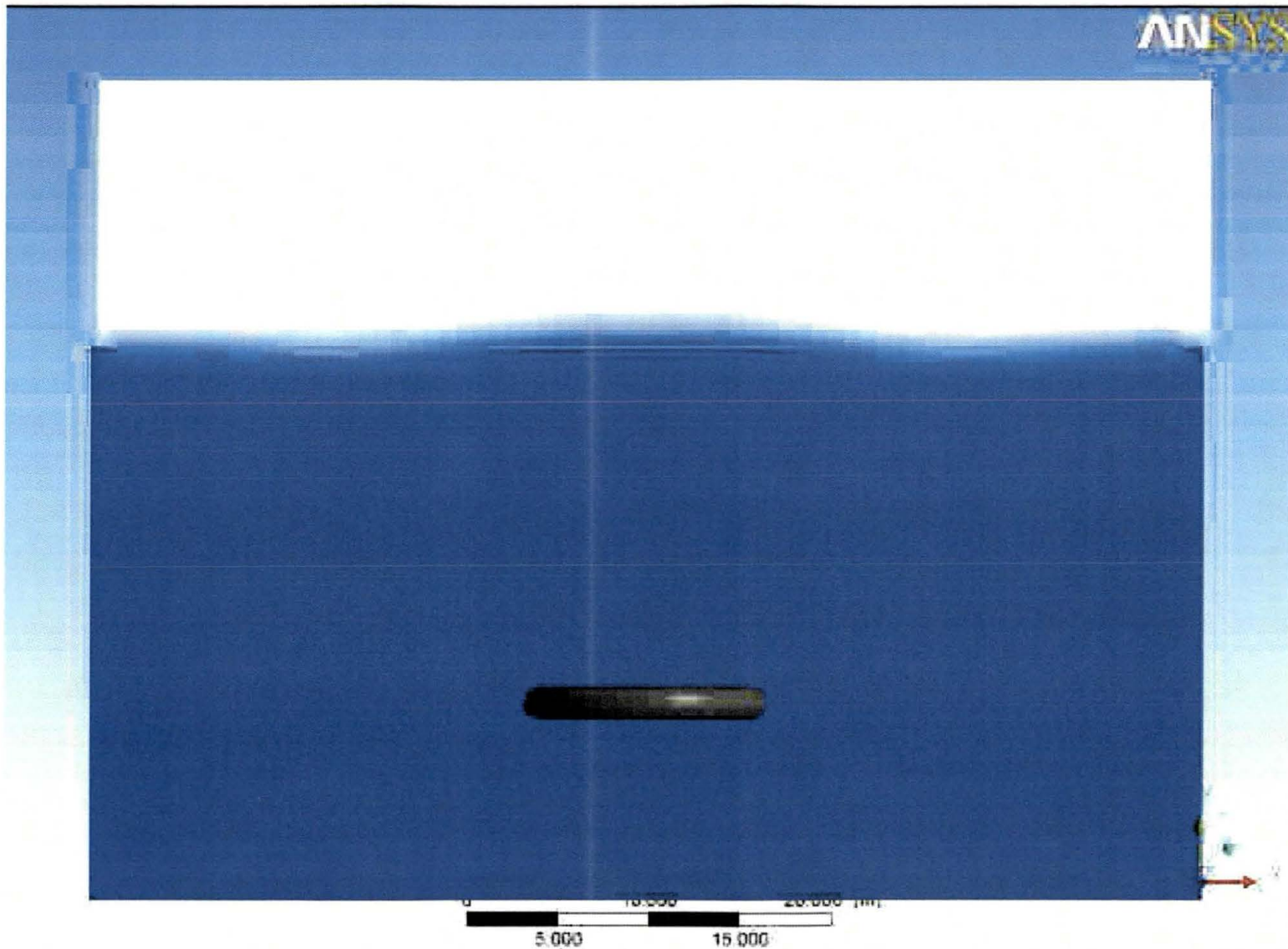


Figure 33. Water Surface Effects From Solid Impact (Side View)

4.1.7 Summary and Conclusions of Numerical Analysis of Incompressible Flow of a UAP Entering Water Results

The CFX-Post generated graphs and animations are illustrative samples of what ANSYS CFX is capable of producing. The scenario was chosen due to its simple geometry, boundary conditions and relative ease of computational requirements. A typical problem of this type when solved by hand, would have taken weeks if not longer. This simulation incorporated a fluid dynamic analysis and further analysis may incorporate numerous other multiphysics attributes in the study of UAP. Heat transfer from a craft entering the earth's atmosphere as well as the effects of varying craft size, shape and speed on wave generation during water impact could be studied just as easily. In addition to determining power requirements, achieved surface temperatures etc., recreations of eyewitness sightings may be.

Furthermore, electromagnetic capabilities allow for modeling of possible magnetohydrodynamic (MHD) affects. Electrodynamics can show the energy required to create magnetic fields with different materials as well as the propagation of electromagnetic waves through solid and liquid mediums. Using careful design and properties of human tissue in the program it would be possible to show effects on the human body from heat and high electric fields. Effects, such as increase in body temperature or nervous system interruption may be able to be quantified in ANSYS. This tool can greatly assist in the goal of studying human effects to reverse engineer UAP technology.

4.2 ANALYSES OF SPHERICAL UAPS

4.2.1 Acoustical Analysis of a Spherical USO

Over the years, there have also been numerous reports USOs. In 1967, a UFO was reported crashing into Shag Harbour, Nova Scotia. It was reported that hovering and flashing orange lights were present, then it tilted at about a 45 degree angle and entered the water. A yellow light was seen in the water moving and leaving a trail of yellow foam. The Canadian Coast Guard was dispatched but by the time they arrived along with other vessels at the point of entry the yellow foam was all that remained.

This is one of very few cases where governmental agency documents have formally declared an unidentified flying object was involved. At least eleven people saw a low-flying lit object head down towards the harbor. Multiple witnesses reported hearing a whistling sound "like a bomb," then a "whoosh," and finally a loud bang. Some reported a flash of light as the object entered the water. Several interviewed military witnesses, including a diver involved in an attempted recovery, have claimed an alien spacecraft was responsible. It was also claimed by several of the witnesses that the U.S. military was involved in recovery attempts. The case was also briefly investigated by the Condon Committee UFO study, which offered no explanation.

It has been proposed that this type of craft may operate using some sort of electromagnetic frequency based propulsion system to control underwater "flight" and to achieve incredible performance capabilities in velocity and acceleration.

The three-dimensional acoustic wave equation is given below in the second order partial differential equation:

$$\frac{\partial^2 p}{\partial x^2} + \frac{\partial^2 p}{\partial y^2} + \frac{\partial^2 p}{\partial z^2} - \frac{1}{c^2} \frac{\partial^2 p}{\partial t^2} = 0$$

and

$$c = \sqrt{\frac{B_a}{\rho}}$$

where

- B_a – adiabatic bulk modulus (Pa)
- c – speed of sound in medium (m/s)
- p – pressure (Pa)
- t – time (sec)
- ρ – density of medium (kg/m^3)
- x – x coordinate
- y – y coordinate
- z – z coordinate

The following solutions are obtained by separation of variables in different coordinate systems. Phasor solutions result, that is they have an implicit time-dependence factor of $e^{i\omega t}$ where $\omega = 2\pi f$ is the angular frequency. The explicit time dependence is given by:

$$p(r, t, k) = \text{Real} [p(r, k)e^{i\omega t}]$$

Here $k = \frac{\omega}{c}$ is the wave number and r is the displacement vector.

In Cartesian coordinates and Cylindrical coordinates respectively:

$$p(r, k) = Ae^{\pm ikr}$$

$$p(r, k) = AH_0^{(1)}(kr) + BH_0^{(2)}(kr)$$

where the asymptotic approximations to the Hankel functions, when $kr \rightarrow \infty$, are

$$H_0^{(1)}(kr) \simeq \sqrt{\frac{2}{\pi kr}} e^{i(kr - \pi/4)}$$

$$H_0^{(2)}(kr) \simeq \sqrt{\frac{2}{\pi kr}} e^{-i(kr - \pi/4)}$$

and in Spherical coordinates:

$$p(r, k) = \frac{A}{r} e^{\pm ikr}$$

Depending on the chosen Fourier convention, one of these represents an outward traveling wave (real) and the other an unphysical inward travelling wave (imaginary).

Assuming USOs operate on a frequency driven system, an ANSYS Multiphysics 1/100th scale ¼ symmetry Acoustical full harmonic analyses was performed to study a spherical object of 10 m in both air and water for a range of frequencies at standard conditions. Provided below are contour plots for the real, imaginary and magnitude components of pressure and plots for pressure as a function of radius in Pa.

Table 3. Properties of Water Used for ANSYS Harmonic Analyses

Property	Value
Water Density	1,000 kg/m ³
Speed of Sound	1,500 m/s
Reference Pressure	1 × 10 ⁻⁶ Pa

Figure 34 and Figure 35 show the FEA mesh for 25 elements per wavelength and 50 elements per wavelength for a 1,000 Hz analysis. Upon inspection of the maximum pressures shown in Figure 36 and Figure 37, it is apparent the FEA model solution was mesh independent with a pressure of 1,052 Pa for the 25 element per wavelength model and 1,103 Pa for the 50 element per wavelength model. Generally higher element models for meshes are considered more accurate, but a cost in computational time may be seen in extremely large models. In the runs performed, the 25 element per wavelength model showed sufficient accuracy and reasonable computation times. As frequency was adjusted higher, the elements per wavelength were adjusted down to limit element numbers.

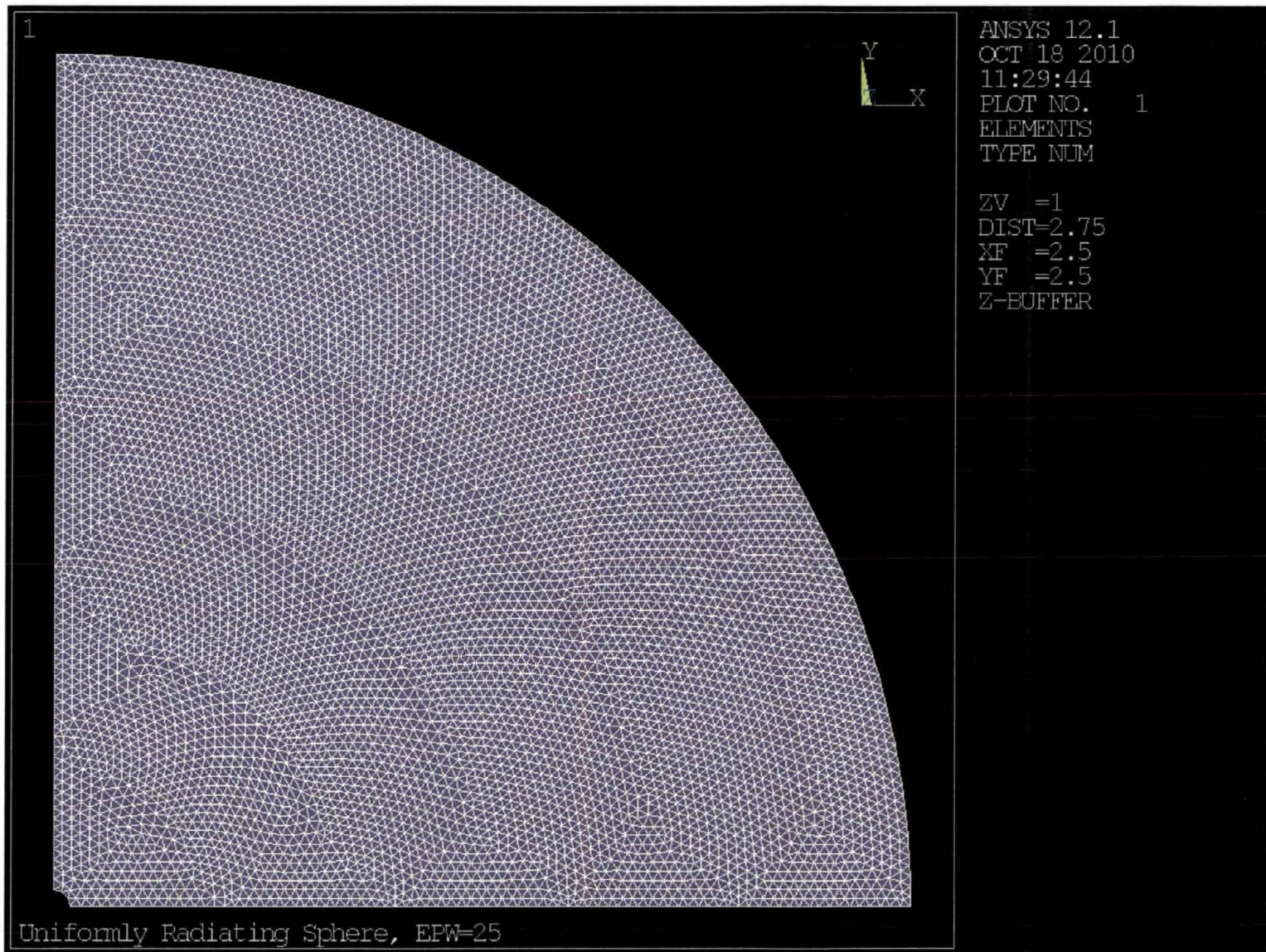


Figure 34. Mesh Plot for 1,000 Hz with 25 Elements per Wavelength in Water

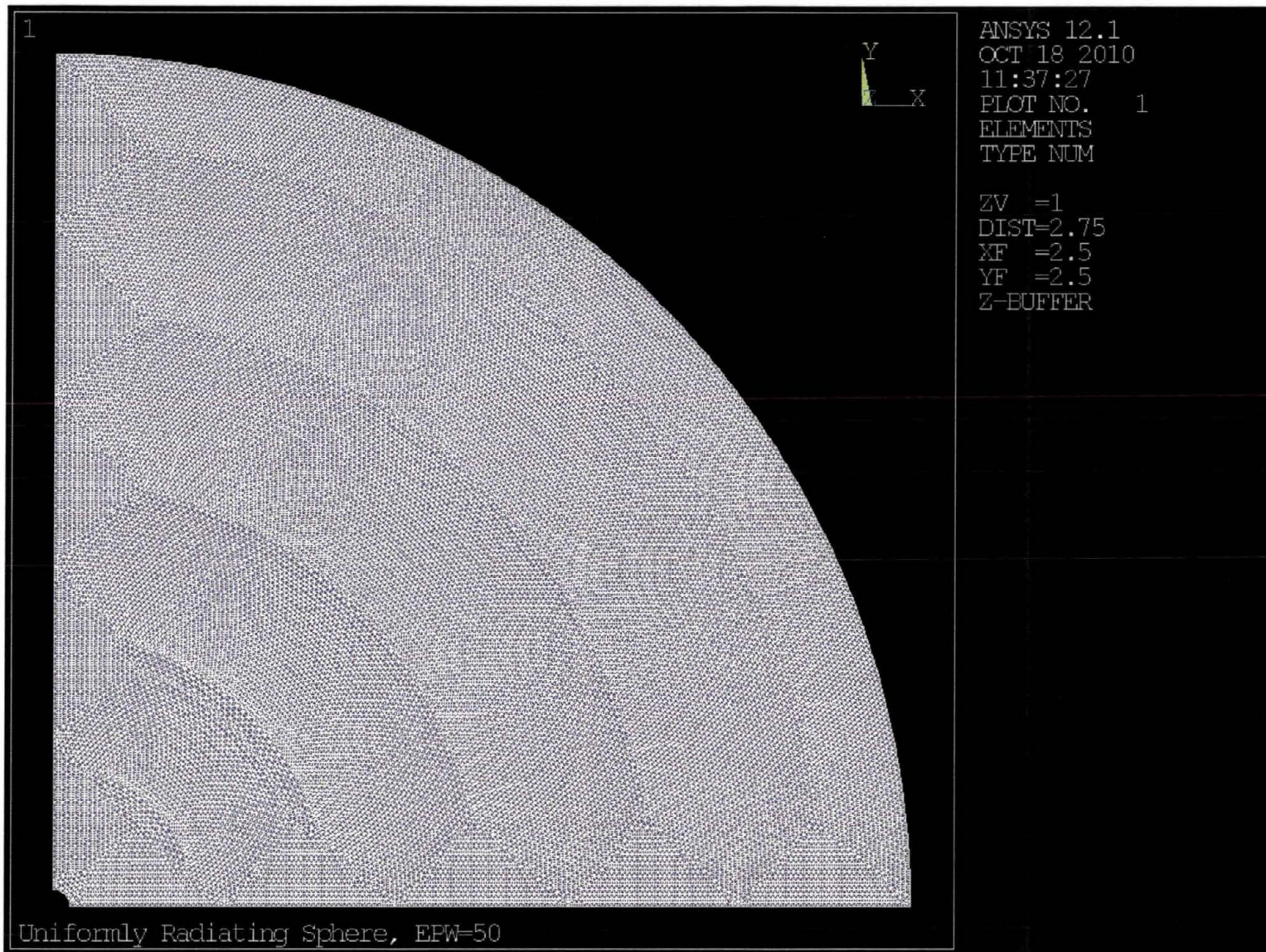


Figure 35. Mesh Plot for 1,000 Hz with 50 Elements per Wavelength in Water

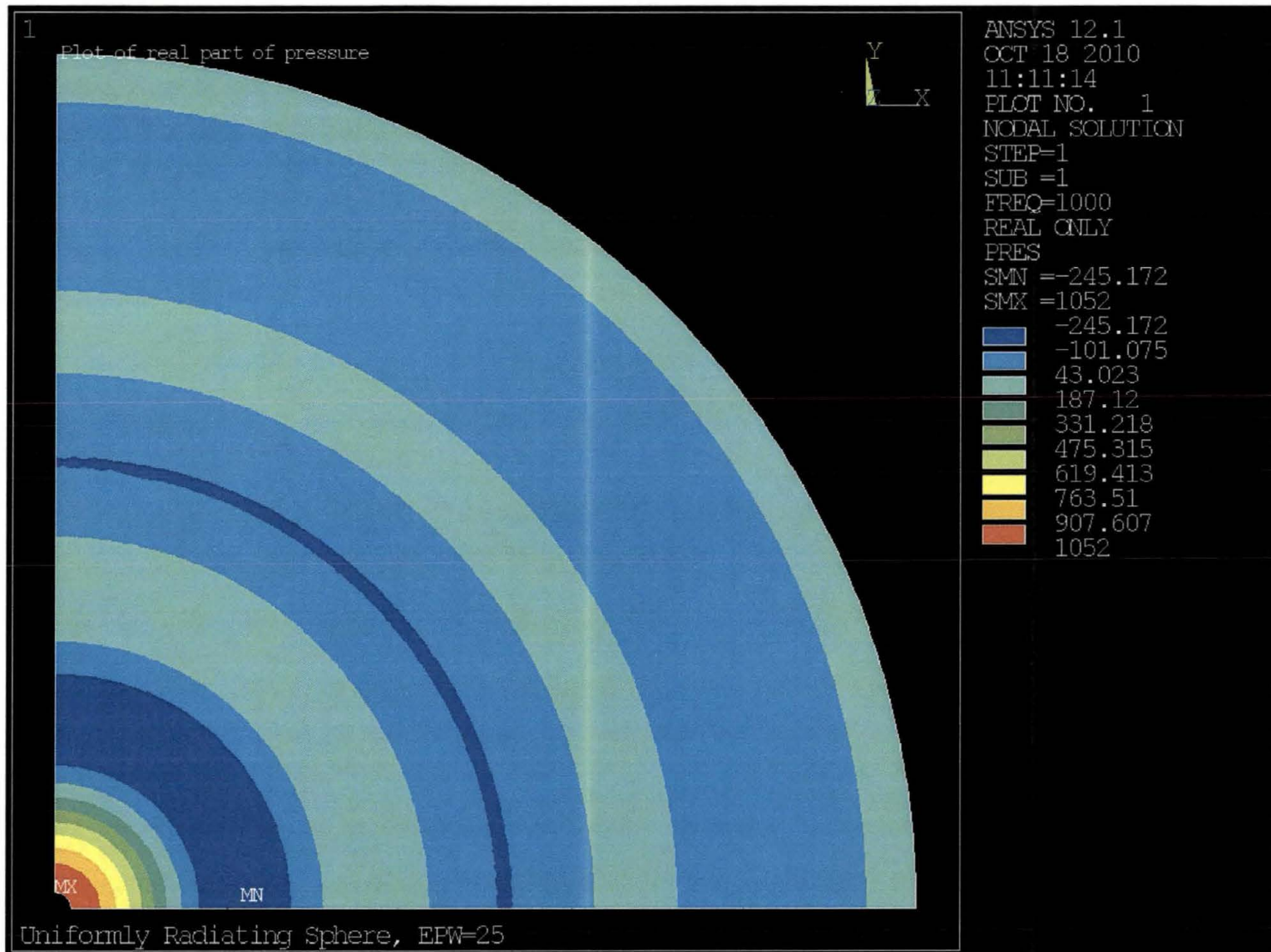


Figure 36. Contour Plot of Real Component of Pressure (Pa) for 1,000 Hz with 50 Elements per Wavelength in Water

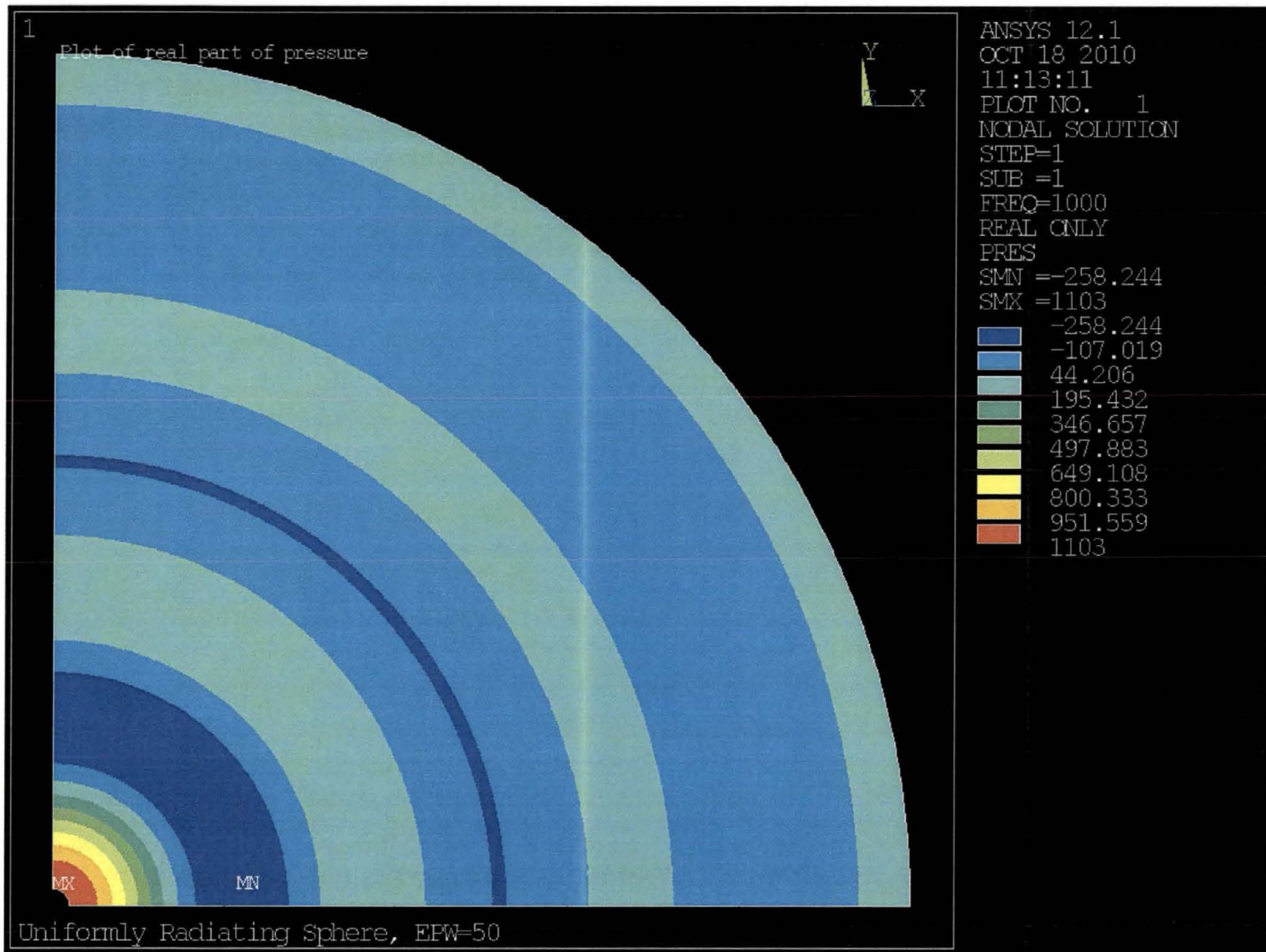


Figure 37. Contour Plot of Real Component of Pressure (Pa) for 1,000 Hz with 50 Elements per Wavelength in Water

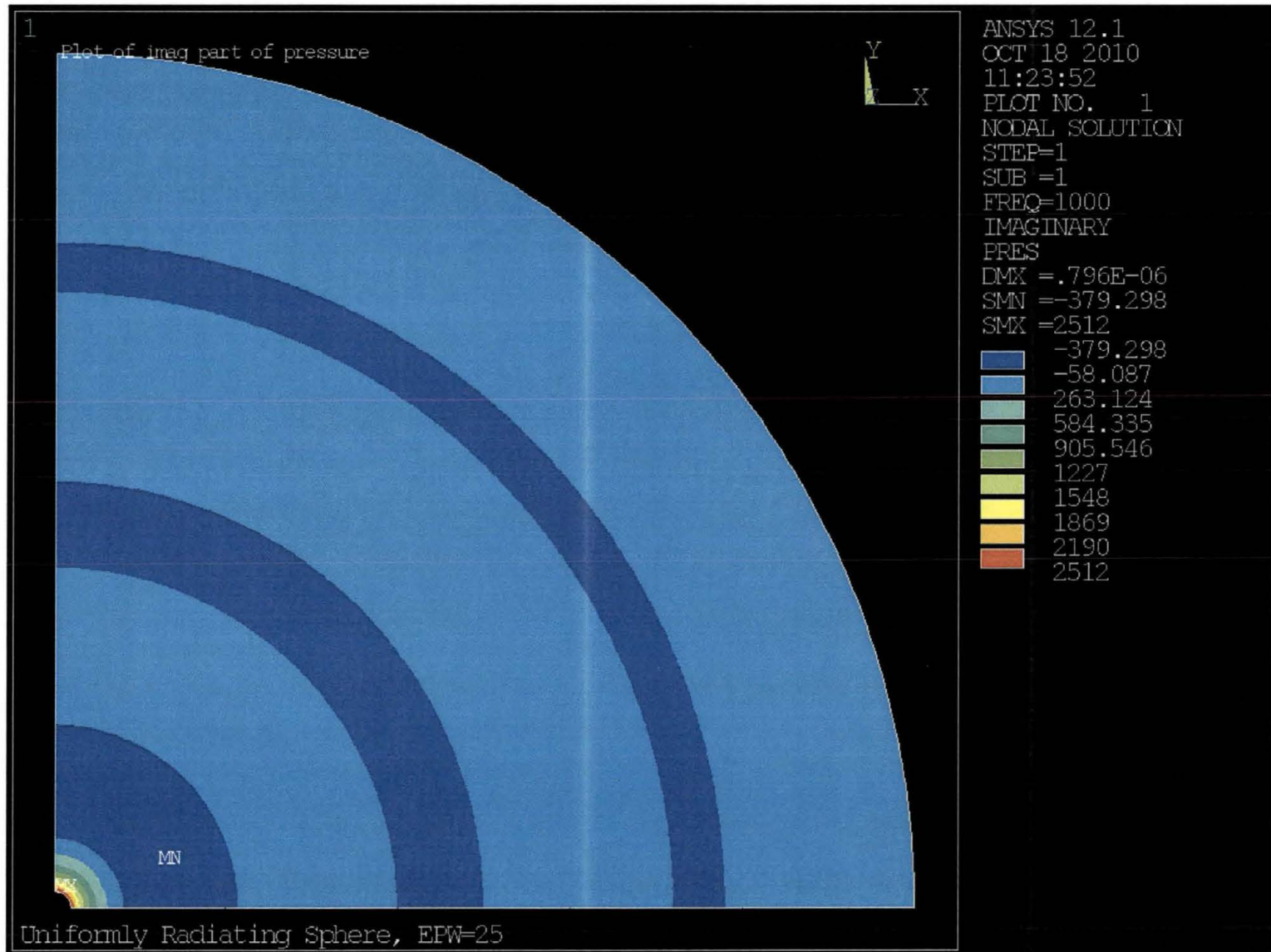


Figure 38. Contour Plot of Imaginary Component of Pressure (Pa) for 1,000 Hz with 25 Elements per Wavelength in Water

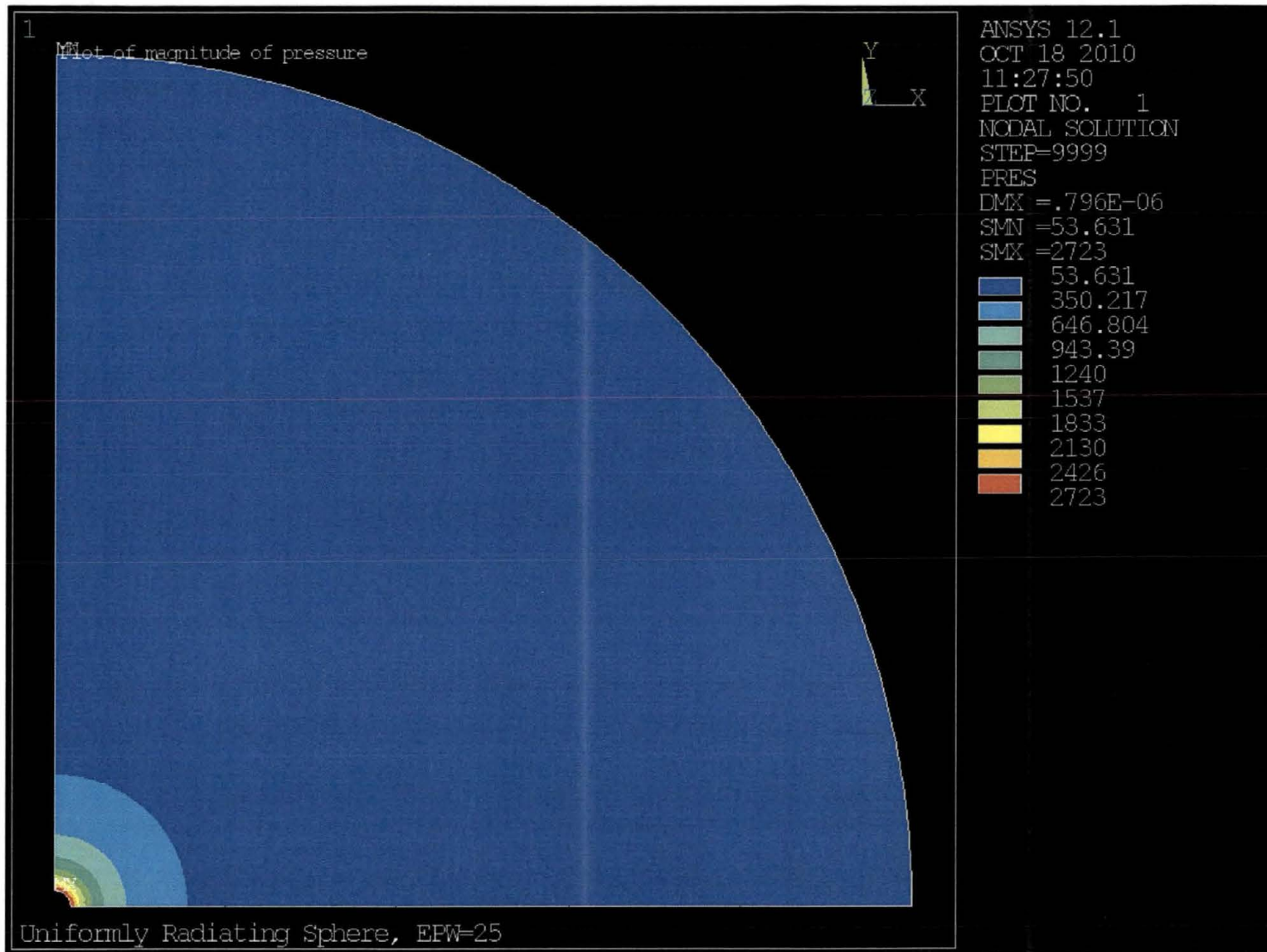


Figure 39. Contour Plot of the Magnitude of Pressure (Pa) for 1,000 Hz with 25 Elements per Wavelength in Water

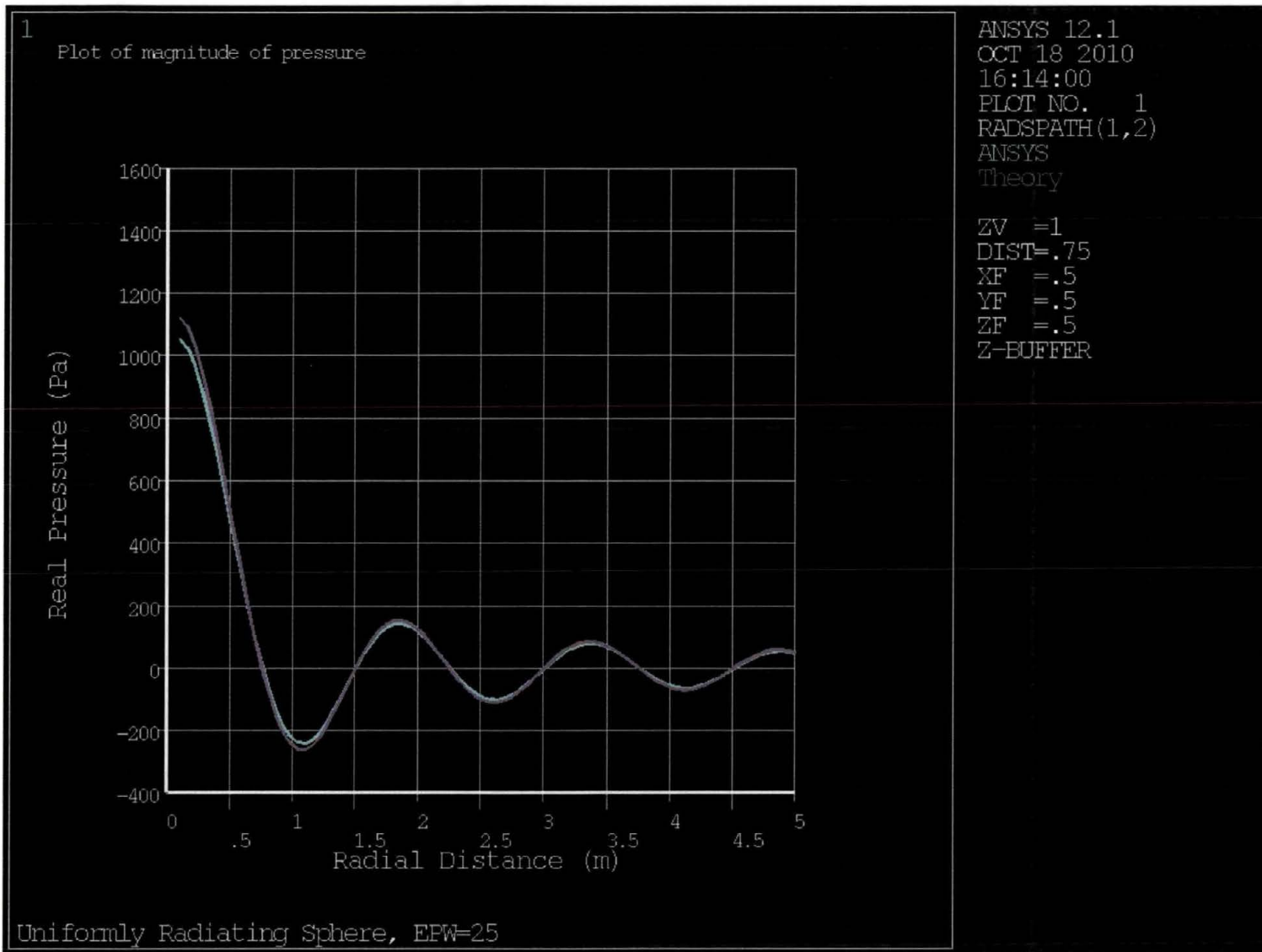


Figure 40. Steady State Real Component of Pressure (Pa) as a Function of Radial Distance (m) Plot for 1,000 Hz with 25 Elements per Wavelength in Water

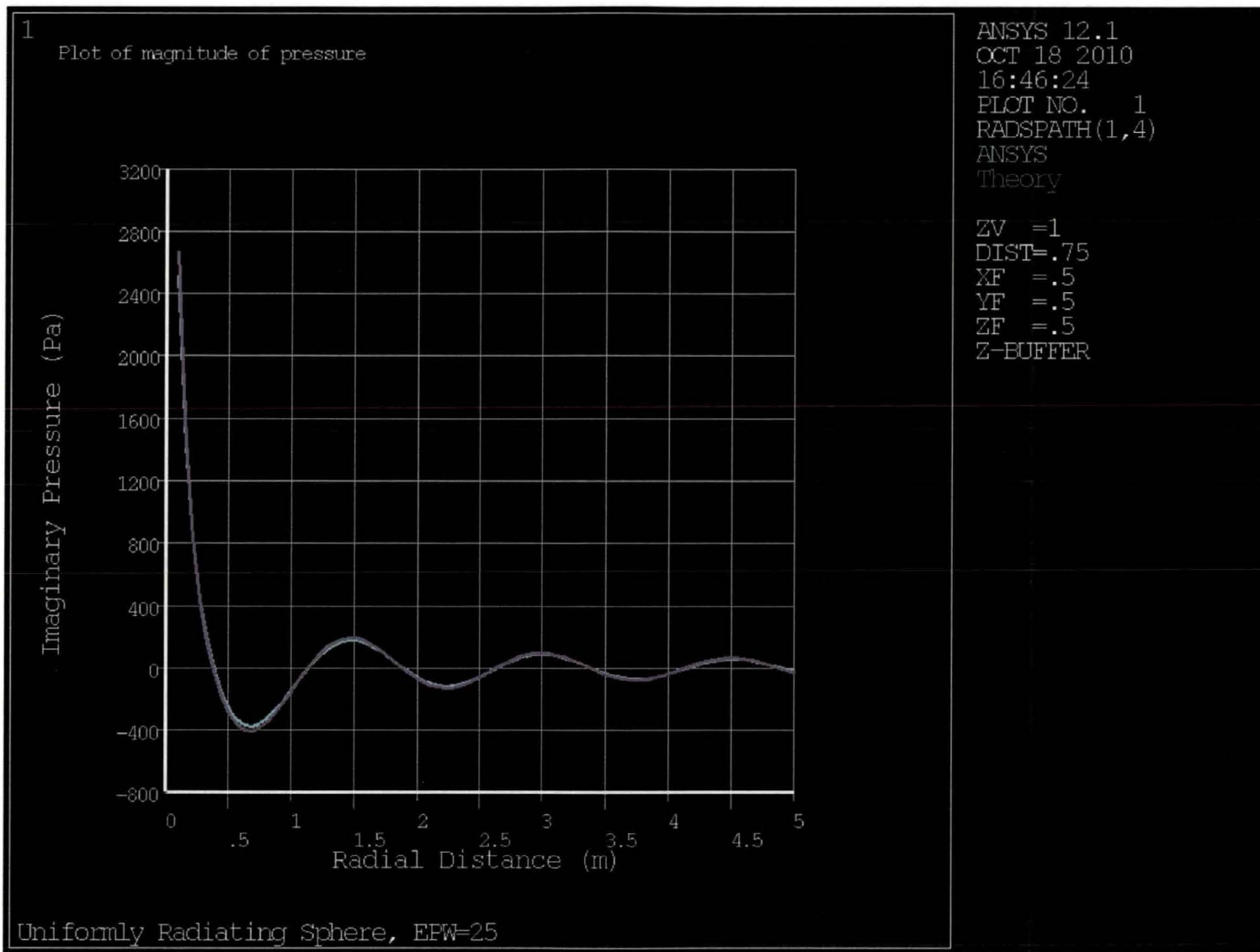


Figure 41. Steady State Imaginary Component of Pressure (Pa) as a Function of Radial Distance (m) Plot for 1,000 Hz with 25 Elements per Wavelength in Water

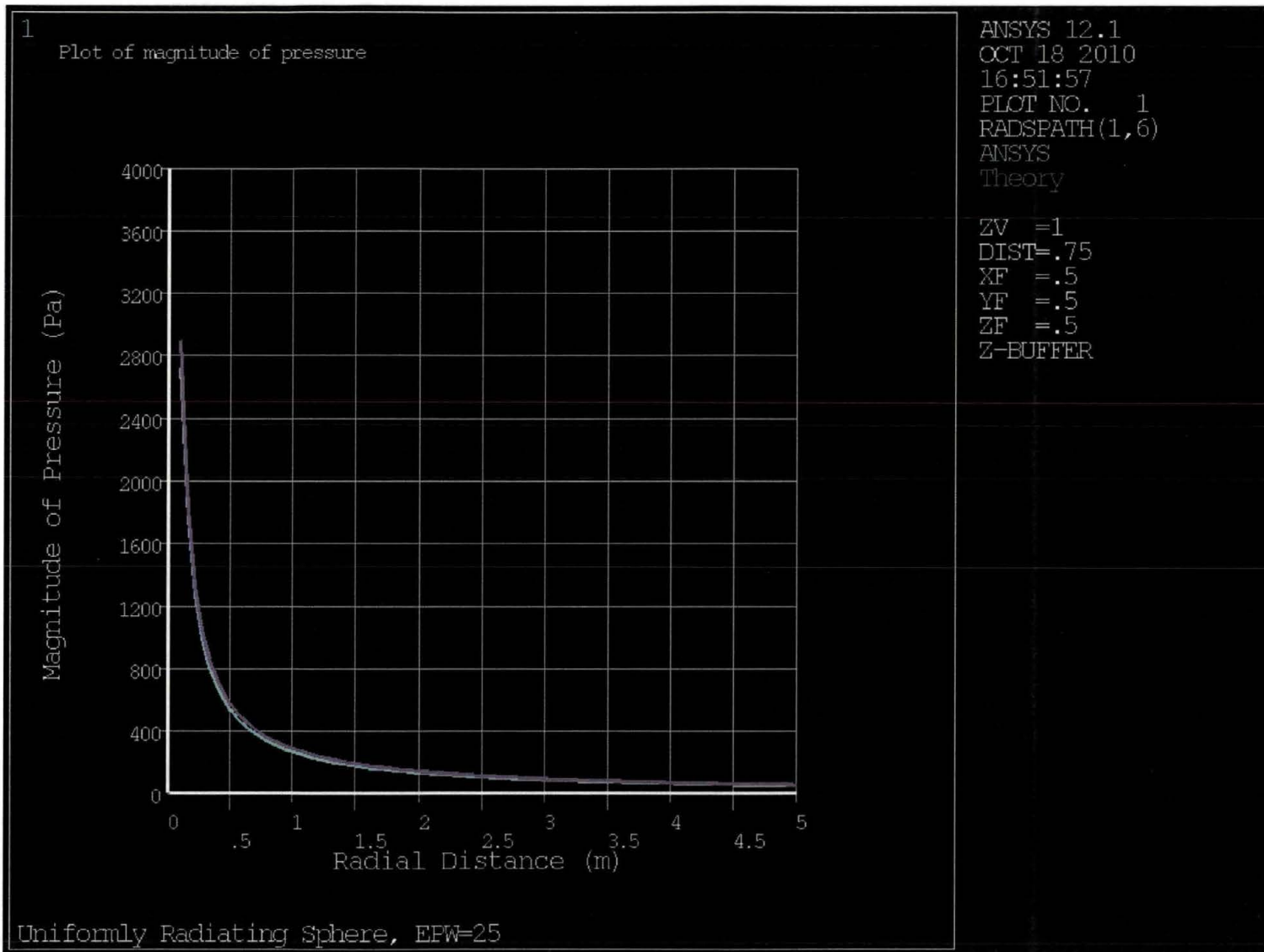


Figure 42. Steady State Magnitude of Pressure (Pa) as a Function of Radial Distance (m) Plot for 1,000 Hz with 25 Elements per Wavelength in Water

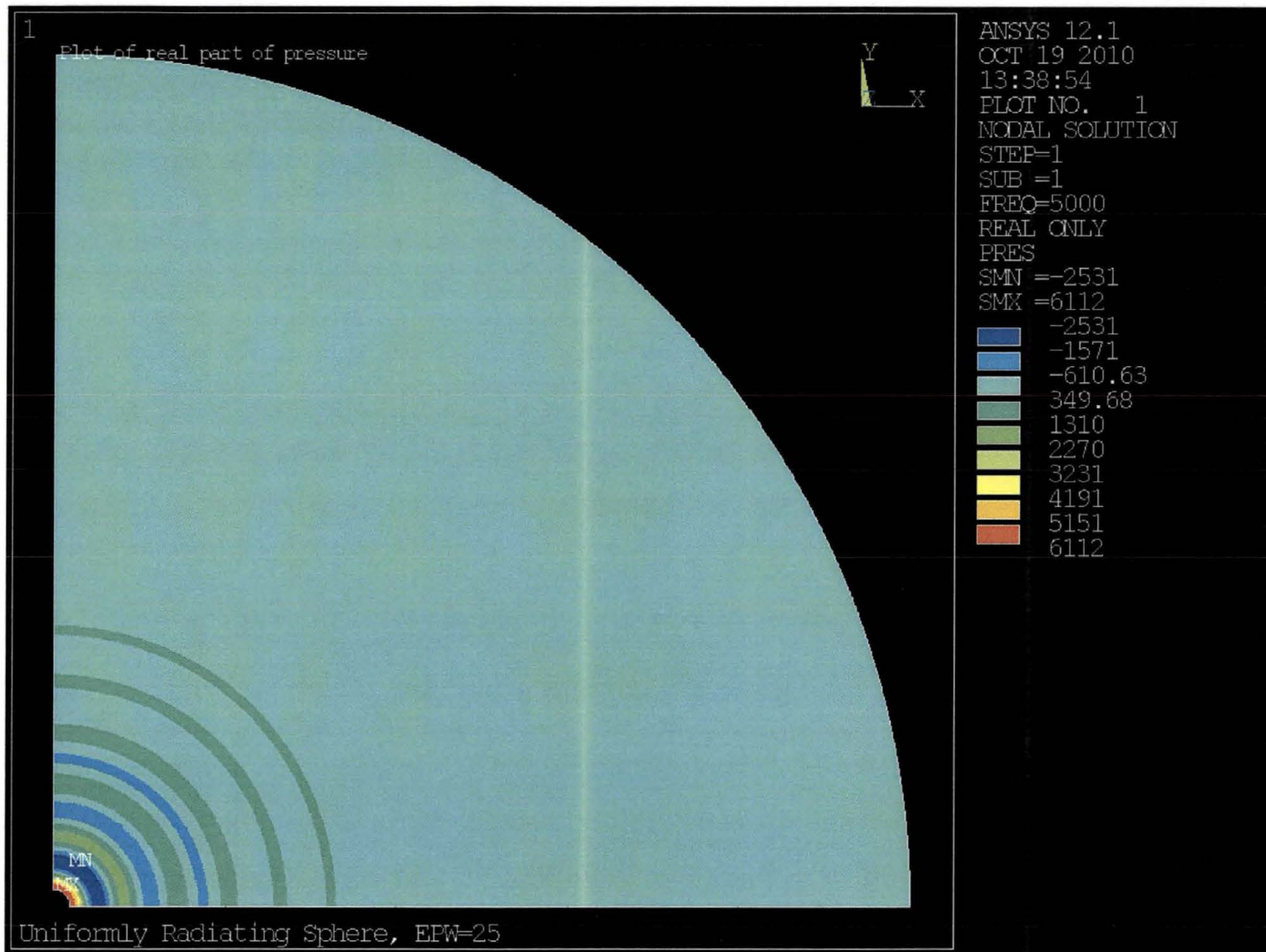


Figure 43. Contour Plot of Real Component of Pressure (Pa) for 5,000 Hz with 25 Elements per Wavelength in Water

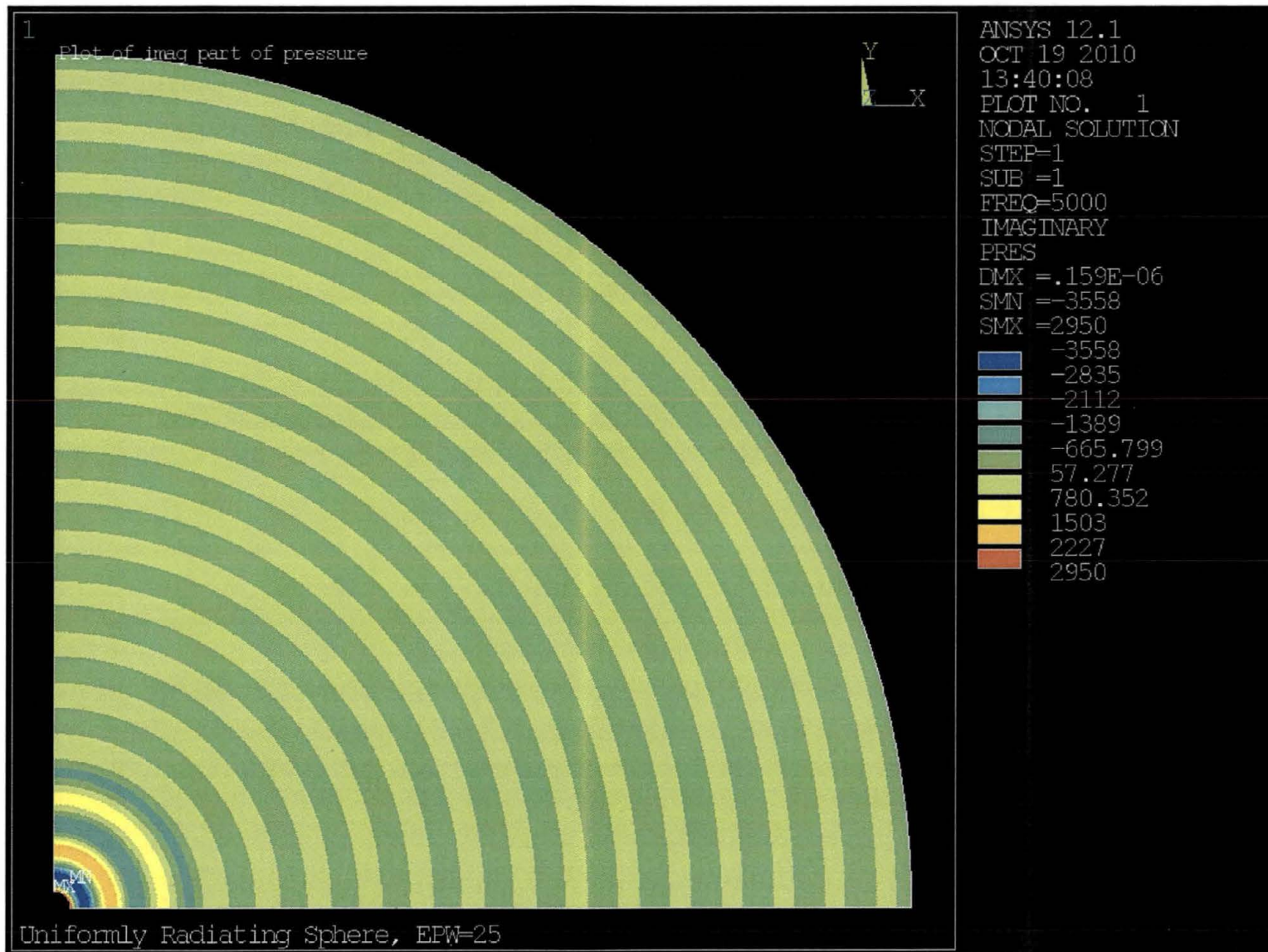


Figure 44. Contour Plot of Imaginary Component of Pressure (Pa) for 5,000 Hz with 25 Elements per Wavelength in Water

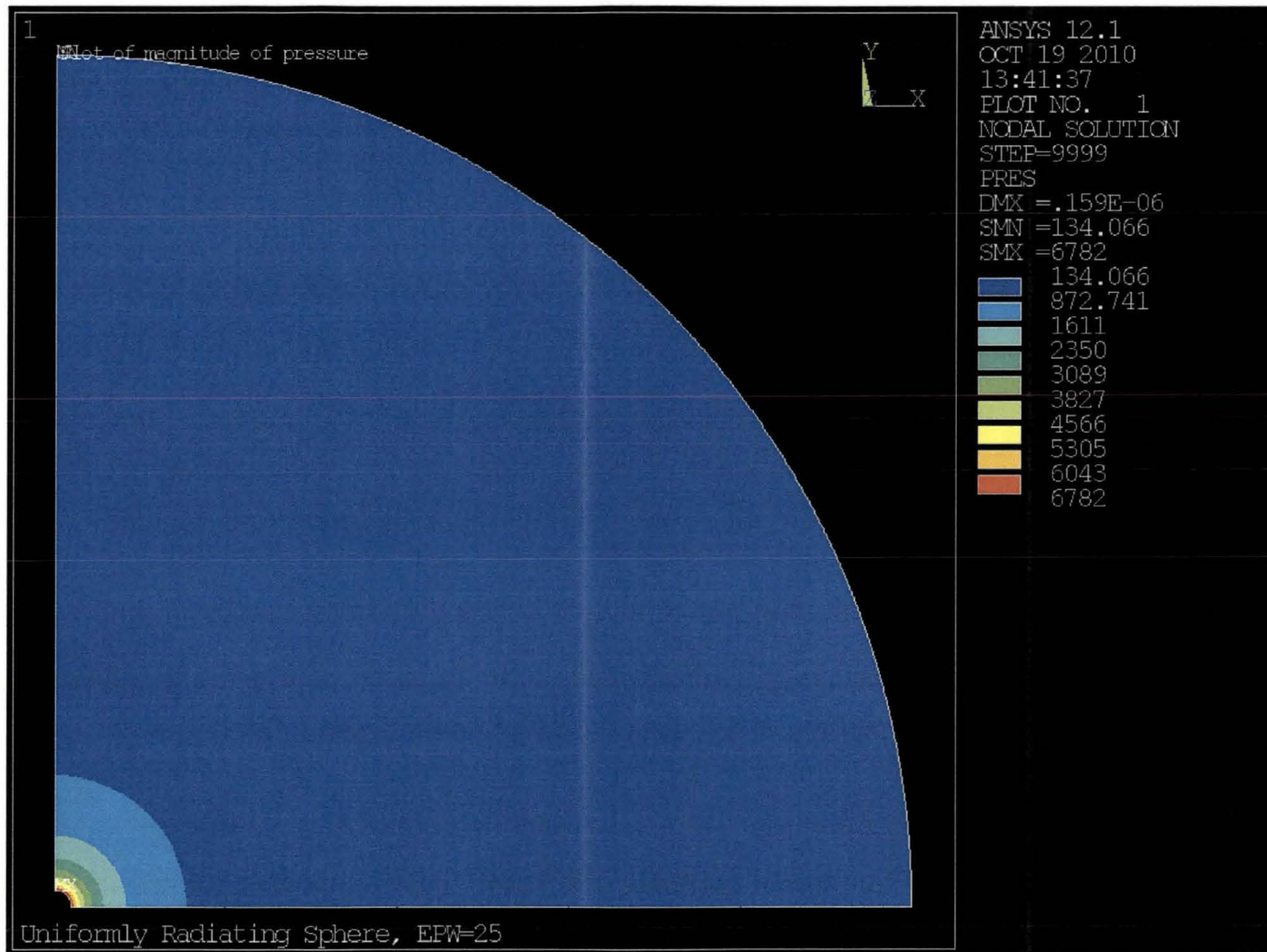


Figure 45. Contour Plot of the Magnitude of Pressure (Pa) for 5,000 Hz with 25 Elements per Wavelength in Water

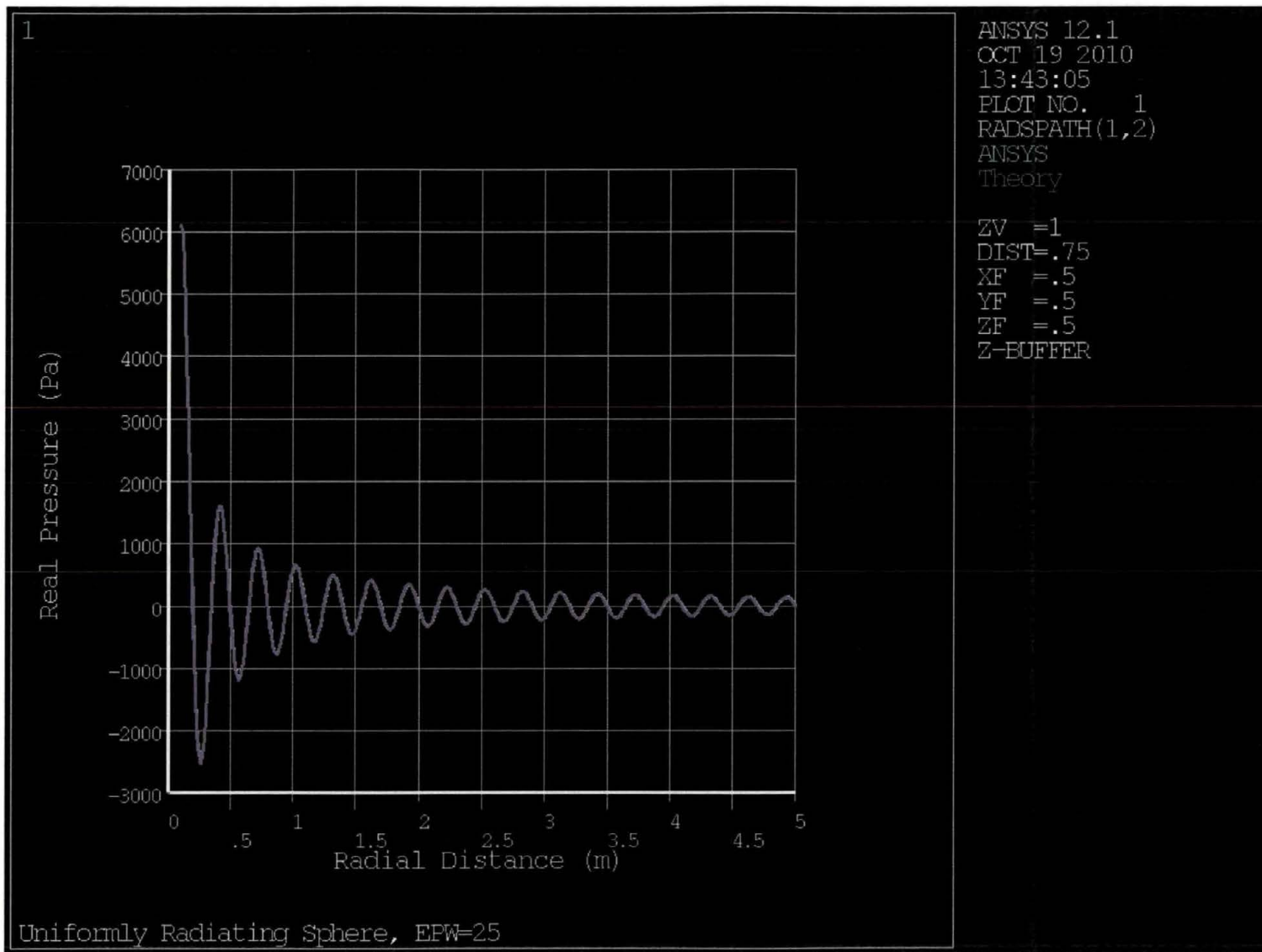


Figure 46. Steady State Real Component of Pressure (Pa) as a Function of Radial Distance (m) Plot for 5,000 Hz with 25 Elements per Wavelength in Water

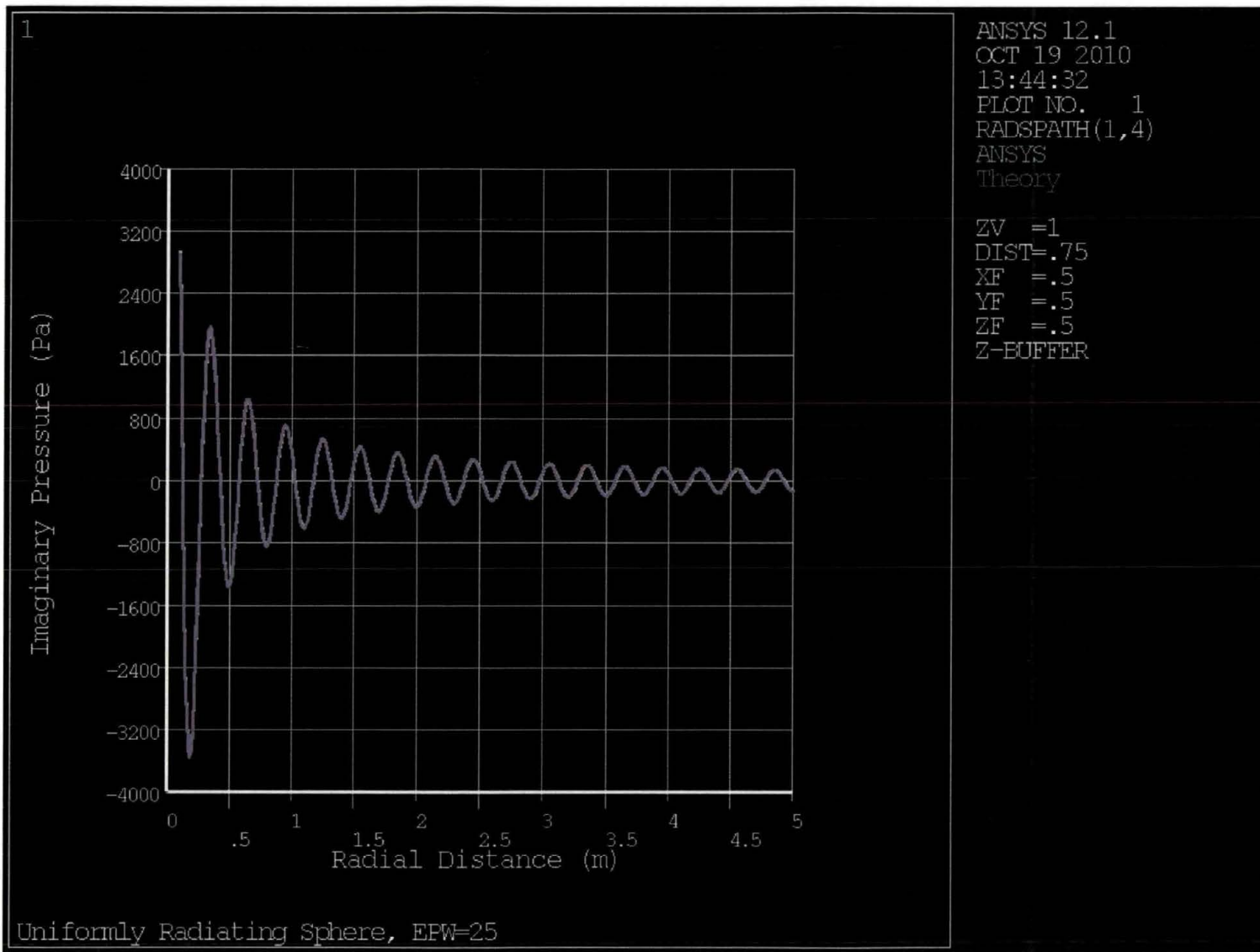


Figure 47. Steady State Imaginary Component of Pressure (Pa) as a Function of Radial Distance (m) Plot for 5,000 Hz with 25 Elements per Wavelength in Water

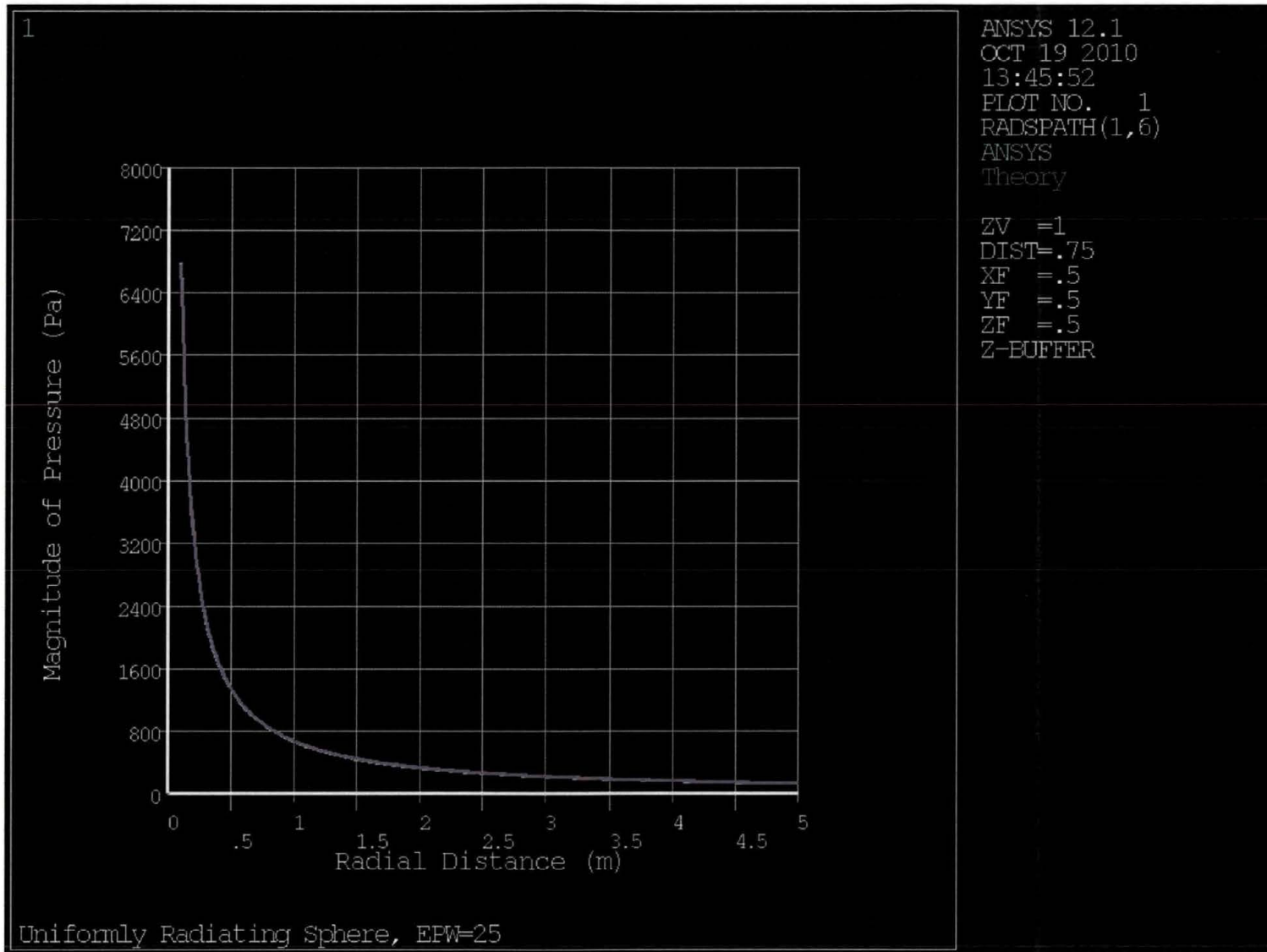


Figure 48. Steady State Magnitude of Pressure (Pa) as a Function of Radial Distance (m) Plot for 5,000 Hz with 25 Elements per Wavelength in Water

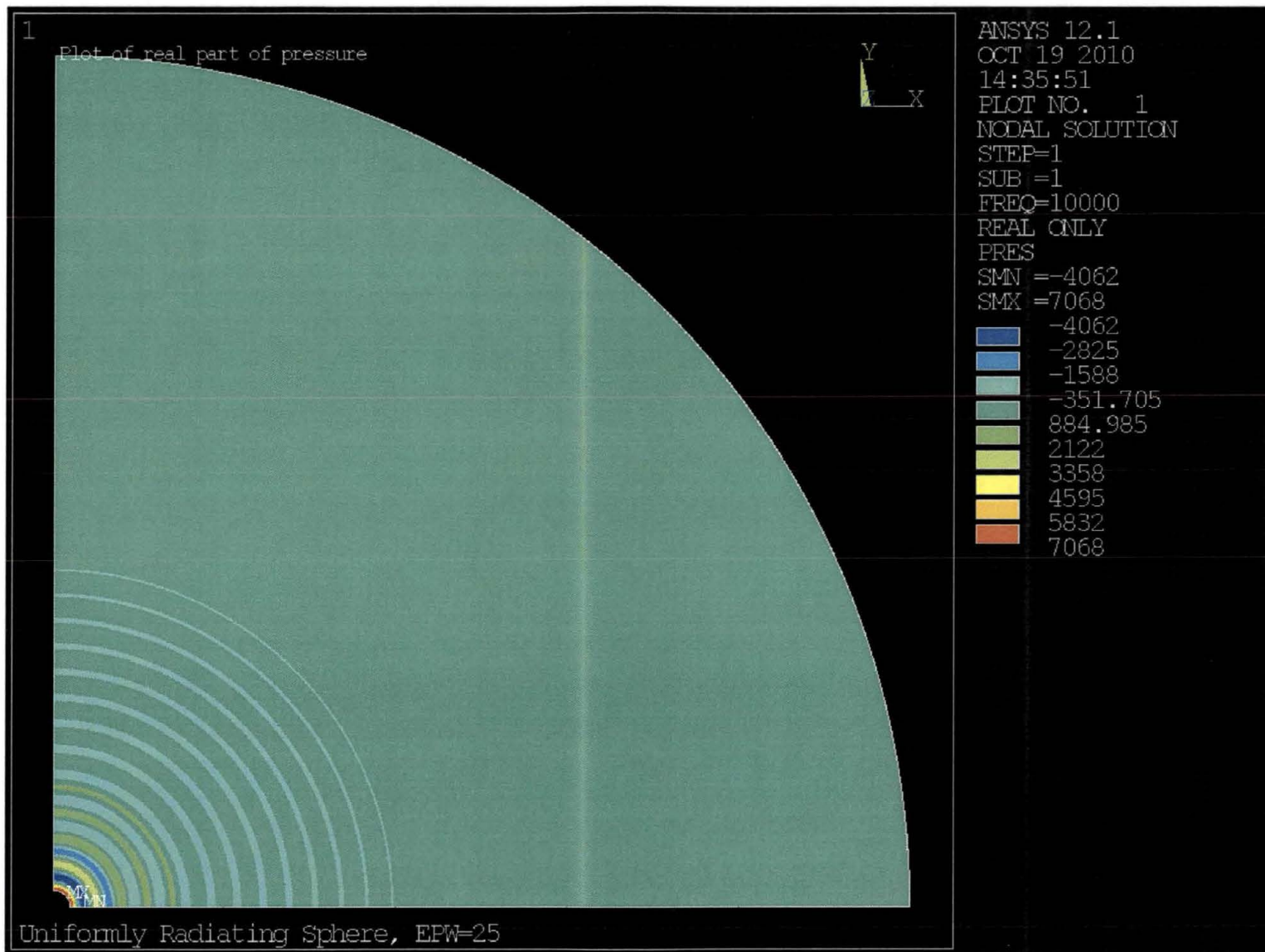


Figure 49. Contour Plot of Real Component of Pressure (Pa) for 10,000 Hz with 25 Elements per Wavelength in Water

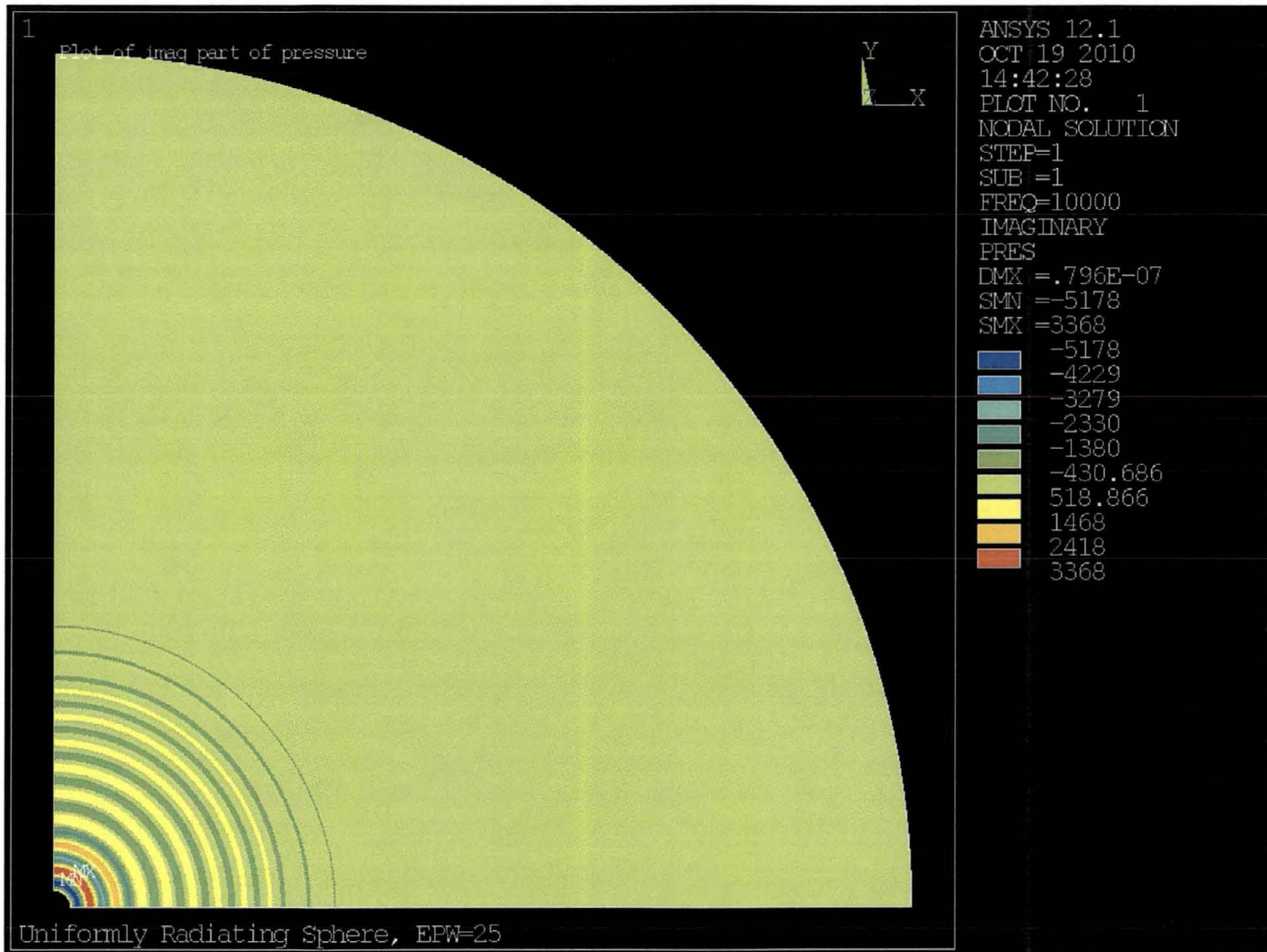


Figure 50. Contour Plot of Imaginary Component of Pressure (Pa) for 10,000 Hz with 25 Elements per Wavelength in Water

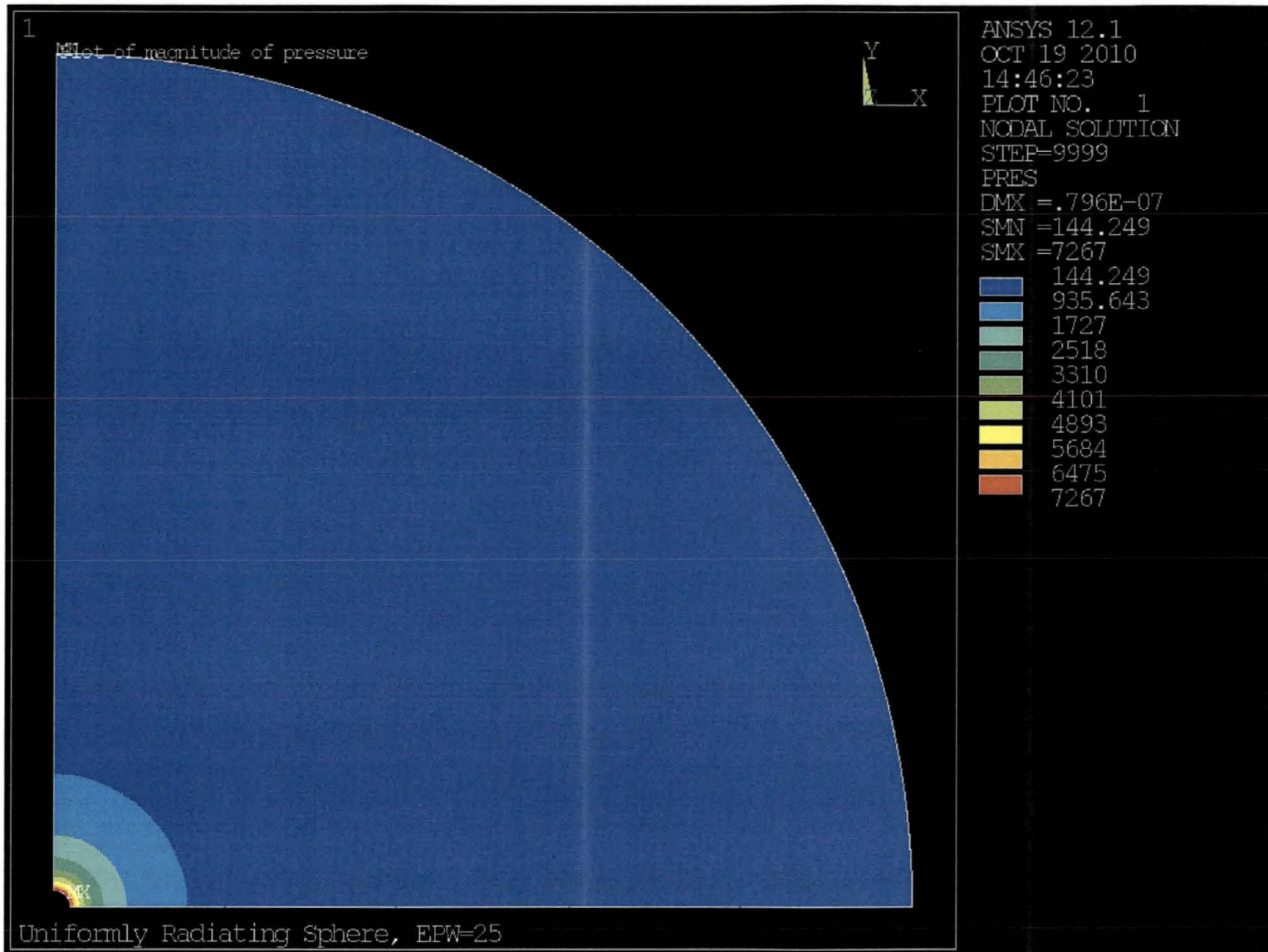


Figure 51. Contour Plot of the Magnitude of Pressure (Pa) for 10,000 Hz with 25 Elements per Wavelength in Water

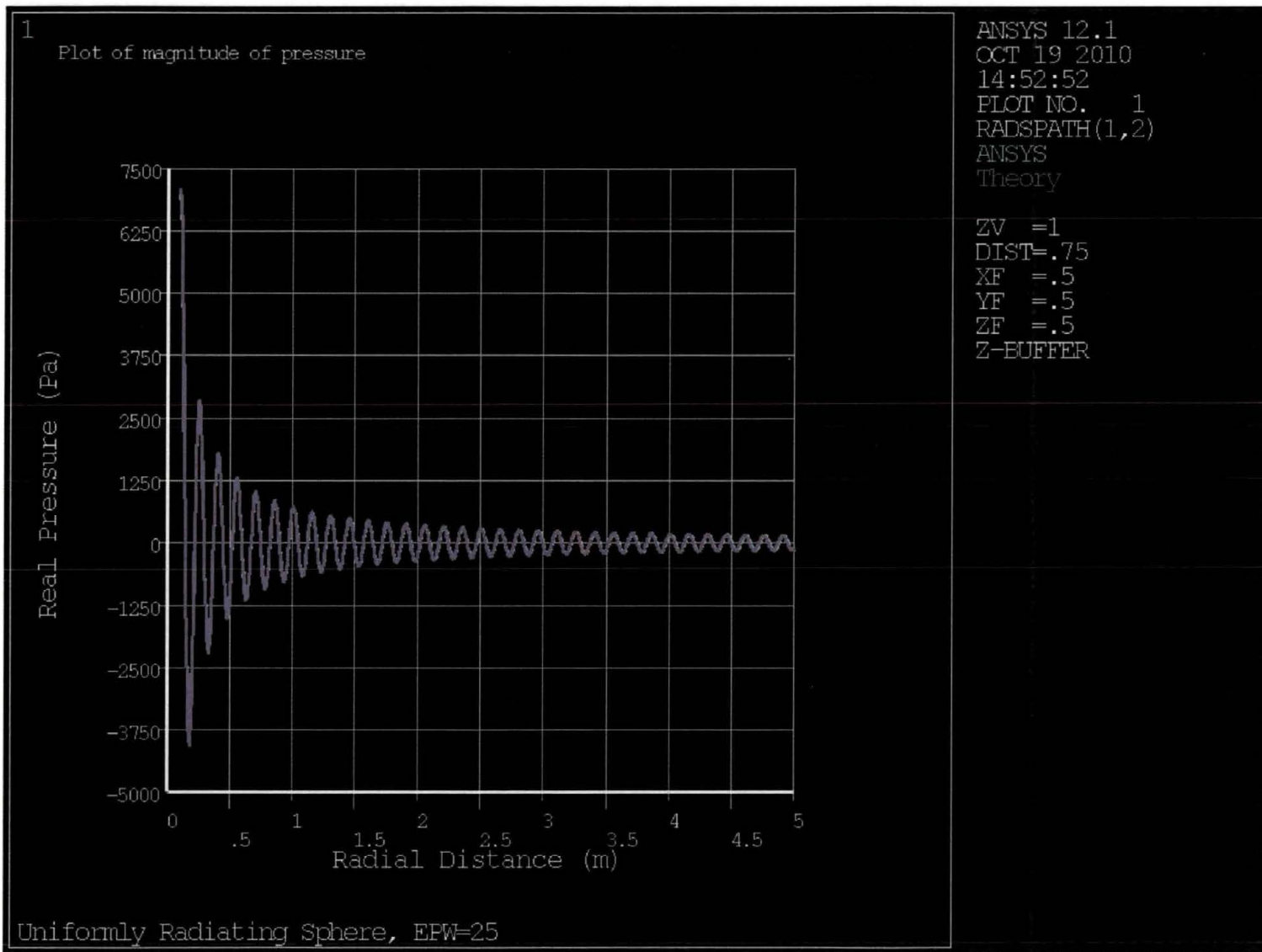


Figure 52. Steady State Real Component of Pressure (Pa) as a Function of Radial Distance (m) Plot for 10,000 Hz with 25 Elements per Wavelength in Water

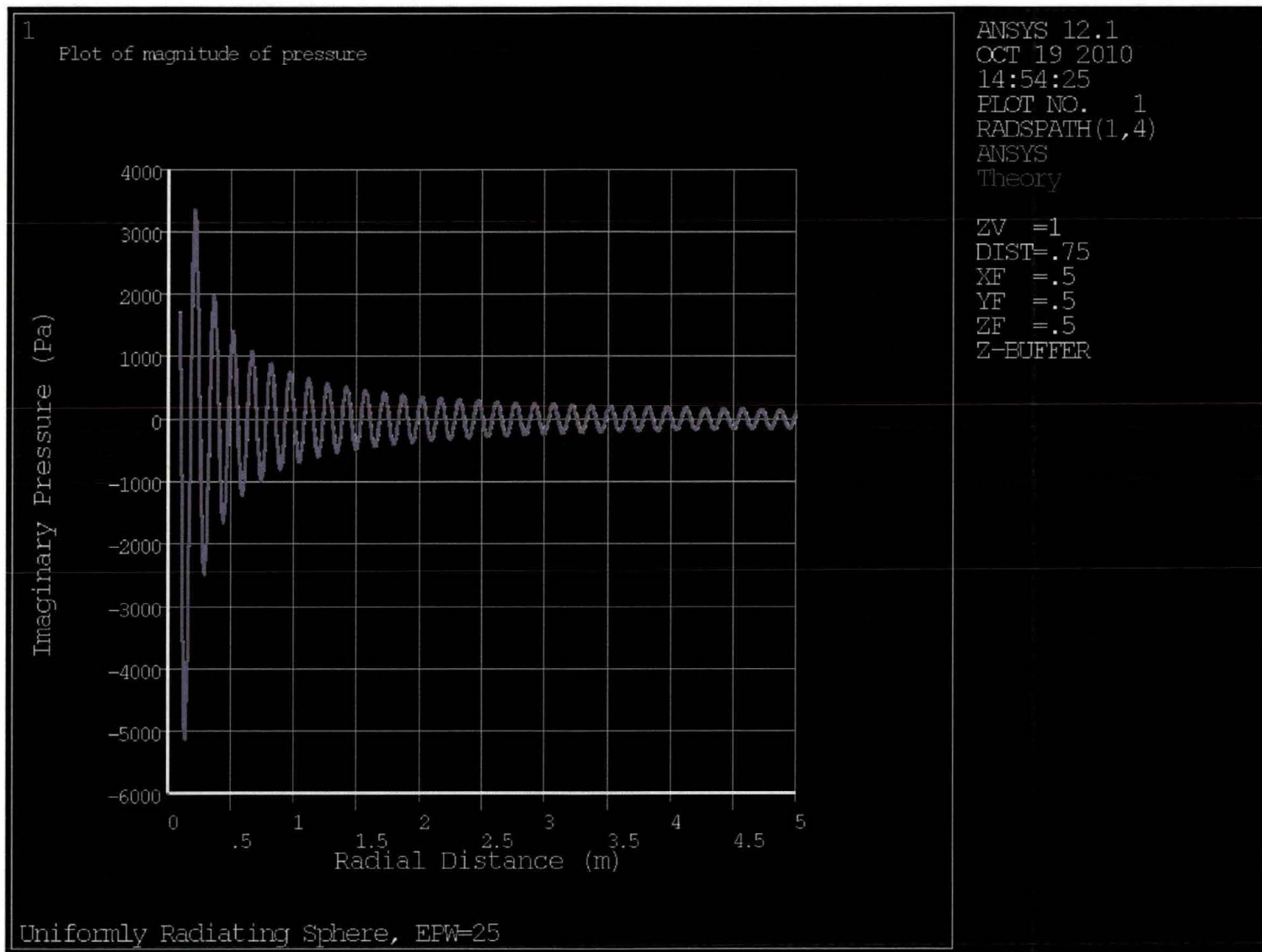


Figure 53. Steady State Imaginary Component of Pressure (Pa) as a Function of Radial Distance (m) Plot for 10,000 Hz with 25 Elements per Wavelength in Water

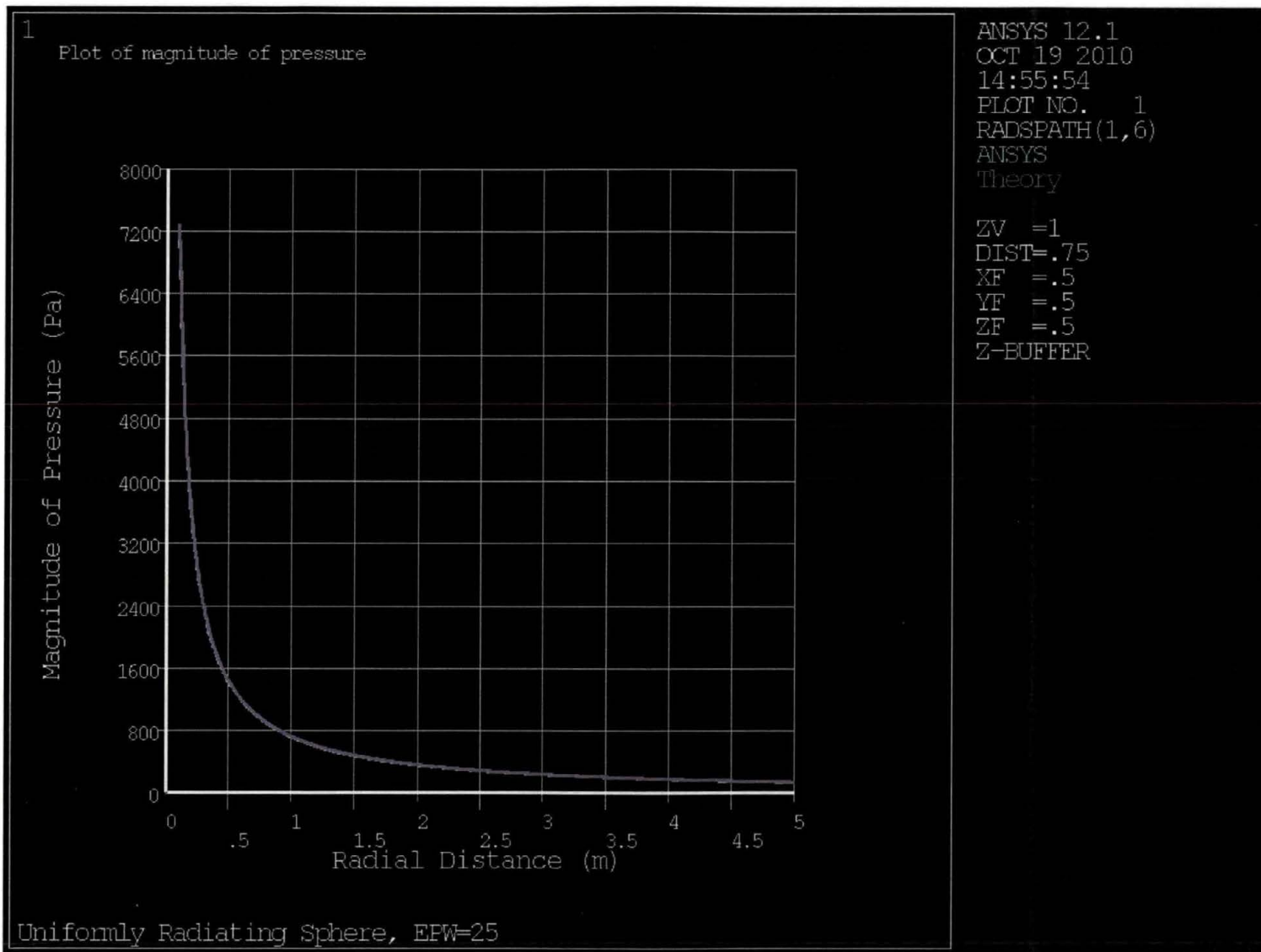


Figure 54. Steady State Magnitude of Pressure (Pa) as a Function of Radial Distance (m) Plot for 10,000 Hz with 25 Elements per Wavelength in Water

4.2.1.1 Summary and Conclusions of Acoustic Analyses

A successful analysis of a USO was conducted using a full harmonic acoustics simulation. The plots of the real and imaginary values showed good agreement with the expected theoretical solutions. It may be concluded from the contour plots and graphs that the varying frequencies produce acoustics pressures far out from the actual source and decline in an inverse square law relationship. In the future, ships and submarines could possibly detect these pressure disturbances and a frequency of the mode of operation could be calculated with a known distance from the vessel.

4.2.2 ANSYS Multiphysics Electromagnetic Capabilities

The electromagnetic capabilities of ANSYS Multiphysics include a full-wave electromagnetic solver applicable to resonant, propagating, radiation and scattering phenomena in the frequency domain. RF or microwave passive components, antennas, attenuators, interconnects and related high frequency structures may be modeled for use in applications of stealth, electronic warfare and directed high energy applications. Post-processing calculations provide electric and magnetic field intensity, quality factor, scattering matrix parameters, voltage, current, characteristic impedance, radar cross section, far and near electromagnetic fields beyond the modeled domain, antenna patterns, including period structures, and Joule losses (ANSYS, Inc., 2009). Magneto hydrodynamics may also be modeled in development of propulsion units and power generation, electron beam dynamics and electrical discharges. The Maxwell Equations below provide the basis for electromagnetic calculations.

$$\nabla \cdot \mathbf{D} = \rho_e$$

$$\nabla \times \mathbf{H} = \mathbf{J} + \frac{\partial \mathbf{D}}{\partial t}$$

$$\nabla \times \mathbf{E} = -\frac{\partial \mathbf{B}}{\partial t}$$

$$\nabla \cdot \mathbf{B} = 0$$

where:

B – magnetic induction field (tesla)

D – displacement field (C/m²)

E – electric field (V/m)

H – magnetic field (A/m)

J – current density

ρ_e – charge density

4.2.3 Radar Cross Section Analysis of a Spherical UFO

Many UAP have been reported across the globe. Pilots have reported seeing these craft in the air, but when asked for confirmation of other aircraft in the area, air traffic control reports nothing on radar.

Only a tiny fraction of energy is bounced back to the receiving antenna, even though many megawatts of power may be transmitted in a single pulse. The amount of power returned from a target to the transmitting radar depends on four major factors:

1. The power transmitted in the direction of the target.
2. The amount of power that impacts the target and is reflected back in the direction of the antenna. This is directly relational to the range between the antenna and target and the target's RCS.
3. The amount of reflected power that is received by the antenna.
4. The length of time in which the antenna is pointed at the target.

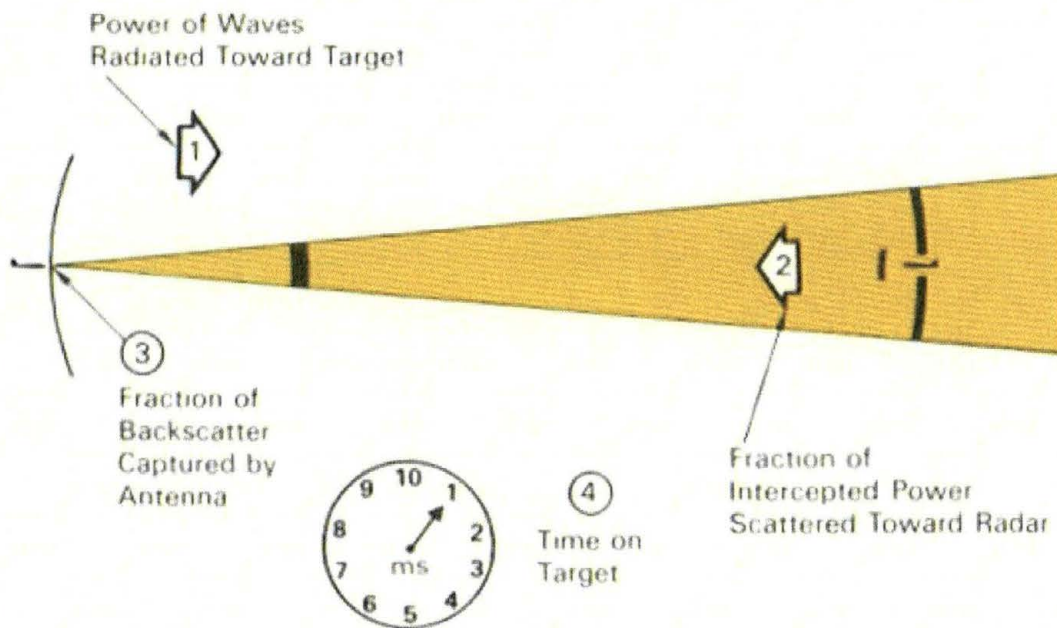


Figure 55. Factors that Determine the Energy Returned by a Target (Aerospaceweb.org , 2010)

Power flux is used to describe the relationship between these variables. The further the radar wave travels, the greater the power transmitted decrease because it is spread over a larger area. The inverse square law of the range R or $1/R^2$ governs the area over which the power is spread from the transmitting radar. The power flux or power density of the transmitted radar wave at the range of the target has a special name called the incident power density (P_{incident}).

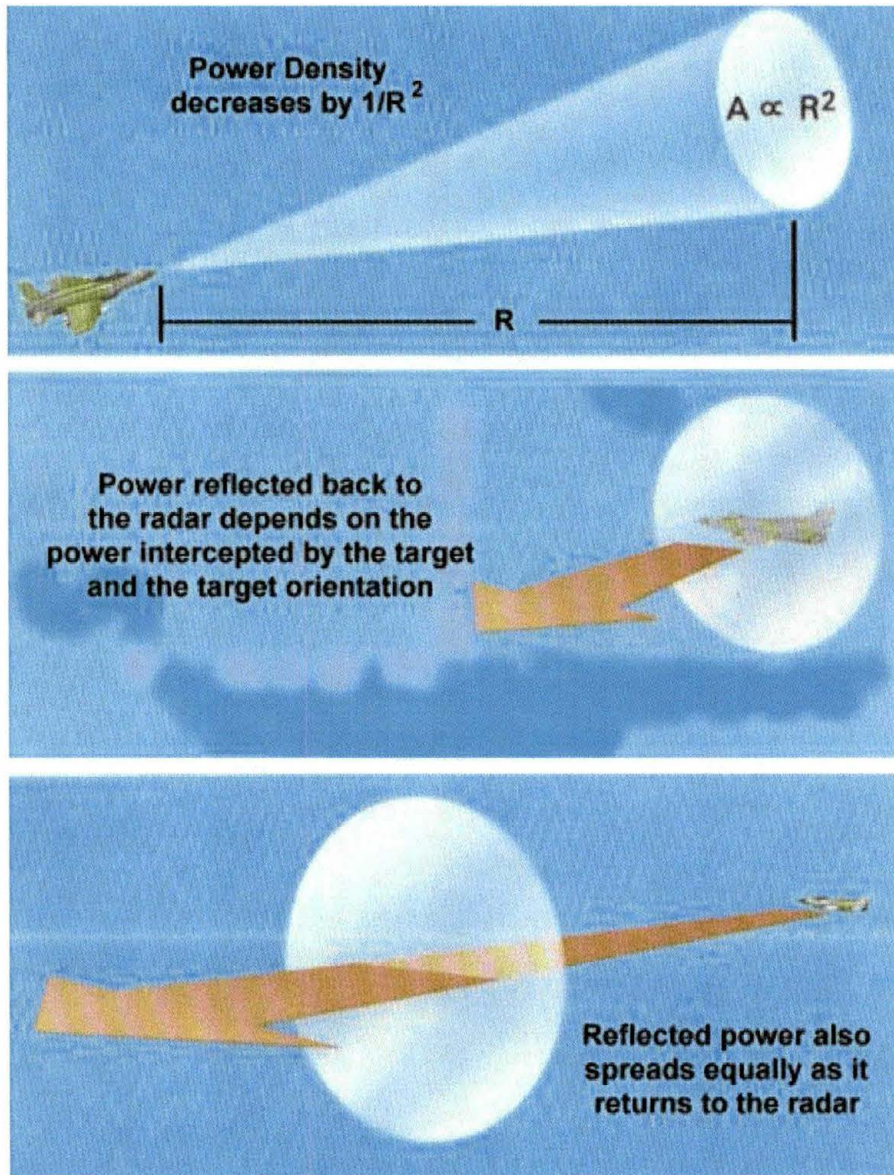


Figure 56. Effect of Distance from the radar to the Target on the Power Density (Aerospaceweb.org , 2010)

When the radar wave reaches the target, a portion is reflected back to the antenna. In addition, the reflected power also dissipates at $1/R^2$ therefore it is reduced by a factor of $1/R^4$ roundtrip by the time it is returned to the antenna. The ability of a radar system to detect a target depends on whether the amount of power returned is great enough to be differentiated from internal noise, ground clutter, background radiation, and other sources of interference. This is defined as the signal to noise ratio. The object of stealth is to absorb or reflect waves away from receiving antenna and/or jam or propagate a false wave back to its source so that the target is nearly impossible to detect or track.

The amount of power that is reflected back to the radar depends largely on a quantity called the radar cross section (RCS). RCS (σ) is technically an area and typically expressed in square meters (m^2) and depends on the following three factors:

Geometric cross section:

The area of the object presented to the antenna or projected area is known as the geometric cross section. The area varies depending on the angle, or aspect, seen by the radar. The geometric cross section (A) determines how much power transmitted by the radar ($P_{incident}$) is intercepted by the target ($P_{intercepted}$) according to the following equation:

$$P_{intercepted} = AP_{incident}$$

Reflectivity:

The reflectivity is the fraction of the intercepted power that is reflected by the target, regardless of direction. An object doesn't always reflect equally from all directions as some parts are flat or curved producing varying radar reflection and some of the power is absorbed by the object. Objects that have radar Absorbent Materials (RAM) and radar Absorbent Structures (RAS) are designed using internal reflectors to trap incoming radar waves. The power received by the antenna after scattering or reflecting off the target is equal to the intercepted power less whatever portion of that power is absorbed by the target. The reflectivity is the ratio of power scattered by the target ($P_{scatter}$) to the power intercepted by the target ($P_{intercepted}$).

$$Reflectivity = \frac{P_{scatter}}{AP_{intercepted}}$$

Directivity:

The directivity is related to reflectivity but refers to the power scattered back in the direction of the receiving antenna. The power that is reflected toward the antenna is called the backscattered power ($P_{backscatter}$). Directivity is the ratio of the power that is backscattered in the direction of the antenna to the power that would have been scattered in that direction if the scattering were in fact uniform in all directions. Isotropic power ($P_{isotropic}$) is the power scattered in a perfect sphere over a unit solid angle of that sphere.

$$Directivity = \frac{P_{backscatter}}{P_{isotropic}} = \frac{P_{backscatter}}{\frac{1}{4\pi} P_{scatter}}$$

The reflected power will be much greater or much smaller than the isotropic power depending on how the target is oriented to the transmitting antenna. The directivity, therefore, will be much greater than 1 when the target returns a strong backscatter in the direction of the receiving antenna and much less than 1 when the backscatter is small.

These three factors can be combined to determine the complete RCS (σ) for a target.

$RCS = \sigma = \text{Geometric Cross Section} \times \text{Reflectivity} \times \text{Directivity}$

$$\sigma = 4\pi \frac{P_{backscatter}}{P_{intercepted}}$$

The importance of RCS can best be understood by looking at an equation relating the RCS of the target to the energy received by the antenna.

$$S \cong \frac{P_{avg} G \sigma A_e t_{ot}}{(4\pi)^2 R^4}$$

where

S = signal energy received by the radar

P_{avg} = average power transmitted by the radar

G = gain of the radar antenna

σ = RCS

A_e = effective area of the radar antenna, or "aperture efficiency"

t_{ot} = time the radar antenna is pointed at the target (time on target)

R = range to the target

Figure 57 shows a target that presents the same aspect to the radar at ranges from 1 to 50 miles. At a range of 50 miles, the relative power received by the radar is only 0.00000016, or 1.6×10^{-7} % of the strength at one mile. This diagram graphically illustrates how significant the effect of energy dissipation is with distance, and how sensitive radars must be to detect targets at even short ranges.

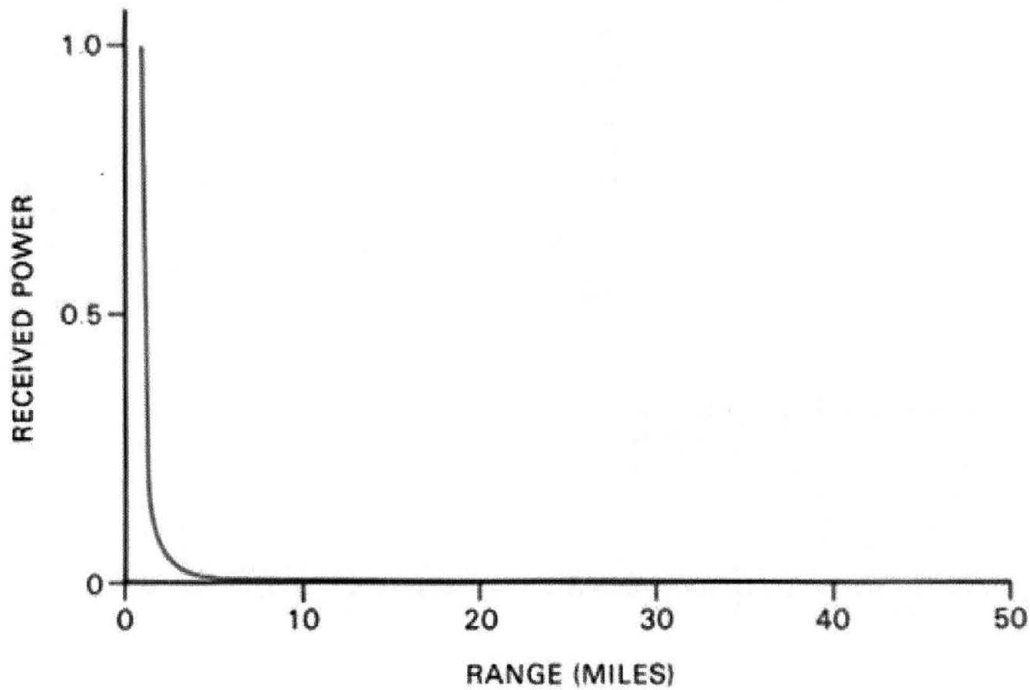


Figure 57. Reduction in the Strength of Target Echoes with Range (Aerospaceweb.org , 2010)

Furthermore, every radar system has a minimum signal energy it can detect, a quantity called S_{\min} . This minimum signal energy along with antenna design and scan rate determine the maximum range (R_{\max}) at which a given radar can detect a given target.

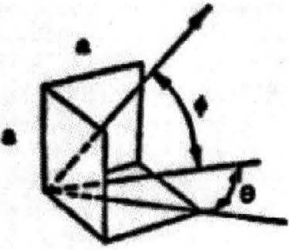
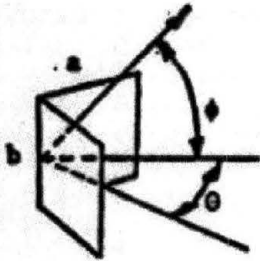
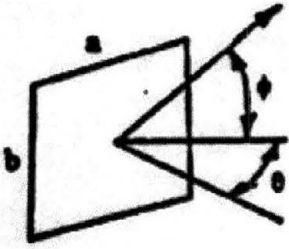
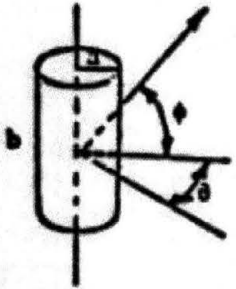
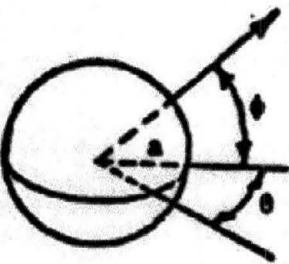
Geometry	Description	Maximum RCS	Comments
	Square trihedral corner reflector	$\sigma = \frac{12\pi a^4}{\lambda^2}$	Strongest radar return due to triple reflection of incident wave
	Right dihedral corner reflector	$\sigma = \frac{8\pi a^2 b^2}{\lambda^2}$	Second strongest radar return due to double reflection of incident wave; decreases from maximum slowly with changing θ and rapidly with changing ϕ
	Flat plate	$\sigma = \frac{4\pi a^2 b^2}{\lambda^2}$	Third strongest radar return due to direct reflection of incident wave; decreases rapidly as incidence angle changes from perpendicular
	Right circular cylinder	$\sigma = \frac{2\pi a b^2}{\lambda}$	Strong radar return as aspect (θ) changes, but decreases rapidly as azimuth (ϕ) changes
	Sphere	$\sigma = \pi a^2$	Produces the same isotropic return in all directions

Figure 58. Geometry, Description and Maximum RCS(Aerospaceweb.org , 2010)

RCS in square meters can be converted to dBsm by the following equation.

$$dBsm = 10\text{Log}(RCS_{m^2})$$

It can be difficult to directly compare RCS estimates from one object to another since the RCS varies wildly depending on aspect, radar frequency and wavelength, and the fidelity of the receiver. Figure 59 illustrates typical RCS values for aircraft and other objects, ranging from insects and birds up to large ground vehicles and ships. The RCS of a stealth aircraft is typically multiple orders of magnitude lower than a conventional plane and is often comparable to that of a small bird or large insect.

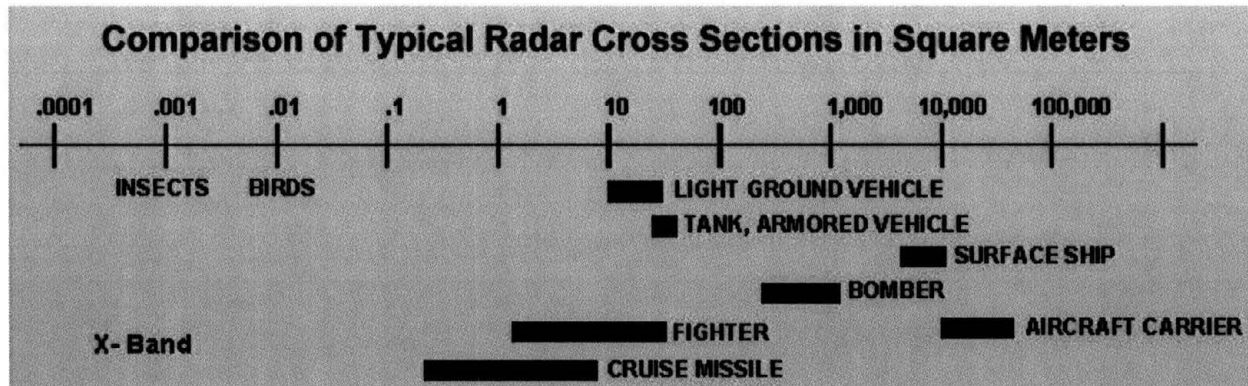


Figure 59. Radar Cross Section Comparison (Aerospaceweb.org , 2010)

A one-half symmetry analysis of the radar cross section of a UAP sphere with a dielectric coating was performed. Assuming the bottom limit of an ultrahigh frequency (UHF) very long range radar system is 300 MHz, a full scale RCS full harmonic analysis was performed to study a spherical object of 10 m in air with a 1 m dielectric coating layer. Provided in Figure 64 is a contour plot for the electric field distribution.

Figure 60 and Figure 61 show the FEA mesh for 25 elements per wavelength and 50 elements per wavelength for a 300 MHz RCS analysis.

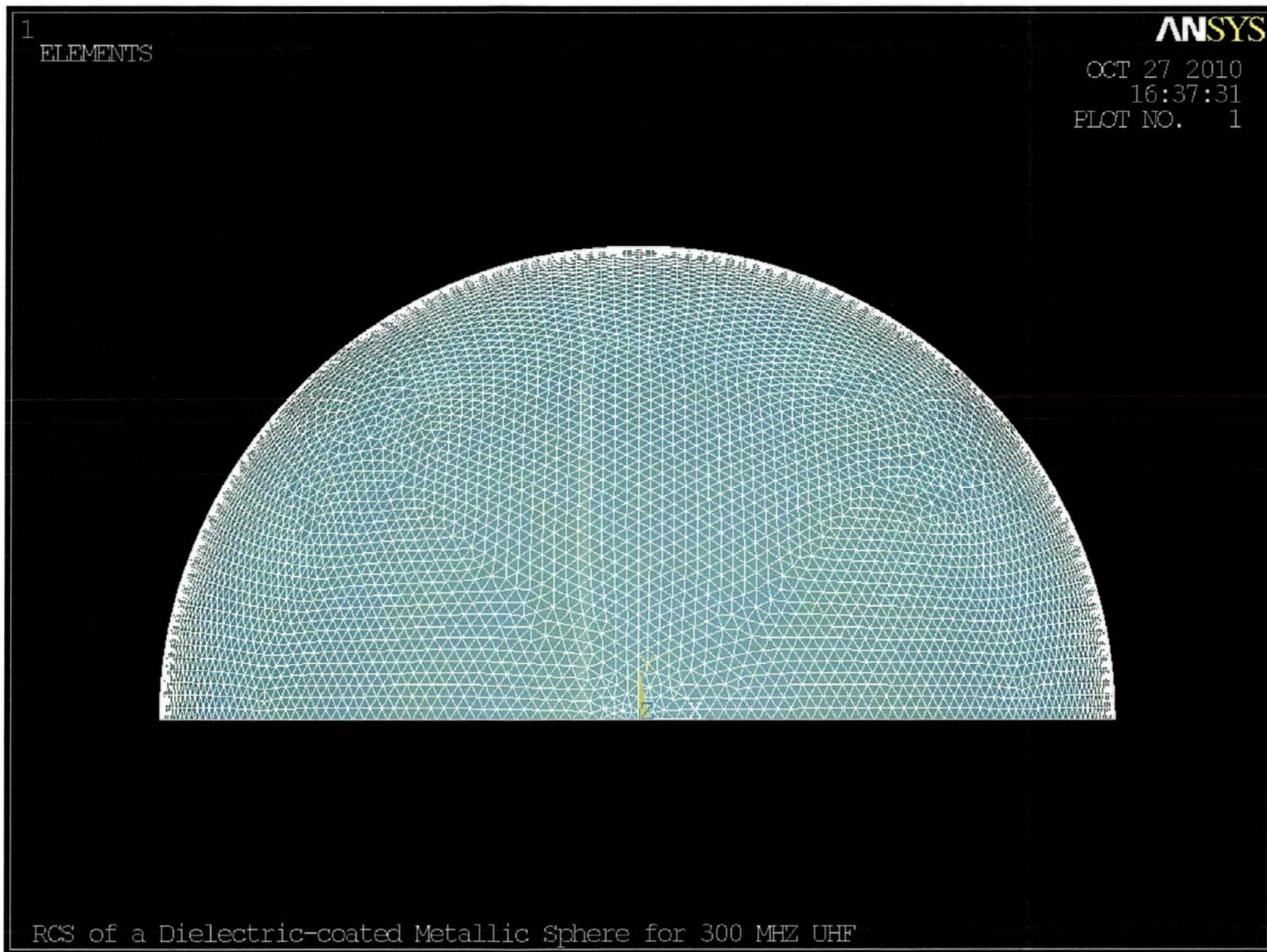


Figure 60. Mesh of 1/2 Symmetry UFO Sphere with 25 Elements per Wavelength



Figure 61. Mesh of 1/2 Symmetry UFO Sphere with 50 Elements per Wavelength

Table 4. Normalized radar Cross Section for a 10 m Metallic Sphere with a 1 m Dielectric Coating in Decibels for 300 MHz and 25 Elements per Wavelength

PHI (Deg)	THETA (Deg)	Normalized RCS (dB)
0.000	0.000	-0.17461E+01
0.000	5.000	-0.18396E+01
0.000	10.000	-0.20891E+01
0.000	15.000	-0.24059E+01
0.000	20.000	-0.26306E+01
0.000	25.000	-0.25683E+01
0.000	30.000	-0.21056E+01
0.000	35.000	-0.13090E+01
0.000	40.000	-0.36528E+00
0.000	45.000	0.54501E+00
0.000	50.000	0.13011E+01
0.000	55.000	0.18315E+01
0.000	60.000	0.20883E+01
0.000	65.000	0.20270E+01
0.000	70.000	0.15903E+01
0.000	75.000	0.69095E+00
0.000	80.000	-0.81414E+00
0.000	85.000	-0.31541E+01
0.000	90.000	-0.64801E+01
0.000	95.000	-0.85723E+01
0.000	100.000	-0.54262E+01
0.000	105.000	-0.16586E+01
0.000	110.000	0.10839E+01
0.000	115.000	0.29983E+01
0.000	120.000	0.43027E+01
0.000	125.000	0.51444E+01
0.000	130.000	0.56415E+01
0.000	135.000	0.59202E+01
0.000	140.000	0.61375E+01
0.000	145.000	0.64662E+01
0.000	150.000	0.70226E+01
0.000	155.000	0.77921E+01
0.000	160.000	0.86493E+01
0.000	165.000	0.94471E+01
0.000	170.000	0.10076E+02
0.000	175.000	0.10474E+02
0.000	180.000	0.10609E+02

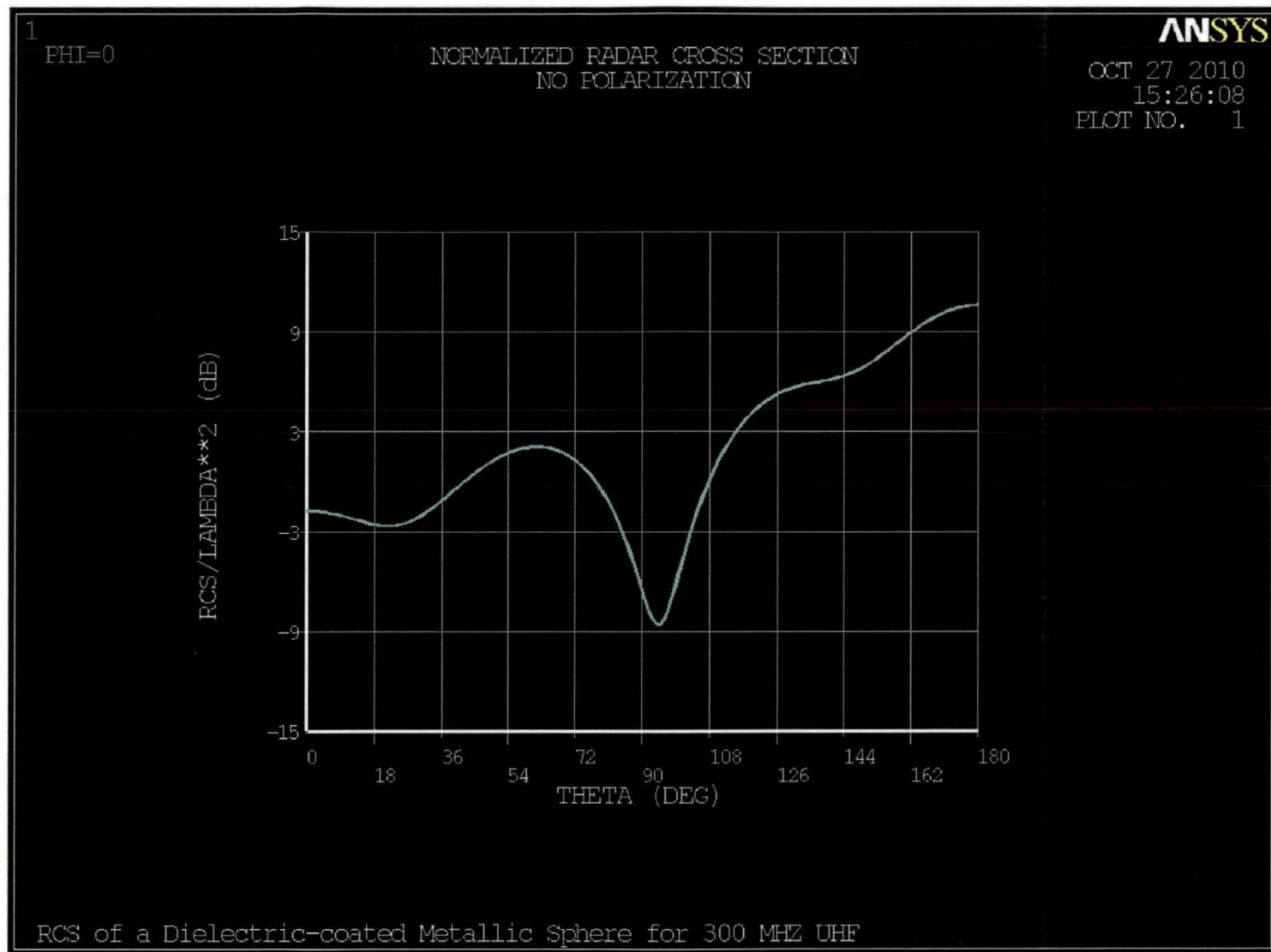


Figure 62. Normalized radar Cross Section Plot for a ½ Symmetry 10 m Metallic Sphere with a 1 m Dielectric Coating in Decibels for 300 MHz and 25 Elements per Wavelength

Table 5. Normalized radar Cross Section for a 10 m Metallic Sphere with a 1 m Dielectric Coating in Decibels for 300 MHz and 50 Elements per Wavelength

PHI (Deg)	THETA (Deg)	Normalized RCS (dB)
0.000	0.000	-0.13803E+01
0.000	5.000	-0.14503E+01
0.000	10.000	-0.16341E+01
0.000	15.000	-0.18535E+01
0.000	20.000	-0.19807E+01
0.000	25.000	-0.18742E+01
0.000	30.000	-0.14592E+01
0.000	35.000	-0.78502E+00
0.000	40.000	0.11714E-01
0.000	45.000	0.78777E+00
0.000	50.000	0.14360E+01
0.000	55.000	0.18849E+01
0.000	60.000	0.20821E+01
0.000	65.000	0.19780E+01
0.000	70.000	0.15109E+01
0.000	75.000	0.58974E+00
0.000	80.000	-0.93250E+00
0.000	85.000	-0.32902E+01
0.000	90.000	-0.66390E+01
0.000	95.000	-0.87047E+01
0.000	100.000	-0.54874E+01
0.000	105.000	-0.17016E+01
0.000	110.000	0.10488E+01
0.000	115.000	0.29700E+01
0.000	120.000	0.42801E+01
0.000	125.000	0.51239E+01
0.000	130.000	0.56159E+01
0.000	135.000	0.58773E+01
0.000	140.000	0.60608E+01
0.000	145.000	0.63411E+01
0.000	150.000	0.68464E+01
0.000	155.000	0.75769E+01
0.000	160.000	0.84125E+01
0.000	165.000	0.92021E+01
0.000	170.000	0.98300E+01
0.000	175.000	0.10228E+02
0.000	180.000	0.10364E+02

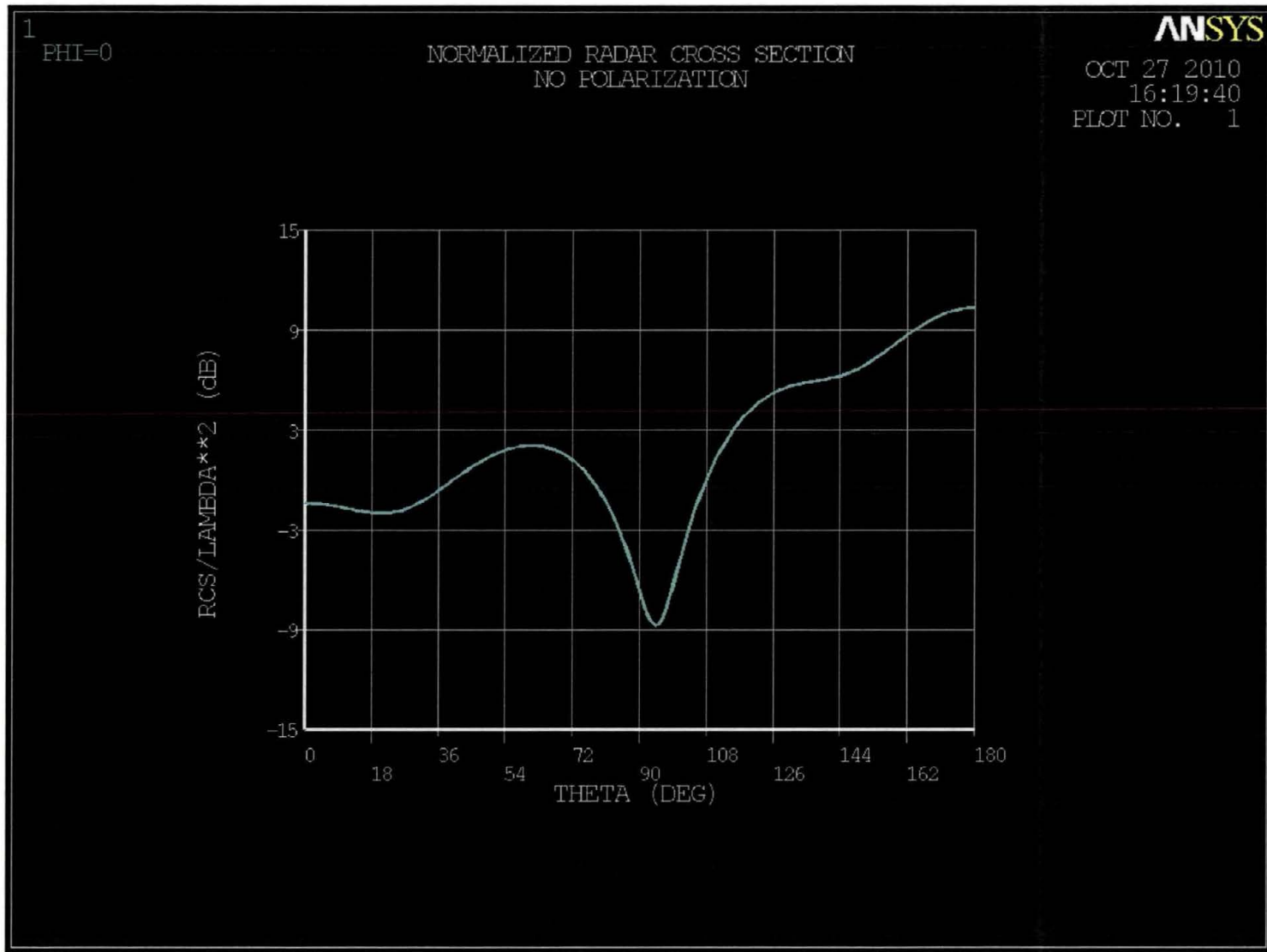


Figure 63. Normalized radar Cross Section Plot for a ½ Symmetry 10 m Metallic Sphere with a 1 m Dielectric Coating in Decibels for 300 MHz and 50 Elements per Wavelength

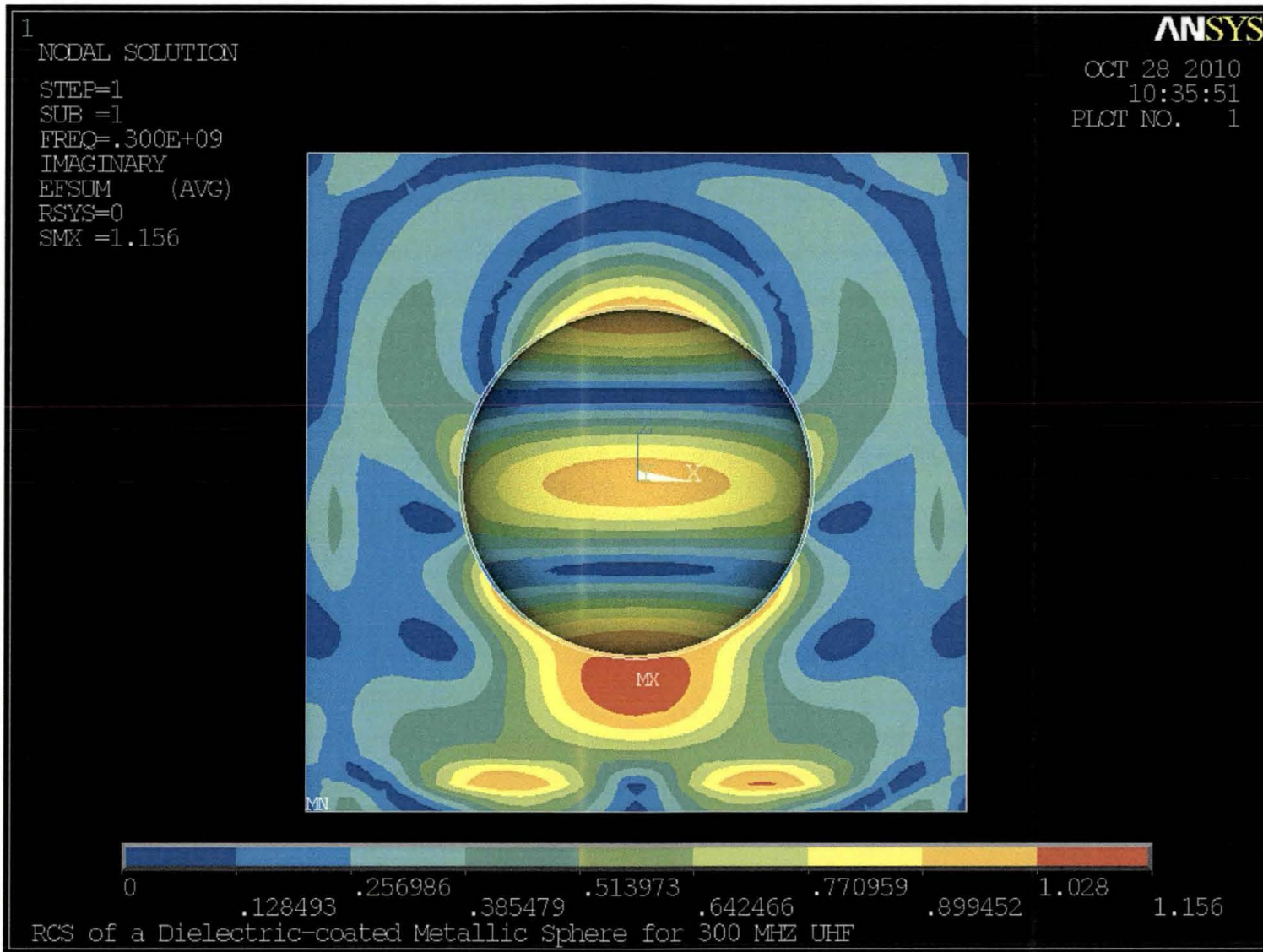


Figure 64. Electric Filed Contour in V/m for a ½ Symmetry 10 m Metallic Sphere with a 1 m Dielectric Coating in Decibels for 300 MHz and 25 Elements per Wavelength

4.2.3.1 Summary and Conclusions of RCS Analysis

A successful analysis of a spherical UAP RCS was conducted using a full harmonic electromagnetic simulation. Upon inspection of the values of normalized RCS at 90°, the dB shown in Table 4 and Table 5, it is apparent the FEA model solution was mesh independent with a pressure of -0.64801E+01 dB for the 25 element per wavelength model and -0.66390E+01 dB for the 50 element per wavelength model. In the runs performed, the 25 element per wavelength model showed sufficient accuracy and reasonable computation times. The normalized RCS plots and electric field contour illustrate the variation of RCS dB and V/m values over a range of 0 to 180°. As one would expect, the values are largest at the point of incident of the radar wave and some reflection and also decrease in magnitude were witnessed around the sphere. Various shapes of UAPs may be evaluated for RCS and the resulting electric field due to an incidental radar wave is also attainable. This information may be used in the future for cases reported to determine the prominence of an object's expected RCS and whether similar radar returns were received.

5. SUMMARY AND CONCLUSION

Compressible and incompressible fluid flow, dynamics, acoustics and radar theory all were provided in this report to give the reader a brief overview and understanding of the numerous physical equations that may be applied to reported UAP and USO behavior. Numerical solutions to these partial differential equation systems (many of which do not possess analytical or closed form solutions) which describe the physics of the event are achieved with millions of elements to model the object domain and medium. Each element may have numerous sets of coupled physical equations that need be solved by passing through many different computational iterations until convergence is achieved. BAASS is one of the few companies possessing the expertise, computer software and computational platforms to achieve such sophistication in numerical studies of UAP.

Compressible fluid flow analyses were performed to calculate and visualize the steady state pressure, temperature and Mach number contours around two non-conventional craft shapes. A solid disc shaped object descending through the air into a body of liquid was investigated to provide visual simulation of the disturbance produced on the surface of the water through use of incompressible fluid flow. The USO analyses were performed using a full harmonic acoustics simulation and a spherical UAP RCS model was completed using a full harmonic electromagnetic simulation. For the individual summary and conclusions of each analytical and numerical study, see Sections 4.1.2, 4.1.4, 4.1.7, 4.2.1.1, and 4.2.3.1 of this report.

From a more general perspective, BAASS was created in 2008 in order to facilitate the long term research and development of novel and emerging future technologies worldwide as they specifically relate to air and spacecraft. A large component of the BAASS mission is to study in depth the performance characteristics of UAP and USOs. From the data accrued, it is also BAASS's mission to produce a Threat Assessment of UAP and USO performance and capabilities. As a first step in accomplishing this mission BAASS has 1) acquired significant field data collection capabilities, both human and instrumented, 2) built the largest known UAP performance and behavior Data Warehouse in the world and 3) acquired advanced computational ability to analyze the data accrued.

Research and development necessary for the procurement of the technology required for advanced space and weapons systems are conducted through use of computational Multiphysics FEA, development of computer code, experimentation, material science testing and manufacturing of prototypes in both BAASS in-house and collaborating facilities and laboratories. Academic areas of concentration include Computational Fluid Dynamics (CFD), Heat Transfer, Nuclear Engineering, Electromagnetics and Radio Frequencies (RF), Theoretical and Computational Physics, Biological Sciences and Chemistry.

Theoretical and computational applications, as well as experimentation on components of non-conventional propulsion systems is under way to provide for future development of vehicles that are capable of operating in the atmosphere, under water and in space. Operation of the vehicle in different mediums, as well as a goal of hypersonic flight would provide superior performance in its ability to reach intended targets, faster delivery of weapons, greater effective

range and an engagement capability enabling employment of complex tactics against multiple targets across multiple domains. This research intends to provide innovative approaches and concepts for aircraft, propulsion, and flight technologies that demonstrate significant advances in performance and capabilities beyond those in operation today.

This report outlined software, equipment and database descriptions along with select theory, analytical and numerical solutions for UAP incidents through engineering and physics analyses. Many analyses of UAP may use analytical or closed form solutions to solve the equations that describe the physics of an event. Where analytical solutions do not exist or the geometry is too complex, BAASS incorporates ANSYS Multiphysics to provide a powerful computational platform to solve large problems numerically, while combining and solving many different physical equations. The combination of computational software with field measurement equipment and historical databases of UAP events allows BAASS to utilize state of the art engineering techniques and tools to assess the operational capabilities of UAP and USOs. A greater understanding of these objects will allow for an accurate threat assessment, as well as provide the physics behind the incredible performance attributes that some have displayed. BAASS' acquired knowledge and capabilities are leading the way to quantum leaps in technology for travel in the atmosphere, space and under water, along with advances in armament and defense systems.

6. REFERENCES

- Aerospaceweb.org . (2010). *Ask Us - Radar Cross Section*. Retrieved October 25, 2010, from Aerospaceweb.org : <http://www.aerospaceweb.org/question/electronics/q0168.shtml>
- Allen, E. (2006, Feb). The Case for Near Space. *Aerospace America* , 31-34.
- Anderson, J. (1990). *Modern Compressible Flow with Historical Perspective*. New York: McGraw-Hill.
- Anderson, J. (1990). *Modern Compressible Flow with Historical Perspective*. New York: McGraw-Hill, Inc.
- ANSYS, Inc. (2009). *ANSYS, Inc. - Corporate Homepage*. Retrieved October 6, 2009, from ANSYS Products Portfolio: <http://www.ansys.com/products/default.asp>
- Arnold, K. (1953). *The Coming of the Saucers*. Private Publication.
- Feindt, C. (2010). *UFOs and Water*. U.S.: Xlibris.
- Foster, A. a. (1983). *Basic Nuclear Engineering*. Boston: Allyn and Bacon, Inc.
- Giancoli, D. (2000). *Phycsis for Scientists and Engineers with Modern Physics*. Upper Saddle River: Prentice Hall.
- Hill, P. (1995). *Unconventional Flying Objects - a scientific analysis*. Charlottesville: Hampton Roads.
- Hughes, W. a. (1991). *Schaum's Outline Theory and Problems: Fuid Dynamics*. New York, New York: McGraw-Hill.
- Hughes, W. a. (1991). *Schaum's Theory and Problems: Fluid Dynamics*. New York: Mc-Graw Hill, Inc.
- Incropera, F. a. (1996). *Fundamentals of Heat and Mass Transfer*. New York: John Wiley & Sons.
- Jackson, G. (2006). *Antimatter Harvesting in Space*. NASA Institute For Advanced Concepts Final Report. <http://www.niac.usra.edu/studies/1107Jackson.html>: NASA.
- Kulikowska, T. (2000). *An Introduction to Neutron Transport Phenomena*. Swierk: Institute of Atomic Energy.
- Los Alamos National Laboratory. (2005, Jan 29). *Los Alamos National Laboratory: MCNP Home Page*. Retrieved Aug 24, 2010, from Los Alamos National Laboratory: <http://mcnp-green.lanl.gov/>

- Miley, G. (1995). Innovative Technology for an Inertial Electrostatic Confinement Fusion Propulsion Unit. (T. Kammash, Ed.) *Fusion Energy in Space Propulsion: Progress in Astronautics and Aeronautics*, 167, 161-177.
- Modest, M. (1993). *Radiative Heat Transfer*. New York: McGraw-Hill.
- Puthoff, H. (2008). *Advanced Aerospace Weapons System Applications Program: BAASS Technical Study 2: Propulsion*. Las Vegas: BAASS.
- Riley, W. a. (1996). *Engineering Mechanics - Dynamics*. New York: John Wiley & Sons.
- Schlichting, H. (1968). *Boundary Layer Theory*. New York: McGraw Hill, Inc.
- Schlichting, H. (1968). *Boundary-Layer Theory*. New York: McGraw-Hill.
- Valleé, J. and Davis, E. (2003). Incommensurability, Orthodoxy and the Physics oh High Strangeness: A 6-layer Model for Anomalous Phenomena. *Science, Religion and Consciousness Forum*. University Fernando Pessoa, Porto.
- Valleé, J. (1998). Estimates of Optical Output in Six Cases of Unexplained Aerial Objects with Defined Luminosity Characteristics. *Journal of Scientific Exploration*, 12 (3), 345-358.
- X-5 Monte Carlo Team. (2003, April 24). MCNP — A General Monte Carlo N-Particle Transport Code, Version 5, Volume I: Overview and Theory. Los Alamos, NM, USA.
- Zill, D. a. (1993). *Differential Equations with Boundary-Value Problems*. Boston: PWS Publishing Company.
- Zucker, R. (1977). *Fundamentals of Gas Dynamics*. Champaign: Matrix.
- Zucker, R. (1977). *Fundamentals of Gas Dynamics*. Champaign: Matrix Publishers, Inc.

SYMBOLS AND ACRONYMS

A – Area

AAV – anomalous aerial vehicle

A_e – effective area of the radar antenna, or "aperture efficiency"

B – magnetic induction field

BAASS – Bigelow Aerospace Advanced Space Studies

B_a – adiabatic bulk modulus

c – speed of sound in medium

CFD – computational fluid dynamics

CSG – Carrier Strike Group

D – displacement field

DIA – Defense Intelligence Agency

E – electric field

FEA – Finite Element Analysis

FLIR – forward looking infrared

fluid structure interaction

g – gravitational acceleration

G – gain of the radar antenna

GB - gigabyte

g_x – x directional component of gravitational acceleration

g_y – y directional component of gravitational acceleration

g_z – z directional component of gravitational acceleration

H – magnetic field

HDV – High Definition Video

J – current density

k – wave number

M – molar mass

MHD – magnetohydrodynamics

p – pressure

P_{avg} – average power transmitted by the radar

$P_{backscatter}$ – backscattered power

$P_{incident}$ – incident power density

$P_{intercepted}$ – power intercepted by the target

$P_{isotropic}$ – isotropic power

$P_{scatter}$ – power scattered by the target

R – range to the target

R_{max} – maximum range

R_u – gas constant

radar – radio detection and ranging

RCS – radar cross section

RF – radio frequency

S – signal energy received by the radar

S_{min} – minimum signal energy

T – temperature

TB – terabyte

t – time

t_{ot} = time the radar antenna is pointed at the target (time on target)

u – x velocity

v – y velocity

w – z velocity

x – x coordinate

y – y coordinate

z – z coordinate

UAP – unidentified aerial phenomena

UAV – unmanned aerial vehicle

UFO – unidentified flying object

UHF – ultra high frequency

USO – unidentified submerged object

ε – specific internal energy

μ – dynamic viscosity of the fluid

ρ – density of the fluid

ρ_e – charge density

σ – radar cross section

ω – angular frequency

ATTACHMENT I – ANSYS INPUT FILES

USO ANSYS Multiphysics Acoustics Input File Example

```
!-----  
! 1/100th Acoustical Model of a 10 m Spherical USO in Water  
! at 1000 Hz  
!-----
```

```
!-----  
! Define variables for problem:  
! Radiating Sphere of Radius SPHRRADS with uniform surface  
! velocity of VELOCITY oscillating at FREQUENC  
!-----
```

```
*set,FREQUENC,1000  
*set,VELOCITY,0.005  
*set,PI ,acos(-1)  
*set,SPHRRADS,0.1  
*set,TOLER,0.0001
```

```
!-----  
! Fluid properties:  
! Density, Speed of sound in water, Reference pressure  
!-----
```

```
*set,WATRDENS,1000  
*set,WATRSONC,1500  
*set,REFEPRES,1E-6
```

```
!-----  
! Geometry info  
! Infinite radius at INFIRADS meters  
! INFIXOFF, INFIYOFF not used right now...  
!-----
```

```
*set,INFIRADS,5  
*set,INFIXOFF,0.0  
*set,INFIYOFF,0.0
```

```
!-----  
! Mesh info  
! Use mapped mesh? YES=1 NO=0 (use NO for now)  
! Elements per wavelength (EPW)  
!-----
```

```
*set,MAPDMESH,0  
*set,TRIMESH ,1  
*set,EPW ,50
```

```
!-----  
! Graphics settings  
! Set title and subtitles  
! Make sure the legend is always on (/plopt,info,on)  
! Put global triad at right top corner (/triad,rtop)  
! Turn on Full Graphics because of DDTSREP#16215  
!-----  
/title,Uniformly Radiating Sphere, EPW=%EPW%  
/stitle,1,Sphere radius of %SPHRRADS%m  
/stitle,2,Frequency at %FREQUENC%Hz  
/stitle,3,Uniform velocity of %VELOCITY%m/s  
/stitle,4,Infinite Boundary of %INFIRADS%m at (%INFIYOFF%,%INFIYOFF%)  
/plopt,info,on  
/triad,rtop  
/graphics,full
```

```
!-----  
! Enter Preprocessor  
!-----  
/prep7  
!-----
```

```
! Define elements  
! 1 = fluid w/ structure  
! 2 = fluid no structure  
! 3 = infinite fluid  
! Define elements and keyopts (et) (keyopt)  
! Define real constants (r)  
! Define material properties (mp)  
!-----
```

```
et,1,fluid29  
keyopt,1,2,0  
keyopt,1,3,1
```

```
et,2,fluid29  
keyopt,2,2,1  
keyopt,2,3,1  
et,3,fluid129  
keyopt,3,3,1
```

```
r,1,REFEPRES  
r,2,REFEPRES  
r,3,INFIRADS,0,0,
```

```
mp,dens,1,WATRDENS  
mp,sonc,1,WATRSONC  
mp,dens,2,WATRDENS
```

```
mp,sonc,2,WATRSONC
mp,sonc,3,WATRSONC
```

```
!-----
! Create geometry
! Create five 90 degree quarter circles (pcirc)
! Merge keypoints (nummrg,kp)
!-----
```

```
pcirc,1,SPHRRADS,0,90,
pcirc,2,1,0,90,
pcirc,3,2,0,90,
pcirc,4,3,0,90,
pcirc,5,4,0,90,
nummrg,kp
```

```
!-----
! Mesh
! Set global element size based on EPW above
! Map with quads, quad-dominant for free mesh (mshape,0)
! Mesh mapped or free (mshkey)
! Set area attributes (aatt)
! Mesh all areas (amesh)
! Set plot controls based on element type number
!-----
```

```
esize,(WATRSONC/FREQUENC)/EPW
mshape,TRIMESH
mshkey,MAPDMESH
aatt,2,2,2
amesh,all
/pnum,type,1
/num,1
/auto
eplot
```

```
!-----
! Rotate all nodes in cylindrical CS
!-----
csys,1
nrotate,all
```

```
!-----
! Change elements near center to fluid with struct present
!-----
type,1
real,1
mat,1
```

```
nsl,s,loc,x,SPHRRADS
esln
nsle
emodif,all
```

```
!-----
```

```
! Apply struct boundary conditions on element type 1
! Constrain all translation DOF (the "free" DOF)
! Reapply velocity as displacement on inner nodes in radial
! dir. (ux)
! Apply FSI (fluid-struct interface) flag to active
```

```
!-----
```

```
d,all,uy
d,all,ux
nsl,s,loc,x,SPHRRADS
d,all,ux,0,-VELOCITY/(2*PI*FREQUENC)
sf,all,fsi
```

```
!-----
```

```
! Mesh Infinite fluid domain
! Instead of meshing, use ESURF to generate elements on      ! existing mesh
```

```
!-----
```

```
type,3
real,3
mat,3
esel,all
nsl,s,loc,x,INFIRADS,INFIRADS+TOLER
esurf,all
allsel,all
finish
```

```
!-----
```

```
! solution options
! Full harmonic analysis
! frequency at FREQUENC
! select everything & solve
```

```
!-----
```

```
/solu
antype,harm
hropt,full
hrout,on
lumpm,0
eqslv,sparse
harfrq,FREQUENC
nsubst,
```

```
kbc,0
allsel,all
solve
finish
```

```
!-----
! postprocessing w/ annotations
! Load real (set,1,1,1,0) and plot pressure
! Load imag (set,1,1,1,1) and plot pressure
! do a load case comb. to SRSS for pressure magnitude
!-----
```

```
/post1
/tsp,,0.75
/ann,dele
/tla,-90,90,Plot of real part of pressure
/dscale,1,off
set,1,1,1,0
plnsol,pres
```

```
/tsp,,0.75
/ann,dele
/tla,-90,90,Plot of imag part of pressure
set,1,1,1,1
/replot
```

```
/tsp,,0.75
/ann,dele
/tla,-90,90,Plot of magnitude of pressure
lcdef,1,1,1,0
lcooper,srss,1
/replot
```

```
!-----
! path operations
!-----
```

```
csys,0
lsel,s,loc,x,0
nsll,s,1
*get,NCOUNT,node,,count
csys,1
nset,s,loc,x,SPHRRADS
nset,r,loc,y,90,90+TOLER
STRTNODE=ndnext(0)
nset,s,loc,x,INFIRADS,INFIRADS+TOLER
nset,r,loc,y,90,90+TOLER
FININODE=ndnext(0)
```

```

allsel,all
path,RADIAL,2,30,(NCOUNT-1)
ppath,1,STRTNODE
ppath,2,FININODE
avprin,0,0,
set,1,1,1,0
pdef,REALPRES,pres,,noavg
set,1,1,1,1
pdef,IMAGPRES,pres,,noavg
paget,trapoin,poin
paget,tracdata,tabl
paget,traclabl,labe

*dim,RADSPATH,table,NCOUNT,7

*do,ICOUNT,1,NCOUNT
  WAVENUMB=2*PI*FREQUENC/WATRSONC
  CURRRADS=TRACDATA(ICOUNT,2,1)

TEMPAMPL=WATRDENS*WATRSONC*VELOCITY*WAVENUMB*(SPHRRADS**2)/CURRRADS
TEMPAMPL=TEMPAMPL/(1+(WAVENUMB*SPHRRADS)**2)
TEMPAMRC=WAVENUMB*SPHRRADS*cos(WAVENUMB*(CURRRADS-SPHRRADS))
TEMPAMRS=sin(WAVENUMB*(CURRRADS-SPHRRADS))
TEMPAMIC=cos(WAVENUMB*(CURRRADS-SPHRRADS))
TEMPAMIS=-WAVENUMB*SPHRRADS*sin(WAVENUMB*(CURRRADS-SPHRRADS))
RADSPATH(ICOUNT,1)=TRACDATA(ICOUNT,2,1)
RADSPATH(ICOUNT,2)=TRACDATA(ICOUNT,5,1)
RADSPATH(ICOUNT,3)=TEMPAMPL*(TEMPAMRC+TEMPAMRS)
RADSPATH(ICOUNT,4)=TRACDATA(ICOUNT,6,1)
RADSPATH(ICOUNT,5)=TEMPAMPL*(TEMPAMIC+TEMPAMIS)

RADSPATH(ICOUNT,6)=sqrt(TRACDATA(ICOUNT,5,1)**2+TRACDATA(ICOUNT,6,1)**2)
TEMP1 =TEMPAMPL*(TEMPAMRC+TEMPAMRS)
TEMP2 =TEMPAMPL*(TEMPAMIC+TEMPAMIS)
RADSPATH(ICOUNT,7)=sqrt(TEMP1**2+TEMP2**2)
*enddo

/gcolumn,1,ANSYS
/gcolumn,2,Theory
/axlab,x,Radial Distance (m)
/axlab,y,Real Pressure (Pa)
*vplot,RADSPATH(1,1),RADSPATH(1,2),3

/axlab,y,Imaginary Pressure (Pa)

```

*vplot,RADSPATH(1,1),RADSPATH(1,4),5

/axlab,y,Magnitude of Pressure (Pa)

*vplot,RADSPATH(1,1),RADSPATH(1,6),7

UAP ANSYS Multiphysics RCS Input File Example

```
/batch,list  
/title, RCS of a Dielectric-coated Metallic Sphere for 300 MHZ UHF  
/com, Problem: A metallic sphere (radius=5.0m) coated by dielectric layer  
/com,      (thickness=1.0m, Er=4)  
/com,      Incident Wave: -x polirazation with PHI = 0 (degree), THETA = 0 (degree)  
/nopr  
/prep7
```

! problem dimensions and set-up

freq=300e6

lambda=3.e8/freq

epsr=4

wave1=lambda/sqrt(epsr)

wave2=lambda

h1=wave1/25

h2=wave2/25

ra=0.5*lambda

s=0.01*lambda

rb=ra+s

a=rb+4*h2

b=a+3*h2

c=b+4*h2

! --- define elements and materials ---

et,1,HF119,1

et,2,HF119,1,,1

mp,murx,1,1.

mp,perx,1,epsr

mp,murx,2,1.

mp,perx,2,1.

! --- set up the geometry ---

sphere,ra,rb,0,180

sphere,rb,a,0,180

vsel,all

cm,vequi,volu

block,-b,b,0,b,-b,b

block,-c,c,0,c,-c,c

vsbv,4,3,,delete,keep

vsbv,3,vequi,,delete,keep

csys,2

vsel,s,loc,x,0,ra/2

vdel,all

alls

csys,0

vglue,all

! --- meshing ---

csys,0

smrtsize,4

! meshing

esize,h1

type,1
mat,1
vmesh,1
mat,2
esize,h2
vmesh,3
esize,h2
vmesh,6

! --- PML element ---

type,2
vmesh,5
alls
nummrg,all

! define equivalent source surface

csys,2
nsel,s,loc,x,0,a
esln,s,1,all
nsel,s,loc,x,a
sf,all,mxwf
alls

! define boundary condition

csys,0
nsel,s,loc,x,c
nsel,a,loc,x,-c

```
nselect,all,loc,y,c
nselect,all,loc,z,-c
nselect,all,loc,z,c
d,all,ax,0.
nselect,all
csys,2
nselect,s,loc,x,ra
d,all,ax,0.
csys,0
allsel,all
! incident plane wave
plwave,-1,0,0,0,0
fini
/solu
hfscat,scat
eqslv,sparse
antype,harmic
harfreq,freq
solve
fini
/post1
set,1,1
hfsym,,,pmc
prfar,rcsn,total,0,0,,0,180,36
/yrange,-35,15
plfar,rcsn,total,0,0,,0,180,180
fini
```

ATTACHMENT II – "TIC TAC" CFD CONTOUR PLOTS FOR PRESSURE, TEMPERATURE AND MACH NUMBER

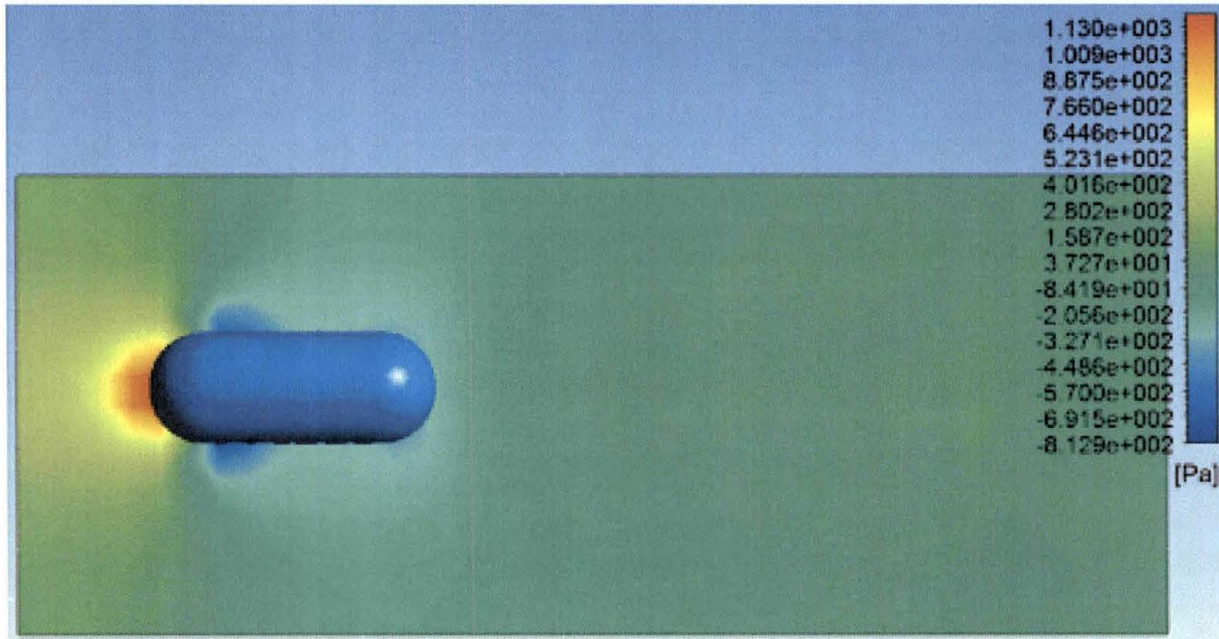


Figure 65. Tic Tac Pressure at 1/6 Scale, Air Temperature 223K and 100 mph with Subsonic Inlet and Subsonic Outlet

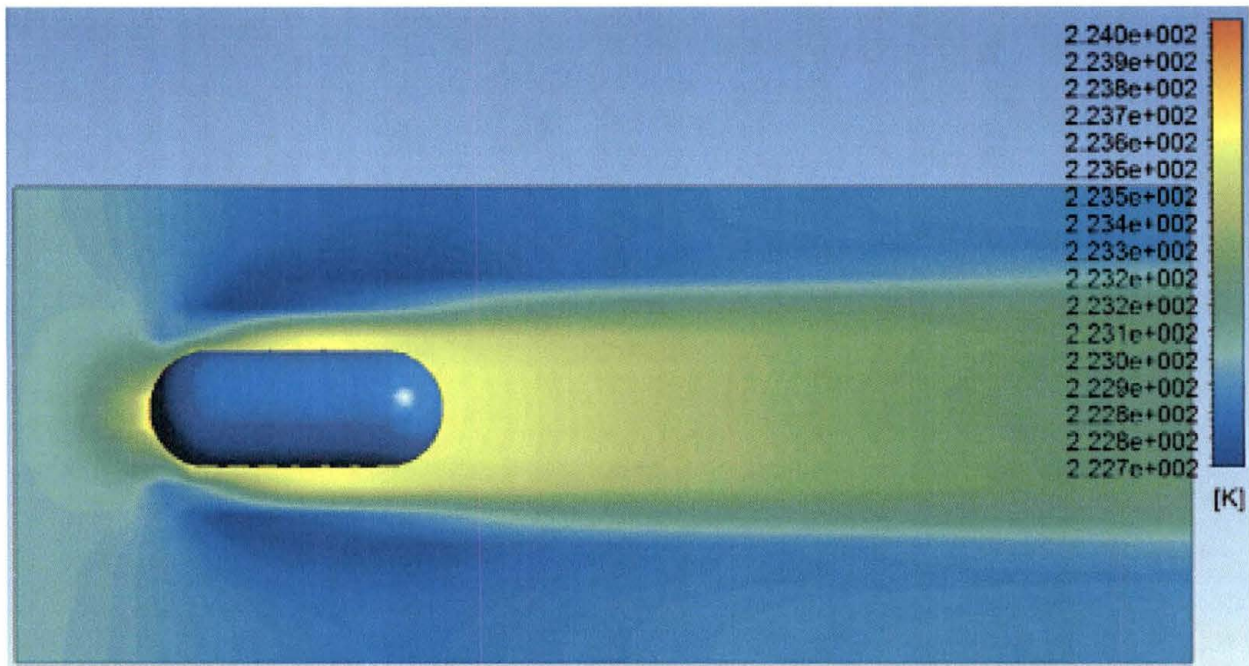


Figure 66. Tic Tac Temperature at 1/6 Scale, Air Temperature 223K and 100 mph with Subsonic Inlet and Subsonic Outlet

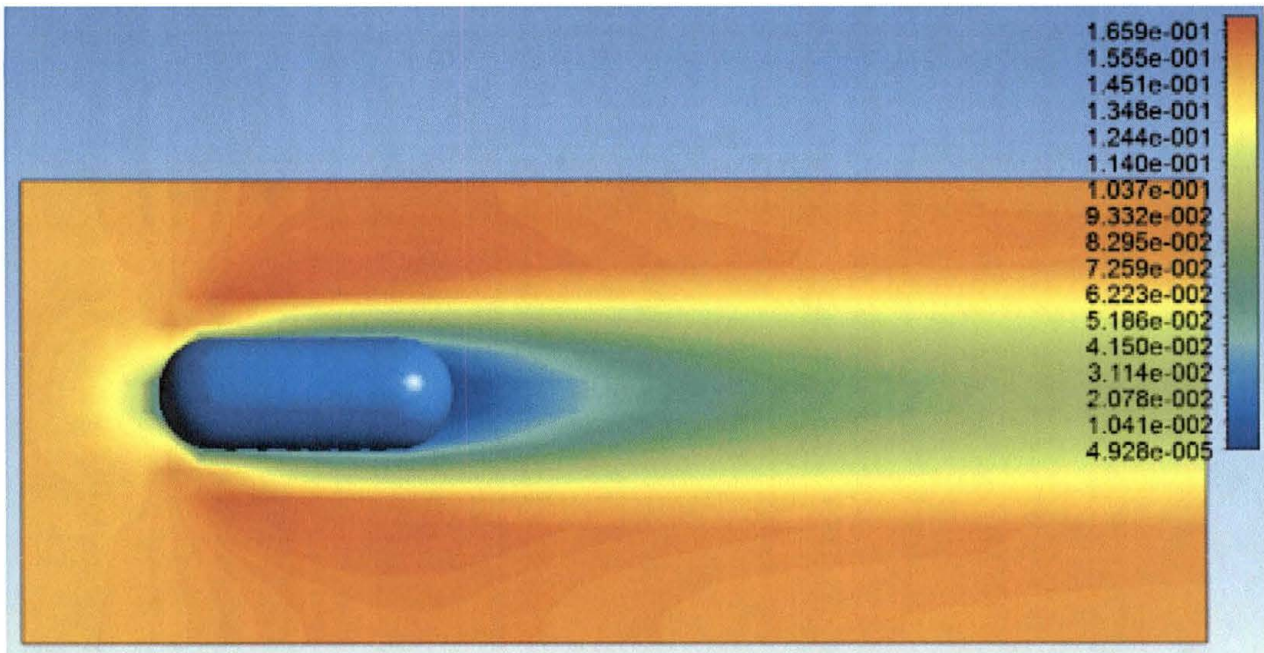


Figure 67. Tic Tac Mach Number at 1/6 Scale, Air Temperature 223K and 100 mph with Subsonic Inlet and Subsonic Outlet

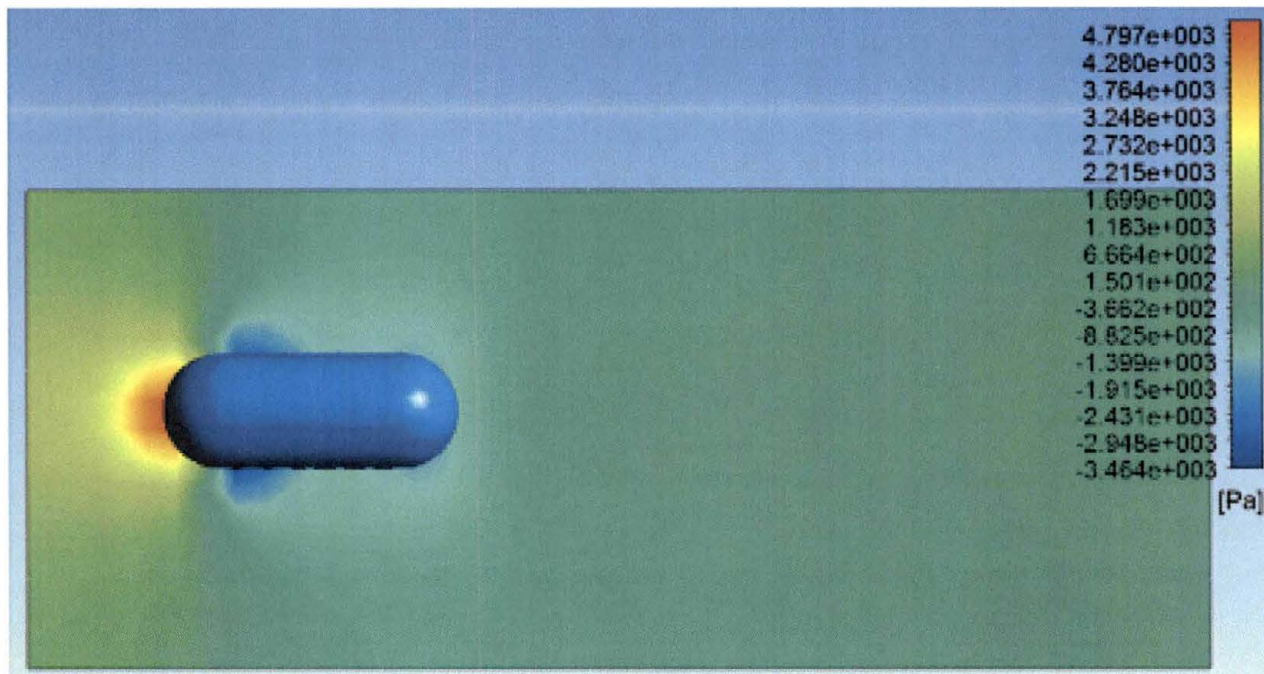


Figure 68. Tic Tac Pressure at 1/6 Scale, Air Temperature 223K and 200 mph with Subsonic Inlet and Subsonic Outlet

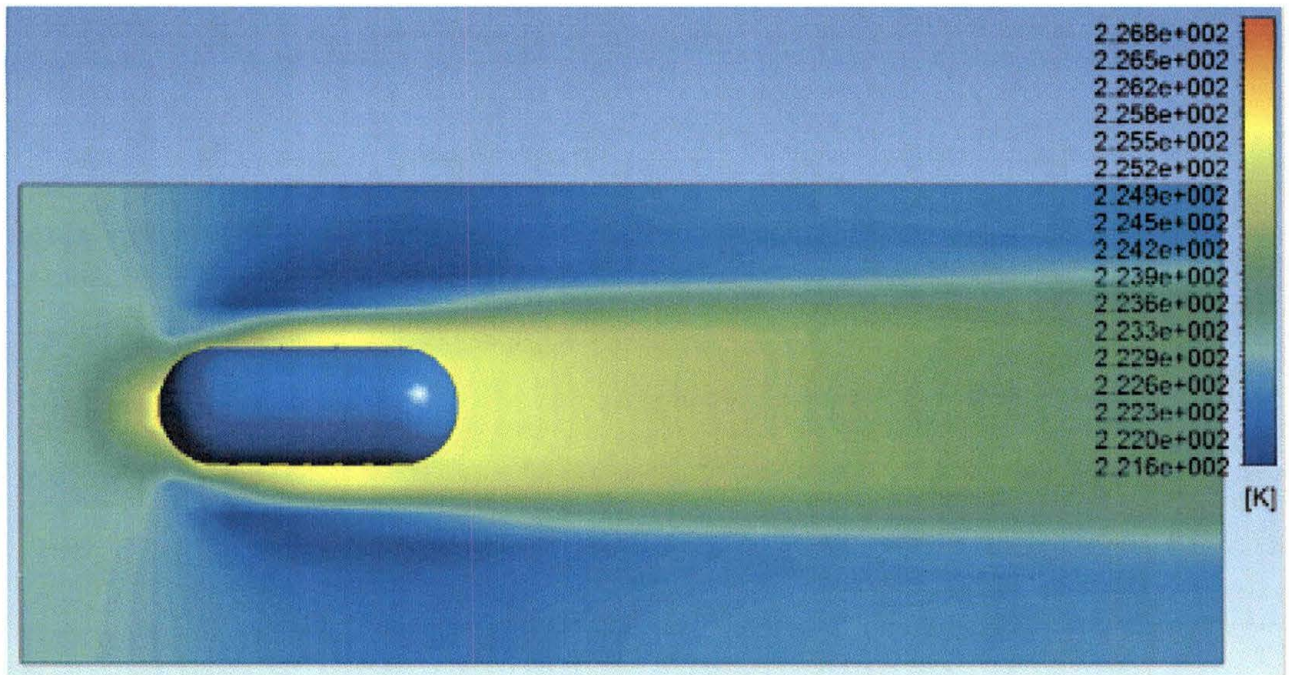


Figure 69. Tic Tac Temperature at 1/6 Scale, Air Temperature 223K and 200 mph with Subsonic Inlet and Subsonic Outlet

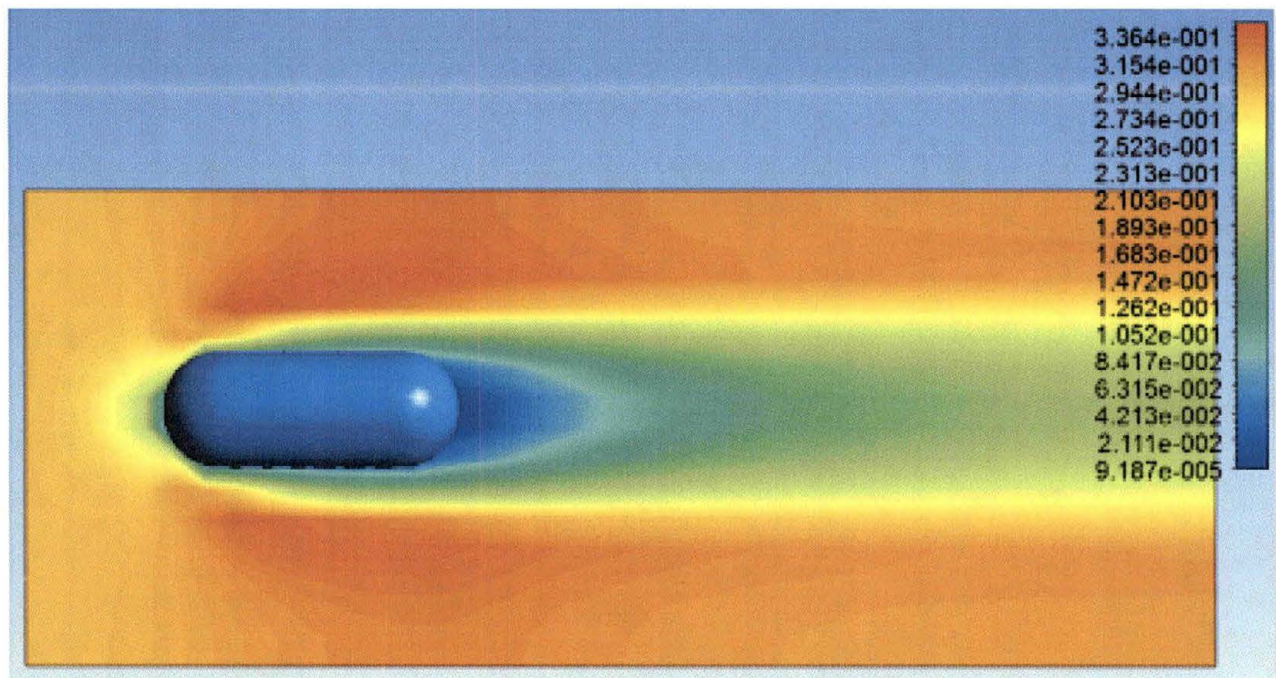


Figure 70. Tic Tac Mach Number at 1/6 Scale, Air Temperature 223K and 200 mph with Subsonic Inlet and Subsonic Outlet

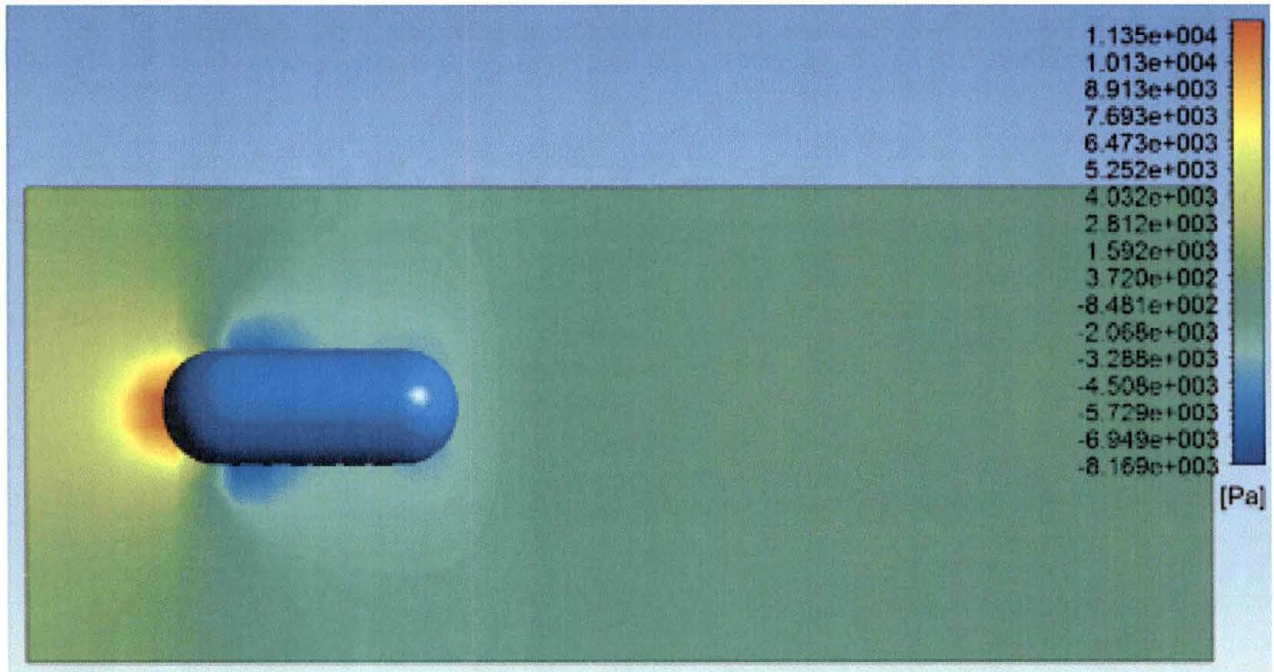


Figure 71. Tic Tac Pressure at 1/6 Scale, Air Temperature 223K and 300 mph with Subsonic Inlet and Subsonic Outlet

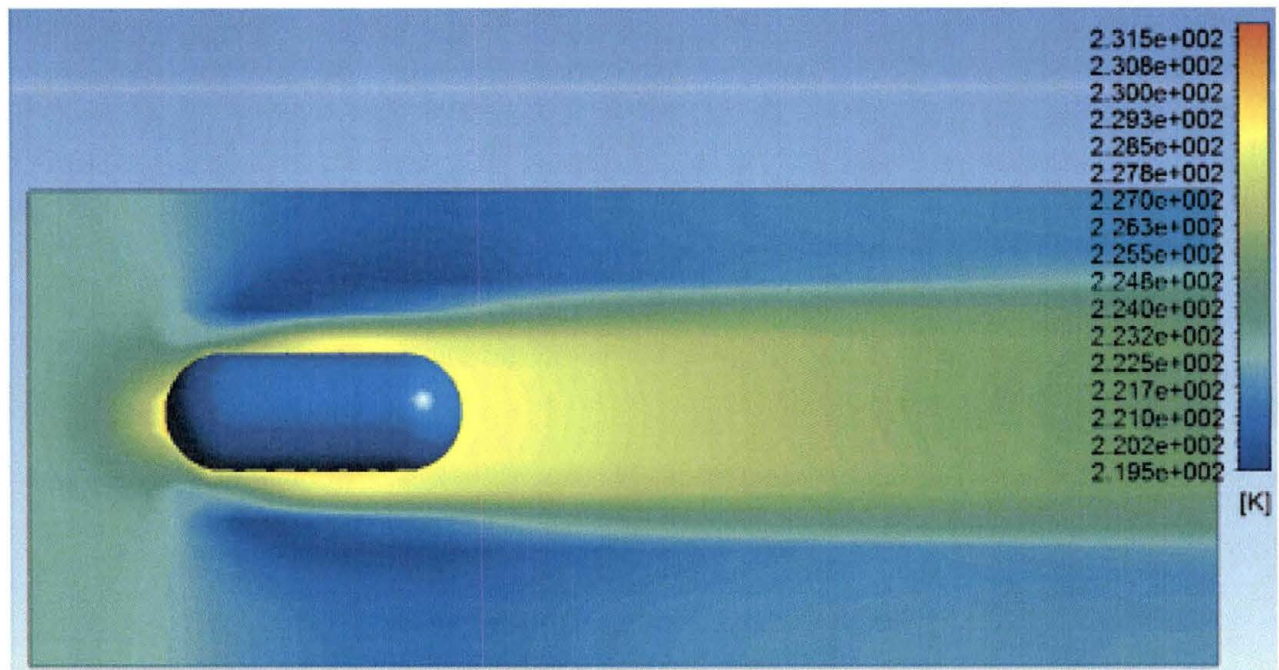


Figure 72. Tic Tac Temperature at 1/6 Scale, Air Temperature 223K and 300 mph with Subsonic Inlet and Subsonic Outlet

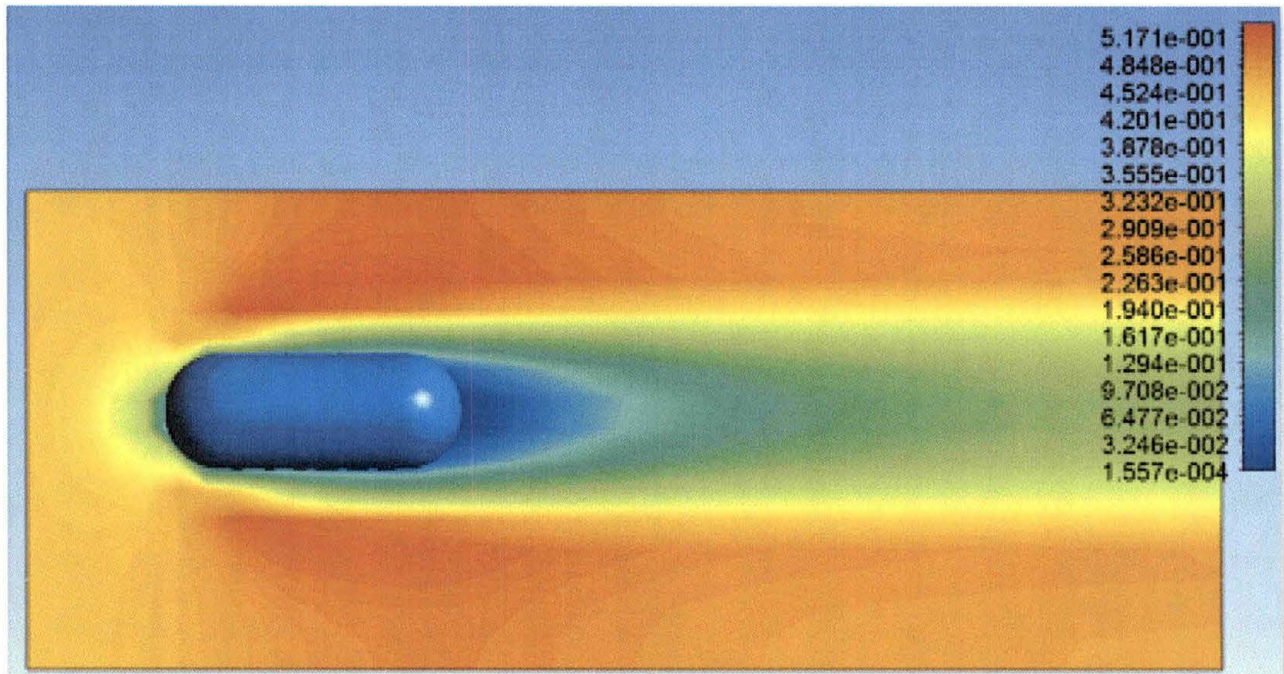


Figure 73. Tic Tac Mach Number at 1/6 Scale, Air Temperature 223K and 300 mph with Subsonic Inlet and Subsonic Outlet

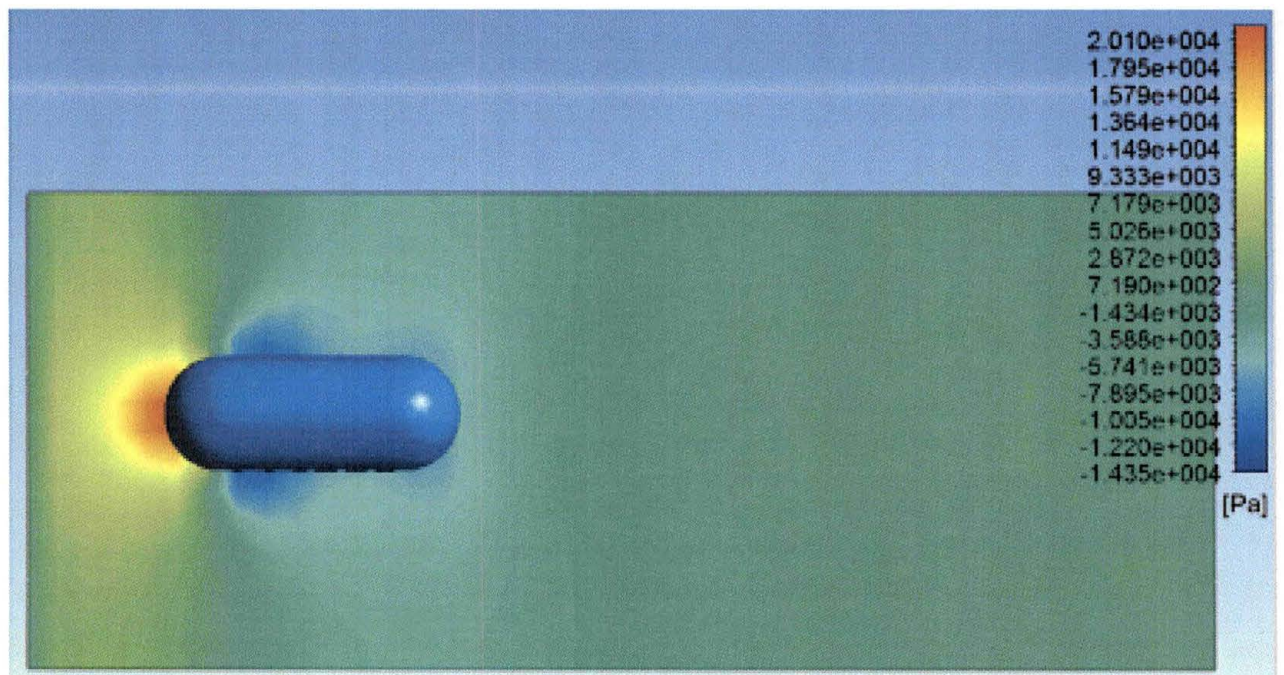


Figure 74. Tic Tac Pressure at 1/6 Scale, Air Temperature 223K and 400 mph with Mixed Inlet and Subsonic Outlet

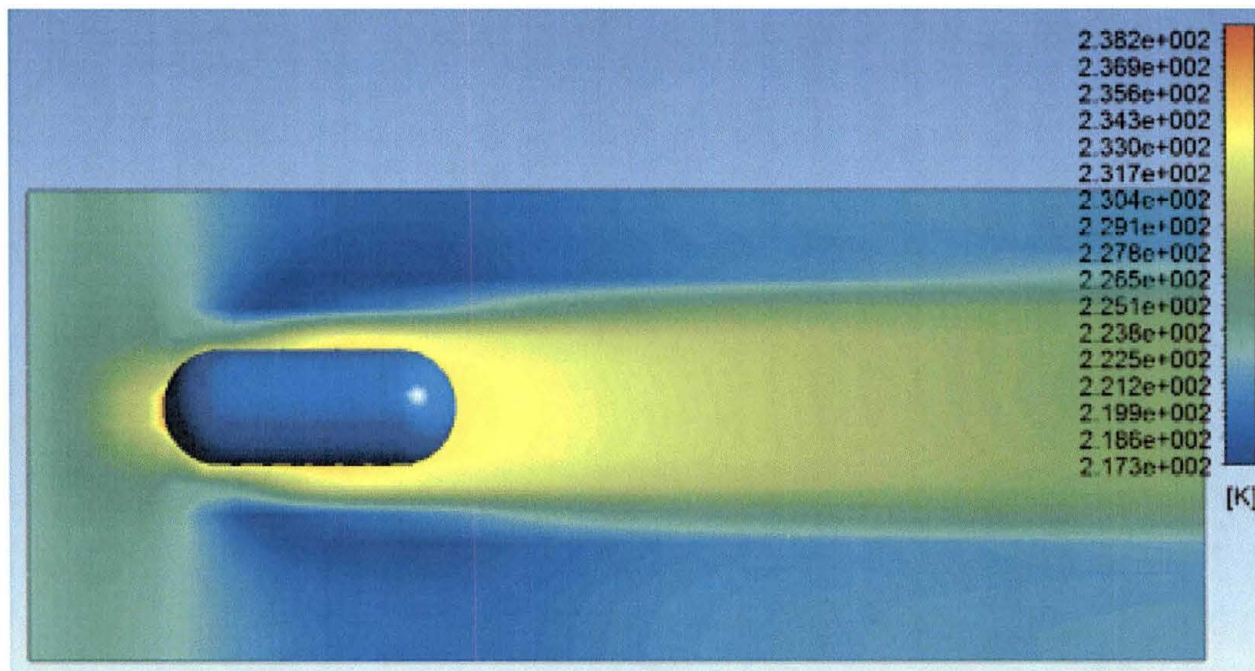


Figure 75. Tic Tac Temperature at 1/6 Scale, Air Temperature 223K and 400 mph with Mixed Inlet and Subsonic Outlet

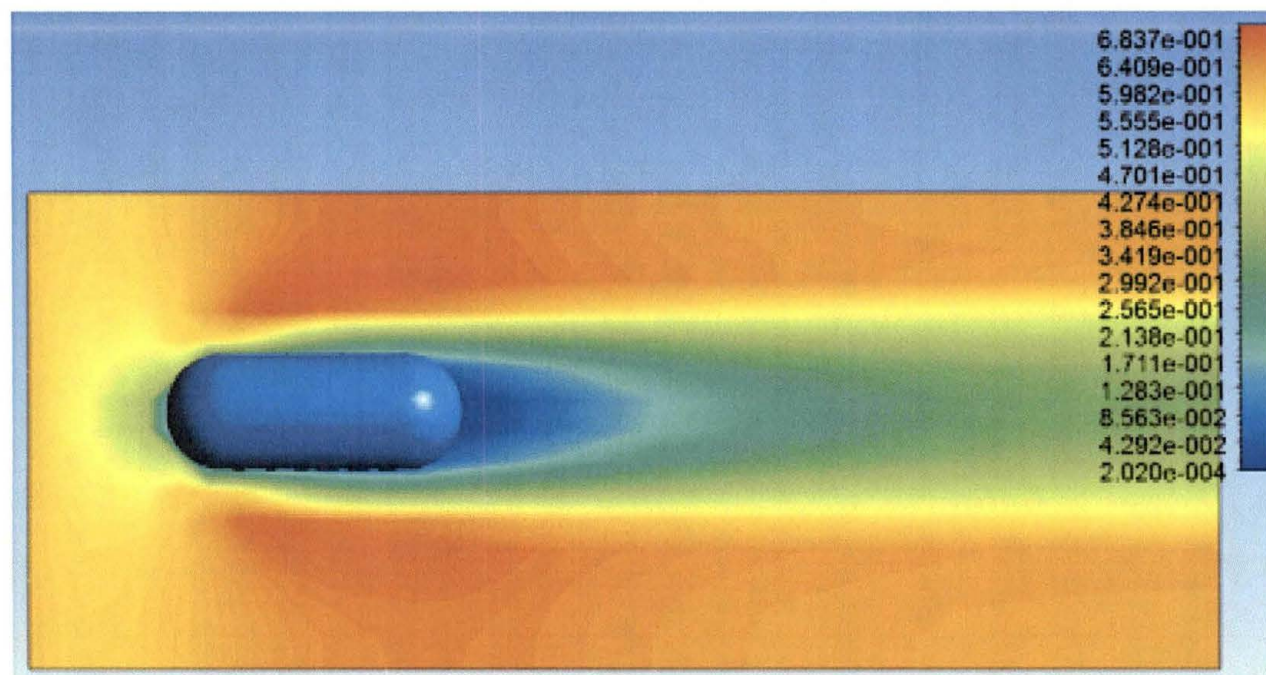


Figure 76. Tic Tac Mach Number at 1/6 Scale, Air Temperature 223K and 400 mph with Mixed Inlet and Subsonic Outlet

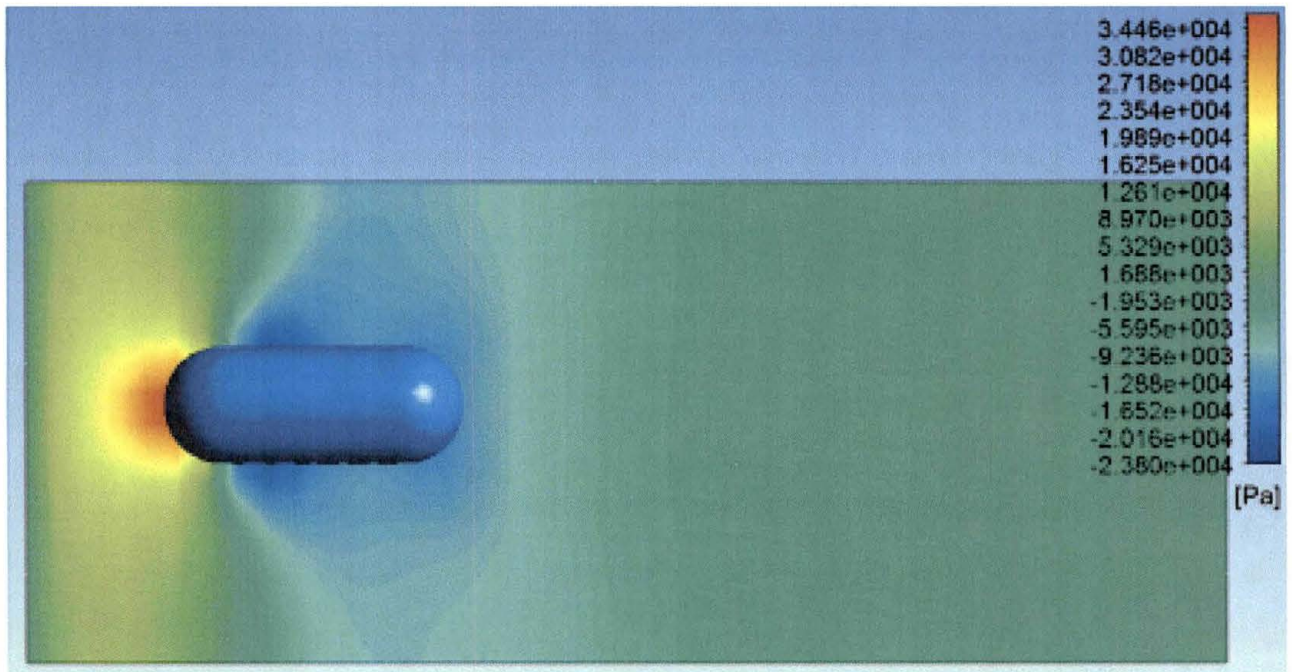


Figure 77. Tic Tac Pressure at 1/6 Scale, Air Temperature 223K and 500 mph with Mixed Inlet and Subsonic Outlet

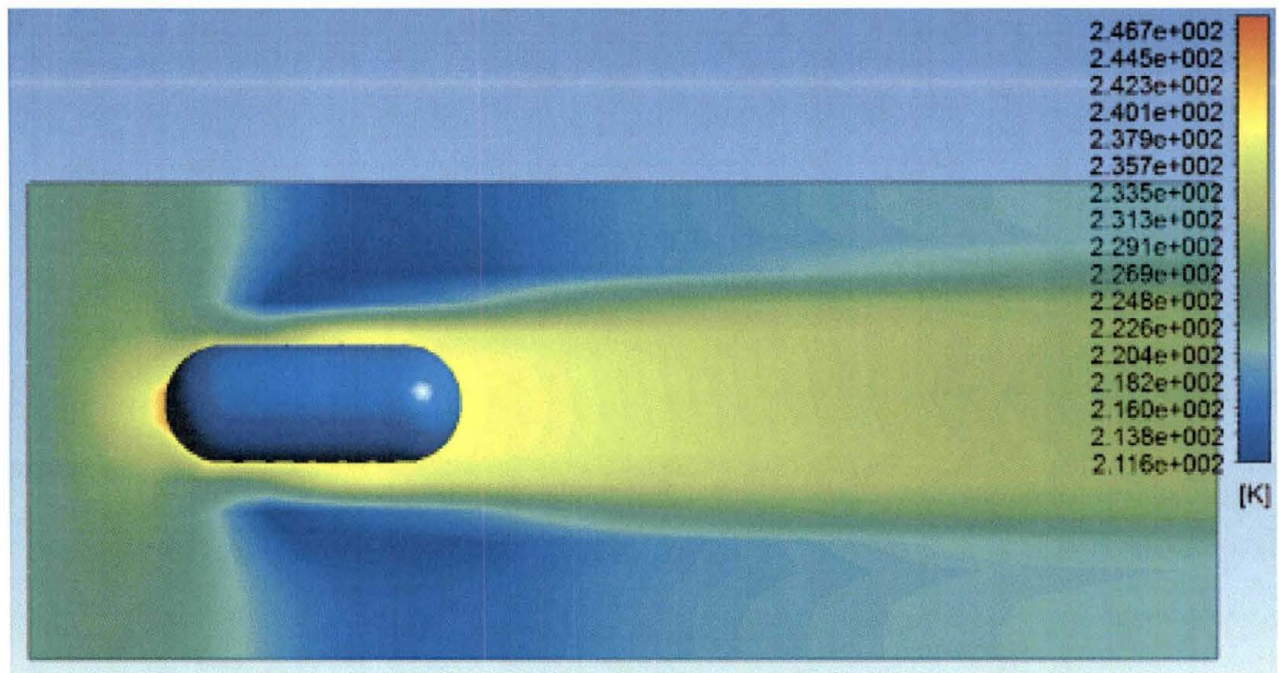


Figure 78. Tic Tac Temperature at 1/6 Scale, Air Temperature 223K and 500 mph with Mixed Inlet and Subsonic Outlet

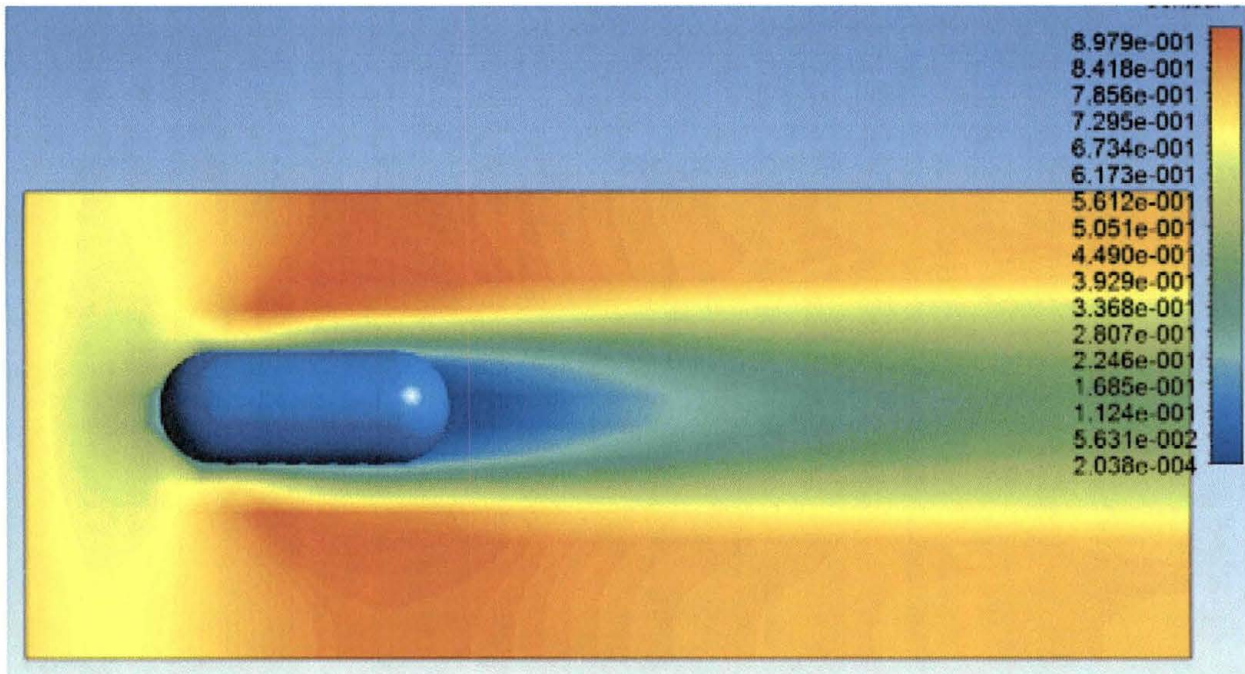


Figure 79. Tic Tac Mach Number at 1/6 Scale, Air Temperature 223K and 500 mph with Mixed Inlet and Subsonic Outlet

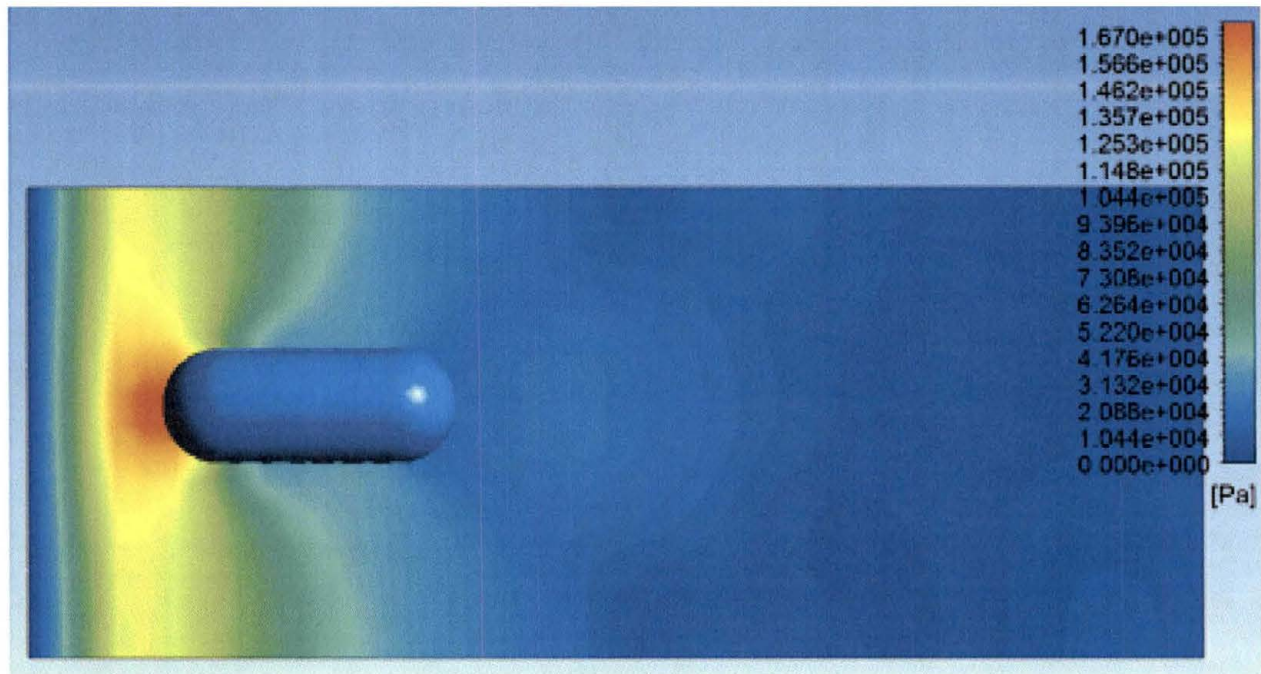


Figure 80. Tic Tac Pressure at 1/6 Scale, Air Temperature 223K and 900 mph with Supersonic Inlet and Supersonic Outlet

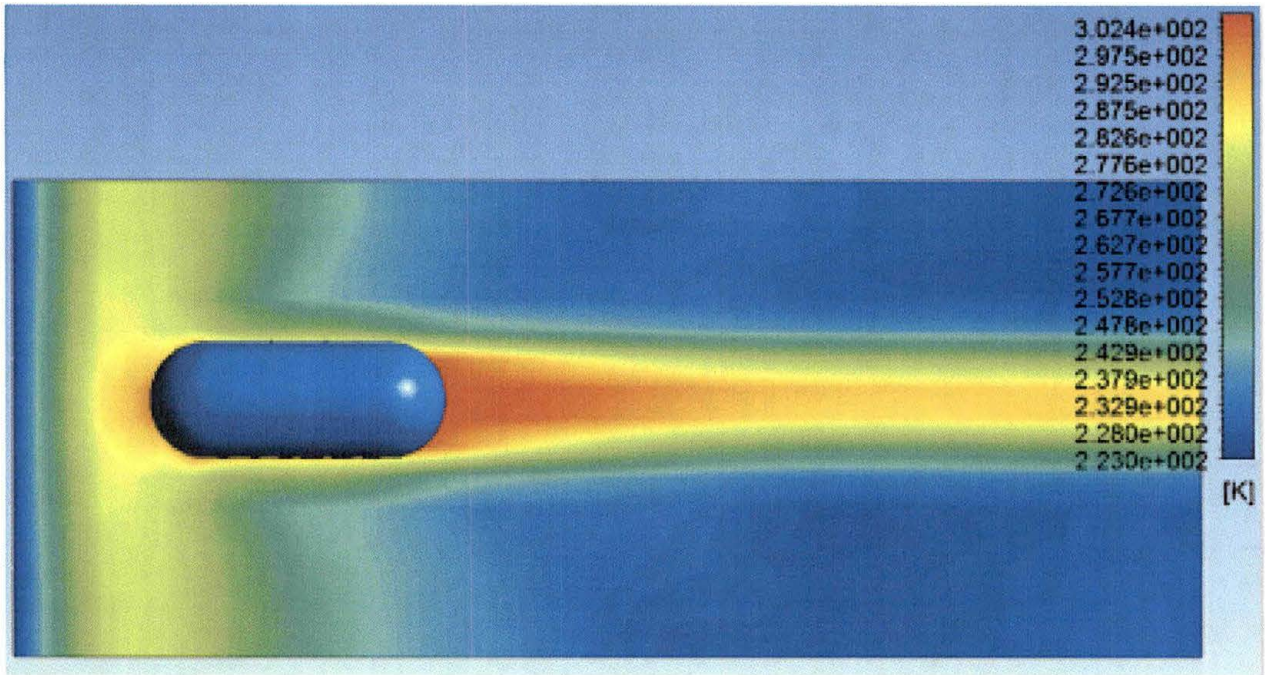


Figure 81. Tic Tac Temperature at 1/6 Scale, Air Temperature 223K and 900 mph with Supersonic Inlet and Supersonic Outlet

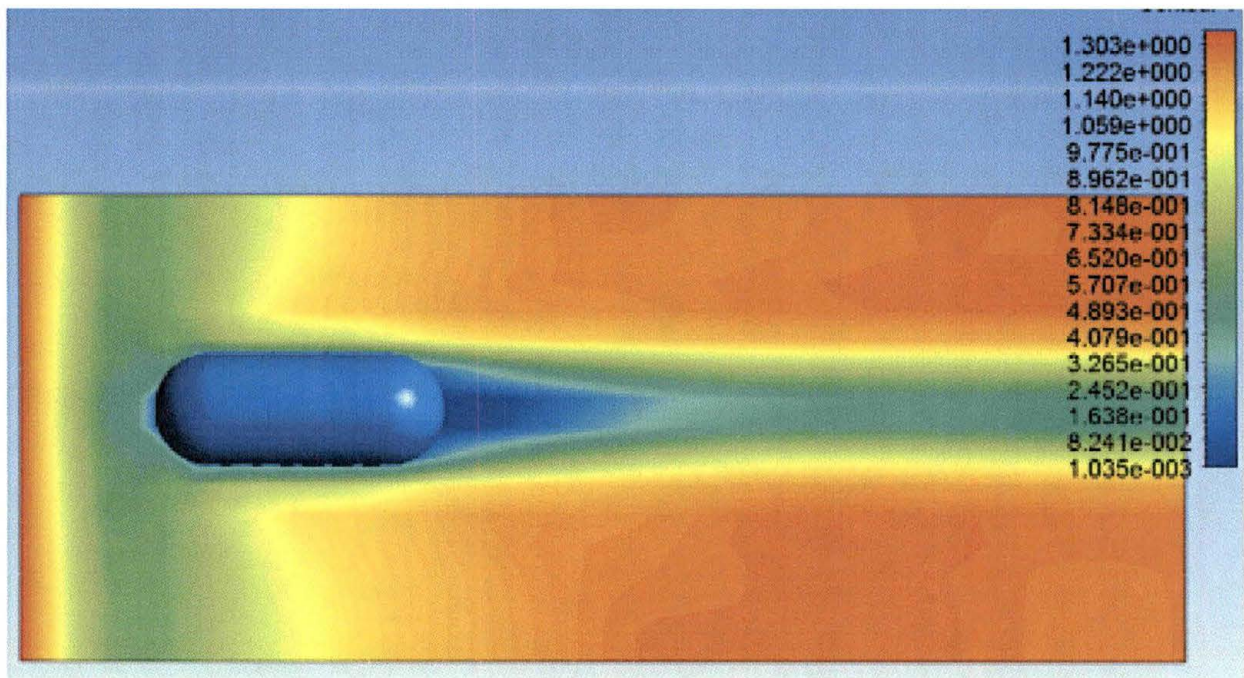


Figure 82. Tic Tac Mach Number at 1/6 Scale, Air Temperature 223K and 900 mph with Supersonic Inlet and Supersonic Outlet

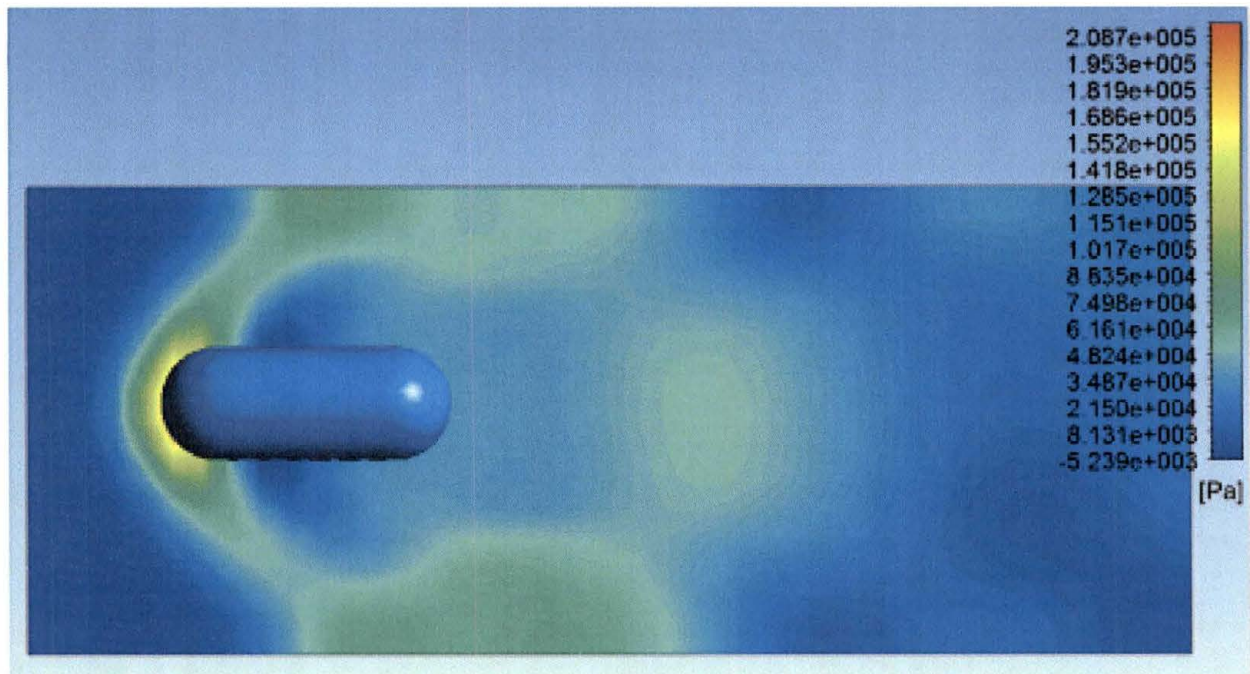


Figure 83. Tic Tac Pressure at 1/6 Scale, Air Temperature 223K and 1100 mph with Supersonic Inlet and Supersonic Outlet

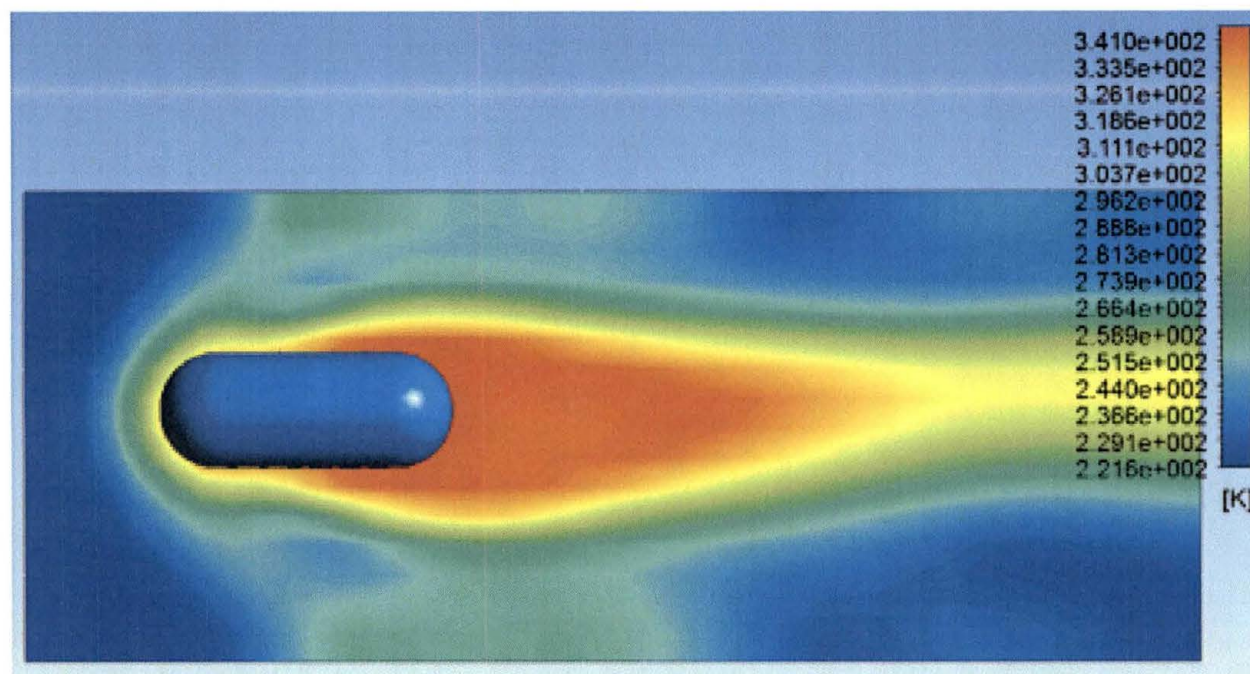


Figure 84. Tic Tac Temperature at 1/6 Scale, Air Temperature 223K and 1100 mph with Supersonic Inlet and Supersonic Outlet

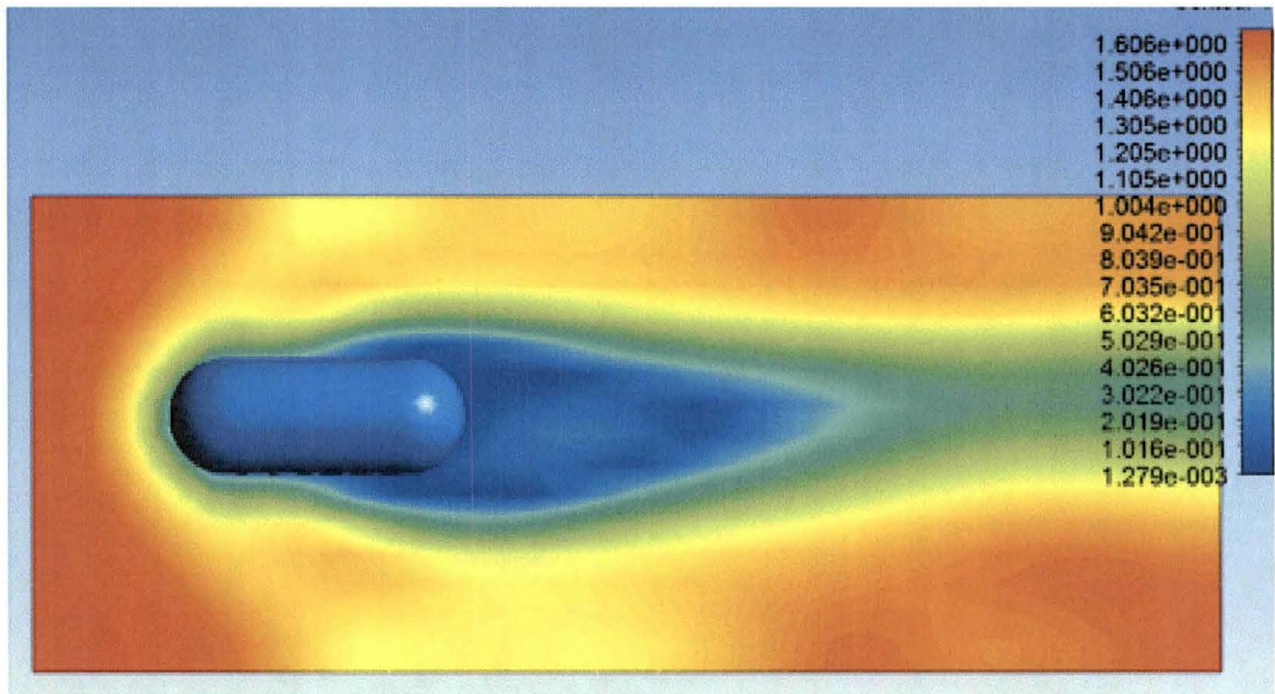


Figure 85. Tic Tac Mach Number at 1/6 Scale, Air Temperature 223K and 1100 mph with Supersonic Inlet and Supersonic Outlet

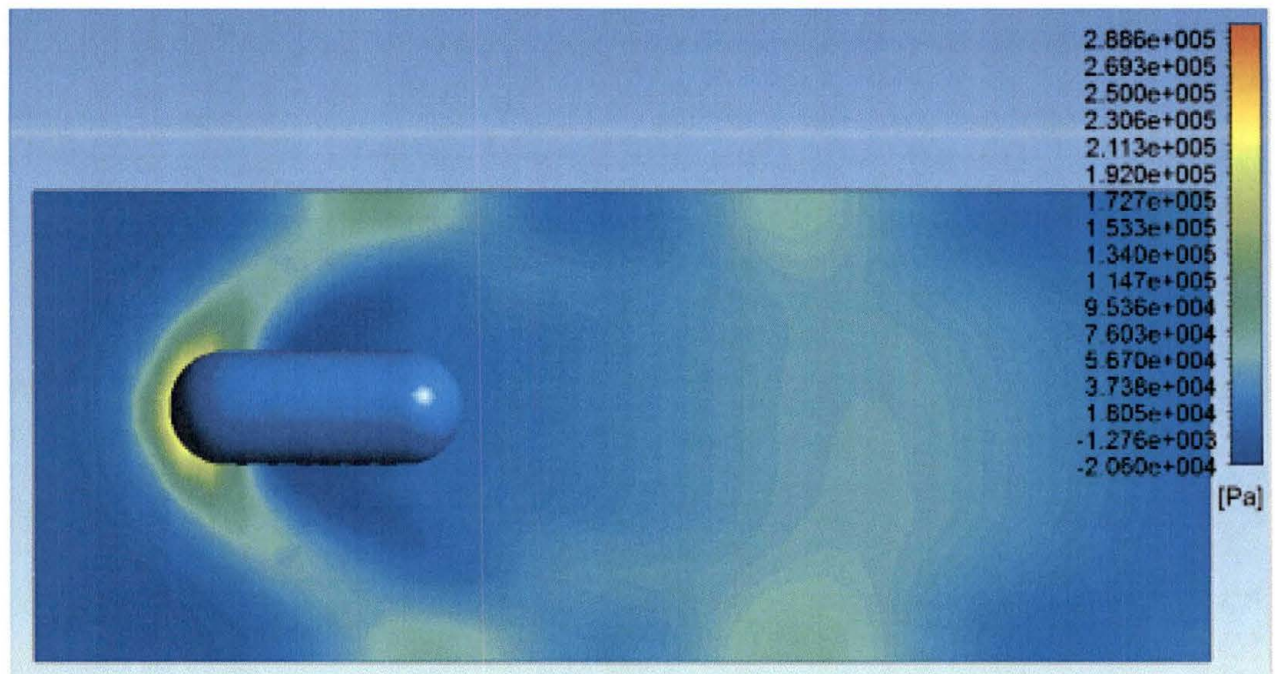


Figure 86. Tic Tac Pressure at 1/6 Scale, Air Temperature 223K and 1300 mph with Supersonic Inlet and Supersonic Outlet

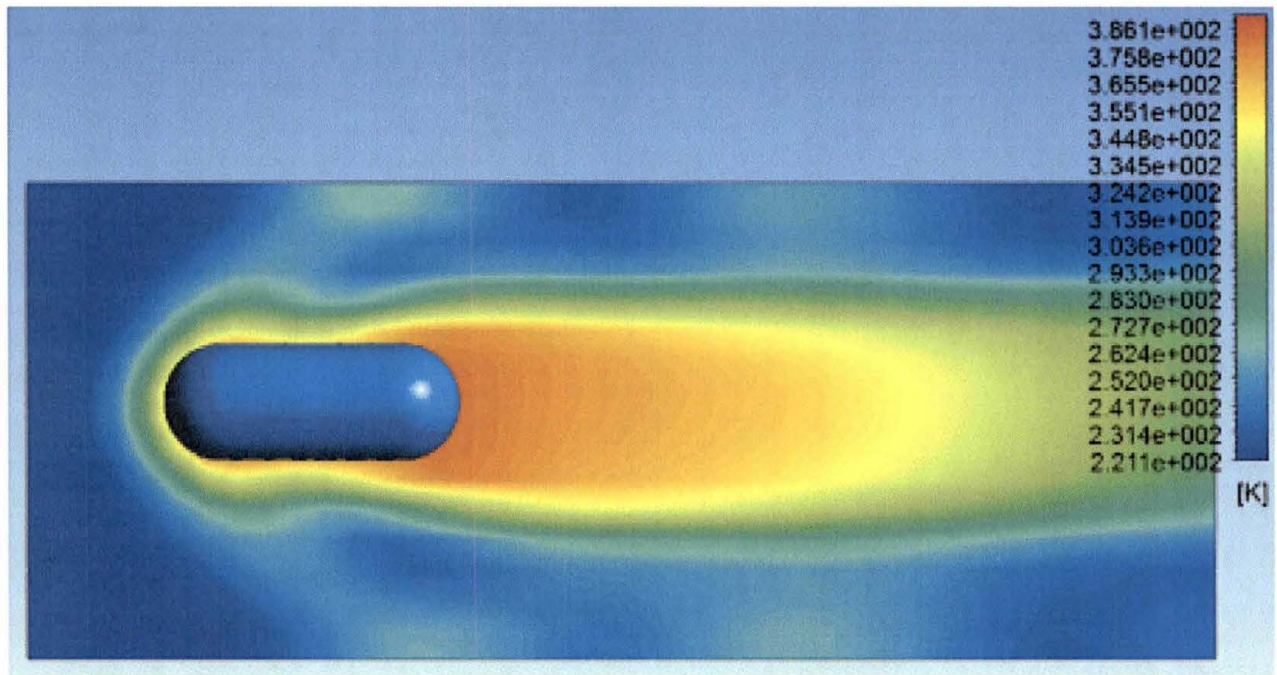


Figure 87. Tic Tac Temperature at 1/6 Scale, Air Temperature 223K and 1300 mph with Supersonic Inlet and Supersonic Outlet

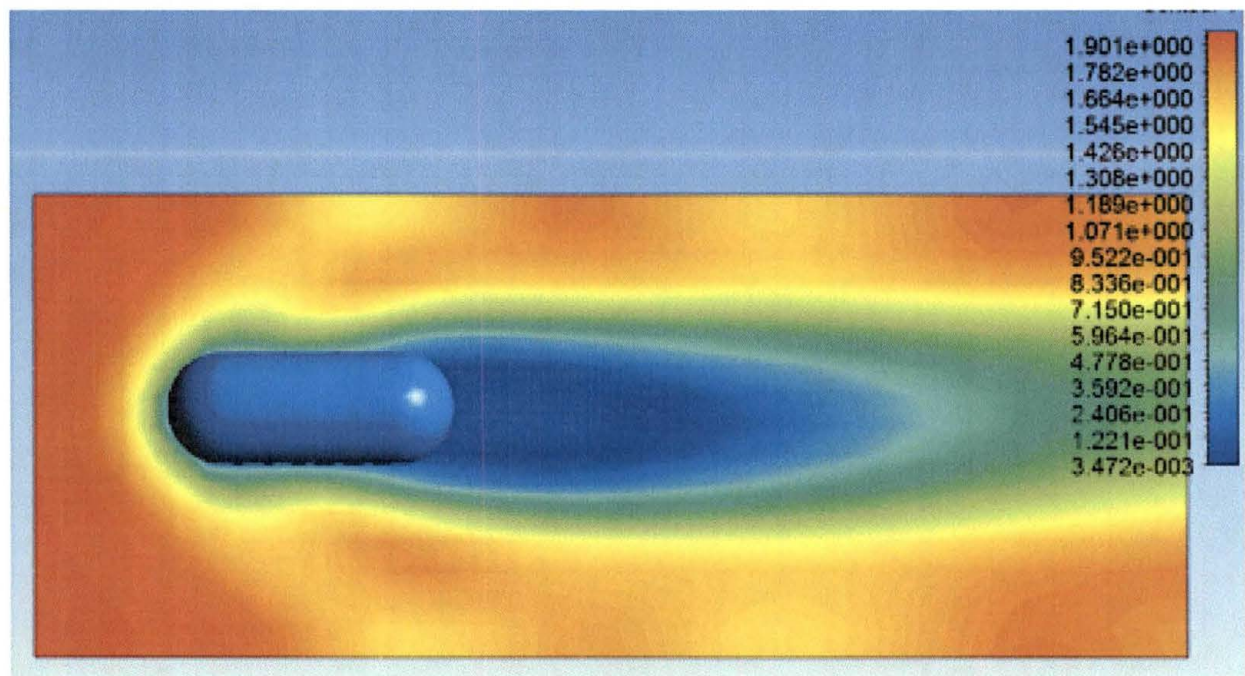


Figure 88. Tic Tac Mach Number at 1/6 Scale, Air Temperature 223K and 1300 mph with Supersonic Inlet and Supersonic Outlet

ATTACHMENT III – RIGHT CIRCULAR CYLINDER CFD CONTOUR PLOTS FOR PRESSURE, TEMPERATURE AND MACH NUMBER

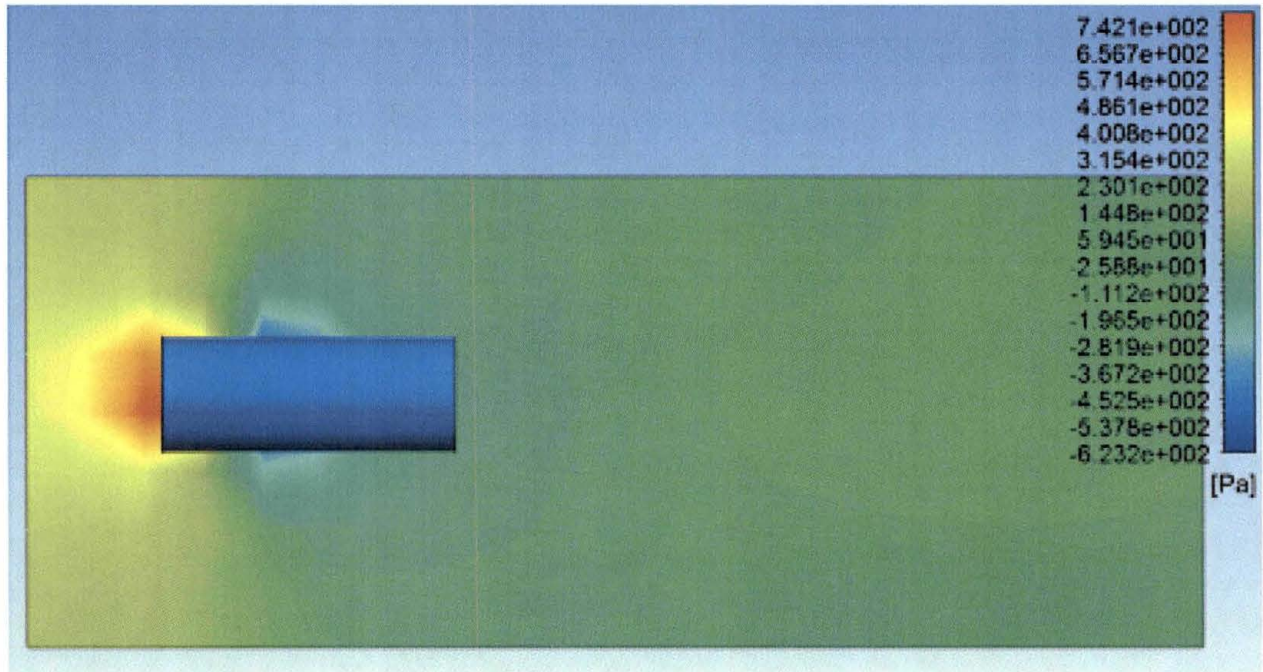


Figure 89. Cylinder Pressure at 1/6 Scale, Air Temperature 223K and 100 mph with Subsonic Inlet and Subsonic Outlet

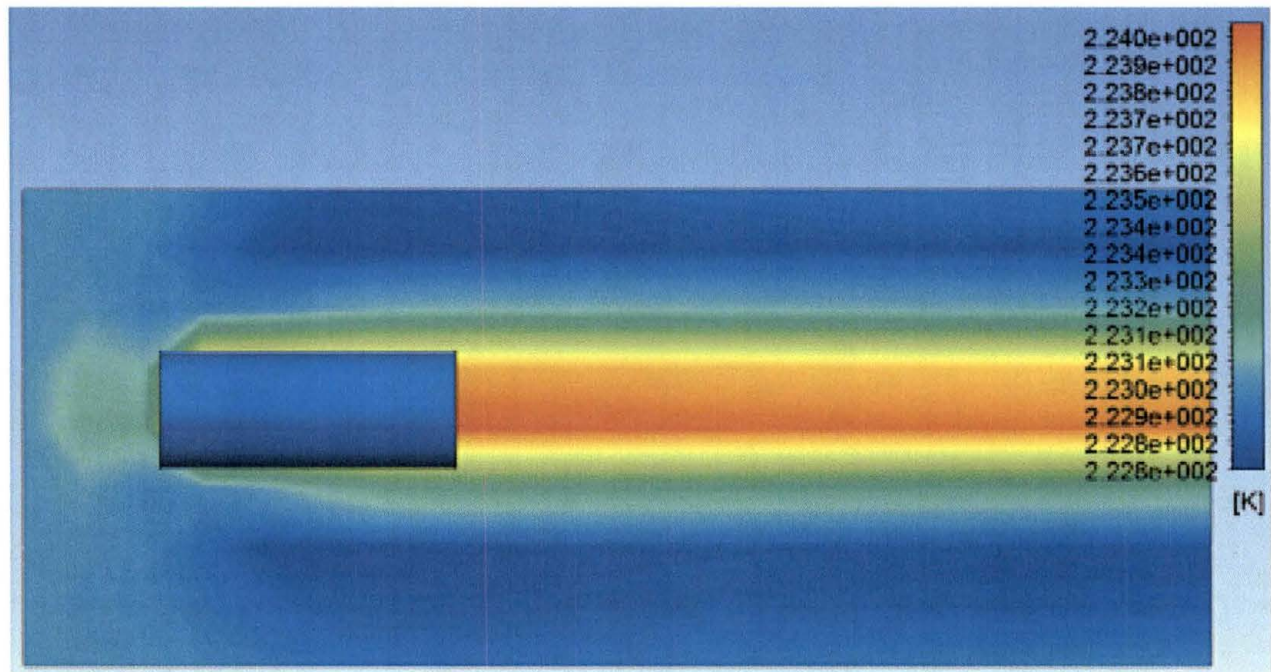


Figure 90. Cylinder Temperature at 1/6 Scale, Air Temperature 223K and 100 mph with Subsonic Inlet and Subsonic Outlet

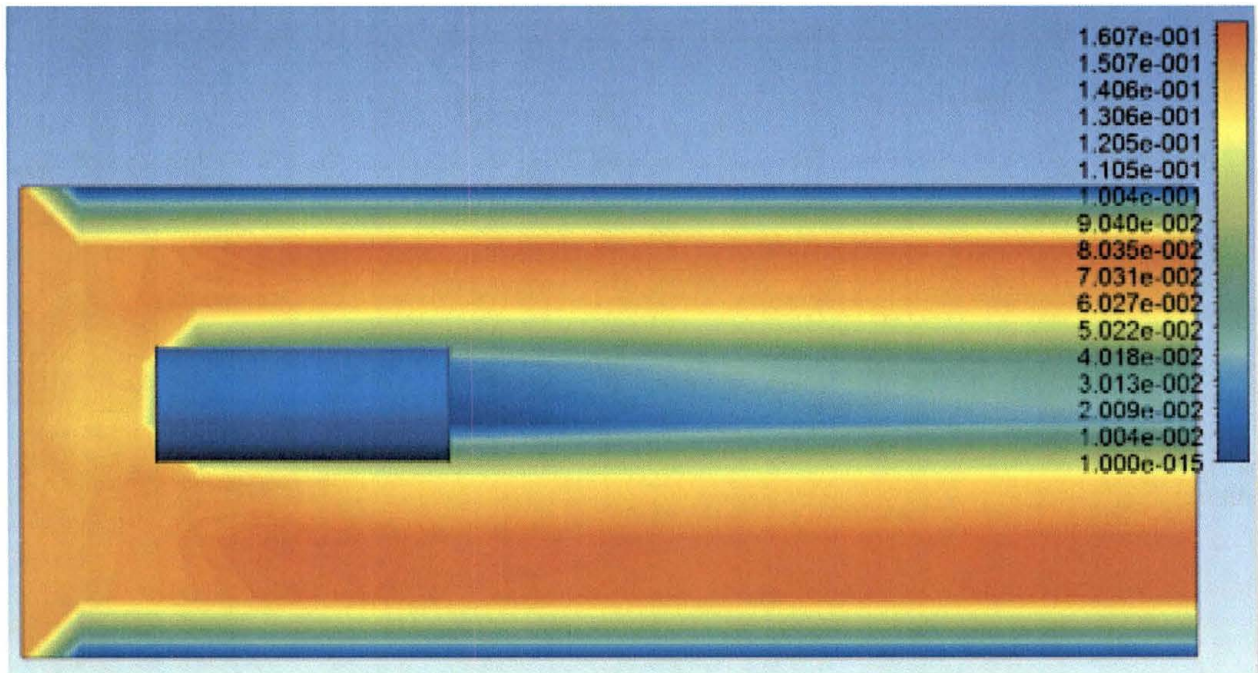


Figure 91. Cylinder Mach Number at 1/6 Scale, Air Temperature 223K and 100 mph with Subsonic Inlet and Subsonic Outlet

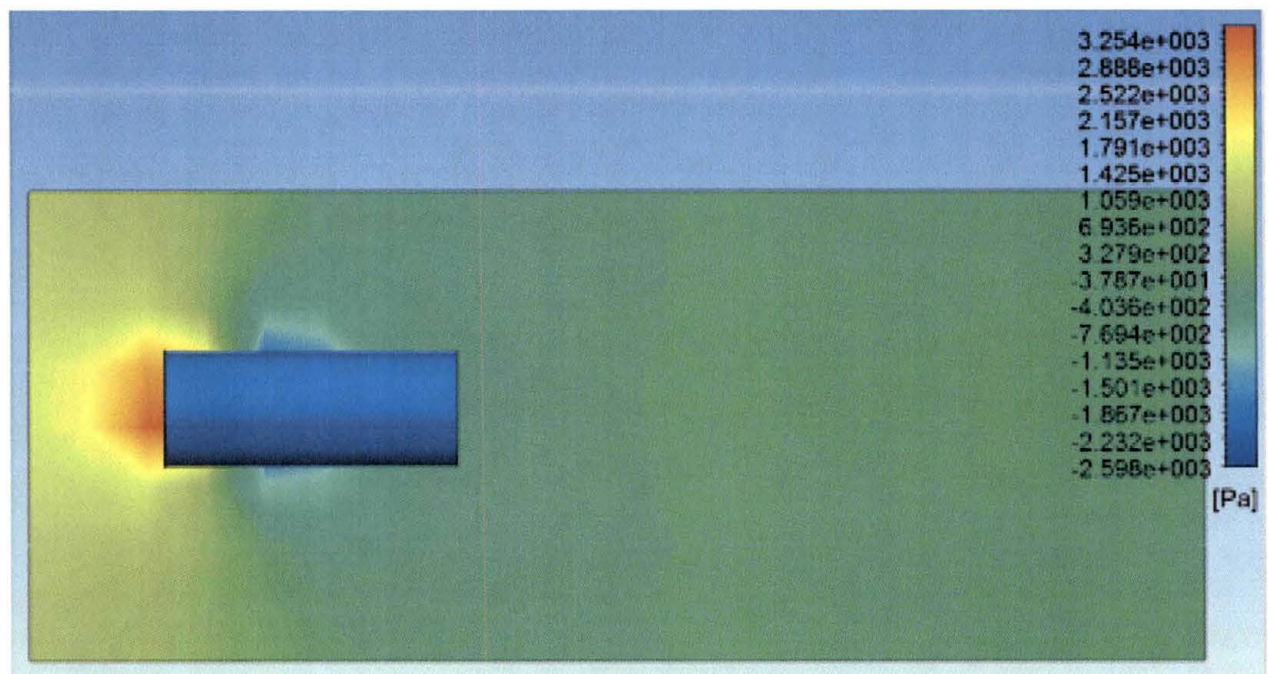


Figure 92. Cylinder Pressure at 1/6 Scale, Air Temperature 223K and 200 mph with Subsonic Inlet and Subsonic Outlet

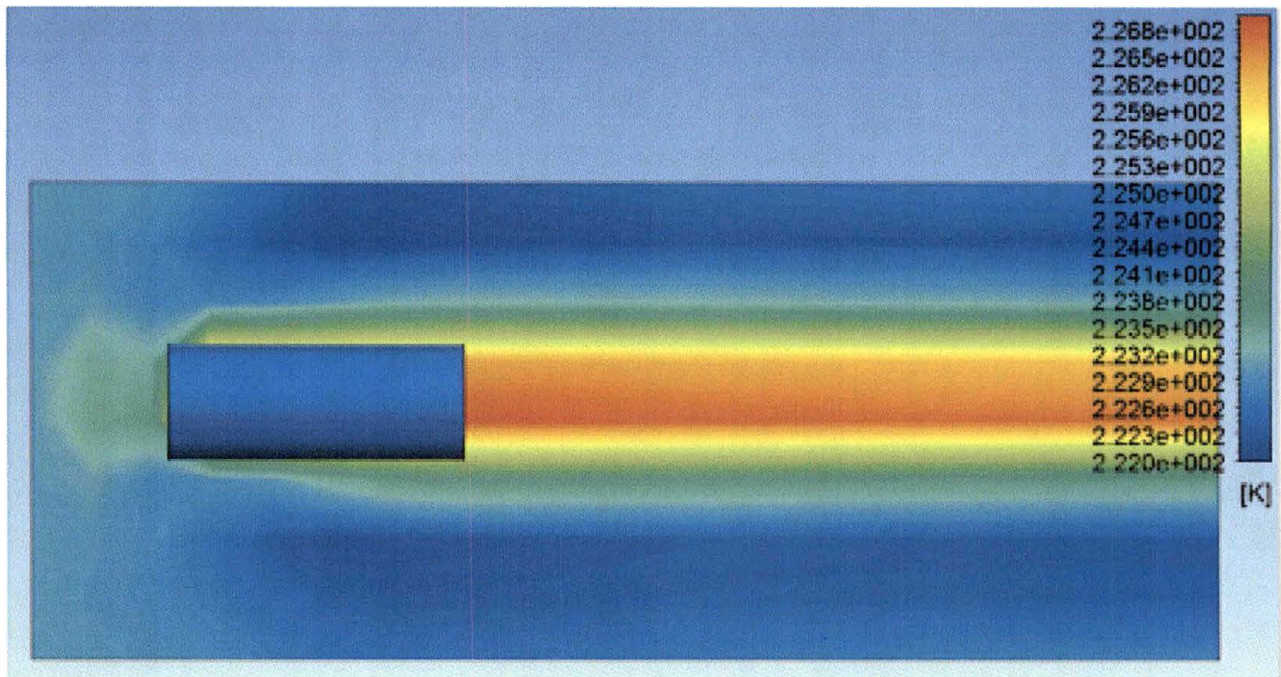


Figure 93. Cylinder Temperature at 1/6 Scale, Air Temperature 223K and 200 mph with Subsonic Inlet and Subsonic Outlet

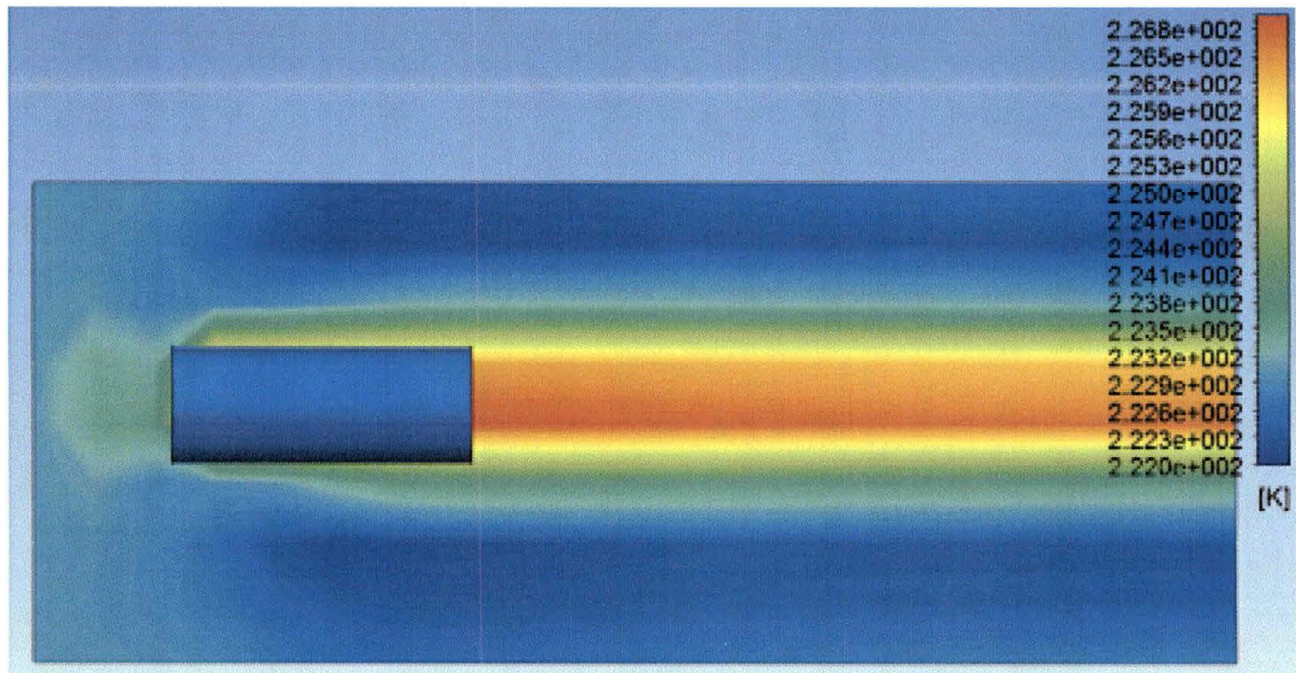


Figure 94. Cylinder Mach Number at 1/6 Scale, Air Temperature 223K and 200 mph with Subsonic Inlet and Subsonic Outlet

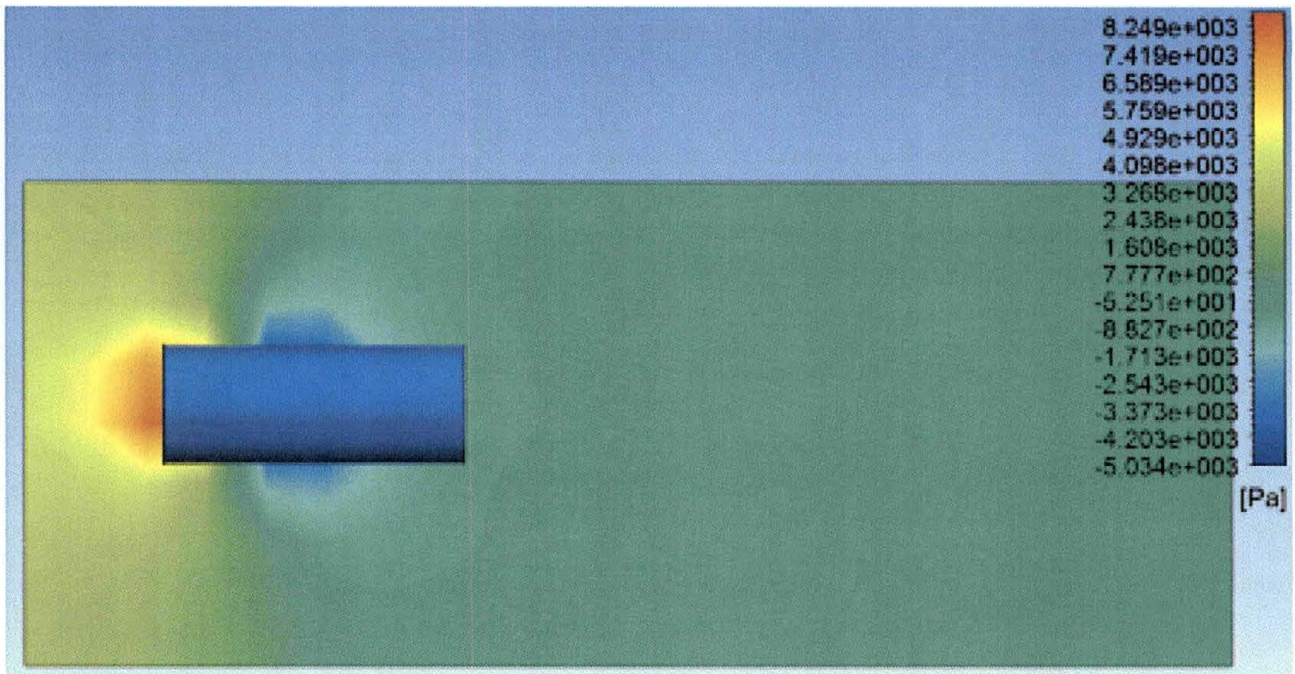


Figure 95. Cylinder Pressure at 1/6 Scale, Air Temperature 223K and 300 mph with Subsonic Inlet and Subsonic Outlet

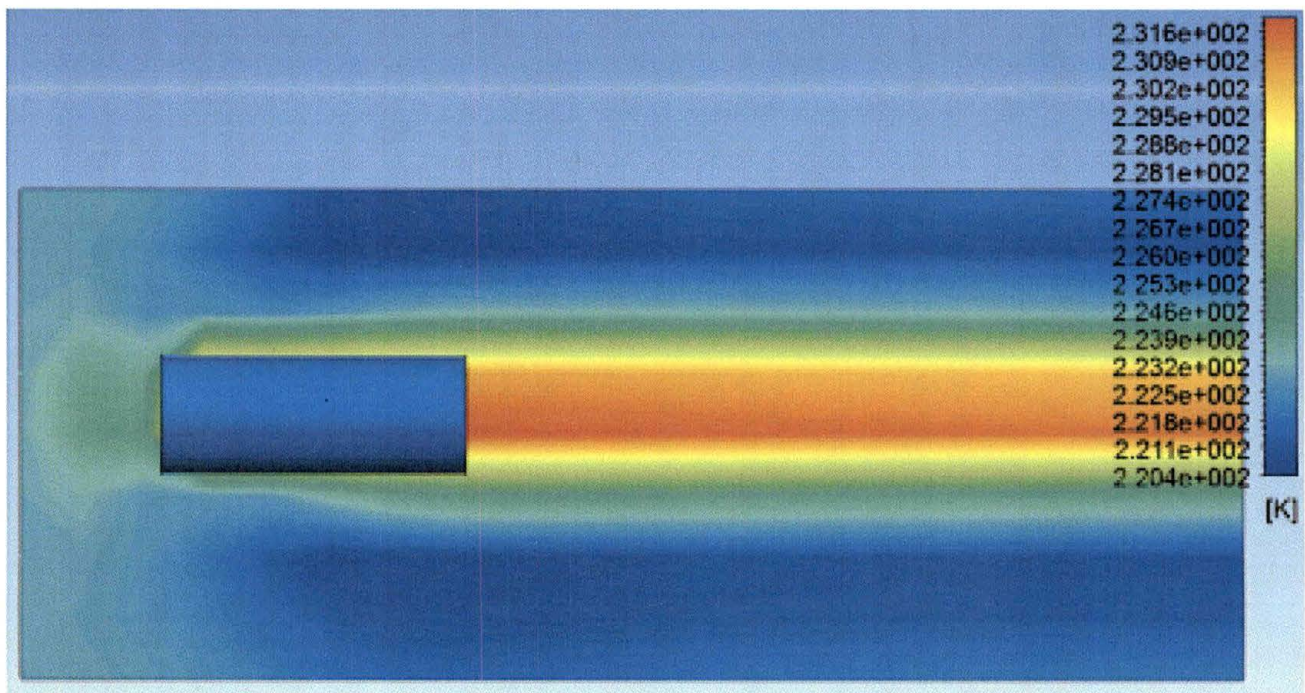


Figure 96. Cylinder Temperature at 1/6 Scale, Air Temperature 223K and 300 mph with Subsonic Inlet and Subsonic Outlet

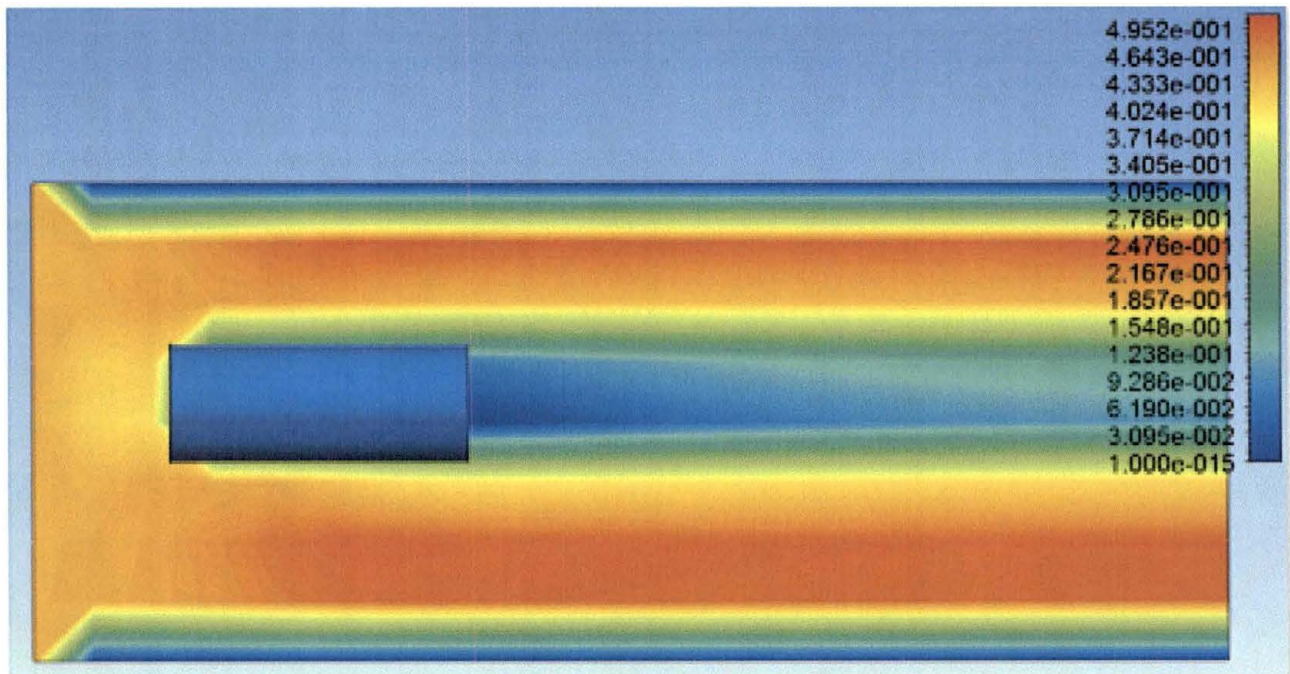


Figure 97. Cylinder Mach Number at 1/6 Scale, Air Temperature 223K and 300 mph with Subsonic Inlet and Subsonic Outlet

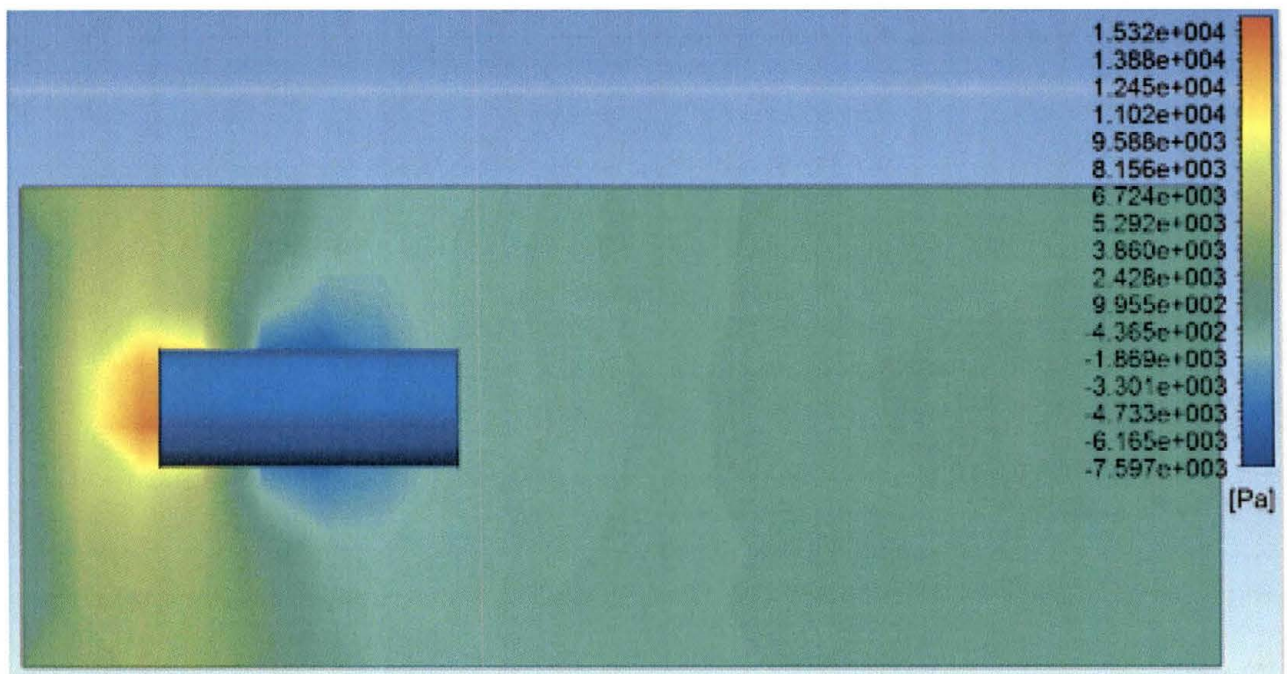


Figure 98. Cylinder Pressure at 1/6 Scale, Air Temperature 223K and 400 mph with Subsonic Inlet and Subsonic Outlet

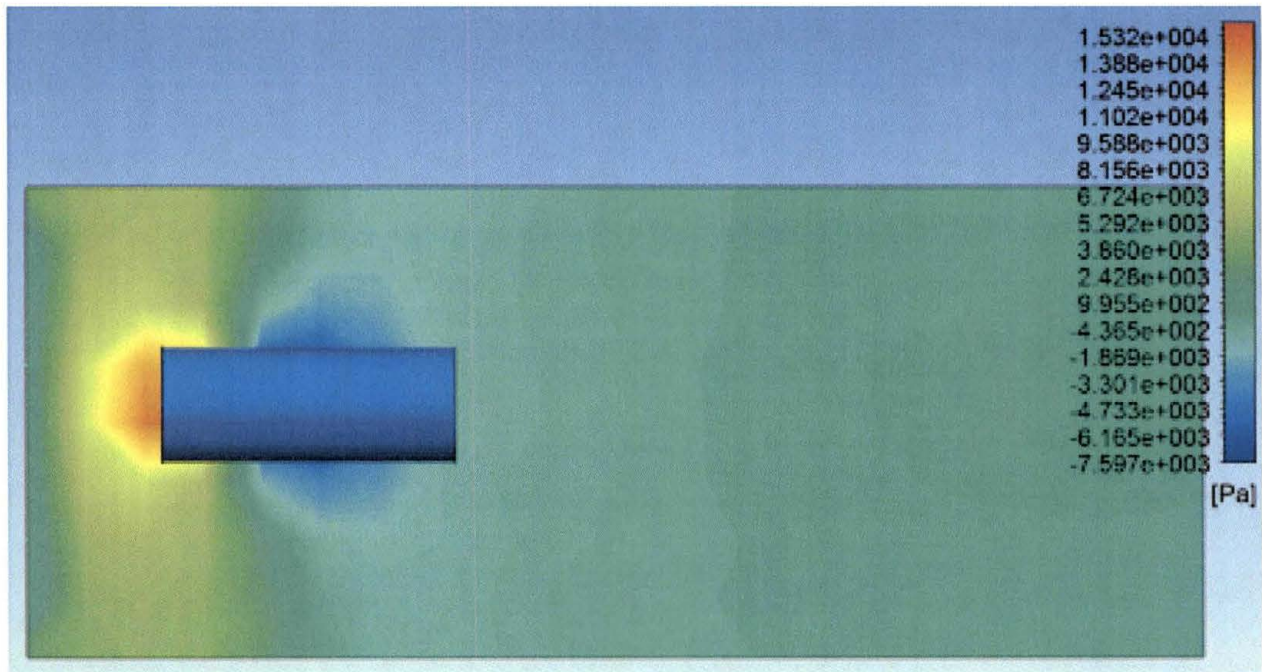


Figure 99. Cylinder Temperature at 1/6 Scale, Air Temperature 223K and 400 mph with Subsonic Inlet and Subsonic Outlet

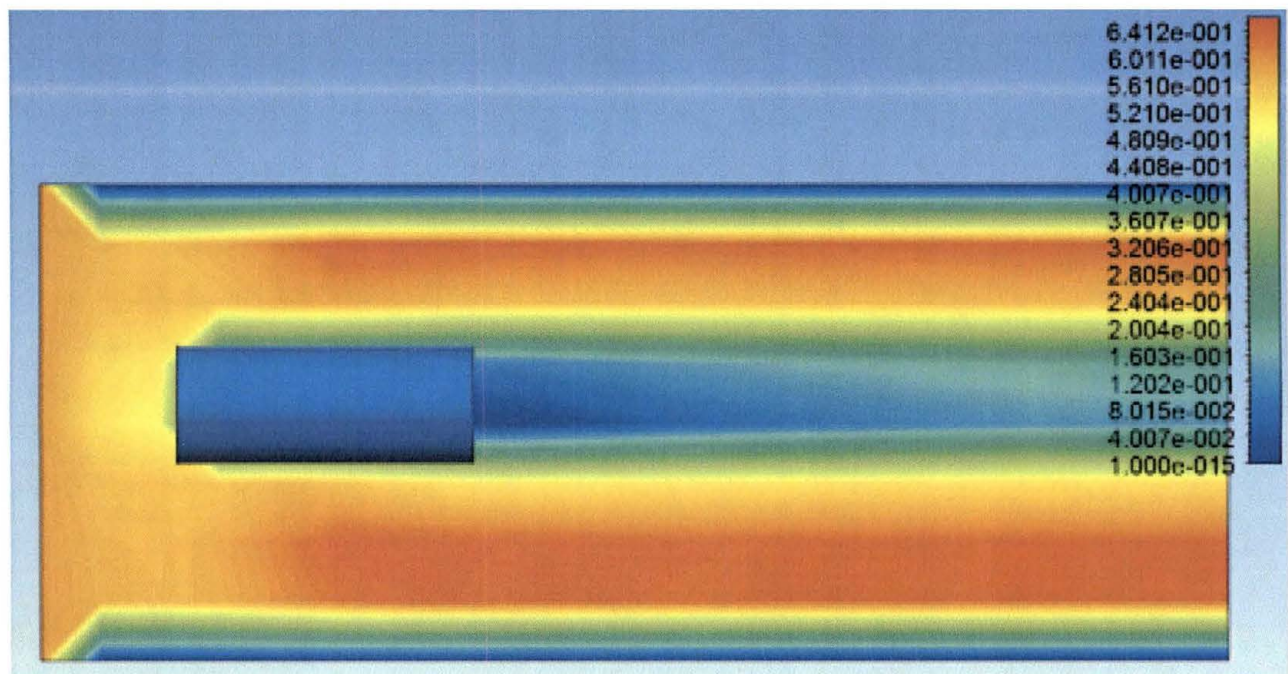


Figure 100. Cylinder Mach Number at 1/6 Scale, Air Temperature 223K and 400 mph with Subsonic Inlet and Subsonic Outlet

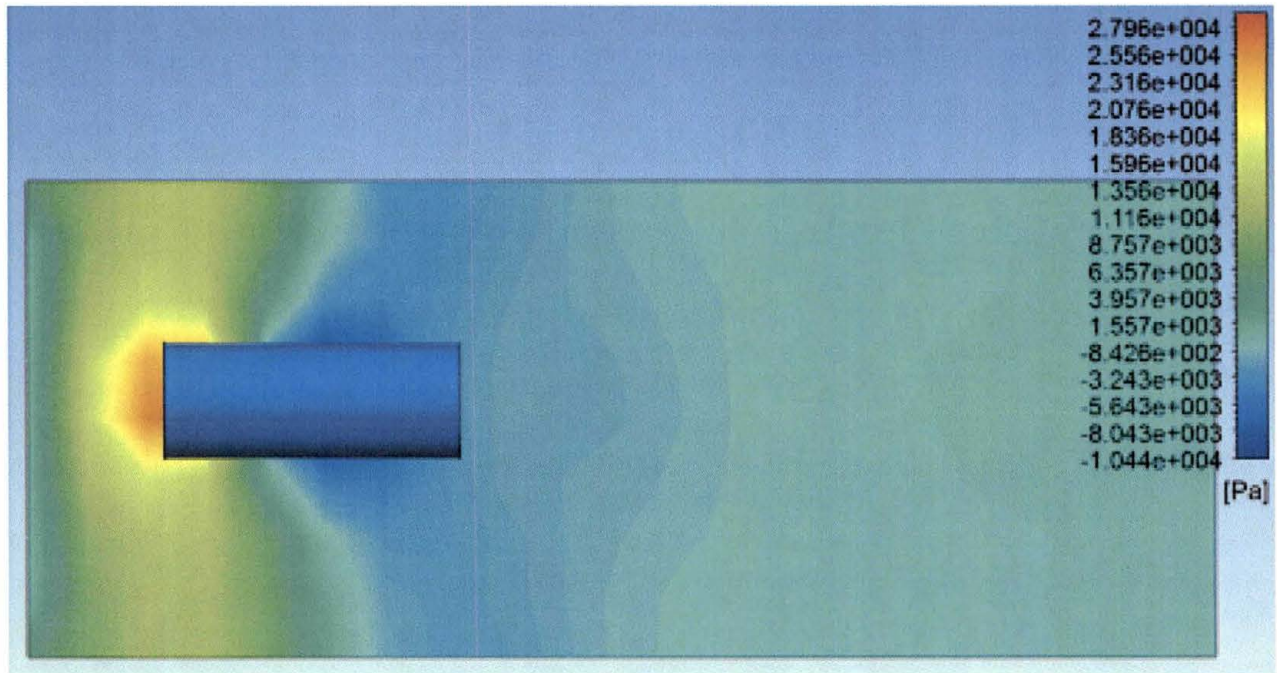


Figure 101. Cylinder Pressure at 1/6 Scale, Air Temperature 223K and 500 mph with Mixed Inlet and Subsonic Outlet

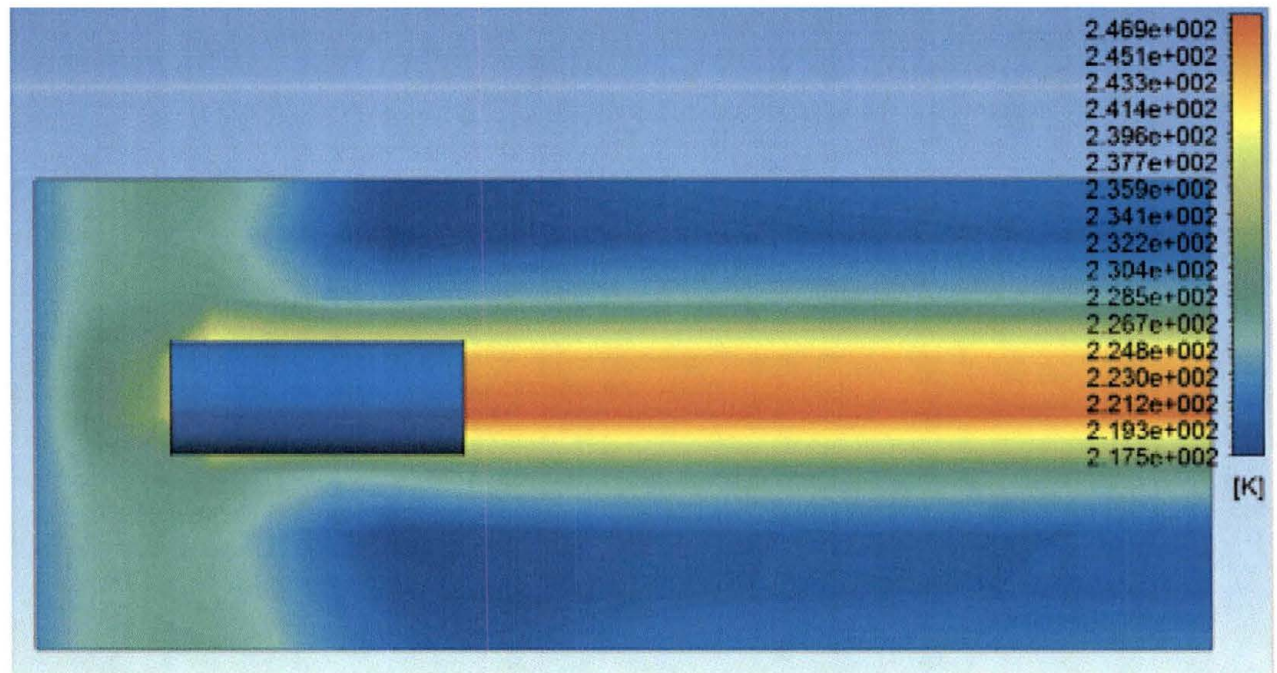


Figure 102. Cylinder Temperature at 1/6 Scale, Air Temperature 223K and 500 mph with Mixed Inlet and Subsonic Outlet

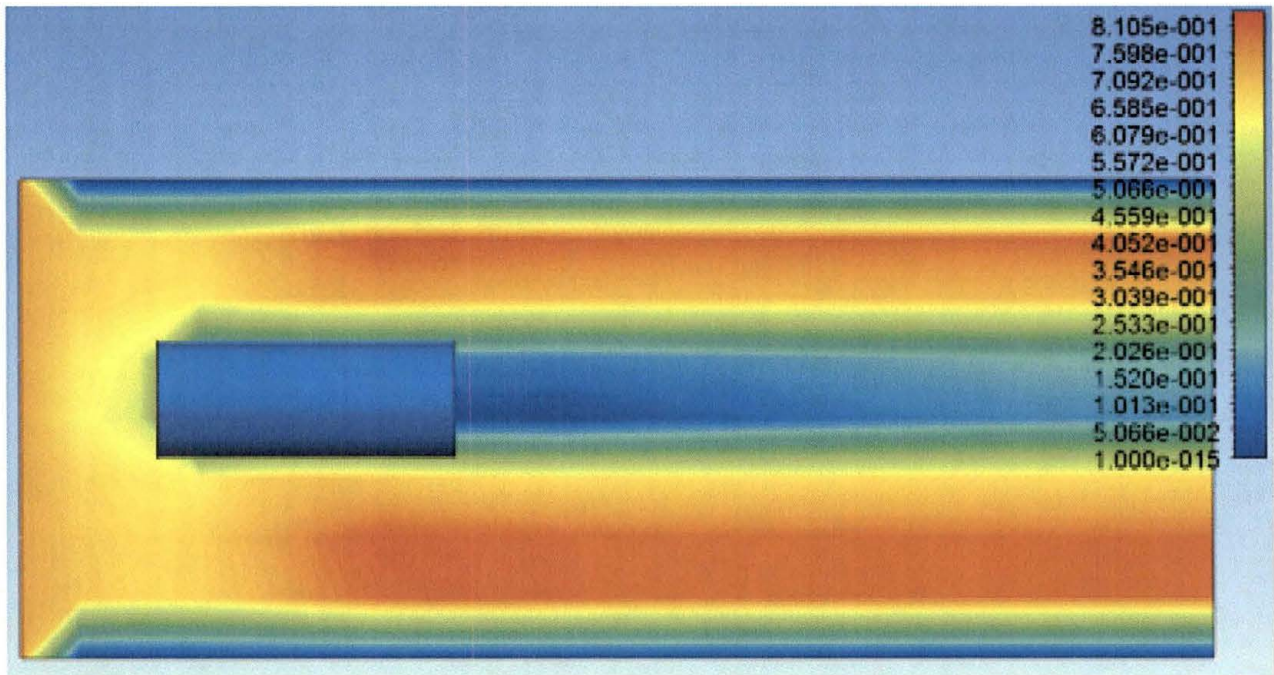


Figure 103. Cylinder Mach Number at 1/6 Scale, Air Temperature 223K and 500 mph with Mixed Inlet and Subsonic Outlet

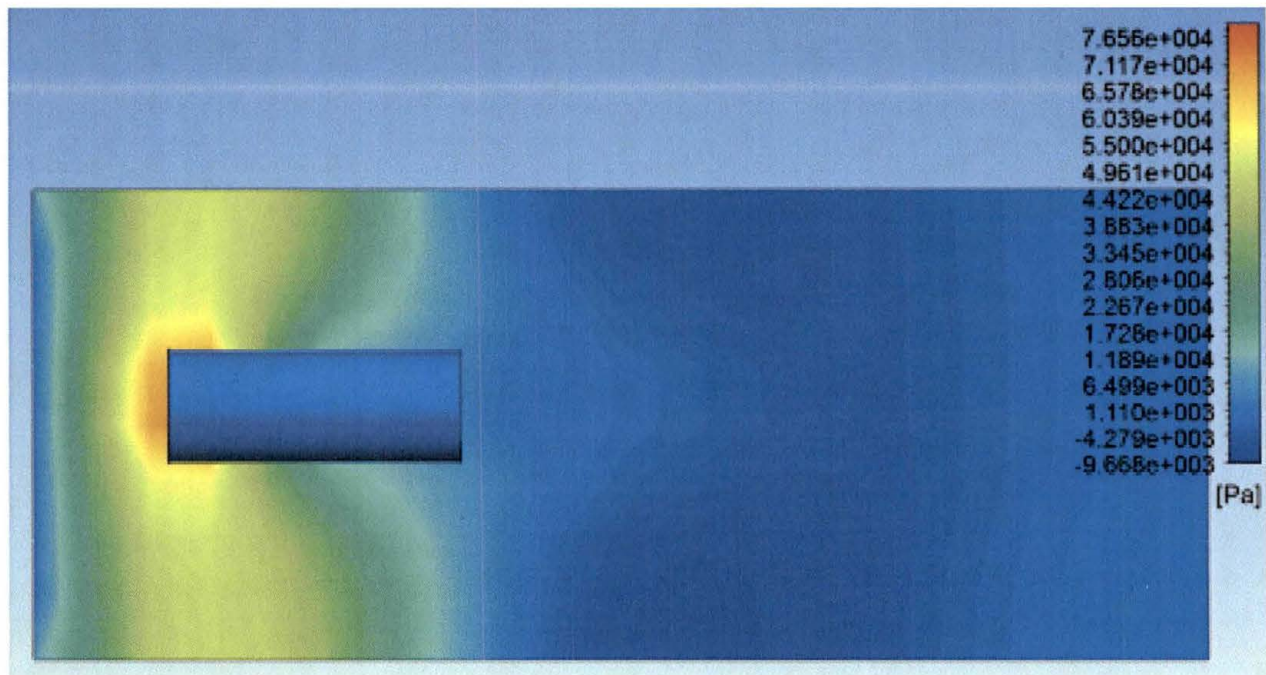


Figure 104. Cylinder Pressure at 1/6 Scale, Air Temperature 223K and 700 mph with Mixed Inlet and Supersonic Outlet

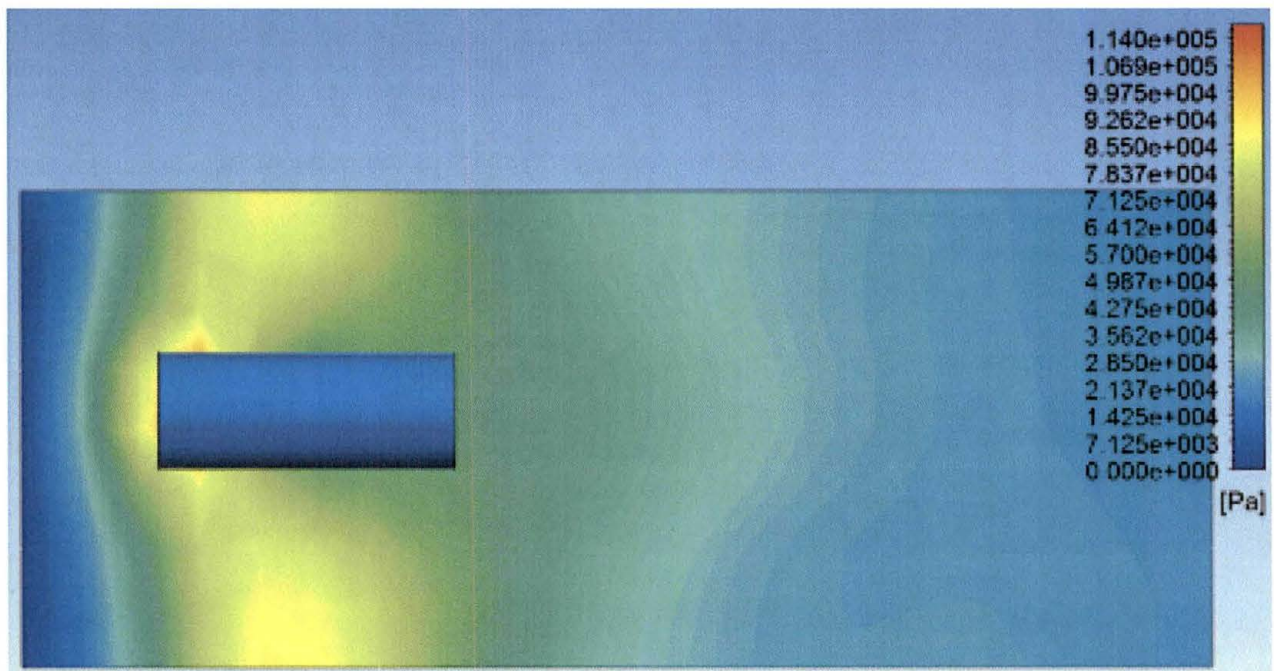


Figure 105. Cylinder Pressure at 1/6 Scale, Air Temperature 223K and 900 mph with Supersonic Inlet and Supersonic Outlet

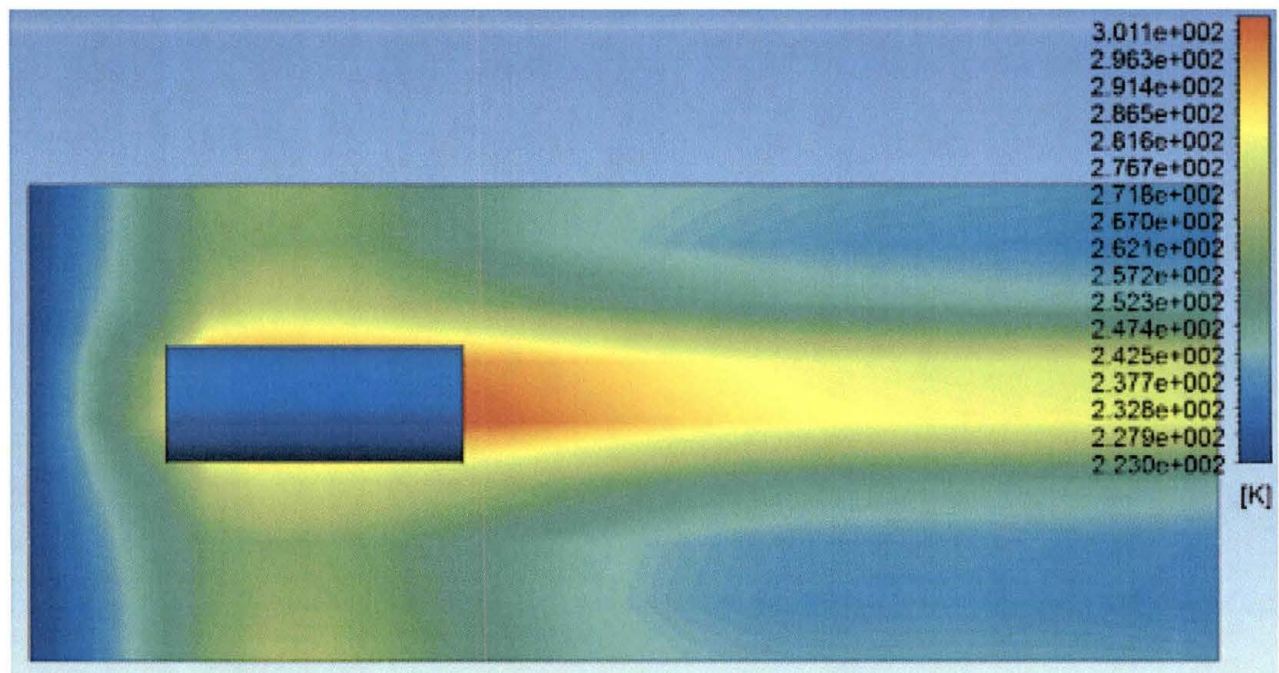


Figure 106. Cylinder Temperature at 1/6 Scale, Air Temperature 223K and 900 mph with Supersonic Inlet and Supersonic Outlet

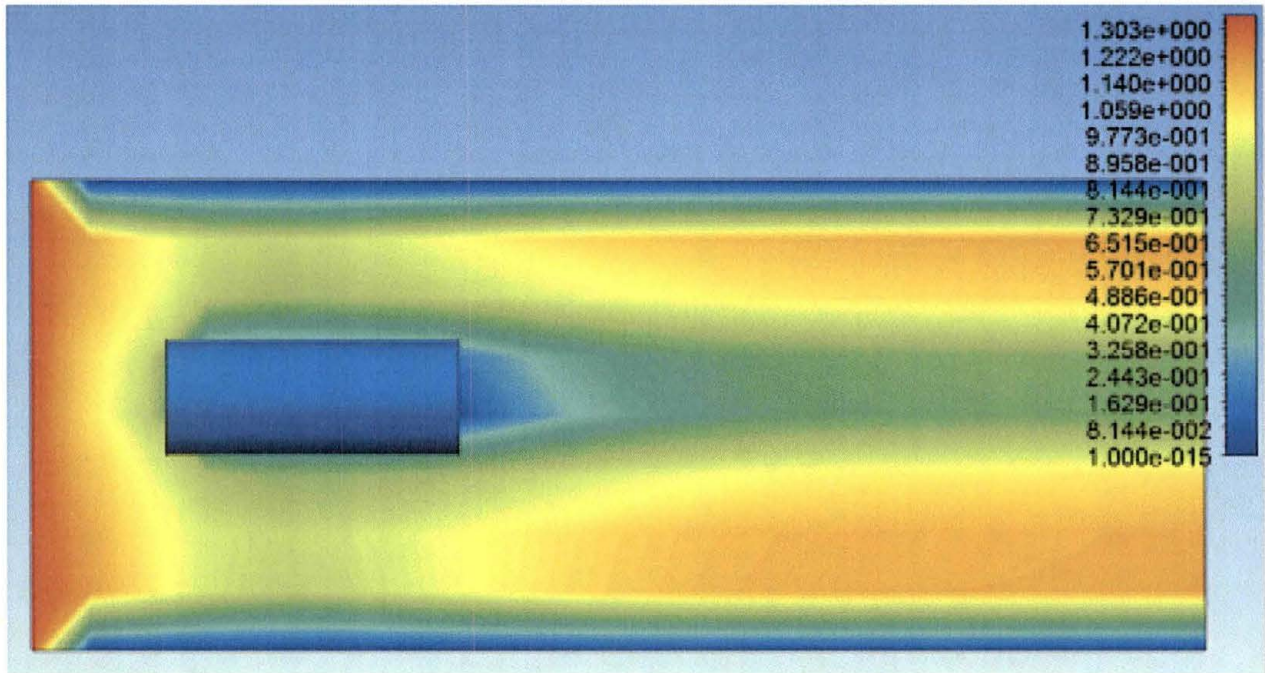


Figure 107. Cylinder Mach Number at 1/6 Scale, Air Temperature 223K and 900 mph with Supersonic Inlet and Supersonic Outlet

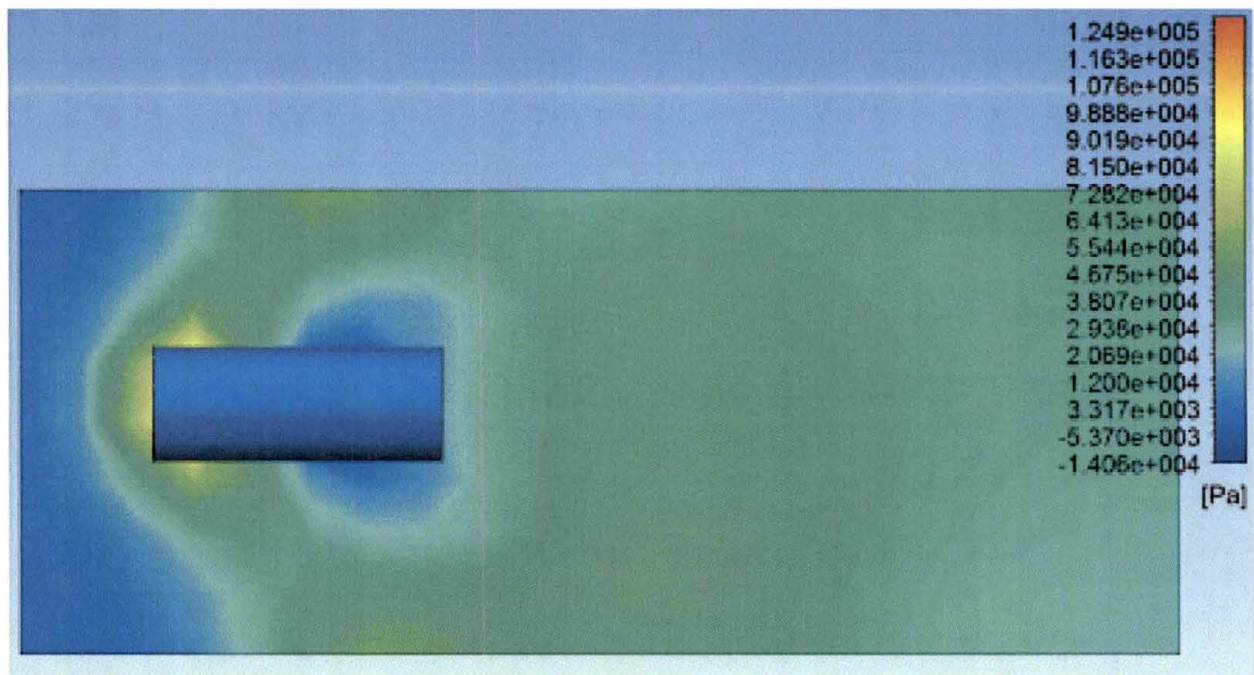


Figure 108. Cylinder Pressure at 1/6 Scale, Air Temperature 223K and 1100 mph with Supersonic Inlet and Supersonic Outlet

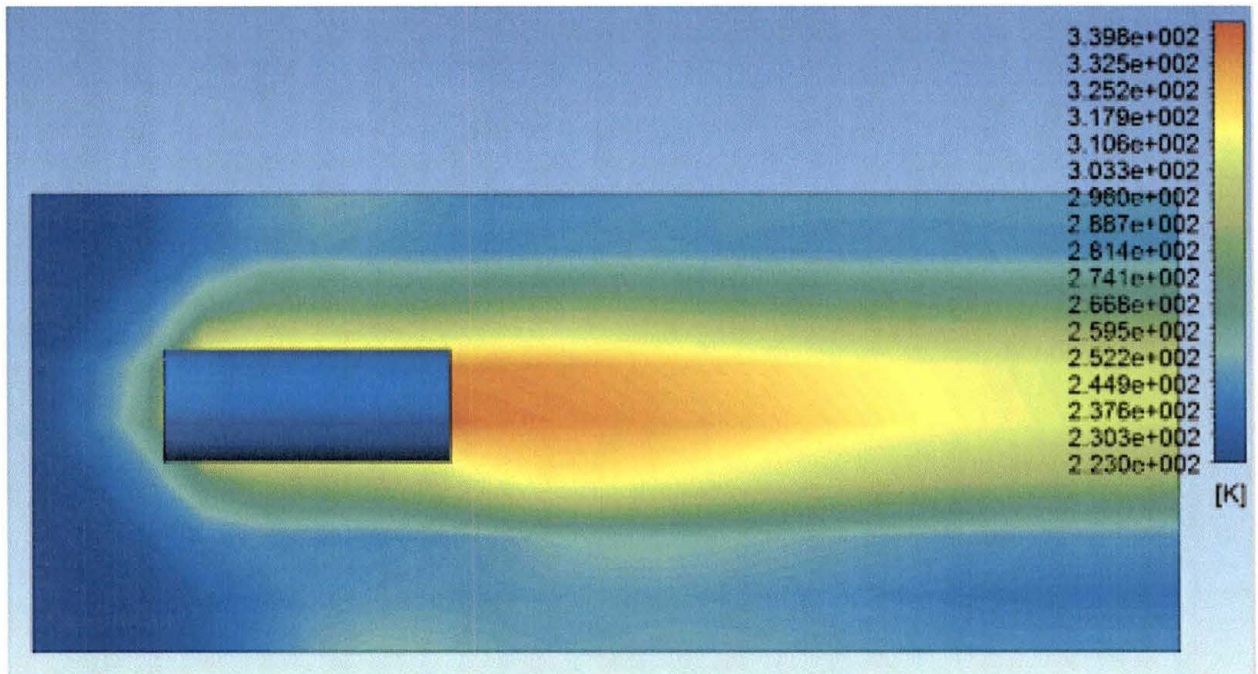


Figure 109. Cylinder Temperature at 1/6 Scale, Air Temperature 223K and 1100 mph with Supersonic Inlet and Supersonic Outlet

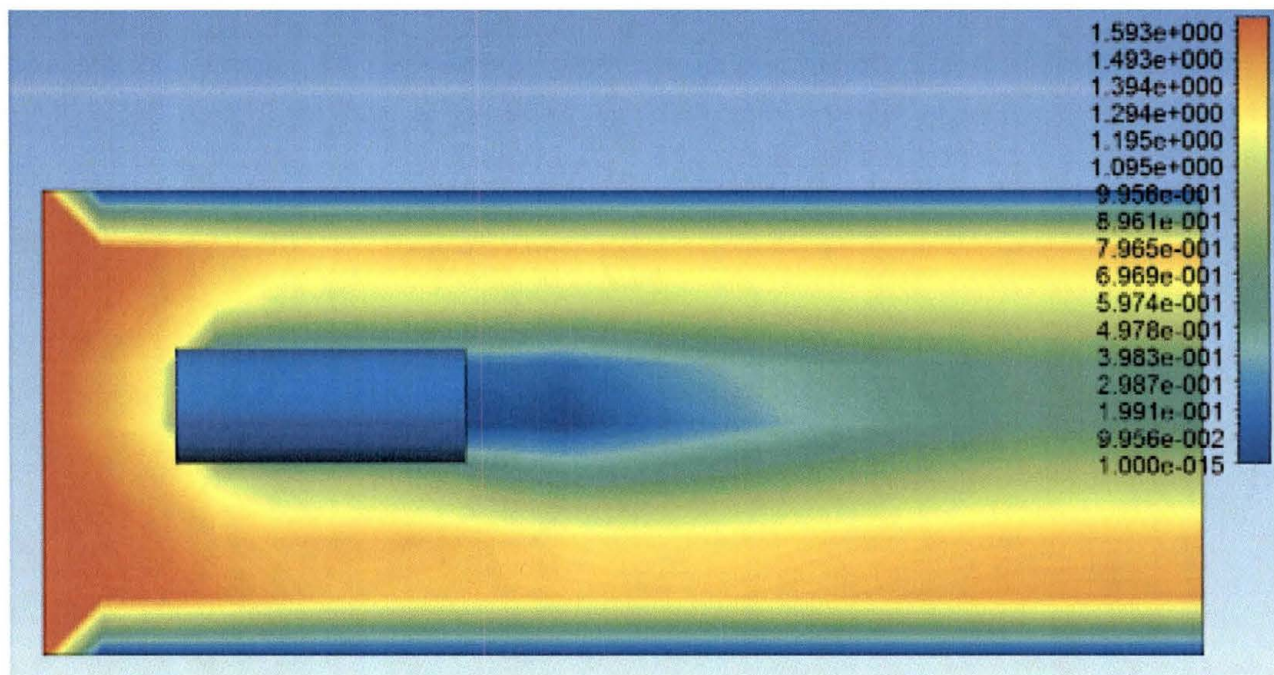


Figure 110. Cylinder Mach Number at 1/6 Scale, Air Temperature 223K and 1100 mph with Supersonic Inlet and Supersonic Outlet

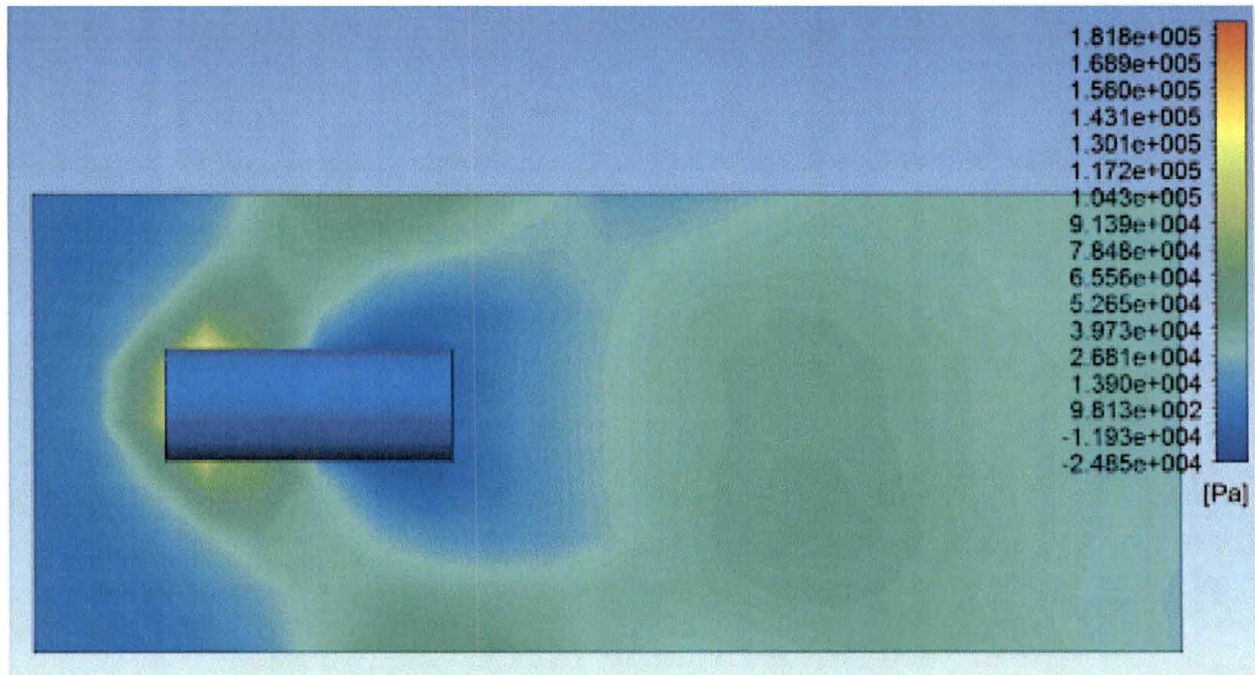


Figure 111. Cylinder Pressure at 1/6 Scale, Air Temperature 223K and 1300 mph with Supersonic Inlet and Supersonic Outlet

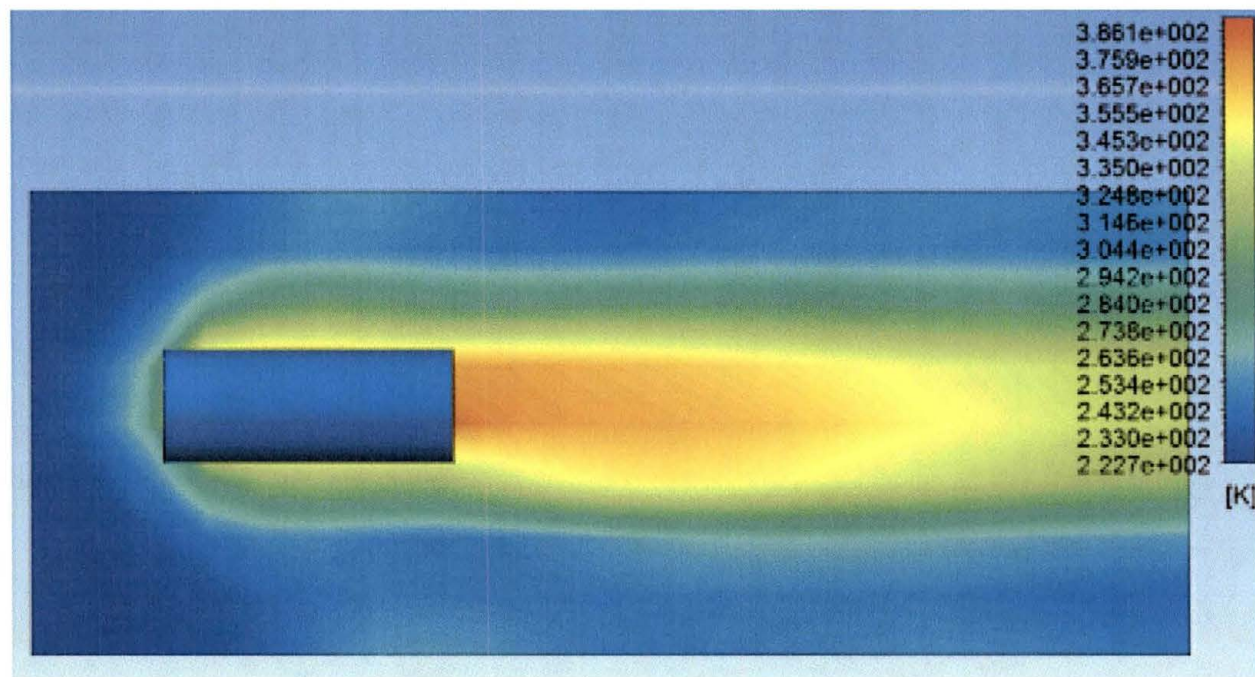


Figure 112. Cylinder Temperature at 1/6 Scale, Air Temperature 223K and 1300 mph with Supersonic Inlet and Supersonic Outlet

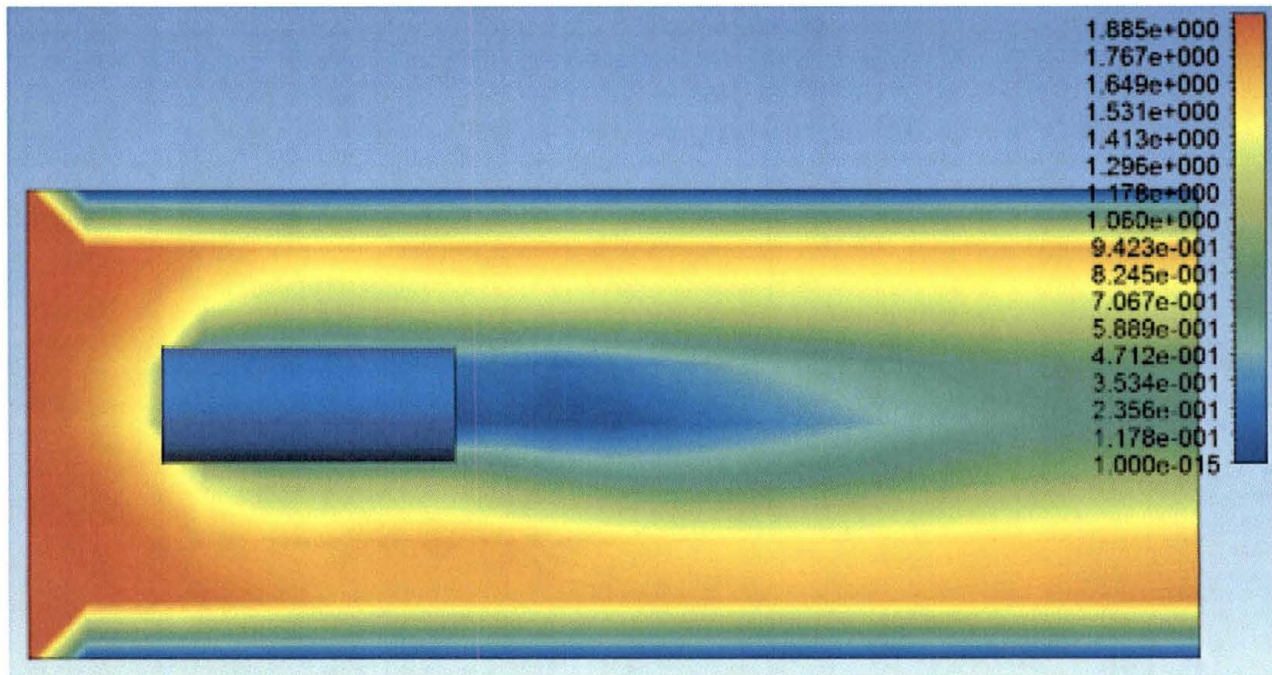


Figure 113. Cylinder Mach Number at 1/6 Scale, Air Temperature 223K and 1300 mph with Supersonic Inlet and Supersonic Outlet